Investigating G protein-coupled receptor 35 signalling and its role in cardiovascular disease

Nina Jennifer Divorty
BSc (Hons), MRes

Submitted in fulfilment of the requirements for the degree of
Doctor of Philosophy

Institute of Molecular, Cell and Systems Biology and
Institute of Cardiovascular and Medical Sciences

College of Medical, Veterinary and Life Sciences

University of Glasgow

February 2017

Abstract

G protein-coupled receptors (GPCRs) are an important source of drug targets with diverse therapeutic applications. Orphan GPCRs, which have unknown endogenous ligands or physiological functions, represent a pool of potential therapeutic targets that could provide novel or improved treatments for a wide range of diseases. G protein-coupled receptor 35 (GPR35) is an orphan receptor that has been associated with several diseases and physiological processes, including gastrointenstinal disease, pain transduction, inflammation and cardiovascular disease. However, the precise function of GPR35 in these processes is yet to be elucidated. Cardiovascular disease, including hypertension and heart failure, remains a large global disease burden, suggesting that current treatments are inadequate and that novel insights might be beneficial. Therefore, the role of GPR35 in cardiovascular disease was investigated in order to assess its potential as a therapeutic target.

To provide insight into the potential mechanisms of GPR35 actions in the cardiovascular system, GPR35 signalling was investigated in detail *in vitro*. Agonist-dependent phosphorylation was observed at five sites in the GPR35 C-terminal tail, which differentially influenced ß-arrestin recruitment. Both agonist-dependent phosphorylation and ß-arrestin-1/2, but not $G\alpha_{12/13}$, were essential for agonist-induced internalisation of GPR35, an important process in the desensitisation of the G protein-mediated response. Conversely, agonist-induced reorganisation of the actin cytoskeleton was dependent on $G\alpha_{12/13}$, but not phosphorylation or ß-arrestin.

To assess the role of GPR35 in cardiovascular disease, its actions were investigated in three *in vivo* models. A GPR35 knockout mouse had no abnormal cardiovascular phenotype under basal conditions, with no detectable differences in blood pressure, cardiac function, vascular reactivity or end-organ morphology compared with the wild type background strain. However, GPR35 knockout mice were resistant to hypertension and cardiac dysfunction induced by 2-week infusion of angiotensin II. Furthermore, administration of the GPR35 agonist amlexanox exacerbated both hypertension and end-organ damage in the stroke-prone spontaneously hypertensive rat.

These findings demonstrate a pathological role for GPR35 in the development of hypertension and its associated end-organ damage. It is likely that this is a result of $G\alpha_{13}$-mediated effects of GPR35 on the actin cytoskeleton in cardiovascular tissues, although this requires further investigation in primary cell models. These studies suggest that antagonism of GPR35 could be a novel therapeutic strategy to treat hypertension and/or heart failure. The findings must now be validated by antagonising GPR35 in *in vivo* disease models, in order to evaluate the therapeutic value of this strategy.

Table of Contents

List of Tables

List of Figures

List of Publications

Manuscripts

- McCallum J.E., Mackenzie A.E., **Divorty N.**, Clarke C., Delles C., Milligan G. and Nicklin S.A. (2016) G protein-coupled receptor 35 mediates human saphenous vein vascular smooth muscle cell migration and endothelial cell proliferation. *Journal of Vascular Research* **52**(6):383-395

- **Divorty N.**, Mackenzie A.E., Nicklin S.A. and Milligan G. (2015) G protein-coupled receptor 35: an emerging target in inflammatory and cardiovascular disease. *Frontiers in Pharmacology* **6**:41

Poster Presentations

- **Divorty N.**, Mackenzie A.E., Butcher A., Hudson B., Tobin A., Nicklin S.A. and Milligan G. Molecular coupling and phosphorylation profile of the orphan receptor GPR35

  British Pharmacological Society 6th Focused Meeting on Cell Signalling

  18–19 April 2016, University of Leicester, Leicester, UK

- **Divorty N.**, Butcher A., McCallum J.E., Tobin A., Graham D., Nicklin S.A. and Milligan G. G protein-coupled receptor 35 signalling and its role in cardiovascular disease.

  G Protein-Coupled Receptors: Structure, Signaling and Drug Discovery

  21–25 February 2016, Keystone Resort, Keystone, Colorado, USA

Acknowledgements

I would firstly like to thank my supervisors, Graeme Milligan, Stuart Nicklin and Delyth Graham, for their support and guidance throughout this project. They have each made enormous contributions to my personal and professional development, and their combined efforts have been instrumental in the planning and execution of this research.

Thanks to all the individuals who contributed to my scientific training and aided in the gathering of data: Laura Jenkins for her endless practical guidance on all things molecular pharmacology, John Pediani for his microscopy expertise, and all members of the Milligan lab for helpful advice and discussion; Stu for in-depth discussions on cloning technique and interpretation of *in vivo* data, and members of the Nicklin lab for their practical advice; Del, Elisabeth Beattie and Leslie Graham for assisting with the animal experiments (special thanks to Del and Elisabeth for many hours in the theatre and for coping with my frustration), the Biological Services staff in the Cardiovascular Research Facility for care and husbandry of the animals, and Jennifer McCallum for conducting a preliminary amlexanox SHRSP study, the data from which are included in the analyses in Chapter 6; Andrew Tobin for hosting me in his lab at the University of Leicester, Adrian Butcher for his assistance with the phospholabelling experiments there, and Andrew Bottrill for carrying out the mass spectrometry analysis reported in Chapter 3; and Asuka Inoue for generously providing the CRISPR-edited cell lines.

I thank the Wellcome Trust for funding my studentship. I extend my gratitude to the directors of the University of Glasgow Wellcome Trust Programme, Darren Monckton and Olwyn Byron; firstly for providing me with the opportunity to join such a fantastic programme, but also for their invaluable guidance in the early stages and their continued mentorship throughout. Thanks also to my fellow programme students, especially the 2012 cohort: Marléne, Catrina, Hussain and Kevin, for sharing the highs and the lows of this journey with me – without you it would have been a lot less fun.

The many friends I have met through this PhD also deserve a heartfelt thanks: my GCRC office-mates – Lisa, Emma, Margaret, Small Hannah, Tall Hannah and

Laura – your constant laughs and emotional support made the whole thing bearable; Laura and Elisa, our coffee breaks together provided a much-needed escape from the lab; Eugenia, your chat and encouragement has kept me going through it all.

I would not even have come close to reaching this goal without the constant, unwavering support of my family. Mum and Dad, you started me on this path by inspiring me to aim high and 'hold fast'. I hope the many emotional phone calls were worth it. Alistair and Adam, your successes have always encouraged me to do better – perhaps sibling rivalry isn't such a bad thing.

Finally, my endless gratitude goes to Pete. Your passion and perseverance inspire me. Thank you for everything: late-night lab troubleshooting, enduring my writing-induced mood swings, and providing me with daily laughter. I simply could not have done it without you.

Author's Declaration

"I declare that, except where explicit reference is made to the contribution of others, this dissertation is the result of my own work and has not been submitted for any other degree at the University of Glasgow or any other institution."

Signature: _____

Printed name: _____

Definitions/Abbreviations

$[Ca^{2+}]_i$	Intracellular calcium
5-HT	5-hydroxytryptamine
ACE	Angiotensin converting enzyme
AEP	Active effective pressure
Ang II	Angiotensin II
AP2	Adaptor protein 2
AR	Adrenergic receptor
Arr	Arrestin
BRET	Bioluminescent resonance energy transfer
cAMP	Cyclic adenosine monophosphate
CNS	Central nervous system
CRISPR	Clustered regularly interspaced short palindromic repeats
C_T	Cycle threshold
CVD	Cardiovascular disease
D	Dopamine
DAG	Diacylglycerol
DHICA	5,6-dihydroxyindole-2-carboxylic acid
DMR	Dynamic mass redistribution
DMSO	Dimethylsulfoxide
Dox	Doxycycline
DRG	Dorsal root ganglion
ECL	Extracellular loop
ELISA	Enzyme-linked immunosorbent assay
EPAC	Exchange protein activated by cAMP
ERK	Extracellular signal-regulated kinase
eYFP	Enhanced yellow fluorescent protein
FFA	Free fatty acid
GDP	Guanosine diphosphate
GEF	Guanine nucleotide exchange factor
GPCR	G protein-coupled receptor
GPR35	G protein-coupled receptor 35
GRK	G protein-coupled receptor kinase
GTP	Guanosine triphosphate
GWAS	Genome-wide association study
$G\alpha_i$	Gα inhibitory

$G\alpha_s$	Gα stimulatory
h	Human
HA	Haemagglutinin
HEK	Human embryonic kidney
IBD	Inflammatory bowel disease
ICL	Intracellular loop
IKK	IκB kinase
IP3	Inositol triphosphate
JNK	c-jun N-terminal kinase
KO	Knockout
LARG	Leukaemia-associated RhoGEF
Lbc	Lymphoid blast crisis
LPA	Lysophosphatidic acid
LPS	Lipopolysaccharide
LV	Left ventricle
m	Mouse
MT	Melatonin
PDE5	cGMP-specific phosphodiesterase type 5
PDM	Phosphorylation-deficient mutant
PKA	cAMP-dependent protein kinase
PKC	Protein kinase C
PSC	Primary sclerosing cholangitis
PTx	*Bordetella pertussis* Toxin
qRT-PCR	Quantitative real-time polymerase chain reaction
r	Rat
RGS	Regulators of G protein signalling
Rluc	*Renilla* luciferase
ROCK	Rho-associated protein kinase
RQ	Relative quantity
SDS-PAGE	Sodium dodecyl sulphate polyacrylamide gel electrophoresis
SHRSP	Stroke-prone spontaneously hypertensive rat
SNP	Single nucleotide polymorphism
TAC	Trans-aortic constriction
TBK	TANK-binding kinase
WT	Wild type

Chapter 1 Introduction

1.1 G protein-coupled receptors in drug discovery

1.1.1 The G protein-coupled receptor superfamily

The G protein-coupled receptor (GPCR) superfamily is the largest family of membrane proteins in the human proteome, comprising cell surface receptors for a wide variety of stimuli including hormones, neurotransmitters, chemokines, metabolites, ions and more. As such, GPCRs have important roles in an extensive range of physiological processes, and have been studied intensively for several decades. The family is characterised by a common seven-transmembrane α-helical fold, with family members sharing a high degree of structural similarity in the transmembrane bundle. Other structural features include an extracellular domain consisting of the N-terminal domain and three flexible extracellular loops (ECLs) and an intracellular domain consisting of three intracellular loops (ICLs) and a C-terminal tail. These regions are more variable and confer much of each receptor's ligand-binding and signalling specificity (Katritch et al., 2012).

1.1.2 GPCRs as therapeutic targets

Due to their ubiquity in physiological processes, GPCRs and their ligands are often implicated in pathophysiology and disease. This, together with their accessibility at the cell membrane, makes the family an important source of therapeutic targets. By various different estimates, approximately 30% of all FDA-approved drugs target GPCRs (Overington et al., 2006, Rask-Andersen et al., 2011, Garland, 2013). These have diverse therapeutic applications including the treatment of neuropsychiatric disorders, cardiovascular disease, allergy, pain, obesity and diabetes, and include many of the all-time bestselling drugs (Table 1-1) (Zambrowicz and Sands, 2003, Garland, 2013). New GPCR-targeting drugs are still being discovered, accounting for 19% of new molecular entities approved between 2010 and 2012 (Garland, 2013). Furthermore, relatively recent developments in the field have uncovered novel facets of GPCR signalling, such as biased agonism, that can be further exploited to develop novel and improved therapeutics (Whalen et al., 2011, Luttrell et al., 2015).

GPCRs therefore remain at the forefront of drug discovery and hold great potential as therapeutic targets for the future.

Table 1-1 Selected bestselling drugs that target GPCRs

Drug	GPCR target	Therapeutic application
Claritin (loratidine)	Histamine H_1 receptor	Allergy
Diovan (valsartan)	AT_1 angiotensin receptor	Hypertension, heart failure
Plavix (clopidogrel)	$P2Y_{12}$ purinergic receptor	Heart attack, stroke
Serevent (salmeterol)	$ß_2$ adrenergic receptor	Asthma, COPD
Seroquel (quetiapine)	5-HT/dopamine receptors	Psychosis, depression
Singulair (montelukast)	Leukotriene receptor	Asthma, allergy
Zyprexa (olanzapine)	5-HT/dopamine receptors	Psychosis

Adapted from (Zambrowicz and Sands, 2003). (COPD = chronic obstructive pulmonary disease; 5-HT = 5-hydroxytryptamine.)

1.1.3 Orphan GPCRs

Although GPCRs are generally very valuable drug targets, the vast majority of approved drugs act at a select few family members: the histamine H_1 receptor, the α_{1A} and α_{2A} adrenergic receptors, the M_1, M_2 and M_3 muscarinic receptors, the dopamine D_2 receptor and the 5-HT_{2A} serotonin receptor (Garland, 2013). Of 365 non-olfactory GPCRs, less than one third are currently utilised as drug targets. More than 120 are orphan GPCRs – receptors that have not yet been paired with a cognate endogenous ligand (Davenport et al., 2013, Alexander et al., 2015). Often, these orphan receptors are poorly characterised and have unknown physiological functions. However, given the importance of GPCR signal transduction in a wide range of cellular processes, it is thought that many orphan GPCRs must have therapeutically relevant roles. These receptors therefore represent a pool of previously unexploited potential therapeutic targets, and ongoing research efforts are being applied to 'deorphanise' these receptors and elucidate their roles in various diseases.

1.1.4 Deorphanisation strategies

Historically, GPCR drug targets were identified using a 'classical pharmacology', ligand-based approach, in which biologically active compounds are isolated, for example from tissue extracts, and used to generate lead compounds,

subsequently leading to target identification. This approach was used for some of the most therapeutically successful GPCR targets, such as the ß-adrenergic receptors – which were identified as receptors for adrenaline in 1948 and subsequently targeted by ß blockers – and the histamine receptors, which were used to screen for early anti-allergy drugs in the 1930s, and remain important targets today (Wachter and Gilbert, 2012, Jones, 2016). However, advances in homology screening techniques (whereby novel genes are amplified using primers for homologous sequences), and later the publication of the human genome, gave rise to a large pool of orphan receptor targets, and so a new strategy for drug discovery emerged (Lander et al., 2001). 'Reverse pharmacology' uses the receptor target as a starting point, utilising the cloned receptor to screen for endogenous and synthetic ligands (Lecca and Abbracchio, 2008). These tool compounds can subsequently be used to investigate the receptor's pharmacological properties and biological function (Lecca and Abbracchio, 2008, Kolar et al., 2016). The reverse pharmacology approach has been applied successfully to deorphanise a number of important drug targets, such as the early deorphanisation of the 5-HT_{1A} serotonin receptor (Fargin et al., 1988) and the dopamine D_2 receptor (Bunzow et al., 1988). It has also been instrumental in the identification of novel endogenous ligands and previously unknown transmitter systems, as with the discovery of orexins and their receptors as regulators of wakefulness and appetite (Sakurai et al., 1998). Following on from these early successes, the approach continues to yield promising new drug targets, such as free fatty acid receptor 1 (FFA_1), formerly the orphan GPR40, which is now an attractive therapeutic target in type 2 diabetes (Itoh et al., 2003, Li et al., 2016).

Some knowledge of the coupling and signalling profile of an orphan GPCR is beneficial to developing screening assays for deorphanisation. G protein and second messenger activity assays such as guanosine triphosphate (GTP)-γS, cyclic adenosine monophosphate (cAMP), and intracellular calcium ($[Ca^{2+}]_i$) assays have proven successful in deorphanisation and surrogate ligand screens (Briscoe et al., 2003, Takeda et al., 2003, Jenkins et al., 2010, Meyer et al., 2013). Components of the desensitisation and internalisation cycle, especially translocation of the adaptor protein ß-arrestin, have also been utilised in screening efforts (Oakley et al., 2006, Neetoo-Isseljee et al., 2013). It is therefore important to

understand how these processes vary among GPCRs in order to properly interpret screens for orphan receptors.

Today, novel technologies are being applied to the reverse pharmacology model in order to deorphanise poorly characterised receptors. The recent accumulation of high quality crystal structures has enabled *in silico* homology modelling, which in combination with virtual screening is a powerful means of identifying surrogate ligands for orphan receptors that have few or no tool compounds with which to probe their function (Ngo et al., 2016b). This approach has been used to identify high potency synthetic 'surrogate' ligands for orphan receptors such as GPR17, a proposed target in neurodegenerative disease (Eberini et al., 2011), and GPR37L1, which has been associated with neuroprotection and hypertension (Ngo et al., 2016a).

1.1.5 Orphan GPCRs as drug targets

While identifying the endogenous ligands for orphan receptors is desirable, deorphanisation is not always necessary to identify potential therapeutic value. In fact, identifying a therapeutically relevant function for an orphan receptor is usually a prerequisite for amassing sufficient interest to make a concerted deorphanisation effort. Often, important physiological and pathophysiological roles can be inferred from tissue distribution or phenotypic studies. Transgenic and knockout mice can be valuable tools in interrogating the functions of poorly characterised receptors. For example, the orphan GPR88 is expressed in areas of the brain associated with schizophrenia (Logue et al., 2009). GPR88 knockout mice showed behavioural defects associated with the striatal dopamine system, implicating it as a potential therapeutic target in CNS disorders (Logue et al., 2009). Similarly, GPR55 – a recently deorphanised endocannabinoid receptor – is moderately expressed in epithelia (Pérez-Gómez et al., 2013). Its role in tumorigenesis was first discovered in a knockout mouse study, and it is now an emerging therapeutic target and biomarker in cancer (Pérez-Gómez et al., 2013, Andradas et al., 2016, Singh et al., 2016).

Another argument for the therapeutic value of orphan GPCRs is the possibility of ligand-independent functions for these receptors (Levoye and Jockers, 2008). This includes both constitutive activity (the ability to activate downstream

signalling in the absence of agonist) and modulation of other proteins' activities. Constitutive activity not only provides a possible rationale for why some receptors defy deorphanisation efforts *via* traditional screening assays (which depend upon agonist-induced stabilisation of the active receptor conformation), but also enables targeting by inverse agonists, which effectively antagonise the receptor by reducing signalling below the constitutive level (Bond and Ijzerman, 2006). Modulation of other proteins, for example through heteromerisation with other GPCRs and membrane proteins, also provides opportunities for therapeutic targeting of orphan GPCRs. The orphan GPR50 has been shown to interact with the closely related MT_1 melatonin receptor and inhibit both high affinity binding of the endogenous agonist and agonist-induced recruitment of G protein (Levoye et al., 2006). Heteromerisation of GPCRs is now known to be an important modulator of trafficking and signalling for many GPCRs, and has been demonstrated in native tissues for several therapeutically relevant receptors (Gomes et al., 2016). There is a strong possibility that some orphan receptors are involved in heteromeric interactions with non-orphan GPCRs, or even with other membrane proteins, and targeting these interactions is another possible therapeutic strategy.

1.2 GPCR signalling

1.2.1 Diversity among GPCRs

There are more than 800 GPCR genes in the human genome, each with a specific set of ligand-binding and downstream signalling capacities. The superfamily can be phylogenetically grouped into six families or classes (Fredriksson et al., 2003, Nordström et al., 2011). The Rhodopsin family, also known as Class A, is by far the largest family, and encompasses a wide range of protein and small-molecule receptors, including a large group of olfactory receptors (Fredriksson et al., 2003). Class A GPCRs have short extracellular N-terminal domains, and ligands generally bind within the transmembrane helical region (Fredriksson et al., 2003). Despite sharing several important anchor motifs in the transmembrane bundle, structural variation in the ligand-binding pockets of Class A receptors provides a diverse array of ligand specificities within the family (Katritch et al., 2012).

The remaining families are considerably smaller and have less diverse ligands than the Rhodopsin family. Class B1 or Secretin family GPCRs bind to a group of peptides with high sequence similarity, including glucagon and glucagon-like peptide, and are characterised by a relatively short N-terminus containing conserved Cys bridges (Fredriksson et al., 2003). Class B2 or Adhesion family GPCRs have heavily glycosylated, variable-length N-termini containing adhesion-like domains; these receptors undergo autocatalytic processing and are involved in cell adhesion signalling (Hamann et al., 2015). Class C or the Glutamate family consists mostly of metabotropic glutamate receptors, which have long N-terminal domains that bind directly to the ligands (Bräuner-Osborne et al., 2007). The Frizzled family bind to Wnt family glycoproteins and are involved in developmental processes (Slusarski et al., 1997). Finally, the Taste2 receptors were previously grouped with the Frizzled family, but have recently been reclassified as a separate family of sensory receptors (Nordström et al., 2011, Munk et al., 2016)

1.2.2 GPCR activation

The fundamental function of GPCRs is to transduce extracellular signals across the plasma membrane to cytoplasmic effectors, enabling the cell to respond to environmental cues. The signal is initiated by ligand binding to the orthosteric binding site (a binding pocket inside the helix bundle in the case of Class A GPCRs). Binding of the ligand induces substantial conformational changes in both the transmembrane helix bundle and the intracellular domain. Recent crystal structures of ligand-bound rhodopsin, β_2 adrenergic receptor and A_{2A} adenosine receptor have revealed that these changes are conserved among Class A GPCRs (Rasmussen et al., 2011, Standfuss et al., 2011, Xu et al., 2011). Stabilisation of this active conformation enables translocation and binding of cytoplasmic effector proteins to the receptor's intracellular domain, which in turn regulates intracellular signalling cascades.

1.2.3 Classical G protein-mediated signalling

GPCR signalling is now known to be a complex network, influenced by many different components and feeding into a multitude of effector pathways. However, the superfamily takes its name from the first of these effectors to be

described – the heterotrimeric G proteins. This family of guanine nucleotide-binding proteins are the major cytoplasmic signalling effectors of most GPCRs. They consist of α, ß and γ subunits, which form a heterotrimeric complex in the inactive, guanosine diphosphate (GDP)-bound state. The complex is tethered to the plasma membrane by lipid modifications on the α and γ subunits (Vögler et al., 2008). Upon ligand binding to the GPCR and stabilisation of its active conformation, the Gα subunit binds to the receptor's intracellular domain. In the case of Class A GPCRs, Gα binds to the cytoplasmic ends of transmembrane helices 5 and 6 (Rasmussen et al., 2011, Standfuss et al., 2011, Xu et al., 2011). This causes a conformational change in the Gα subunit which promotes GDP/GTP exchange, thus activating the G protein and allowing the Gα subunit to dissociate from both the βγ dimer and the receptor (Figure 1-1 A) (Chung et al., 2011). The active Gα and Gβγ subunits can then regulate various second messengers until the intrinsic GTPase activity of the Gα subunit hydrolyses GTP to GDP (Higashijima et al., 1987, Sprang et al., 2007). This allows reassociation of the inactive heterotrimer and terminates the signal. The GTPase activity of Gα can be accelerated by a family of GTPase activating proteins called regulators of G protein signalling (RGS), which mediate rapid termination of the signal (Woodard et al., 2015). G proteins can continue to be activated and inactivated *via* this GDP/GTP cycle until either ligand dissociation returns the GPCR to its inactive conformation, or desensitisation mechanisms preclude further Gα binding.

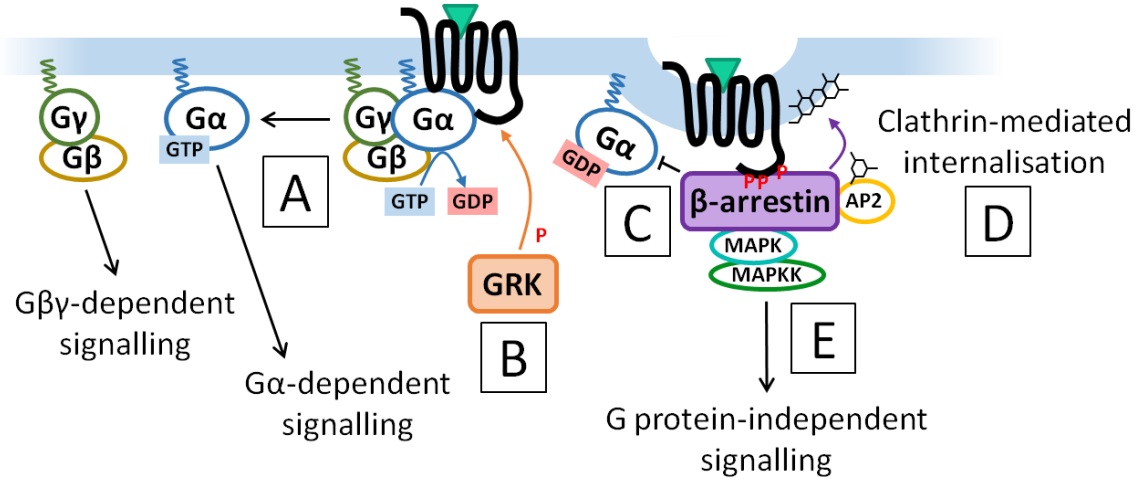

Figure 1-1 GPCR signalling (A) Upon ligand binding, Gα binds to the GPCR, promoting GDP/GTP exchange and allowing dissociation of the Gα and Gβγ subunits and G protein-dependent signalling. **(B)** G protein-coupled receptor kinases phosphorylate the agonist-occupied GPCR. **(C)** Recruitment of β-arrestin to the phosphorylated GPCR sterically hinders further G protein activation. **(D)** β-arrestin recruits proteins that initiate clathrin-mediated internalisation. **(E)** β-arrestin can also act as a scaffold to recruit proteins involved in G protein-independent signalling.

The G protein family contains multiple α, ß and γ isoforms, each of which has a specific tissue distribution and downstream signalling profile (Wettschureck and Offermanns, 2005). G proteins can interact with multiple GPCRs and GPCRs can interact with multiple Gα family members. Thus, the availability of the GPCR, its interacting G protein subunits and their cytoplasmic effector proteins all contribute to the signalling outcome in response to a stimulus in any given cell. The Gα proteins can be split into several sub-families, each of which has a characteristic signalling profile.

1.2.3.1 The $G\alpha_s$ sub-family

Gα 'stimulatory' ($G\alpha_s$) subunits are ubiquitously expressed, and transduce their signals by increasing intracellular levels of the second messenger cAMP. Active $G\alpha_s$ diffuses within the plasma membrane and binds to and activates the transmembrane enzyme adenylate cyclase, which converts adenosine triphosphate (ATP) into cAMP. cAMP has diverse cellular effects depending on the cell type in question, including the activation of glycogenolysis and lipolysis, hormone release, smooth muscle relaxation and neuronal activation (Sutherland, 1972, Wettschureck and Offermanns, 2005). These effects are mediated by cAMP-dependent proteins, such as cAMP-dependent protein kinase (PKA) and exchange proteins activated by cAMP (EPACs).

1.2.3.2 The $G\alpha_{i/o}$ sub-family

The Gα 'inhibitory' ($G\alpha_{i/o}$) sub-family has eight members, which exert their effects by decreasing intracellular cAMP and by regulating a variety of ion channels. $G\alpha_{i1}$, $G\alpha_{i2}$ and $G\alpha_{i3}$ are the most abundant in most tissues and are widely distributed. They decrease cAMP by inhibiting various isoforms of adenylate cyclase. Other $G\alpha_{i/o}$ members have restricted expression, such as $G\alpha_o$ in neurons and $G\alpha_z$ in neurons and platelets. It is thought that these primarily mediate their effects indirectly through the release of their βγ subunits (Wettschureck and Offermanns, 2005). Because of their role in decreasing cAMP, the cellular effects of $G\alpha_{i/o}$ proteins are largely antagonistic to those of $G\alpha_s$.

1.2.3.3 The $G\alpha_{q/11}$ sub-family

Like the $G\alpha_{i/o}$ sub-family, the $G\alpha_{q/11}$ sub-family includes both ubiquitous and tissue-specific members. $G\alpha_q$ and $G\alpha_{11}$ are ubiquitously expressed, whereas $G\alpha_{14}$ is restricted to kidney, lung and spleen and $G\alpha_{16}$ is expressed only in hematopoietic cells (Wettschureck and Offermanns, 2005). All of these transduce their signals by recruiting and activating phospholipase C-β, which catalyses the breakdown of phosphatidylinositol 4,5-bisphosphate into inositol 1,4,5-trisphosphate (IP3) and diacylglycerol (DAG) (Wettschureck and Offermanns, 2005, Litosch, 2016). IP3 mediates the release of intracellular calcium and DAG activates protein kinase C (PKC). $G\alpha_{q/11}$ can also activate RhoA *via* p63RhoGEF (Litosch, 2016). These multiple effectors perform a range of signalling functions, with outcomes such as smooth muscle contraction, cellular hypertrophy and synaptic transmission (Wettschureck and Offermanns, 2005).

1.2.3.4 The $G\alpha_{12/13}$ sub-family

$G\alpha_{12}$ and $G\alpha_{13}$ are both ubiquitously expressed, but frequently couple to GPCRs that also activate other Gα subunits. Since specific inhibitors of $G\alpha_{12/13}$ are not available, their precise signalling roles have been difficult to define. The best-characterised role of $G\alpha_{12}$ and $G\alpha_{13}$ is their RhoA-mediated effects on the actin cytoskeleton. $G\alpha_{12/13}$ binds to and activates a panel of four Rho guanine nucleotide exchange factors (RhoGEFs), which promote RhoA GDP/GTP exchange (Siehler, 2009). RhoA activates a number of downstream pathways that lead to

changes in cell shape, polarity and adhesion, cell migration and cellular hypertrophy (Worzfeld et al., 2008, Siehler, 2009).

1.2.3.5 Gβγ signalling

In addition to signalling *via* the four Gα sub-families, GPCRs can also signal through the Gβγ complex, which often complements the Gα-mediated response. Following GPCR-mediated dissociation of the Gα subunit, Gβγ is free to regulate a number of its own targets, including the G protein-regulated inward rectifier K^+ channel, phospholipase C-ß and adenylate cyclase (Clapham and Neer, 1997). Because $G\alpha_i$ subunits are the most highly expressed Gα subunit in most tissues, Gβγ complexes released from $G\alpha_i$-containing heterotrimers are thought to be primarily responsible for Gβγ-mediated signalling (Wettschureck and Offermanns, 2005).

1.2.4 GPCR desensitisation

GPCRs have a range of mechanisms for desensitisation, that is, a decline in the magnitude of the response as a result of continued or repeated stimulation. These mechanisms enable highly regulated termination of the agonist-induced response, and are carried out by cytoplasmic proteins which act on the ICLs and C-terminal tail of the receptor (Lohse, 1993, Tobin et al., 2008). Thus, desensitisation mechanisms are dependent on both the GPCR amino acid sequence and the expression of various cytoplasmic mediators.

1.2.4.1 Heterologous desensitisation by effector kinases

Heterologous desensitisation concerns the desensitisation of receptors by effector kinases. Because this is independent of agonist occupancy and is not receptor-specific, it can occur as a result of ligand binding to a receptor other than the one that is ultimately desensitised. Both PKA and PKC can phosphorylate certain receptors on serine and threonine residues at consensus sites in the ICLs and C-terminal tail, which disrupts the G protein binding site and thus uncouples the receptor from the G protein-mediated response (Lohse, 1993, Tobin, 2008).

1.2.4.2 Homologous desensitisation by arrestins

Homologous desensitisation is the desensitisation of agonist-occupied, activated GPCRs, and occurs more rapidly than heterologous desensitisation (Lohse, 1993). G protein-coupled receptor kinases (GRKs) phosphorylate the ICLs and C-terminal tails of agonist-bound GPCRs at serine and threonine residues distinct from those phosphorylated by effector kinases (Figure 1-1 B) (Seibold et al., 2000). Unlike in heterologous desensitisation, phosphorylation by GRKs alone is not sufficient to uncouple the receptor from the G protein (Benovic et al., 1987). Instead, GRK-mediated phosphorylation leads to the recruitment and binding of the adaptor protein arrestin to the GPCR, which mediates the desensitisation by sterically hindering binding of the Gα subunit (Gimenez et al., 2012).

The arrestins are a family of four proteins: visual arrestin and cone arrestin, which are expressed only in the retina; and ß-arrestins 1 and 2, which are ubiquitously expressed and thus are responsible for homologous desensitisation of most non-visual GPCRs (Luttrell and Lefkowitz, 2002). Since the ß-arrestin and Gα binding interfaces overlap, the immediate consequence of ß-arrestin binding to the GPCR is steric hindrance of further Gα-GDP binding to the agonist-occupied receptor (Figure 1-1 C) (Szczepek et al., 2014). This rapidly terminates the activation of G protein-dependent signalling (Benovic et al., 1987, Lohse, 1993).

A secondary desensitising role of ß-arrestin is to initiate clathrin-mediated internalisation of an agonist-occupied receptor (Figure 1-1 D). Receptor-bound ß-arrestin recruits adaptor protein 2 complex (AP2) and clathrin to the plasma membrane to initiate the formation of clathrin-coated pits (Goodman et al., 1996, Laporte et al., 1999). This leads to internalisation of the agonist-occupied receptor. There are two potential modes of ß-arrestin-mediated internalisation. Depending on the GPCR involved, the ß-arrestin either dissociates prior to endocytosis, or remains in complex with the receptor and co-localises to the endosome (Zhang et al., 1999). This is determined at least in part by the GRK-mediated phosphorylation of serine and threonine residues in the C-terminal tail (Gimenez et al., 2012). Both sorting signals in the receptor intracellular domain and the stability of the interaction with ß-arrestin determine the fate of the

endocytosed receptor – it can either be recycled back to the plasma membrane or targeted for degradation by ubiquitination (Marchese and Trejo, 2013). For receptors that dissociate from ß-arrestin prior to endocytosis, the receptor can resume G protein-dependent signalling in a spatially compartmentalised manner (Calebiro et al., 2009, Tsvetanova and von Zastrow, 2014). However, very recent reports suggest that this may also be possible for ß-arrestin-bound internalised GPCRs, giving rise to sustained G protein signalling from within the endosomal compartment (Thomsen et al., 2016). These features of the internalisation cycle provide additional spatiotemporal regulation of the G protein-dependent response.

1.2.4.3 G protein-independent signalling

In addition to its role in desensitisation, ß-arrestin has recently come to be recognised as an important mediator of signalling in its own right. β-arrestin can be recruited to agonist-occupied GPCRs at the plasma membrane independently of G protein activation, where it can act as a scaffold for cytoplasmic signalling proteins (Figure 1-1 E) (Wei et al., 2003, Shenoy et al., 2006). GPCR-bound ß-arrestin has been shown to bind and activate members of several important pathways including the Src-family kinases, extracellular signal-regulated kinase (ERK) and c-jun N-terminal kinase (JNK) mitogen-activated protein kinases and phosphodiesterases (Luttrell et al., 1999, McDonald et al., 2000, Houslay and Baillie, 2005, Shenoy et al., 2006, DeWire et al., 2007). This ß-arrestin-mediated signalling is slower-onset and more sustained than G protein-dependent responses, adding further temporal regulation and heterogeneity to GPCR signalling (Shenoy et al., 2006). ß-arrestin-mediated signalling has been shown to have physiological relevance *in vivo* in a number of contexts, including development, the central nervous system and the cardiovascular system (Luttrell and Gesty-Palmer, 2010). It is therefore an important consideration in drug discovery, both as a specific target and as a mediator of undesirable on-target effects.

1.2.5 The phosphorylation barcode and tissue-specific GPCR signalling

Out of many possible signalling fates that might result from a ligand binding to a GPCR, how is one specific outcome selected? Much of the signal specificity described above is conferred by phosphorylation of the GPCR by several different kinases, but primarily the GRK family. There is an emerging paradigm that this phosphorylation pattern or 'barcode' can affect cellular responses to receptor activation, with different kinases differentially promoting G protein- versus ß-arrestin-mediated signalling, or favouring desensitisation or internalisation of the receptor (Innamorati et al., 1998, Ren et al., 2005, Nobles et al., 2011). The potential phosphorylation pattern of the GPCR intracellular domain is defined by the presence of phospho-acceptor residues in the GPCR sequence, but also depends on the expression of the relevant GRKs or other kinases. This reasoning has led to a theory of cell type-specific signalling, whereby the kinases expressed in a particular cell type determine the specificity of the GPCR signalling profile (Tobin et al., 2008, Liggett, 2011). Cell type-specific GRK activity has been demonstrated *in vivo* for therapeutically relevant GPCRs such as the dopamine and muscarinic receptors (Walker et al., 2004, Gurevich et al., 2016). This shows that GPCRs have the potential to perform distinct functions in different tissues or cell types, or in different physiological and pathophysiological settings. Once again, developing an understanding of how this applies to individual GPCRs will be beneficial in utilising them as drug targets.

1.2.6 Ligand-specific GPCR signalling

In addition to the GPCR sequence and the available kinases and signalling mediators, one fundamental factor influencing signal specificity remains: the ligand. Certain ligands bind in such a way as to stabilise a receptor conformation that selectively activates a particular signalling pathway – so-called biased ligands. Ligand-specific receptor conformations can favour a particular G protein coupling specificity, promote ß-arrestin-mediated signalling, or determine how rapidly a receptor is internalised or recycled (Maudsley et al., 2005). Biased ligands of GPCRs have great potential in drug discovery in terms of increasing the specificity of responses and reducing on-target side effects caused by

unwanted activation of deleterious pathways (Whalen et al., 2011). To this end, biased ligands are being pursued as therapeutics for a range of applications, most promisingly G protein-biased agonists of the μ-opioid receptor as analgesics, as well as ß-arrestin-biased agonists of the angiotensin II receptor as heart failure treatments (DeWire et al., 2013, Luttrell et al., 2015). Ligand-specific signalling, especially G protein versus ß-arrestin bias, has been shown to be linked to receptor phosphorylation, such that different ligand-receptor conformations favour phosphorylation by different GRKs to determine the signalling response (Wisler et al., 2007, Nobles et al., 2011). Understanding how therapeutically relevant GPCRs are phosphorylated and how this contributes to downstream signalling will be key to harnessing the power of this 'functional selectivity' for drug discovery applications.

1.3 GPCRs in cardiovascular function and disease

1.3.1 Cardiovascular disease

As in all physiological systems, GPCR signalling plays major roles in both normal and aberrant cardiovascular function, and, just as GPCRs are extremely important drug targets in general (as discussed in section 1.1.2), they are commonly targeted in the treatment of cardiovascular disease (CVD).

According to the World Health Organization, CVD is now the leading cause of death worldwide, being the primary cause for an estimated 17.5 million deaths annually (www.who.int/cardiovascular_diseases). The term CVD encompasses a group of diseases affecting the heart and circulation, including arterial disease, heart failure, heart attack and stroke. These diseases are usually associated with hypertension (high blood pressure) and/or atherosclerosis (a build-up of fatty deposits in the arteries that increases the risk of blood clots). The effects of CVD are often accompanied by damage to end organs including the heart, blood vessels, kidney and brain, which can manifest as injury, scarring or impaired function of the affected tissue.

The causes of CVD are complex and multifactorial and involve multiple signalling networks. Although many pharmacological treatments for CVD exist, it nonetheless remains a significant global disease burden. There is therefore a

continuous need to improve our understanding of cardiovascular pathophysiology in order to develop novel therapeutics.

1.3.2 GPCR signalling in the cardiovascular system and CVD

Many different GPCRs have overlapping roles in the neural, hormonal and biochemical regulation of both cardiac and vascular function, as well as in the interconnected systems that influence these, such as the CNS, the renal system and various endocrine glands. The adrenergic system and the renin-angiotensin system are the two major regulators of cardiovascular function, and components of these comprise the major CVD drug targets, although many other GPCRs – including muscarinic, adenosine, endothelin, apelin and vasopressin receptors, to name but a few – also play meaningful roles.

1.3.2.1 The adrenergic receptors

Sympathetic input to the cardiovascular system occurs *via* the actions of adrenaline and noradrenaline at members of the adrenergic receptor (AR) family, consisting of three α_1-ARs, three α_2-ARs and three ß-ARs (Philipp and Hein, 2004). In the heart, the ß-ARs (mostly the $ß_1$-AR) regulate heart rate and cardiac contractility through $G\alpha_s$-mediated increases in cAMP (Philipp and Hein, 2004, Lymperopoulos et al., 2013). This leads to PKA-mediated $[Ca^{2+}]_i$ release, which stimulates cardiac muscle contraction through well-characterised mechanisms (Bers, 2008). The α_2-ARs have an indirect effect on cardiac function by inhibiting norepinephrine release from cardiac sympathetic nerve terminals through their activation of $G\alpha_{i/o}$ (Philipp and Hein, 2004, Lymperopoulos et al., 2013).

Not only do ARs have actions in cardiac muscle, they also regulate vascular smooth muscle contraction and thus directly impact blood pressure. In vascular smooth muscle cells, norepinephrine and epinephrine have antagonistic effects through α- and ß-ARs, respectively (Rohrer and Kobilka, 1998). Norepinephrine binds α_1- and α_2-ARs and causes smooth muscle contraction *via* $G\alpha_{q/11}$- and $G\alpha_{i/o}$-mediated $[Ca^{2+}]_i$ release, which causes vasoconstriction and thus raises blood pressure. Conversely, epinephrine binds $ß_2$-ARs and stimulates $G\alpha_s$-mediated

smooth muscle relaxation and vasodilation, which reduces blood pressure (Rohrer and Kobilka, 1998).

The ARs are subject to GRK-mediated phosphorylation and internalisation, and can also transactivate other receptors or signalling pathways in a GRK- and ß-arrestin-dependent manner (Harris et al., 2008, Capote et al., 2015). The upregulation of certain GRKs in the heart and the resultant desensitisation and downregulation of the $ß_1$-AR is a major pathological mechanism in heart failure (Ungerer et al., 1993). This exemplifies how important the 'phosphorylation barcode' (discussed in section 1.2.5) can be in cardiovascular pathophysiology, and how it might be targeted in the treatment of CVD.

1.3.2.2 Receptors for angiotensin II and the renin-angiotensin system

Angiotensin II (Ang II) is a peptide ligand that has a great many effects on cardiovascular, endocrine and renal function, the combined outcome of which is increased blood pressure. Its release is controlled by the renin-angiotensin system, a hormonal axis responsible for blood pressure homeostasis. The activating stimulus for the pathway is hypotension sensed by the juxtaglomerular cells in the kidney, which respond by initiating an enzymatic cascade through release of the peptidase renin (Davis and Freeman, 1976). Renin cleaves the precursor angiotensinogen into angiotensin I, which can then be converted into the active signalling peptide angiotensin II by angiotensin converting enzyme (ACE) (Te Riet et al., 2015).

Ang II has immediate cardiovascular effects through the angiotensin II type 1 receptor (AT_1R) expressed on the vascular smooth muscle cells of resistance arteries. Both $G\alpha_{q/11}$-mediated $[Ca^{2+}]_i$ release and $G\alpha_{12/13}$-mediated myosin phosphatase inhibition contribute to contraction of the smooth muscle, resulting in vasoconstriction (Wynne et al., 2009). Ang II also has acute actions both directly on the kidney and on endocrine tissues to stimulate aldosterone and anti-diuretic hormone secretion, which have the combined effect of increasing water reuptake by the kidneys and thus increasing blood volume and therefore blood pressure (Te Riet et al., 2015).

As well as acutely raising blood pressure through these mechanisms, Ang II also regulates cell growth and morphology in a number of cardiovascular cell types, promoting hypertrophy and remodelling in both the heart and the vasculature *via* several G protein-dependent and -independent pathways (Mehta and Griendling, 2007). In particular, it has been shown to stimulate proliferation, migration and hypertrophy of vascular smooth muscle cells (Ruiz-Ortega et al., 2001), and to contribute to cardiac hypertrophy and fibrosis through direct effects on cardiomyocytes and cardiac fibroblasts (Capote et al., 2015). Thus, Ang II and the AT_1R have profound effects on the cardiovascular system, and unsurprisingly are often implicated in the development and progression of CVD.

1.3.2.3 GPCR biased signalling in the cardiovascular system

A novel and exciting development in GPCR drug discovery in all therapeutic areas is the discovery of biased agonists – ligands that can selectively activate signalling through a particular pathway (discussed in section 1.2.6). Biased agonists of GPCRs involved in cardiovascular regulation have already shown immense potential in the treatment of CVD. ß blockers (ß-AR antagonists) are a class of drugs historically used to treat hypertension and ischemic heart disease. However, a subset of these, including the third-generation drug carvedilol, have been found to have superior survival effects in chronic heart failure (Poole-Wilson et al., 2003). On closer inspection *in vitro*, it was found that this subset of ß blockers are actually ß-arrestin-biased agonists that promote ß-arrestin-mediated ERK phosphorylation and thus induce specific signalling outcomes in the heart that have cardioprotective effects (Noma et al., 2007, Wisler et al., 2007). Conversely, GRK2-mediated phosphorylation of ß2-AR has been shown to bias the receptor towards $G\alpha_{i/o}$ signalling, which exacerbates pressure overload-induced pathological remodelling in mice (Zhu et al., 2012).

The AT_1R is also a promising target for biased agonists. The ß-arrestin-biased agonist TRV120027 has been shown to improve cardiac function but also actively reduce blood pressure independently of the pressor response to angiotensin II in rats (Violin et al., 2010). This dual effect is not achieved with traditional AT_1R antagonists or ACE inhibitors, and so in this case the biased agonist has a unique therapeutic impact (Violin et al., 2010). TRV120027 entered Phase II clinical trials in 2011, but has recently been discontinued due to a lack of efficacy

(Soergel et al., 2013, Felker et al., 2015). Nonetheless, biased agonists of the AT_1R remain a promising strategy for the treatment of heart failure.

The evident therapeutic potential of biased ligands in CVD highlights a need to investigate the signalling mechanisms of poorly characterised GPCRs that have potential as CVD targets. The power of biased ligands can only be exploited by developing a detailed understanding of how such receptors achieve their signal specificity, through mechanisms such as post-translational modification and interactions with cytoplasmic signalling mediators.

1.4 G protein-coupled receptor 35

G protein-coupled receptor 35 (GPR35) is a poorly characterised orphan GPCR, which nonetheless has potential therapeutic value based on its association with a range of diseases, including cardiovascular disease (Divorty et al., 2015). Despite being discovered nearly two decades ago, its endogenous ligand and physiological function remain undefined. However, with several proposed endogenous ligands and a range of high-potency surrogate ligands now available, studies into GPR35 pharmacology and function are beginning to shed more light on its therapeutic potential (Divorty et al., 2015, Mackenzie and Milligan, 2015).

1.4.1 Discovery and basic characteristics

GPR35 was originally identified in a genomic DNA homology screen, in which it was amplified from human genomic DNA using degenerate primers for GPR1 (O'Dowd et al., 1998). In this first report, a single open reading frame was found to encode a protein of 309 amino acids, which showed highest identity with lysophosphatidic acid (LPA) receptor 4 (also known as P2Y9/GPR23) (32%), the hydroxycarboxylic acid receptor HM74 (30%) and several members of the purinergic P2Y receptor family (29%). This study mapped the novel GPR35 gene to human chromosome 2q37.3.

A subsequent study identified two splice variants of GPR35 in a cDNA screen of human gastric cancer tissue: the previously-identified short isoform GPR35a and a multi-exon variant, GPR35b, which has a 31 amino acid N-terminal extension (Okumura et al., 2004). Although this study found enrichment of GPR35b in

gastric cancer samples, the functional significance of this long variant is still unclear. GPR35b has only ever been detected in humans; mouse and rat GPR35 are 307 and 306 amino acids in length, respectively, and both share 72% identity with human GPR35a and 85% identity with each other (Figure 1-2) (Taniguchi et al., 2006). GPR35a and GPR35b appear to share similar pharmacological properties, with agonists displaying similar potency at the two isoforms in both G protein- and ß-arrestin-based assays (Guo et al., 2008, MacKenzie et al., 2014). The N-terminal extension on GPR35b does not appear to affect expression or trafficking, as both isoforms have similar subcellular localisation (Guo et al., 2008). For these reasons, the large majority of studies on GPR35, including those described in this thesis, have used the GPR35a isoform.

GPR35 is in the δ group of Class A Rhodopsin family of GPCRs, and is phylogenetically grouped into the purin receptor cluster (Fredriksson et al., 2003). Its closest relatives are the aforementioned LPA4 and HM74, along with hydroxycarboxylic acid receptor HCA1/GPR81, the succinate receptor SUCNR1/GPR91, LPA6/P2Y5, and the putative lysophosphatidylinositol receptor GPR55 (Fredriksson et al., 2003). The basic structure of GPR35 is the same as most Class A GPCRs, comprising seven transmembrane helices, a relatively short N-terminal domain and a cytosolic helix 8 preceding a short C-terminal tail (Figure 1-2). The amino acid sequence of the transmembrane helices is highly conserved between the human and rodent orthologues, whereas the ECLs, ICLs and C-terminal tail are more variable (Figure 1-2).

The GPR35 gene is relatively polymorphic, with non-synonymous, coding region single nucleotide polymorphisms (SNPs) leading to seven natural variants of the protein in humans (Figure 1-2). Of these, only the V76M variant (minor allele frequency 0.02) has a significant effect on ligand binding (MacKenzie et al., 2014). Notably, the T108M and S294R variants have been associated with disease (discussed in section 1.4.6), although the mechanistic significance of these associations is unknown (Sun et al., 2008, Ellinghaus et al., 2013).

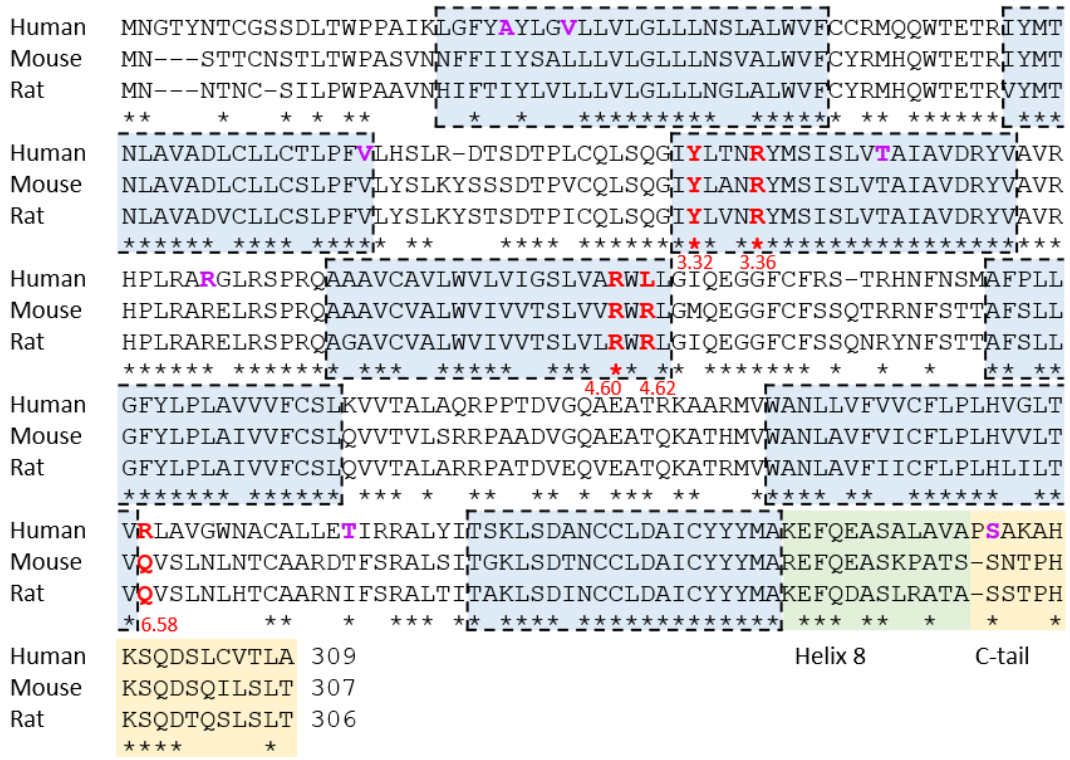

Figure 1-2 Species alignment of human GPR35a with mouse and rat GPR35 showing notable features Human, rat and mouse sequences were aligned using Jalview Online. Conserved residues are marked with an asterix. Transmembrane regions are shown in blue, Helix 8 in green and the C-terminal tail in yellow. Residues essential for ligand binding (Y3.32, R3.36, R4.60, L/R4.62 and R/Q6.58) are highlighted in red. Single nucleotide polymorphisms of the human orthologue (A25T, V29I, V76M, T108M, R125S, T253M and S294R) are highlighted in pink.

1.4.2 Proposed endogenous ligands of GPR35

Over the years, several endogenous molecules have been found to have agonist activity at GPR35, a number of which are summarised below (Figure 1-3 and Table 1-2). Some reports have attempted to designate these as the endogenous ligands, but they have each been rejected for various reasons (discussed below) and the receptor is still officially classified as an orphan by the International Union of Basic and Clinical Pharmacology (Davenport et al., 2013).

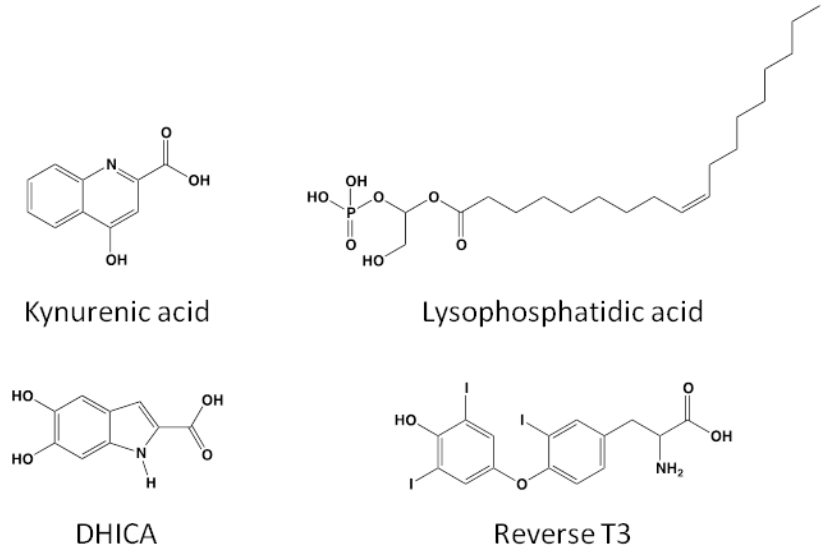

Figure 1-3 Structures of proposed endogenous ligands of GPR35 (DHICA = 5,6-dihydroxyindole-2-carboxylic acid.)

1.4.2.1 Kynurenic acid

The first endogenously occurring molecule reported to have agonist activity at GPR35 was kynurenic acid, a product of tryptophan metabolism with signalling functions that mostly occur in the central and peripheral nervous systems (Stone and Darlington, 2002). Kynurenic acid is well characterised as a competitive antagonist of all three ionotropic glutamate receptors, with potency in the high micromolar range (Schwarcz et al., 2012). However, it also has actions at a number of other targets, including agonism at GPR35 (Wang et al., 2006, Zhao et al., 2010, Jenkins et al., 2011, Deng et al., 2012, Berlinguer-Palmini et al., 2013). Wang et al. were the first to report this activity, demonstrating kynurenic acid-induced activation of $G\alpha_{i/o}$ and internalisation of GPR35 in cells overexpressing the receptor, with mid to low micromolar-range potency at the human, mouse and rat orthologues (Wang et al., 2006). The pharmacological action of this ligand at GPR35 was subsequently confirmed by other groups, but with wide variations in potency between 40 and 200 μM depending on the assay system used (Zhao et al., 2010, Jenkins et al., 2011, Deng et al., 2012, Berlinguer-Palmini et al., 2013).

The reported micromolar potency at rat GPR35 is consistent with the concentration of kynurenic acid present in rat small intestine, where GPR35 is most highly expressed (Wang et al., 2006, Kuc et al., 2008). However, the

potency at the human orthologue has been found in some studies to be in excess of 100 μM (Jenkins et al., 2011, Deng et al., 2012). Based on these findings, the concentration of kynurenic acid required for GPR35 activation in humans exceeds physiological levels (Forrest et al., 2002). However, since the potency of kynurenic acid at human GPR35 is comparable to that at glutamate receptors, its effects in the nervous system might be attributable to GPR35 in the specific regions where its expression has been observed (discussed in section 1.4.6.4). Due to the conflicting nature of the current findings, kynurenic acid is yet to be officially designated as the endogenous ligand for GPR35, despite being widely referred to as such in the literature (Davenport et al., 2013).

Table 1-2 Proposed endogenous ligands of GPR35

Endogenous agonist	G protein pathway	ß-arrestin recruitment?	EC_{50} (human)	Efficacy (human)	Reference
Kynurenic acid	$G\alpha_{i/o}$	Yes	40–>200 μM	Partial	(Wang et al., 2006)
LPA	$G\alpha_{q/11}$	No	Not reported	Unknown	(Oka et al., 2010)
DHICA	Unknown	Yes	22–25 μM	Partial	(Deng et al., 2012)
Reverse T3	Unknown	No	5–100 μM	Full	(Deng et al., 2012)
CXCL17	$G\alpha_{q/11}$	Unknown	nM range	Unknown	(Maravillas-Montero et al., 2015)

EC_{50} range is estimated from results of all reported assays. Efficacy describes maximal response compared with reference agonist zaprinast. (LPA = lysophosphatidic acid; DHICA = 5,6-dihydroxyindole-2-carboxylic acid.)

1.4.2.2 Lysophosphatidic acid

In a screen for endogenous ligands of GPR35 based on its homology with lysophospholipid and purinergic receptors, Oka *et al*. identified three derivatives of LPA as agonists of GPR35 (Oka et al., 2010). In this study, 2-arachidonoyl LPA, 2-linoleoyl LPA and 2-oleoyl LPA induced increases in $[Ca^{2+}]_i$ to a greater extent in human embryonic kidney (HEK) cells stably expressing GPR35 than in HEK cells expressing endogenous levels of LPA receptors. GPR35 overexpression also enhanced 2-oleoyl LPA-induced RhoA activation and ERK phosphorylation. These findings suggest a $G\alpha_{q/11}$-mediated signalling profile, which is consistent with that of the existing LPA receptors, although GPR35 coupling to $G\alpha_{q/11}$ has never been directly demonstrated (Choi et al., 2010). This could be indicative of ligand bias at GPR35, since other agonists have been shown to promote coupling to other G proteins and ß-arrestin (Jenkins et al., 2010, Jenkins et al., 2011, Guo

et al., 2008, Ohshiro et al., 2008). LPA was found in two separate studies not to induce ß-arrestin recruitment to GPR35, a response that is robust and reproducible for the majority of other GPR35 agonists (Southern et al., 2013, Zhao et al., 2010). This would suggest a unique mechanism of action for LPA compared with kynurenic acid and synthetic GPR35 agonists. However, since no antagonists were available at the time of this study, the specific contribution of GPR35 could not be verified, and has not been reported on since. In addition, LPA is known to exert its physiological actions through a well-characterised family of LPA receptors, and so it is unlikely that LPA could have specific GPR35-mediated effects (Choi et al., 2010).

1.4.2.3 Tyrosine metabolites

In a label-free dynamic mass redistribution (DMR) screen of the endogenously GPR35-expressing HT-29 human colon adenocarcinoma cell line, Deng et al. identified several tyrosine derivatives as potent agonists of GPR35 (Deng et al., 2011). This led to the screening of a panel of endogenously-produced tyrosine metabolites in the hope of identifying an endogenous ligand for GPR35 (Deng et al., 2012). Again using DMR in the HT-29 cell line, this screen identified the melanin biosynthesis intermediate 5,6-dihydroxyindole-2-carboxylic acid (DHICA) and the thyroid hormone synthesis intermediate 3,3,5-triiodothyronine (reverse T3) as GPR35 agonists with low micromolar-range potency. These agonists were susceptible to antagonism by the competitive GPR35 antagonist CID-2745687 and also promoted GPR35 internalisation, which verified GPR35 as the target (Heynen-Genel et al., 2011, Deng et al., 2012). However, only DHICA was able to induce ß-arrestin recruitment with comparable potency in a fluorescence resonance energy transfer-based assay, which again might suggest that reverse T3 is a biased agonist (Deng et al., 2012). Unfortunately, as with kynurenic acid, these ligands do not appear to be present *in vivo* at concentrations that could activate GPR35 based on *in vitro* estimations of potency. Circulating levels of reverse T3 are in the low nanomolar range and do not reach the micromolar concentrations required to activate GPR35, although the levels have been shown to increase under pathophysiological conditions, including during heart failure (Peeters et al., 2005, Hamilton et al., 1990). More evidence is required to assess this potential ligand-receptor pairing.

1.4.2.4 CXCL17

The most recently proposed endogenous ligand for GPR35 is the orphan chemokine CXCL17. Maravillas-Montero et al. reported that CXCL17 was able to induce dose-dependent $[Ca^{2+}]_i$ release in pro-B cells and HEK cells transfected with GPR35 (Maravillas-Montero et al., 2015). These effects were observed at nanomolar concentrations, suggesting CXCL17 to be significantly more potent than other endogenous agonists. However, as with LPA, the effect on $[Ca^{2+}]_i$ suggests $G\alpha_{q/11}$ coupling, which is uncharacteristic of GPR35. These findings were also not validated with the use of a GPR35 antagonist, so it is difficult to assess the specific contribution of GPR35 to changes in $[Ca^{2+}]_i$. Although these findings are not sufficient to designate GPR35 as the CXCL17 receptor, existing reports of GPR35 expression and function in leukocytes (discussed in section 1.4.6.3) (Yang et al., 2010, Fallarini et al., 2010, Barth et al., 2009) suggest that a potential role for GPR35 as a chemokine receptor deserves further investigation.

1.4.3 Synthetic ligands of GPR35

In spite of uncertainty surrounding the 'true' endogenous ligand of GPR35, screening efforts have yielded a number of synthetic surrogate ligands with different pharmacological properties. These have proven useful as tool compounds and have facilitated studies into GPR35 pharmacology and function (Divorty et al., 2015). The available panel of synthetic ligands have a range of potencies and efficacies and vary in species selectivity and mode of action (Table 1-3), and so can be used to address a wide variety of questions provided their pharmacological properties are taken into account when interpreting results.

1.4.3.1 Synthetic agonists of GPR35

The structures and properties of a selection of relevant synthetic GPR35 agonists are summarised below (Figure 1-4 and Table 1-3). One of the first synthetic GPR35 agonists to be discovered was the cGMP-specific phosphodiesterase type 5 (PDE5) inhibitor, zaprinast (Taniguchi et al., 2006). It acts with moderate potency but elicits a robust and high efficacy response *in vitro,* and is therefore often used as a reference ligand against which other agonists are assessed. However, like many of the agonists described since, zaprinast displays significant

selectivity for the rat orthologue, with a 50-fold greater EC_{50} at the human receptor (Taniguchi et al., 2006, Milligan, 2011). The anti-asthma drugs cromolyn disodium and dicumarol show lower potency than zaprinast, but are equipotent at the rat and human orthologues (Jenkins et al., 2010). This shows that the apparent species orthologue selectivity of most GPR35 agonists does not apply to all ligands, and may in fact be exploited to probe the intricacies of ligand binding at this receptor (discussed in section 1.4.4) (Yang et al., 2010, Jenkins et al., 2010).

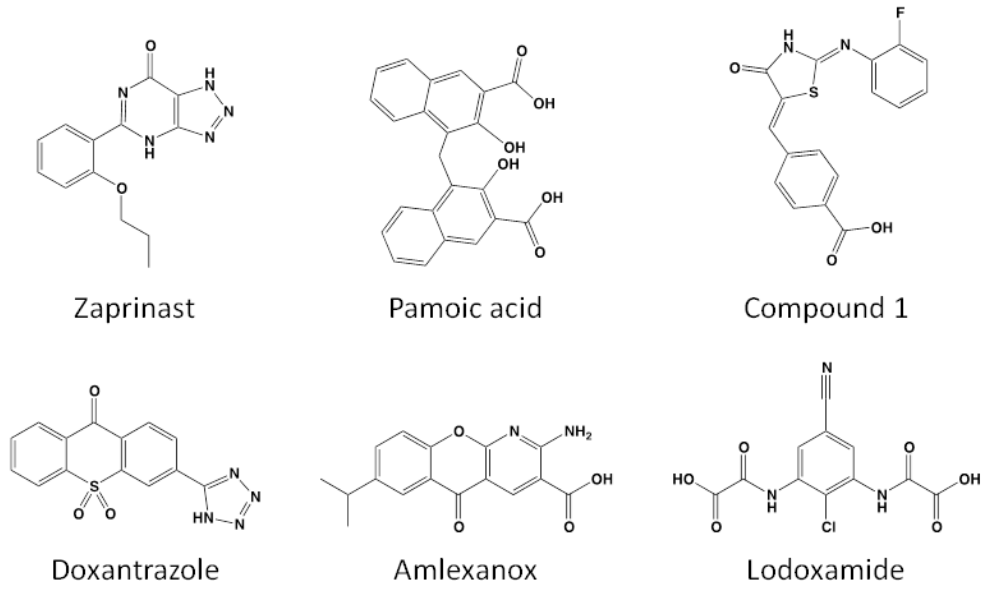

Figure 1-4 Structures of selected synthetic agonists of GPR35

Besides zaprinast, several other agonists with high potency at human GPR35 have been reported. Pamoic acid was identified as a partial but potent agonist in two independent screens of the Prestwick Chemical Library®, with an EC_{50} of 50-80 nM at human GPR35 in ß-arrestin recruitment assays (Zhao et al., 2010, Jenkins et al., 2010). However, pamoic acid is highly selective for the human orthologue, with negligible potency at mouse and rat GPR35 (Jenkins et al., 2012). Neetoo-Isseljee et al. described a high potency, human-selective agonist, "compound 1", that at the rodent orthologues acted as a partial agonist in ß-arrestin recruitment assays, but as a full agonist with markedly higher potency in G protein activation assays (Neetoo-Isseljee et al., 2013). Conversely, the anti-allergic drug doxantrazole is a partial agonist at human GPR35, but a full agonist at rat GPR35 (MacKenzie et al., 2014). These examples demonstrate that

the pharmacology of GPR35 is complex, with different agonist-occupied conformations capable of eliciting distinct signalling outcomes.

Recently, the anti-inflammatory mast cell stabiliser amlexanox was identified as a potent partial agonist at human GPR35, which prompted a screen of other mast cell stabilisers that led to the identification of lodoxamide and bufrolin as high potency, full agonists at both rat and human GPR35 (Southern et al., 2013, MacKenzie et al., 2014). These agonists will all serve as useful tools in the study of GPR35 signalling and function.

Table 1-3 Selected synthetic agonists of GPR35

Synthetic agonist	EC_{50} (human)	EC_{50} (mouse)	EC_{50} (rat)	Efficacy	Notes	Reference
Zaprinast	2–8 μM	1 μM	100 nM	Full	PDE5 inhibitor	(Jenkins et al., 2010, Jenkins et al., 2012)
Pamoic acid	30–50 nM	Inactive	> 100 μM	Partial	DNA pol. ß inhibitor	(Jenkins et al., 2012, Zhao et al., 2010)
Compound 1	26 nM	17 μM	8 μM	Full (human) Partial (rodent)	ß-arr-biased at human	(Neetoo-Isseljee et al., 2013)
Doxantrazole	3.4 μM	Untested	300 nM	Partial (human) Full (rat)	Mast cell stabiliser	(MacKenzie et al., 2014)
Amlexanox (Aphthasol®)	4 μM	Untested	23 nM	Partial	TBK1/IKK-ε inhibitor	(MacKenzie et al., 2014, Southern et al., 2013)
Lodoxamide (Alomide®)	4 nM	Untested	13 nM	Full	Commercial anti-allergic	(MacKenzie et al., 2014)

EC_{50} values are those obtained in BRET-based β-arrestin recruitment assays. Nanomolar-range EC_{50} values are highlighted in grey to show orthologue selectivity. (PDE5 = phosphodiesterase 5; TBK1 = TANK-binding kinase 1; IKK-ε = inhibitor of NFκB kinase ε.)

1.4.3.2 Synthetic antagonists of GPR35

Selective competitive antagonists are essential to verify the specificity of GPCR-mediated responses. Two potent antagonists of GPR35, ML-145 and CID-2745687, have been reported (summarised in Figure 1-5 and Table 1-4) (Zhao et al., 2010, Heynen-Genel et al., 2010, Heynen-Genel et al., 2011). These are both selective for GPR35 over the closely-related receptor GPR55, and exhibit inverse agonist activity at human GPR35 (Heynen-Genel et al., 2010, Heynen-Genel et al., 2011, Jenkins et al., 2012). Interestingly, both antagonists act competitively with zaprinast and cromolyn disodium, but CID-2745687 appears to act non-competitively with pamoic acid, suggesting both that the partial agonist pamoic

acid may have a different binding mode, and that the two antagonists have distinct modes of action (Jenkins et al., 2012).

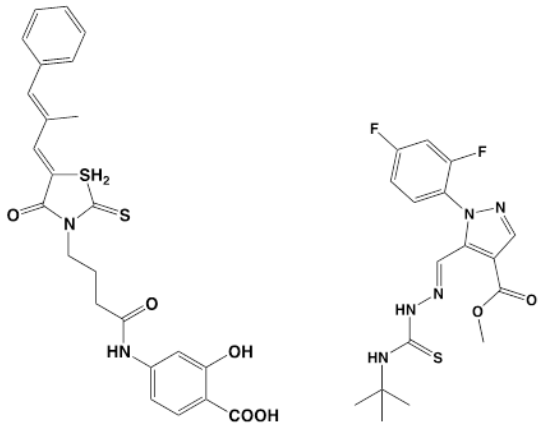

Figure 1-5 Structures of synthetic antagonists of GPR35

Despite good potency at human GPR35, both antagonists display significant species selectivity, inhibiting ß-arrestin recruitment only at the human receptor and not at the rat or mouse orthologues (Jenkins et al., 2012). Therefore, although these compounds will be useful in studying human GPR35 *in vitro*, they cannot be utilised to probe GPR35 function in rodent *in vivo* disease models. No equipotent alternatives are currently available, which presents a significant challenge in investigating the function of this receptor.

Table 1-4 Synthetic antagonists of GPR35

Antagonist	IC_{50} (human)	Notes	Reference
ML-145	27 nM	Competitive antagonist	(Heynen-Genel et al., 2010, Jenkins et al., 2012)
CID-2745687	200 nM	Non-competitive with pamoic acid	(Heynen-Genel et al., 2011, Jenkins et al., 2012)

IC_{50} values are those obtained against zaprinast EC_{80} in BRET-based β-arrestin recruitment assays.

1.4.4 GPR35 ligand binding and species selectivity

The orthosteric ligand binding site of most Class A receptors consists of a pocket within the transmembrane bundle, with the most conserved ligand-contacting residues residing in transmembrane helices 3, 6 and 7 (Venkatakrishnan et al., 2013). The evidence to date suggests that GPR35 ligand binding is typical of

Class A GPCRs, with several important interacting residues in TM3, TM4, TM6 and TM7 identified by mutagenesis studies (Figure 1-2) (Jenkins et al., 2011, MacKenzie et al., 2014). Since most GPR35 ligands contain a carboxylate group or a carboxylate bioisostere (Figure 1-3, Figure 1-4 and Figure 1-5), it is likely that positively-charged residues in the binding pocket are important in ligand binding. An arginine at position 3.36 (using Ballesteros and Weinstein nomenclature[1] (Ballesteros and Weinstein, 1995)) (R3.36) is conserved among several GPCRs related to GPR35 that have small, acidic ligands (Liu et al., 2009). Alanine substitution of this residue or a tyrosine one turn of the helix towards the extracellular side (Y3.32) eliminates ligand binding at both human and rat GPR35 (Figure 1-2) (Jenkins et al., 2011). Studies using species swap mutations that exchange non-conserved residues between the rat and human orthologues identified some additional important features of ligand binding (MacKenzie et al., 2014). Specifically, R6.58 in human GPR35 and R4.60 in both orthologues were identified as essential residues in ligand binding, which were confirmed to interact with ligand in homology model docking studies. Furthermore, a non-conserved residue at position 4.62 (leucine in human GPR35, arginine in rat) was identified which, when swapped between the human and rat orthologues, was sufficient to reverse the species selectivity of zaprinast. This residue is therefore highly likely to be involved in binding of the equipotent agonists, an observation that could prove useful in the search for further equipotent ligands.

1.4.5 GPR35 signalling

Insights into ligand binding and the increasing availability of synthetic tool compounds have aided studies into the downstream signalling and functional consequences of GPR35 activation. Elucidating the signalling pathways influenced by the receptor and the cellular outcomes of GPR35 activity will be vital in understanding its physiological function. Several GPCR signalling mediators have been shown to be regulated by GPR35 *in vitro*, and studies in physiological systems have provided insight into the pathways and responses that

[1] Ballesteros and Weinstein nomenclature is a system of numbering whereby the most conserved residue in a helix 'x' is given the value x.50 (e.g. 3.50 for helix 3) and residues decrease in value towards the N-terminus and increase in value towards the C-terminus (e.g. one residue towards the N-terminus is 3.49 and one residue towards the C-terminus is 3.51).

could potentially be manipulated through pharmacological targeting of this receptor (summarised in Figure 1-6).

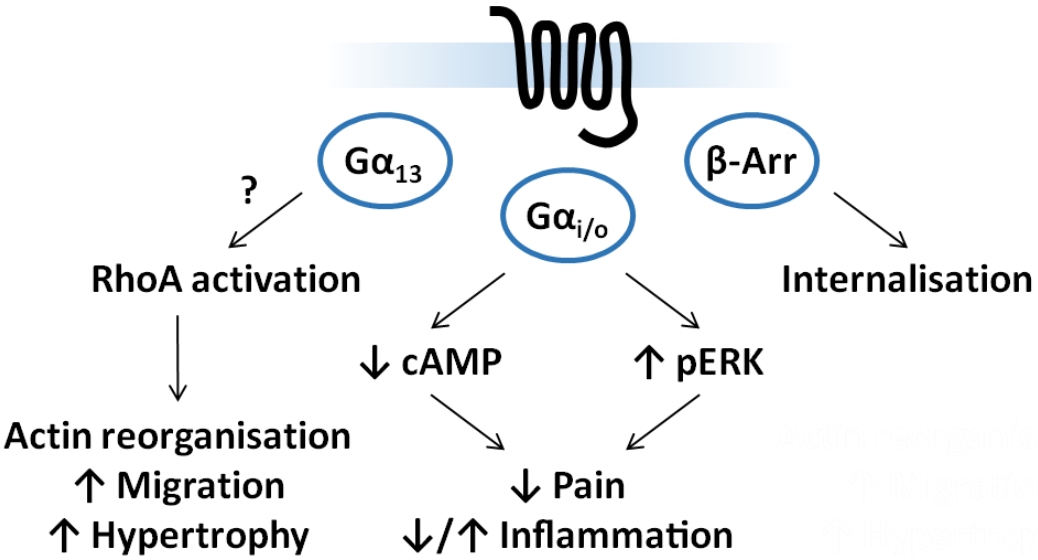

Figure 1-6 Current model of GPR35 signalling GPR35 has been shown to couple to $G\alpha_{i/o}$, $G\alpha_{13}$ and β-arrestin. Signalling pathways and physiological outcomes associated with GPR35 activity are summarised.

In terms of classical G protein-mediated signalling, investigating poorly characterised GPCRs can be challenging due to the fact that most assays measure the signalling outcome of a single G protein family. A common solution to this problem is the use of chimeric G proteins, where the GPCR-coupling portion (i.e. the C-terminal tail) of various G proteins are fused with the signalling portion of a G protein with an easy-to-measure signalling output, such as $G\alpha_q$, whose activity can easily be monitored by measuring accumulation of IP1 (a metabolite of IP3) or $[Ca^{2+}]_i$ mobilisation (Kostenis et al., 2005). Despite being a slightly crude and indirect method, chimeric G proteins are valuable as a starting point to guide studies into GPCR-G protein interactions. This technique has enabled the identification of a number of Gα subunits that can couple to GPR35 with varying efficacy and in a context-dependent manner.

1.4.5.1 GPR35 coupling to $G\alpha_{i/o}$ proteins

Early reports of GPR35 signalling designated it as a $G\alpha_{i/o}$-coupled receptor. Wang et al. used chimeric G proteins to demonstrate that in Chinese hamster ovary cells heterologously expressing human GPR35 and transfected with $G\alpha_i/G\alpha_q$ or $G\alpha_o/G\alpha_q$ chimeras, kynurenic acid elicited $G\alpha_q$-associated signalling (Wang et al.,

2006). They also showed that kynurenic acid-induced [^{35}S]-GTPγS binding in these cells was sensitive to *Bordetella pertussis* toxin (PTx), which ADP-ribosylates and specifically inhibits $G\alpha_{i/o}$ family G proteins (Wang et al., 2006). Furthermore, in Chinese hamster ovary cells overexpressing rat GPR35, both kynurenic acid and zaprinast treatment inhibited forskolin-induced cAMP production, indicating activation of $G\alpha_{i/o}$ protein (Ohshiro et al., 2008). Similarly, Guo et al. reported PTx-sensitive effects on N-type calcium channels in rat neurons heterologously expressing human GPR35, and Zhao et al. reported PTx-sensitive ERK phosphorylation by both zaprinast and pamoic acid in U2OS osteosarcoma cells stably expressing human GPR35 (Guo et al., 2008, Zhao et al., 2010). Together, these findings demonstrate that a number of $G\alpha_{i/o}$-associated signalling outcomes in a range of cell types occur in response to GPR35 stimulation, and these effects are sensitive to specific inhibition of $G\alpha_{i/o}$ proteins.

1.4.5.2 GPR35 coupling to $G\alpha_{12/13}$ proteins

As well as a role for $G\alpha_{i/o}$ signalling in GPR35-mediated responses, more recent reports have demonstrated $G\alpha_{13}$ coupling to GPR35. Using a conformational active-state-sensing GTP-$G\alpha_{13}$ antibody, Jenkins et al. observed zaprinast-induced activation of $G\alpha_{13}$ in HEK cells transfected with either human or rat GPR35 (Jenkins et al., 2011). The same study also demonstrated zaprinast-induced $[Ca^{2+}]_i$ release in these cells when co-transfected with a $G\alpha_{13}/G\alpha_q$ chimera, an effect that was specific for $G\alpha_{13}$ over the other subfamily member $G\alpha_{12}$. $G\alpha_{13}$ and $G\alpha_{12}$ have very similar but subtly different roles within the cell. Of the four RhoGEF proteins that are effectors for this G protein family, leukemia-associated RhoGEF (LARG) and lymphoid blast crisis (Lbc)-RhoGEF can be activated by both $G\alpha_{12}$ and $G\alpha_{13}$, whereas p115-RhoGEF and PDZ-RhoGEF can only be activated by $G\alpha_{13}$ (Siehler, 2009). This results in slightly different signalling profiles, though the differences between the two subfamily members are not well defined (Siehler, 2009). It is of note, however, that homozygous inactivation of $G\alpha_{13}$ is embryonically lethal due to defects in vascular development, whereas $G\alpha_{12}$ knockout mice are viable and lack apparent defects (Gu et al., 2002, Offermanns et al., 1997). A $G\alpha_{13}$-specific signalling profile is unusual among GPCRs, but interestingly is a feature of the orphan receptor GPR55, which is phylogenetically similar to GPR35 (Ryberg et al., 2007). This

potentially suggests similar signalling roles for these two receptors, but their functional relationship is yet to be properly investigated (Zhao and Abood, 2013).

1.4.5.3 Recruitment of β-arrestin to GPR35

In addition to eliciting G protein-mediated responses, GPR35 has been shown to directly recruit β-arrestin-2 following agonist stimulation (Jenkins et al., 2010). All of the synthetic agonists, as well as the endogenous agonists kynurenic acid and DHICA, induce recruitment of β-arrestin-2 to GPR35 (Table 1-2 and Table 1-3). This is followed by agonist-dependent internalisation of both the receptor and β-arrestin, which is indicative of a strong interaction between GPR35 and β-arrestin that is likely driven by phosphorylation of the receptor (see section 1.2.4.2) (Jenkins et al., 2012, Zhao et al., 2010).

While β-arrestin-mediated internalisation is clearly important in regulating the GPR35/G protein signalling axis, β-arrestin-mediated signalling has not yet been reported for GPR35. GPR35 stimulation can lead to phosphorylation of ERK, but this is PTx-sensitive and thus is assumed to be mediated by $G\alpha_{i/o}$ proteins. However, given the diversity of physiological processes seemingly influenced by GPR35 (discussed in section 1.4.6), an understanding of G protein- and β-arrestin-regulated processes may be key to elucidating this receptor's functions in different cellular contexts and harnessing its therapeutic potential.

1.4.6 Physiological function of GPR35

Amid uncertainty regarding the endogenous ligand of GPR35 and following the development of insights into its cellular signalling profile, this orphan receptor's physiological function and importance remain poorly understood. In recent years, however, GPR35 has been suggested to have roles in a range of physiological and pathophysiological settings. Its association with several diverse disease areas hints at potentially far-reaching therapeutic value. It is therefore of significant interest to investigate the physiological functions of this receptor, both in health and disease, in order to evaluate its potential as a novel therapeutic target.

1.4.6.1 GPR35 expression profile

Expression of *GPR35* mRNA has been detected in a number of diverse tissues in both rodent and human studies. In the study that first cloned GPR35 from human genomic DNA, tissue distribution of *GPR35*/*Gpr35* mRNA was investigated by performing Northern blot analysis on a range of human and rat tissues including various parts of the brain and digestive tract (O'Dowd et al., 1998). Although no data were shown, the authors reported that *Gpr35* mRNA was only detected in rat small intestine, and could not be detected in any of the human tissues tested. This is likely due to quite low expression levels of GPCRs in general and of GPR35 in particular. However, since this initial study, technical advancements have enabled much more sensitive methods for detection of mRNA. Using quantitative real-time polymerase chain reaction (qRT-PCR), Wang et al. amplified *GPR35*/*Gpr35* mRNA from lung, stomach, small intestine, colon and spleen in both human and mouse tissues, and also detected *GPR35* in human peripheral lymphocytes (Wang et al., 2006). In a mouse tissue array, *in situ* hybridisation with *Gpr35* mRNA probes revealed expression throughout the lower digestive tract, including duodenum, jejunum, ileum, cecum, colon and rectum (Wang et al., 2006). Taniguchi et al. used qRT-PCR in rat tissues to confirm high expression levels in lung, stomach, small intestine and colon, as previously reported, but also detected high levels in skeletal muscle, dorsal root ganglion (DRG) and uterus, and lower levels in spinal cord, heart, liver, bladder, whole brain and cerebrum (Taniguchi et al., 2006). Several other groups have confirmed expression in rat spinal cord and DRG and additionally reported expression in mouse astrocytes (Ohshiro et al., 2008, Cosi et al., 2011, Berlinguer-Palmini et al., 2013). *GPR35* mRNA has also been detected in various human immune cells, including mast cells, basophils, eosinophils and invariant natural killer-like T cells (Yang et al., 2010, Fallarini et al., 2010). Recently, *GPR35* mRNA was found to be expressed in a number of human vascular cell types, including human saphenous vein smooth muscle cells, human saphenous vein endothelial cells and human umbilical cord endothelial cells (McCallum et al., 2015). The collective evidence suggests expression and therefore possible roles for GPR35 in four key physiological systems: the gastrointestinal system, the immune system, the nervous system and the cardiovascular system.

1.4.6.2 GPR35 in gastrointestinal disease

Since GPR35 is expressed most highly in the gastrointestinal tract, this would be an obvious starting point in the search for a physiological function for GPR35. A genome-wide association study (GWAS) for early-onset inflammatory bowel disease (IBD), including Crohn's disease and ulcerative colitis, identified a *GPR35* SNP associated with ulcerative colitis (Imielinski et al., 2009). The rs4676410 SNP is located upstream of the open reading frame and so does not alter the coding sequence, but this SNP was also not associated with any change in *GPR35* expression level in IBD patients when compared with genetically related healthy controls. However, in a linkage disequilibrium analysis, rs4676410 was associated with the *CAPN10, KIF1A* and *RNPEPL1* genes (Imielinski et al., 2009). *CAPN10*, which encodes the calcium-regulated intracellular cysteine protease calpain 10, was found to be significantly downregulated in individuals with ulcerative colitis, and is therefore likely to be the disease-related gene in the linkage disequilibrium block (Imielinski et al., 2009).

A more recent study investigating genetic risk factors in the chronic cholestatic liver disease, primary sclerosing cholangitis (PSC), has provided further evidence of a possible role for GPR35 in IBD (Ellinghaus et al., 2013). Since most patients with PSC have concurrent ulcerative colitis and these two conditions appear to have shared genetic susceptibility factors, the study performed an integrated analysis of GWAS's for both diseases (Bergquist et al., 2008). Two *GPR35* SNPs were found to have a significant association with PSC, one of which was the upstream intron variant previously identified in the IBD GWAS (Imielinski et al., 2009). The other SNP encodes a threonine to methionine substitution in helix 3 (Figure 1-2) with a minor allele frequency of 0.15. Based on the expression of GPR35 in both the liver and gastrointestinal tract, and the presence of kynurenic acid both in bile and the gut, the authors of this report speculated that GPR35 may have a role in the regulation of inflammation in the biliary and gastrointestinal tracts. However, all the existing evidence for a role for GPR35 in gut inflammation is from genetic association studies. This is yet to be examined experimentally, and so no firm conclusions can currently be drawn regarding the role of this receptor in gut homeostasis and disease.

1.4.6.3 GPR35 in immunity and inflammation

As in the gastrointestinal system, the relatively high expression of GPR35 in various types of immune cell suggests a possible role in the immune system. GPR35 has been implicated in inflammation in several studies, though it remains unclear whether its effects are pro- or anti-inflammatory. GPR35 is suggested to have anti-inflammatory effects through its possible role as a 'metabolite-sensing' receptor for endogenous kynurenic acid (discussed in section 1.4.2.1). Kynurenic acid is produced *via* the kynurenine pathway in the small intestine following consumption of tryptophan-rich foods such as red meat, fish and eggs (Thorburn et al., 2014, Stone and Darlington, 2002). The kynurenine pathway is activated under inflammatory conditions, and kynurenic acid levels are elevated during inflammatory disease (Larkin et al., 2016, Forrest et al., 2002). In the study by Wang et al., kynurenic acid was found to inhibit lipopolysaccharide (LPS)-induced release of tumour necrosis factor-α from human peripheral blood mononuclear cells and purified peripheral blood monocytes, which was proposed to be mediated by agonism of GPR35 (Wang et al., 2006). This was also demonstrated *in vivo* in a mouse model of LPS-induced endotoxic shock (Moroni et al., 2012). Additionally, Kuc et al. have reported that kynurenine can be converted into kynurenic acid by *Escherichia coli*, which may provide a link between the gut microbiota and GPR35-mediated effects on gut inflammation (Kuc et al., 2008, Thorburn et al., 2014).

A conflicting study found that kynurenic acid treatment induced arrest of monocytes and neutrophils onto intracellular adhesion molecule 1-expressing monolayers of vascular endothelial cells (Barth et al., 2009). This was sensitive both to PTx, suggesting $G\alpha_{i/o}$ involvement, and to GPR35 knockdown by short hairpin RNA (Barth et al., 2009). This report suggests a role for GPR35 in leukocyte infiltration, a pro-inflammatory process. However, the effect on leukocyte arrest was observed at nanomolar concentrations of kynurenic acid, which is far lower than the potency range at GPR35 reported in overexpression systems (Wang et al., 2006, Zhao et al., 2010, Jenkins et al., 2011, Deng et al., 2012). More direct evidence that these effects are mediated by GPR35 and not through other receptors modulated by kynurenic acid is required to clarify this discrepancy. Additional support for a pro-inflammatory role for GPR35 comes from its effects on invariant natural killer-like T cells, which are involved in

dendritic cell maturation and protect against autoimmunity. Treatment with either kynurenic acid or zaprinast was shown to reduce interleukin-4 release by these cells in a dose-dependent and PTx-sensitive manner (Fallarini 2010). However, in this study, the agonists had no effect on the level of interferon-γ, which tends to increase as interleukin-4 decreases, and *vice versa*, in a manner that reflects Th1/Th2 cell polarisation (Paludan, 1998). It is therefore difficult to interpret this finding in terms of its physiological significance to pro-/anti-inflammatory signalling.

Considering these studies demonstrating kynurenic acid-induced effects on inflammation, it is noteworthy that several synthetic agonists of GPR35 are known anti-inflammatory agents. Yang et al. reported the anti-allergic and anti-asthma drugs cromolyn disodium and nedocromyl sodium to be moderately potent agonists of GPR35, and also demonstrated upregulation of GPR35 in response to challenge with IgE antibodies (Yang et al., 2010). An independent study reported potency of several related anti-allergic mast cell stabilisers at GPR35 (Table 1-3) (MacKenzie et al., 2014). These findings suggest a possible role for GPR35 in the attenuation of IgE-mediated inflammation and allergy, though this has not been followed up to date.

An additional link between GPR35 and the immune system is the suggestion that GPR35 might be a chemokine receptor for CXCL17 (discussed in section 1.4.2.4) (Maravillas-Montero et al., 2015). CXCL17 is a mucosal macrophage chemoattractant that is upregulated in idiopathic pulmonary fibrosis (Burkhardt 2012). Lung tissue from CXCL17 knockout mice was shown to have significantly reduced expression of GPR35, along with several macrophage markers, compared with lung tissue from wild type mice (Maravillas-Montero et al., 2015). The authors of this report concluded that CXCL17 is required to recruit GPR35-expressing macrophages to the lungs, where they may play a role in pulmonary inflammation. However, this is an isolated report and further investigation is required to determine whether GPR35 is indeed involved in chemoattraction.

1.4.6.4 GPR35 in the nervous system and nociception

A role for GPR35 in the central nervous system has been investigated following reports of its expression in rat spinal cord and DRG neurons (Ohshiro et al., 2008,

Cosi et al., 2011). Kynurenic acid and zaprinast were shown to have PTx-sensitive effects on forskolin-induced cAMP generation in both rat DRG neurons and mouse glial cells endogenously expressing GPR35, (Ohshiro et al., 2008, Cosi et al., 2011). Furthermore, administration of either kynurenine or zaprinast had anti-nociceptive effects in a mouse 'writhing test' pain model, significantly reducing the number of writhes by a maximum of 58% and 54%, respectively (Cosi et al., 2011). This *in vivo* finding has recently been recapitulated in a rat pain withdrawal model (Resta et al., 2016). This study also demonstrated that kynurenic acid and zaprinast can counteract prostaglandin-E_2-induced hyperalgesia by inhibiting its cAMP-mediated effect on neuronal excitability, which is regulated by hyperpolarisation-activated cyclic nucleotide-gated channels (Resta et al., 2016). These findings highlight the $G\alpha_{i/o}$-coupled GPR35 pathway as a potential therapeutic target in the treatment of pain, though it remains to be seen whether these promising findings will translate into humans.

A further potential function of GPR35 in the nervous system is to attenuate excitatory post-synaptic currents in the central nervous system. Berlinguer-Palmini et al. detected *GPR35* expression in mouse cortical astrocytes, and demonstrated that kynurenic acid can inhibit forskolin-mediated cAMP production (Berlinguer-Palmini et al., 2013). This effect was sensitive both to the GPR35 antagonist CID-2745687 and to RNA interference-mediated GPR35 knockdown. The inhibitory capacity of the antagonist should be interpreted with caution, however, considering that a previous study found it to be practically inactive at the rodent orthologues (Jenkins et al., 2012). Berlinguer-Palmini et al. also reported that kynurenic acid and zaprinast altered calcium waves in mouse astrocytes and reduced evoked excitatory post-synaptic currents in rat hippocampal neurons (Berlinguer-Palmini et al., 2013). As kynurenic acid is also an agonist of N-methyl-D-aspartate and α7-nicotinic receptors, the investigators showed that the kynurenic acid-mediated effects on both calcium waves and synaptic currents were insensitive to antagonists of these receptors. This suggests that these effects are indeed mediated by agonism of GPR35, although, once again, these findings are yet to be validated in human cells. Translation into human models is now required to determine the potential of GPR35 as a target in analgesia or in the prevention of excitotoxic damage.

1.4.6.5 GPR35 in the cardiovascular system

Although GPR35 is expressed more highly in other tissues, several studies have highlighted roles for GPR35 in the heart and vasculature. The first report to suggest a link between GPR35 and CVD described a GWAS that aimed to identify novel risk genes for coronary artery disease in a population of hypertensive individuals (Sun et al., 2008). This study identified an association between a GPR35 SNP and coronary artery calcification, a risk factor in coronary artery disease. The SNP, which has a minor allele frequency of 0.48, encodes a serine to arginine substitution in the receptor C-terminal tail (Figure 1-2), a region known to be important in binding cytoplasmic mediator proteins (Szczepek et al., 2014). Since phosphorylation of the C-terminal tail is known to influence the specificity of the downstream response to GPCR activation, and the SNP affects a potential phospho-acceptor serine residue, it is tempting to speculate that it may alter the selectivity of G protein- versus ß-arrestin-mediated responses to GPR35. However, in a more recent study, the S294R substitution had no effect on either cell surface expression or ligand potency in a ß-arrestin recruitment assay (MacKenzie et al., 2014). The mechanism by which this SNP could alter receptor function and contribute to disease therefore remains unclear.

Further evidence of GPR35 contributing to CVD was found in a study investigating myocardial gene expression in twelve patients with chronic heart failure (Min et al., 2010). In this microarray analysis, GPR35 expression was found to be upregulated in the myocardial tissue of these patients compared with healthy controls, suggesting that although GPR35 is not highly expressed in the heart under basal conditions, it is induced at some point during the development of disease. The same study found that adenovirus-mediated overexpression of GPR35 in primary rat cardiomyocytes resulted in cellular hypertrophy, which is a feature of the pathological cardiac hypertrophy that leads to heart failure. Follow-up analysis in a global GPR35 knockout mouse revealed a significant 37.5 mmHg increase in systolic blood pressure compared with the wild type background strain, strongly suggesting that GPR35 has an important role in blood pressure regulation (Min et al., 2010).

A subsequent investigation of GPR35 expression in cardiomyocytes found both mRNA and cell surface protein levels to increase in response to hypoxia and

hypoxia-inducible factor 1 activation (Ronkainen et al., 2014). As hypoxia is a feature of most cardiac pathologies, this provides a possible rationale for the apparently broad involvement of GPR35 in cardiovascular disease. The same study found that GPR35 expression is induced in the heart tissue of experimental mouse models of myocardial infarction and pathological hypertrophy, and this induction precedes cardiac remodelling and heart failure. However, in this study, overexpression of GPR35 in mouse cardiomyocytes led to membrane ruffling and formation of retraction fibres, but no change in cell size. This conflicts with the previous finding in rat cardiomyocytes (Min et al., 2010), suggesting possible species variation in the specific cellular effects of GPR35 overexpression. Since overexpression alone was sufficient to initiate cardiomyocyte remodelling in both cases, these effects may be due either to a constitutive signalling capacity of GPR35 or the presence of a GPR35 agonist in the extracellular environment. Once again, however, the lack of antagonists with efficacy at the rodent orthologues has hindered a more detailed understanding of these findings.

In addition to an apparent role in regulating cell size and shape in cardiomyocytes, GPR35 has been reported to have effects in vascular cells. McCallum et al. demonstrated that GPR35 is expressed in vascular smooth muscle and endothelial cells, and that GPR35 agonists can induce both actin fibre reorganisation and migration in vascular smooth muscle cells (McCallum et al., 2015). These effects were blocked by the antagonists CID-2745687 and ML-145, and also by inhibitors of members of the RhoA signalling pathway, indicating that endogenous GPR35 mediates its effects on vascular cells through its coupling to $G\alpha_{13}$, as previously demonstrated in GPR35-overexpressing HEK293 cells (Jenkins et al., 2011). These findings suggest a potential role for GPR35 in the regulation of vascular remodelling, which is an important element of pathological processes such as intimal hyperplasia, restenosis and vein graft failure.

1.5 GPR35 as a potential therapeutic target in CVD

The evidence reported to date indicates broad functions of GPR35 in various tissues and physiological systems. The emerging roles of GPR35 in the cardiovascular system implicate it as a novel contributor to cardiovascular

dysfunction and a potential therapeutic target in CVD (Divorty et al., 2015). Importantly, CVD is one of the areas in which research into orphan GPCRs has revealed previously unknown transmitter systems and novel therapeutic opportunities (Maguire and Davenport, 2005). Investigating the role of GPR35 in cardiovascular regulation could therefore yield similar novel insights.

1.5.1 $G\alpha_{12/13}$-mediated signalling in CVD

GPR35 is known to couple to both $G\alpha_{i/o}$ and $G\alpha_{13}$ (see section 1.4.5) (Wang et al., 2006, Jenkins et al., 2011). However, all of the direct experimental evidence of a role for GPR35 in the cardiovascular system revolves around its ability to regulate cell size and shape (discussed in section 1.4.6.5), which strongly suggests that its cardiovascular functions are mediated primarily by $G\alpha_{13}$ (Ronkainen et al., 2014, McCallum et al., 2015). Furthermore, McCallum et al. demonstrated that its effects on vascular smooth muscle cell morphology are inhibited by disrupting the RhoA pathway (McCallum et al., 2015). Although $G\alpha_{12/13}$ signalling is still relatively poorly understood compared with the other G protein subfamilies, its primary effects seem to be mediated by its activation of RhoA and its effector Rho-associated kinase (ROCK), which phosphorylates a number of targets involved in shape change and migration (Worzfeld et al., 2008).

While many $G\alpha_{12/13}$-coupled receptors can also couple to $G\alpha_{q/11}$, $G\alpha_{12/13}$ effectors have been shown to have important $G\alpha_{q/11}$-independent roles in cardiovascular physiology and pathophysiology. Studies in smooth muscle-specific $G\alpha_{12/13}$ knockout mice have shown that while $G\alpha_{12}$ and $G\alpha_{13}$ are not required for basal maintenance of vascular tone, they and their RhoGEF target LARG are required for the development of salt-induced hypertension (Wirth et al., 2008). This appears to be due to direct effects on vascular contractility, as expression of dominant-negative forms of $G\alpha_{12/13}$ has been shown to inhibit vascular smooth muscle cell contraction in response to endothelin-1 (Gohla et al., 2000). In addition to direct effects on vascular smooth muscle contraction, $G\alpha_{13}$ has been implicated in pathological remodelling of the heart. A study in inducible cardiomyocyte-specific $G\alpha_{12}$ and $G\alpha_{13}$ knockout mice identified a $G\alpha_{13}$-specific role in pressure overload-induced cardiac remodelling and the subsequent development of heart failure, which was mediated by RhoA/myocardin-related

transcription factor (Takefuji et al., 2012). These findings suggest that $G\alpha_{13}$-coupled GPCRs that are expressed in the cardiovascular system (especially those that are upregulated in cardiovascular tissues during disease, as GPR35 is) are potential therapeutic targets in CVD, particularly in hypertension and heart failure.

1.5.2 GPR35 as a potential therapeutic target in hypertension

As discussed in section 1.4.6.5, GPR35 has been associated with adverse coronary artery remodelling in hypertensive human subjects (Sun et al., 2008), and its deficiency reportedly has a significant impact on blood pressure in knockout mice (Min et al., 2010). These reports implicate GPR35 in the pathogenesis of hypertension, though it is uncertain whether loss, gain or alteration of receptor function is to blame.

1.5.2.1 Causes of hypertension

Hypertension occurs in over a third of adults worldwide, and is a major risk factor for cardiovascular morbidity and mortality (Campbell et al., 2016). If left untreated, hypertension leads to a range of secondary diseases including coronary artery disease, heart failure, renal failure and stroke, and contributed to an estimated 10.3 million deaths globally in 2013 (Chobanian et al., 2003, Campbell et al., 2016). It is defined as a systolic blood pressure greater than 140 mmHg with a diastolic blood pressure greater than 90 mmHg (Williams et al., 2004). The causes of hypertension are multifarious and complex, with lifestyle, genetic susceptibility factors and various diseases and medications all contributing to its development and progression (Williams et al., 2004). On the molecular level, things are no simpler. There are many molecular and cellular mechanisms involved in the pathogenesis of hypertension, including altered vasoreactivity, excessive production of vasoactive hormones, and endothelial dysfunction resulting from oxidative stress or chronic inflammation (Daiber et al., 2016, Grassi et al., 2015, Harris et al., 2008).

1.5.2.2 Current treatments for hypertension and their limitations

Due to the multitude of interacting factors, it is challenging to resolve hypertension by eliminating its primary cause. Instead, management relies on a

combination of lifestyle alterations and pharmacological intervention with one or more of several classes of drug (Williams et al., 2004). First-line treatments include ACE inhibitors, AT_1R antagonists, ß blockers, calcium channel blockers and diuretics, and various combinations thereof (Williams et al., 2004). ACE inhibitors and AT_1R antagonists block elevated activity of the renin-angiotensin system, whereas ß blockers attenuate the hypertensive effects of excessive adrenergic stimulation. Calcium channel blockers and diuretics are less specific approaches, which reduce the sensitivity of vascular smooth muscle cells to vasoconstrictors or decrease blood volume by inhibiting water reabsorption, respectively. Most patients require a combination of drugs from at least two of these four classes to appreciably reduce blood pressure (Williams et al., 2004). However, about a quarter of patients fail to respond at all to this treatment strategy, and are classed as having 'treatment-resistant' or 'uncontrolled' hypertension (Calhoun et al., 2008, Eirin et al., 2016). While alternative therapeutic strategies are emerging, the identification of novel pharmacological targets can only be beneficial in combating this type of hypertension. This is especially relevant for poorly-characterised potential targets like GPR35, the study of which may reveal novel signalling systems whose contributions are currently underappreciated.

1.5.3 GPR35 as a potential therapeutic target in heart failure

Some of the strongest evidence for a pathophysiological role for GPR35 comes from studies in both humans and mice that demonstrate upregulation of GPR35 in the heart during heart failure (discussed in section 1.4.6.5) (Min et al., 2010, Ronkainen et al., 2014). However, whether the induction of GPR35 is an adaptive response or contributes to pathogenesis in these contexts is unclear. Since heterologous overexpression of GPR35 in rat cardiomyocytes has been shown to promote either cytoskeletal rearrangements or hypertrophy (Min et al., 2010, Ronkainen et al., 2014), it is possible that GPR35 is part of the pathological signalling involved in the progression of cardiac hypertrophy to heart failure, and could therefore constitute a therapeutic target.

1.5.3.1 Causes of pathological cardiac remodelling

Heart failure is the end-point of progressive and debilitating alterations in the heart's size, shape and function in response to stress or injury, leading to impaired contractile function and reduced blood flow (Bisping et al., 2014). Pathological remodelling of the heart can be triggered by many different stressors, such as chronic hypertension, myocardial infarction, or inflammation, and can be exacerbated by both lifestyle and genetic factors (Bisping et al., 2014).

Cardiac hypertrophy and increased contractility is initially an adaptive response to cardiovascular stress that progresses to pathological remodelling in response to persistent overload (Burchfield et al., 2013). Pressure overload resulting from excessive afterload – as a consequence of hypertension, for example – leads to concentric hypertrophy, where cardiomyocytes increase in width leading to wall thickening and reduced chamber area (Kehat et al., 2011). Concentric hypertrophy is a compensatory mechanism and allows the heart to maintain normal function (Cohn et al., 2000). On the other hand, volume overload or myocardial infarction leads to eccentric hypertrophy, where cardiomyocytes elongate without increasing in width (Kehat et al., 2011). This leads to wall thinning and dilation of the ventricles, which is detrimental to function (Cohn et al., 2000). Concentric hypertrophy progresses to eccentric hypertrophy, and this transition, along with increased collagen deposition and ventricular stiffening, marks the progression to maladaptive remodelling and failure to pump adequately (Cohn et al., 2000).

In molecular terms, pathological cardiac remodelling is driven by pro-apoptotic, pro-hypertrophic and pro-fibrotic signalling, directed largely by the adrenergic and angiotensin receptor systems but also by other GPCRs, receptor tyrosine kinases, inflammatory mediators and mechanical stimuli (Bisping et al., 2014, Capote et al., 2015). The effector pathways involved include the PKC, Ca^{2+}/Calmodulin, RhoA/ROCK and mitogen-activated protein kinase pathways, all of which are potential clinical targets (van Berlo et al., 2013, Bisping et al., 2014).

1.5.3.2 Current treatments for heart failure and their limitations

In similarity to hypertension (which is the single biggest risk factor for heart failure), the primary drug interventions for adverse cardiac remodelling and prevention of heart failure are usually ß blockers, ACE inhibitors or AT_1R antagonists, along with mineralocorticoid receptor antagonists, which target the aldosterone-mediated actions of the renin-angiotensin system (Hunt et al., 2009). These are effective both in controlling hypertension and therefore minimising this risk factor, and in actively inhibiting or even reversing hypertrophy and fibrosis (Xie et al., 2013). Advanced heart failure may also be treated with implantable devices including cardioverter-defibrillators and ventricular assist devices (Hunt et al., 2009). However, heart failure remains a significant cause of death worldwide, indicating that current treatments are not sufficient in the long term (Hunt et al., 2009). This is probably due to the multitude of signalling pathways and cell types involved in the pathogenesis of the disease, and so understanding the different mechanisms that lead to adverse remodelling of the heart is still a necessity. Elucidating the role of GPR35 in this process therefore has therapeutic relevance.

1.6 Aims and objectives

Recent findings of both human and animal studies contribute towards an emerging link between GPR35 and CVD (Sun et al., 2008, Min et al., 2010, Ronkainen et al., 2014, McCallum et al., 2015). This link appears to have justification at the biochemical and cellular levels in terms of G protein coupling and the possible signalling pathways involved, and brings us closer to assigning a function to the orphan receptor, although its precise role in disease remains unclear. Given the historical success of GPCRs (including orphan GPCRs) as drug targets, the link between GPR35 and CVD makes it a potential therapeutic target in diseases such as hypertension and its associated pathological cardiac remodelling and heart failure. The treatment of these diseases remains a global health challenge, and so there is a need to identify novel mechanisms and therapeutic targets. This thesis aims to address this need by characterising GPR35 signalling and its role in the cardiovascular system, to investigate the hypothesis that GPR35 is a potential therapeutic target in CVD. To this end, the work presented in this thesis is based on three objectives:

1. Investigate GPR35 signalling *in vitro*

Determining the specific downstream consequences of GPR35 activation is necessary to place it into context as a signalling mediator in the cardiovascular system. Elucidating the signalling pathways activated by GPR35 and how these are regulated, for example by investigating the contributions of G protein, ß-arrestin and receptor phosphorylation, will be valuable in assessing how GPR35 signalling might be targeted using emerging therapeutic strategies such as the use of biased agonists to increase the specificity of drug responses.

> **Hypothesis:** GPR35 activates signalling pathways *in vitro* that are consistent with a role in regulation of the cardiovascular system.

2. Examine the role of GPR35 in the cardiovascular system by assessing the cardiovascular phenotype of a GPR35 knockout mouse

Studies in knockout animals have been very valuable in linking orphan receptors to disease phenotypes. Although GPR35 has been linked with CVD, and a knockout mouse has been briefly reported on, the consequences of GPR35 deficiency on cardiovascular function are yet to be examined in detail. This has been addressed through a study into the basal cardiovascular phenotype of a GPR35 knockout mouse.

> **Hypothesis**: GPR35 is essential for normal cardiovascular function in the mouse.

3. Determine the contribution of GPR35 to cardiovascular pathophysiology using rodent models of CVD

To assess the potential of GPR35 as a therapeutic target, it is necessary to investigate its function in the context of cardiovascular dysfunction. This has been addressed using rodent models of CVD, including a study of hypertension in the knockout mouse and an agonist study in an inbred rat model of hypertension and end-organ damage.

> **Hypotheses**: GPR35 is essential for the development of Ang II-induced hypertension in the mouse; and pharmacological agonism of GPR35 exacerbates cardiovascular disease in the stroke-prone spontaneously hypertensive rat.

Chapter 2 Materials and Methods

2.1 Pharmacological reagents

- **Amlexanox** (2-Amino-7-(1-methylethyl)-5-oxo-5H- [1]Benzopyrano[2,3-b]pyridine-3-carboxylic acid): Tocris Bioscience.

- **CID-2745687** (1-(2,4- Difluorophenyl)-5-[[2-[[(1,1-dimethylehyl)amino]thioxomethyl]hydrazinylidene]methyl]-1H-pyrazole-4-carboxylic acid methyl ester): Tocris Bioscience.

- **Doxantrazole** (3-(1*H*-tetrazol-5-yl)-9*H*-thioxanthen-9-one 10,10-dioxide monohydrate): Sigma-Aldrich

- **Lodoxamide** (2-[2-chloro-5-cyano-3-(oxaloamino)anilino]-2-oxoacetic acid): synthesised in collaboration with MRCT (London, UK).

- **ML-145** (-Hydroxy-4-[4-(5Z)-5-[(E)-2-methyl-3-phenylprop-2- enylidene]-4-oxo-2-sulfanylidene-1,3-thiazolidin-3-yl]butanoylamino]benzoic acid): Tocris Bioscience.

- **Pamoic acid** (1, 1′-Methylene-bis(2-hydroxy-3-naphthoic acid)): Sigma-Aldrich.

- **Zaprinast** (2-(2-Propyloxyphenyl)-8-azapurin-6-one): Tocris Bioscience.

All pharmacological agents were dissolved in dimethyl sulfoxide (DMSO) at stock concentrations of 1–100 mM depending on solubility.

2.2 Buffers and solutions

- **Competent bacteria solution 1**: 30 mM CH_3CO_2K, 10 mM $RbCl_2$, 10 mM $CaCl_2$, 50 mM $MnCl_2$, 15% (v/v) glycerol, pH 5.8 with acetic acid

- **Competent bacteria solution 2**: 10 mM 3-morpholinopropane-1-sulfonic acid (MOPS), 10 mM $RbCl_2$, 75 mM $CaCl_2$, 15% (v/v) glycerol, pH 6.5 with HCl

- **DMEM-HEPES**: 1x Dulbecco's modified Eagle's medium (DMEM) High Glucose, 20 mM 4-(2-hydroxyethyl)-1-piperazineethanesulfonic acid (HEPES), pH 7.4

- **DNA loading buffer (6x)**: 0.4 mg/mL sucrose, 0.25% (w/v) bromophenol blue

- **Hank's balanced salt solution (HBSS)**: 137 mM NaCl, 5.3 mM KCl, 0.34 mM Na_2HPO_4, 0.44 mM KH_2PO_4, 4 mM $NaHCO_3$, 1.26 mM $CaCl_2$, 0.5 mM $MgCl_2$, 0.4 mM $MgSO_4$, pH 7.3

- **HEPES microscope buffer**: 130 mM NaCl, 5 mM KCl, 20 mM HEPES, 10 mM glucose, 1 µM $MgCl_2$, 1 µM $CaCl_2$, pH 7.2

- **Krebs/HEPES buffer (phospholabelling)**: 118 mM NaCl, 1.3 mM $CaCl_2$, 4.3 mM KCl, 1.17 $MgSO_4$, 4.17 mM $NaHCO_3$, 11.7 mM glucose, 10 mM HEPES, pH 7.4

- **Laemmli buffer (2x)**: 60 mM Tris, 80 mM sodium dodecyl sulphate (SDS), 50 mM dithiothreitol, 10% (v/v) glycerol, 0.25% (w/v) bromophenol blue

- **Luria-Bertani (LB) agar**: 10 g/L tryptone, 5 g/L yeast extract, 10 g/L NaCl, 15 g/L agar, pH 7

- **Luria-Bertani (LB) broth**: 10 g/L tryptone, 5 g/L yeast extract, 10 g/L NaCl, pH 7

- **Lysis buffer (phospholabelling)**: 20 mM Tris (pH 7.4), 150 mM NaCl, 3 mM ethylenediaminetetraacetic acid (EDTA), 1% (v/v) NP-40, 0.5% (w/v) sodium deoxycholate

- **Phosphate-buffered saline (PBS)**: 137 mM NaCl, 2.7 mM KCl, 1.8 mM KH_2PO_4, 10 mM Na_2HPO_4, pH 7.4

- **Physiological salt solution (PSS)**: 118.3 mM NaCl, 4.7 mM KCl, 1.2 mM $MgSO_4$, 25 mM $NaHCO_3$, 1.19 mM KH_2PO_4, 11.7 mM glucose, 2.5 mM $CaCl_2$, bubbled with O_2 15 min

- **Physiological salt solution high potassium (KPSS)**: 120 mM KCl, 1.2 mM $MgSO_4$, 25 mM $NaHCO_3$, 1.19 mM KH_2PO_4, 11.7 mM glucose, 2.5 mM $CaCl_2$, bubbled with O_2 15 min

- **Radioimmunoprecipitation assay (RIPA) buffer**: 50 mM HEPES (pH 7.4), 150 mM NaCl, 1% (v/v) Triton X-100, 0.5% (w/v) sodium deoxycholate, 0.1% (w/v) SDS, 10 mM NaF, 5 mM EDTA, 10 mM Na_2HPO_4, 5% (v/v) ethylene glycol, pH 7.3

- **Transfer buffer**: 200 mM glycine, 25 mM Tris, 20% (v/v) methanol

- **Tris-acetate-EDTA (TAE) buffer**: 40 mM Tris, 1 mM EDTA (pH 8), 20 mM acetic acid

- **Tris-buffered saline (TBS)**: 20 mM Tris, 150 mM NaCl, 3 mM EDTA, pH 7.4

- **Tris-EDTA (TE) buffer**: 10 mM Tris, 0.1 mM EDTA, pH 7.4

2.3 Molecular biology and cloning

2.3.1 Preparation of competent bacteria

To prepare competent bacteria for chemical transformation, XL1-Blue competent bacteria were streaked onto LB agar and grown overnight at 37°C. A single colony was inoculated into 5 mL LB broth and grown overnight at 37°C, then subcultured into 100 mL LB broth and grown at 37°C until reaching an optical density at 550 nm of 0.48. The culture was chilled on ice for 5 min and two 50 mL aliquots were subjected to centrifugation at 1750 x *g* for 10 min at 4°C. Each pellet was resuspended in 20 mL solution 1, then chilled on ice for 5 min and subjected to centrifugation as before. Each pellet was resuspended in 2 mL solution 2 and chilled on ice for 15 min. The resulting XL1-Blue competent bacteria were aliquoted and stored at − 80°C.

2.3.2 Chemical transformation

XL1-Blue competent bacteria were transformed with plasmid DNA using chemical transformation. 100–500 ng plasmid DNA was added to 50 µL competent bacteria in pre-chilled microcentrifuge tubes and incubated on ice for 20 min. Samples were heat-shocked for 90 sec at 42°C, then incubated on ice for 2 min. Next, 450 µL LB broth was added and samples were incubated with shaking for 60 min at 37°C, before plating 100–250 µL onto LB agar containing 50 µg/mL ampicillin. Plates were incubated overnight at 37°C.

2.3.3 Purification of plasmid DNA

2.3.3.1 Miniprep purification

Microgram quantities of plasmid DNA were purified using the Wizard® Plus SV Minipreps DNA Purification System (Promega) as per the manufacturer's instructions. Briefly, 3–5 mL overnight culture was subjected to centrifugation at 10,000 x *g* for 5 min. The bacterial pellet was resuspended in kit buffer and lysed by the addition of SDS-containing lysis solution. Lysates were incubated with alkaline phosphatase for 5 min at room temperature, then neutralised by the addition of a neutralising buffer. The resulting solution was applied to a spin column and subjected to centrifugation at 16,000 x *g* for 1 min to allow the DNA

to bind the column. The flow-through was discarded and the column washed twice, centrifuging at 16,000 x *g* for 1 min each time. DNA was eluted in 50–100 µL nuclease-free water into a sterile microcentrifuge tube and stored at – 20°C.

2.3.3.2 Maxiprep purification

Milligram quantities of plasmid DNA were purified using the QIAGEN® Plasmid Maxi Kit as per the manufacturer's instructions. Briefly, 200–500 mL overnight culture was subjected to centrifugation at 3000 x *g* for 30 min at 4°C. The bacterial pellet was resuspended in pre-chilled resuspension buffer and lysed by the addition of lysis buffer. Lysate was incubated for 5 min at room temperature, then neutralised by the addition of pre-chilled neutralisation buffer and incubated on ice for 20 min. The resulting solution was subjected to centrifugation at 3000 x *g* for 15 min at 4°C. A QIAGEN-tip 100 column was equilibrated with 15 mL equilibration buffer, and the lysate supernatant applied and allowed to pass through the column by gravity flow. The flow-through was discarded and the column was washed twice with wash buffer. DNA was eluted in 15 mL elution buffer and precipitated by adding 10.5 mL isopropanol, then subjected to centrifugation at 3000 x *g* for 30 min. The pellet was air-dried, desalted by washing with 2 mL 70% (v/v) ethanol, transferred to a sterile microcentrifuge tube and subjected to centrifugation at 16,000 x *g* for 15 min. The pellet containing purified DNA was air-dried, then dissolved in 0.5–1 mL nuclease-free water.

2.3.3.3 Ethanol precipitation

Prior to using maxiprep-purified plasmid vectors for cloning, DNA was further purified using ethanol precipitation to remove residual contaminants such as excess salt. Two volumes of 100% ethanol and 0.1 volumes of 3 M sodium acetate (pH 5.2) were added to the DNA, and the mixture incubated at – 80°C for 30 min. The precipitated DNA was subjected to centrifugation at 16,000 x *g* for 15 min. The pellet was desalted by washing with 100 µL 70% (v/v) ethanol and subjected to centrifugation as before. The pellet containing purified DNA was air-dried, then dissolved in the original volume of nuclease-free water.

2.3.3.4 Determination of DNA concentration

Plasmid DNA concentration was determined by measuring absorbance at 260 nm of a 1:100 dilution using a spectrophotometer. DNA purity was assessed using the A_{260}/A_{280} ratio, with a ratio between 1.7 and 2.0 considered pure.

2.3.4 Polymerase chain reaction (PCR)

PCR was used to introduce restriction sites or epitope tags and to amplify specific DNA fragments. Reactions of 50 µL were set up in sterile 500 µL PCR tubes with the following components:

- 1 x Colourless GoTaq® Buffer (Promega)
- 0.8 mM deoxyribonucleotides (dNTPs) (0.2 mM each deoxyadenosine triphosphate, deoxycytidine triphosphate, deoxyguanosine triphosphate and deoxythymidine triphosphate) (Promega)
- 0.5 µM each forward and reverse primers
- 100 ng template DNA
- 5 units GoTaq® DNA Polymerase (Promega)

Reaction mixtures were subjected to thermal cycling using the following conditions:

1.	Preheating	95°C	2 min
2.	Denaturing	95°C	30 sec
3.	Annealing	50–60°C*	30 sec
4.	Extension	72°C	2 min
5.	Repeat steps 2–4 (x 29)		
6.	Final extension	72°C	10 min
7.	Hold	4°C	∞

*Depending on melting temperature (T_m) of primers.

2.3.5 PCR Purification

PCR products were purified using the QIAquick® PCR Purification Kit (QIAGEN) as per the manufacturer's instructions. Briefly, PCR product was diluted in five

volumes of binding buffer, applied to a QIAquick spin column and subjected to centrifugation at 16,000 x *g* for 1 min. The flow-through was discarded and the column washed once, centrifuging as before. The flow-through was discarded and the column subjected to centrifugation once more to remove residual ethanol. DNA was eluted in 50 µL nuclease-free water into a sterile microcentrifuge tube, allowing the water to stand on the column for 1 min before centrifuging.

2.3.6 Restriction endonuclease digestion

Digestion by restriction endonuclease enzymes was used to generate sticky-end DNA fragments for ligation. pcDNA3.1(+), pcDNA3.1/Hygro(+) or pcDNA5/FRT/TO plasmid vectors and relevant insert fragments were digested overnight at 37°C in 50–100 µL digests containing the following components:

- 1 x CutSmart® Buffer (New England Biolabs)
- 10–50 µg vector DNA or 50 µL PCR product
- 1–10 units (depending on manufacturer's recommendation for supercoiled plasmid DNA) High Fidelity (HF®) restriction endonucleases (New England Biolabs)

2.3.7 Agarose gel electrophoresis

DNA insert and vector fragments were separated by agarose gel electrophoresis. Gels were prepared by dissolving 1% (w/v) agarose and 1 x SYBR® Safe DNA stain (Life Technologies) in TAE buffer. Once set, gels were immersed in TAE buffer and samples were prepared by adding 1 x DNA loading buffer before loading 5–50 µL/well onto the gel. Samples were subjected to electrophoresis at 125 V for 20–30 min. The size and concentration of the DNA fragments were estimated by running 5 µL Hyperladder™ 1kb (Bioline) alongside the samples.

2.3.8 Gel extraction

After gel electrophoresis, DNA insert and vector fragments were extracted from the gel using the QIAquick Gel Extraction Kit (QIAGEN) as per the manufacturer's instructions. Briefly, bands were visualised using ultraviolet light and excised from the gel with a razor blade. Gel pieces were put into sterile microcentrifuge

tubes and weighed. Three gel volumes of solubilisation buffer was added and the gel pieces dissolved by incubating at 50°C for 10 min, vortexing every 2–3 min. One gel volume of isopropanol was added, and the resulting solution was applied to a QIAquick spin column and subjected to centrifugation at 16,000 x *g* for 1 min. The flow-through was discarded and the column washed once, repeating the cenntrifugation step. The flow-through was discarded and the column subjected to centrifugation once more to remove residual ethanol. DNA was eluted in 30–50 µL nuclease-free water into a sterile microcentrifuge tube, allowing the water to stand on the column for 1 min before centrifuging.

2.3.9 DNA dephosphorylation

To remove 5' phosphate groups from digested vector fragments and thus minimise re-ligation of empty vector, vector fragments were treated with Antarctic Phosphatase (New England Biolabs). 1 unit of Antarctic Phosphatase was added per µg of vector, along with 0.1 volumes of 10 x Antarctic Phosphatase Reaction Buffer. Samples were incubated for 30 min at 37°C, then the enzyme was inactivated by incubating at 65°C for 5 min.

2.3.10 DNA ligation

Ligation of DNA sticky ends was carried out to produce recombinant plasmid DNA. Insert and vector fragments were added at molar ratios of 1:3, 1:1 and 3:1 to 20 µL ligation reactions containing the following components:

- 1 x T4 DNA Ligase Reaction Buffer (New England Biolabs)
- 100 ng vector DNA
- X ng insert DNA
- 400 units (1 µL) T4 DNA Ligase (New England Biolabs)

Ligation reactions were incubated overnight at 16°C and 5 µL of ligated product was transformed into XL1-Blue competent bacteria as described in section 2.3.2.

2.3.11 Site-directed mutagenesis

Point mutations were introduced into DNA sequences using the Stratagene QuikChange® system. Mutagenic primer pairs containing the desired base substitution(s) with a T_m ≥78°C were designed using the formula:

$$T_m = 81.5 + 0.41(\%GC) - 675/n - \%\ \text{mismatch}$$

(n = primer length in base pairs.)

To amplify mutagenised plasmid DNA, 50 µL reactions were set up in sterile 500 µL PCR tubes with the following components:

- 1 x Pfu Turbo Reaction Buffer (Agilent Technologies)
- 0.8 mM dNTPs
- 1 µM each forward and reverse primers
- 20 ng template DNA
- 2.5 units Pfu Turbo DNA Polymerase (Agilent Technologies)

Reaction mixtures were subjected to thermal cycling using the following conditions:

1.	Preheating	95°C	30 sec
2.	Denaturing	95°C	30 sec
3.	Annealing	55°C	1 min
4.	Extension	72°C	10 min
5.	Repeat steps 2–4 (x 17)		
6.	Hold	4°C	∞

Methylated parental template DNA was digested using *Dpn*I restriction enzyme by adding 10 units of *Dpn*I (Promega) directly to the PCR product and incubating for 2 hours at 37°C. Following incubation, 1 µL digested PCR product was transformed into XL1-Blue competent bacteria as described in section 2.3.2.

2.3.12 DNA sequencing

Cloning and mutagenesis products were sequenced to verify that the correct changes had been introduced. DNA sequencing was performed by DNA Sequencing & Services (MRC I PPU, College of Life Sciences, University of Dundee, Scotland, www.dnaseq.co.uk) using Applied Biosystems Big-Dye Ver 3.1 chemistry on an Applied Biosystems model 3730 automated capillary DNA sequencer. DNA sequences were assessed using Chromas software and NCBI Basic Local Alignment Search Tool (BLAST) (www.blast.ncbi.nlm.nih.gov).

2.3.13 Generation of hemagglutinin (HA)-tagged GPR35 constructs

Human (hGPR35), rat (rGPR35) and mouse (mGPR35) GPR35 constructs with N-terminal FLAG epitope tags (amino acid sequence DYKDDDDK) and C-terminal enhanced yellow fluorescent protein (eYFP) tags (FLAG-hGPR35-eYFP, FLAG-rGPR35-eYFP, and FLAG-mGPR35-eYFP) in pcDNA3.1(+) (Jenkins et al., 2010, Jenkins et al., 2012) were used as PCR templates. An HA tag (amino acid sequence YPYDVPDYA) was introduced to the C-terminus and restriction sites introduced to both 5' and 3' termini by PCR using the following primers (restriction sites are underlined):

*Hin*dIII hGPR35 Forward:
5' GATCAAGCTTGCCACCATGAATGGCACCTACAACACCTGT 3'
hGPR35-HA *Bam*HI Reverse:
5' TATTGGATCCTTAAGCGTAATCTGGAACATCGTATGGGTAGGCGAGGGTCACGCACAG 3'
*Kpn*I rGPR35 Forward:
5' GCGCGGTACCGCCACCATGAACAATACAAATTGTAGCATCCTCCC 3'
rGPR35-HA *Bam*HI Reverse:
5' GCGCGGTACCGCCACCATGAACAATACAAATTGTAGCATCCTCCC 3'
*Hin*dIII mGPR35 Forward:
5' GCGCAAGCTTGCCACCATGAATAGTACAACCTGTAACAGCACC 3'
mGPR35-HA *Bam*HI Reverse:
5' TACTGGATCCTTAAGCGTAATCTGGAACATCGTATGGGTAGGTGAGGCTCAGGATCTGGG 3'

PCR products were cloned into pcDNA5/FRT/TO for subsequent use in the Flp-In™ T-REx™ system.

2.3.14 Generation of GPR35 phospho-acceptor site mutant constructs

Phospho-acceptor serine and threonine residues in the GPR35 C-terminal tail were mutated to alanine in order to preclude phosphorylation. FLAG-hGPR35-eYFP, FLAG-rGPR35-eYFP and FLAG-mGPR35-eYFP in pcDNA3.1(+) or hGPR35-HA and mGPR35-HA in pcDNA5/FRT/TO were used as templates for site-directed mutagenesis. S/T to A substitutions were introduced using a series of mutagenic primers as detailed in Table 2-1, Table 2-2 and Table 2-3. For multiple mutations spread across >10 bp, site-directed mutagenesis was carried out sequentially using multiple primer pairs. Phosphorylation-deficient mutants (PDMs) of hGPR35, rGPR35 and mGPR35 with all of the C-terminal tail S/T residues mutated were generated in this manner.

2.3.15 Generation of phosphorylation-deficient hGPR35 intramolecular BRET sensor constructs

An intramolecular bioluminescence resonance energy transfer (BRET) sensor construct was generated in order to test the capacity of phosphorylation-deficient GPR35 to couple to $G\alpha_{13}$. FLAG-hGPR35(PDM)-eYFP in pcDNA3.1(+) was used as a PCR template. *Hin*dIII and *Kpn*I restriction sites were introduced to the 5' and 3' termini of the FLAG-hGPR35 open reading frame using the following primers (restriction sites are underlined):

*Hin*dIII FLAG Forward:
5' ACTTAAGCTTGCCACCATGGATTACAAGGATGACG 3'
hGPR35 T307A *Kpn*I Reverse:
5' TAATGGTACCGGCGAGGGCCACGCACAG 3'

The PCR product was inserted upstream of an intramolecular BRET sensor construct in pcDNA5/FRT/TO, consisting of mCitrine linked to NanoLuc® luciferase by an ER/K α-helical linker and fused with the C-terminal 27 amino acids of $G\alpha_{13}$ (mCitrine-ER/K-NanoLuc-$G\alpha_{13}$) or the same construct with no peptide (mCitrine-ER/K-NanoLuc-NP).

Table 2-1 hGPR35 mutagenic primers

Primer sequence (5' to 3')	Template	Mutation	For/Rev
CCAGGAGGCGGCTGCACTGGCCGTG	hGPR35	S287A	For
CACGGCCAGTGCAGCCGCCTCCTGG	hGPR35	S287A	Rev
CCGTGGCTCCCGCTGCTAAGGCCC	hGPR35	S294A	For
GGGCCTTAGCAGCGGGAGCCACGG	hGPR35	S294A	Rev
GGCCCACAAAGCCCAGGACGCTCTGTGCGTG	hGPR35	S300A/S303A	For
CACGCACAGAGCGTCCTGGGCTTTGTGGGCC	hGPR35	S300A/S303A	Rev
GGCCCACAAAGCCCAGGACTCTC	hGPR35	S300A	For
GAGAGTCCTGGGCTTTGTGGGCC	hGPR35	S300A	Rev
CAAAAGCCAGGACGCTCTGTGCGTG	hGPR35	S303A	For
CACGCACAGAGCGTCCTGGCTTTTG	hGPR35	S303A	Rev
CTGTGCGTGGCCCTCGCCGCG	hGPR35-eYFP	T307A	For
CGCGGCGAGGGCCACGCACAG	hGPR35-eYFP	T307A	Rev
CTGTGCGTGGCCCTCGCCTACCC	hGPR35-HA	T307A	For
GGGTAGGCGAGGGCCACGCACAG	hGPR35-HA	T307A	Rev

Mutagenic primer pairs used to introduce Ser/Thr to Ala substitutions to hGPR35 constructs. Altered codons are underlined. For = forward; Rev = reverse; eYFP = enhanced yellow fluorescent protein; HA = haemagglutinin

Table 2-2 mGPR35 mutagenic primers

Primer sequence (5' to 3')	Template	Mutation	Rev
CCAGGAAGCGGCCAAGCCAGCCACG	mGPR35	S286A	For
CGTGGCTGGCTTGGCCGCTTCCTGG	mGPR35	S286A	Rev
TCCAAGCCAGCCACGGCTGCCAACACACCCC	mGPR35	S291A/S292A	For
GGGGTGTGTTGGCAGCCGTGGCTGGCTTGGA	mGPR35	S291A/S292A	Rev
CCCCACAAGGCCCAAGATGCCCAGATCCTGAGC	mGPR35	S298A/S301A	For
GCTCAGGATCTGGGCATCTTGGGCCTTGTGGGG	mGPR35	S298A/S301A	Rev
CCCAGATCCTGGCCCTCGCCTGCGGCCGCATGG	mGPR35-eYFP	S305A/T307A	For
CCATGCGGCCGCAGGCGAGGGCCAGGATCTGGG	mGPR35-eYFP	S305A/T307A	Rev
CCAAGCCAGCCGCGGCTGCCAACACACC	mGPR35-eYFP (S291A/S292A)	T290A	For
GGTGTGTTGGCAGCCGCGGCTGGCTTGG	mGPR35-eYFP (S291A/S292A)	T290A	Rev
CCGCGGCTGCCAACGCACCCCACAAGAGC	mGPR35-eYFP (T290A/S291A/S292A)	T294A	For
GCTCTTGTGGGGTGCGTTGGCAGCCGCGG	mGPR35-eYFP (T290A/S291A/S292A)	T294A	Rev
CCCAGATCCTGGCCCTCGCCTACCCATACGATGTTCC	mGPR35-HA/rGPR35-HA	S305A/T307A	For
GGAACATCGTATGGGTAGGCGAGGGCCAGGATCTGGG	mGPR35-HA/rGPR35-HA	S305A/T307A	Rev

Mutagenic primer pairs used to introduce Ser/Thr to Ala substitutions to mGPR35 constructs. Altered codons are underlined. For = forward; Rev = reverse; eYFP = enhanced yellow fluorescent protein; HA = haemagglutinin

Table 2-3 rGPR35 mutagenic primers

Primer sequence (5' to 3')	Template	Mutation	For/Rev
CCAGGATGCGGCCTTGCGGGCC	rGPR35	S285A	For
GGCCCGCAAGGCCGCATCCTGG	rGPR35	S285A	Rev
CCTTGCGGGCCGCAGCCTCTAGC	rGPR35	T289A	For
GCTAGAGGCTGCGGCCCGCAAGG	rGPR35	T289A	Rev
GCCGCAGCCGCTGCCGCACCCCACAAGAGCC	rGPR35	S291A/S292A/T293A	For
GGCTCTTGTGGGGTGCGGCAGCGGCTGCGGC	rGPR35	S291A/S292A/T293A	Rev
CCCCACAAGGCCCAAGATGCTCAGAGCCTGAGCC	rGPR35	S297A/T300A	For
GGCTCAGGCTCTGAGCATCTTGGGCCTTGTGGGG	rGPR35	S297A/T300A	Rev
CCAAGATACTCAGGCCCTGGCCCTCGCCAGCGGCCGC	rGPR35-eYFP	S302A/S304A/T306A	For
GCGGCCGCTGGCGAGGGCCAGGGCCTGAGTATCTTGG	rGPR35-eYFP	S302A/S304A/T306A	Rev
GCGGGCCGCAGCCGCTGCCGCACCCCACAAGGCCC	rGPR35-eYFP (T289A/S297A)	S291A/S292A/T293A	For
GGGCCTTGTGGGGTGCGGCAGCGGCTGCGGCCCGC	rGPR35-eYFP (T289A/S297A)	S291A/S292A/T293A	Rev
CCCAAGATGCTCAGGCCCTGGCCCTCGCCAGCGGCCGC	rGPR35-eYFP (S289A/S301A)	S302A/S304A/T306A	For
GCGGCCGCTGGCGAGGGCCAGGGCCTGAGCATCTTGGG	rGPR35-eYFP (S289A/S301A)	S302A/S304A/T306A	Rev

Mutagenic primer pairs used to introduce Ser/Thr to Ala substitutions to rGPR35 constructs. Altered codons are underlined. For = forward; Rev = reverse; eYFP = enhanced yellow fluorescent protein; HA = haemagglutinin

2.4 Mammalian cell culture

2.4.1 Maintenance of mammalian cell lines

2.4.1.1 HEK293T cells

Human embryonic kidney 293 cells transformed with large T-antigen (HEK293T cells) were maintained in Dulbecco's Modified Eagle's Medium supplemented with 10% (v/v) heat-inactivated foetal calf serum (FCS), 2 mM L-glutamine., 100 units/mL penicillin and 100 µg/mL streptomycin at 37°C and 5% CO_2 in a humidified atmosphere.

2.4.1.2 Flp-In T-REx-293 cells

Flp-In T-REx HEK293 cells (Life Technologies) were maintained in Dulbecco's Modified Eagle's Medium High Glucose without Sodium Pyruvate supplemented with 10% (v/v) heat-inactivated FCS, 100 units/mL penicillin, 100 µg/mL streptomycin and 10 µg/mL blasticidin at 37°C and 5% CO2 in a humidified atmosphere.

2.4.1.3 Cryopreservation

Cell lines were cryopreserved for long-term storage in liquid nitrogen. Confluent cells were detached by incubating with trypsin-EDTA and subjected to centrifugation at 500 x *g* for 5 min. The pellet was resuspended in 2-3 mL FCS + 10% (v/v) DMSO and 1 mL aliquots frozen at − 80°C before transferring to liquid nitrogen storage. Cryopreserved cells were revived by thawing rapidly in a 37°C water bath and transferring to 10 mL pre-warmed culture medium in a flask. Medium was changed after 8-16 hours to remove DMSO.

2.4.2 Transient transfection of cell lines

2.4.2.1 Polyethyleimine (PEI)

PEI transient transfection was used as the default method of transient transfection. For a 10 cm^2 culture dish, 5 µg of DNA was diluted in 250 µL 150 mM NaCl and mixed 1:1 with 250 µL 150 mM NaCl containing 30 µg PEI. The mixture was vortexed for 10 sec and incubated for 10 min at room temperature

before adding dropwise to the dish. This procedure was scaled down for 6-well plates. Cells were incubated with the PEI overnight at 37°C, then transfection medium was replaced with fresh culture medium. Cells were incubated for a further 24–48 hours before using in assays.

2.4.2.2 Lipofectamine®

For applications where PEI transfection negatively affected cell morphology and assay reliability, cells were transiently transfected using Lipofectamine (Life Technologies) as per the manufacturer's instructions. For a 6-well plate, 0.5–2.5 µg DNA was diluted in 100 µL Opti-MEM® and mixed 1:1 with 100 µL Opti-MEM containing 5 µL Lipofectamine reagent. The mixture was incubated for 5 min at room temperature before adding dropwise to the well. Cells were incubated with the Lipofectamine for 4–5 hours, then transfection medium was replaced with fresh culture medium or induction medium. Cells were incubated for a further 24–48 hours before using in assays.

2.4.3 Stable transfection of cell lines

2.4.3.1 Flp-In T-REx doxycyline-inducible 293 cells

GPR35-HA and GPR35 intramolecular BRET sensors were stably transfected into HEK293 cells using the Flp-In T-REx system. The pcDNA5/FRT/TO vector containing the relevant cDNA was transfected into Flp-In T-REx-293 parental cells using the FRT stable integration site. Cells were co-transfected with the relevant cDNA/pcDNA5/FRT/TO construct and the pOG44 Flp recombinase vector in a 1:8 ratio using PEI. After 48 hours, cells were subcultured 1:10 and 1:30, and 24 hours later medium was changed to maintenance medium plus 10 µg/mL blasticidin and 200 µg/mL hygromycin to select for stable transfectants. Medium was changed every three days until individual colonies were visible by eye (10–14 days). Cells were then detached by incubating with trypsin-EDTA and pooled to give polyclonal cell lines which were maintained in blasticidin/hygromycin selection medium. When required, expression of the integrated gene was induced by addition of 100 ng/mL doxycycline (Dox) for 18-24 h.

2.4.3.2 CRISPR-modified HEK293T cells

Clustered regularly interspaced short palindromic repeats (CRISPR)-modified HEK293T cell lines with ß-arrestin-1/2 or $G\alpha_{12/13}$ knocked out (Arr KO and $G_{12/13}$ KO, respectively) and the equivalent parental cell line were obtained from Asuka Inoue (Tohoku University, Japan). Stable cell lines constitutively expressing FLAG-hGPR35-eYFP or FLAG-hGPR35(PDM)-eYFP were generated in order to assess ß-arrestin- and $G\alpha_{12/13}$-mediated responses. Cells were transfected with the relevant cDNA in pcDNA3.1/Hygro(+) using PEI as described in section 2.4.2.1. After 48 hours, cells were subcultured 1:500, 1:1000 and 1:2000, and 24 hours later medium was changed to maintenance medium plus 200 µg/mL hygromycin to select for stable transfectants. Medium was changed every three days until individual colonies were visible by eye (10–14 days). Individual colonies were picked into 24-well plates and scaled up to give monoclonal cell lines which were maintained in hygromycin selection medium.

2.5 Assessing receptor expression

2.5.1 Immunocytochemistry

Immunocytochemistry was used to assess receptor expression and subcellular localisation. Cells were seeded at 3 x 10^5 cells/well on poly-D-lysine-coated 22 mm round coverslips in 6-well plates and incubated overnight at 37°C. Cells were washed twice in PBS and fixed with 3.7% (w/v) paraformaldehyde (PFA) in PBS for 10 min at room temperature. Fixed cells were washed 3 x 5 min in PBS and blocked with 3% (w/v) non-fat milk in PBS or blocked and permeabilised with 3% (w/v) non-fat milk and 0.15% (v/v) Triton-X100 in PBS for 10 min at room temperature. Cells were then incubated with primary antibody (rat anti-HA High Affinity (Roche) 1:100 dilution) in 3% (w/v) non-fat milk for 1 hour at room temperature, washed 3 x 5 min in PBS, then incubated with secondary antibody (Alexa Fluor® 594-goat anti-rat IgG (Molecular Probes) 1:500 dilution) in 3% (w/v) non-fat milk for 1 hour at room temperature. Cells were washed 3 x 5 min in PBS and coverslips were mounted onto glass slides using Immu-Mount™ (Fisher Scientific). Images were taken using a Nikon Eclipse TE2000 epifluorescence microscope with Coolsnap HQ camera using the rhodamine filter and x40 oil immersion objective.

2.5.2 Cell surface enzyme-linked immunosorbent assay (ELISA)

Cell surface expression of receptors was quantified by live-cell ELISA. Cells were seeded at 6 x 10^4 cells/well in poly-D-lysine-coated clear 96-well plates and incubated overnight at 37°C. Cells were incubated with primary antibody (mouse monoclonal anti-FLAG M2 (Sigma-Aldrich) 1:1000) in culture medium for 30 min at 37°C, then washed once with DMEM-HEPES and incubated with secondary antibody (Horseradish peroxidase (HRP)-sheep anti-mouse IgG (GE Healthcare) 1:5000) and 10 µg/mL Hoechst 33342 in culture medium for 30 min at 37°C protected from light. Cells were then washed twice with warmed (37°C) PBS. During the second wash, the Hoechst 33342 signal (excitation 355 nm, emission 460 nm) was read on a POLARStar® Omega (BMG Labtech). Finally, PBS was removed and 100 µL/well room temperature TMB substrate was added. The plate was incubated for 5 min at room temperature protected from light, then the absorbance at 620 nm was read on a POLARStar Omega. Absorbance was corrected for cell number by dividing by the Hoechst 33342 signal.

2.6 Pharmacological and functional assays

2.6.1 [^{32}P] phospholabelling assay

Flp-In T-REx-293 GPR35-HA cells were seeded in 6-well plates at 2 x 10^5 cells/well and incubated overnight at 37°C. GPR35-HA expression was induced by adding 100 ng/mL doxycycline and incubating overnight at 37°C. Cells were washed three times with Krebs/HEPES buffer without phosphate and incubated in this buffer plus 100 µCi/mL [^{32}P]-orthophosphate for 90 min at 37°C. Cells were pre-treated with antagonist for 5 min where stated, then stimulated for 5 min with vehicle only (DMSO) or agonist and immediately lysed by addition of 750 µL/well lysis buffer containing cOmplete™ EDTA-free Protease Inhibitor Cocktail (Roche) and PhosSTOP™ Phosphatase Inhibitor Cocktail (Roche). Lysates were incubated on ice for 5 min, then cleared by centrifugation at 20,000 x *g* for 20 min at 4°C. GPR35-HA was immunoprecipitated from the cleared lysates using anti-HA affinity matrix (Roche). Lysates were incubated with 50 µL affinity matrix suspension with rotation for 2 h at 4°C. Immunoprecipitate was collected by centrifuging at 1000 x *g* for 1 min and washed 3 x with lysis buffer, subjecting to centrifugation and aspirating supernatant after each wash. GPR35-HA was

eluted from the matrix by adding 50 µL Laemmli buffer, vortexing and incubating at 65°C for 10 min. Immunoprecipitates were separated by SDS-PAGE on 10% Bis-Tris acrylamide gels, which were dried and exposed to X-ray film overnight at − 80°C. A small amount of each sample was run in parallel on a separate gel, then transferred to PVDF membrane and immunoblotted for GPR35-HA. Bands were quantified by densitometry using ImageJ software.

2.6.2 β-arrestin recruitment BRET assay

A BRET-based ß-arrestin recruitment assay was used to assess the effect of C-terminal tail mutations on ß-arrestin coupling. HEK293T cells were seeded in 10 cm^2 dishes and transiently co-transfected with wild type or mutant FLAG-GPR35-eYFP and ß-arrestin-2 fused with *Renilla* luciferase (ß-arrestin-2-RLuc) in a 4:1 ratio using PEI, as described in section 2.4.2.1. Control cells were transfected with ß-arrestin-2-RLuc only. After 24 hours, cells were detached by incubating with trypsin-EDTA and seeded at 6 x 10^4 cells/well in poly-D-lysine-coated white 96-well plates, then incubated overnight at 37°C. Cells were washed once with pre-warmed (37°C) HBSS and incubated in HBSS for 30–60 min at 37°C. During incubation, the eYFP signal (excitation 485 nm, emission 520 nm) was read on a PHERAstar® FS (BMG Labtech) to estimate relative receptor expression. The RLuc substrate coelenterazine-h (Promega) was added to a final concentration of 5 µM and the plate incubated for 10 min at 37°C protected from light. Agonist was added at the relevant concentrations in triplicate and the plate incubated for a further 5 min at 37°C, then the emissions at 475 nm and 535 nm were read on a PHERAstar FS. Since coelenterazine h luminesces at 475 nm and eYFP is excited at 475 nm and emits at 535 nm, net BRET values were obtained by dividing the emission at 535 nm by the emission at 475 nm and subtracting the 535 nm/475 nm ratio for cells expressing only the ß-arrestin-2-RLuc donor (the basal BRET):

Net BRET = (em535 nm/em475 nm) – (em535 nm/em475 nm (RLuc only))

2.6.3 $G\alpha_{13}$ intramolecular BRET sensor assay

An assay using the $G\alpha_{13}$ intramolecular BRET sensor described in section 1.1.1 was used to assess the effect of C-terminal mutations on $G\alpha_{13}$ recruitment.

Flp-In T-REx-293 cells stably transfected with the relevant GPR35 sensor were seeded at 6 x 10^4 cells/well in poly-D-lysine-coated white 96-well plates and incubated for 6 hours at 37°C before adding 100 ng/mL doxycycline and incubating overnight at 37°C to induce GPR35 sensor expression. Cells were washed once with pre-warmed (37°C) HBSS and incubated in HBSS for 30–60 min at 37°C. During incubation, the mCitrine signal (excitation 485 nm, emission 520 nm) was read on a PHERAstar FS to estimate receptor expression. The NanoLuc substrate Nano-Glo® (Promega) was added to a final dilution of 1:800 and the plate incubated for 10 min at 37°C protected from light. Agonist was added at the relevant concentrations in triplicate and the plate incubated for a further 5 min at 37°C, then the emissions at 455 nm and 530 nm were read on a CLARIOstar® (BMG Labtech). Since NanoGlo luminesces at 455 nm and mCitrine is excited at 455 nm and emits at 530 nm, BRET Ratio values were obtained by dividing the emission at 530 nm by the emission at 455 nm:

BRET Ratio = (em530 nm/em455 nm)

2.6.4 Receptor internalisation

2.6.4.1 Qualitative receptor internalisation

Receptor internalisation was qualitatively examined using live-cell confocal microscopy. Cells were seeded at 0.5–1 x 10^5 cells/well on poly-D-lysine-coated 30 mm round coverslips in 6-well plates and incubated for at least 48 hours at 37°C to recover normal morphology after seeding. For transient transfection, cells were transfected using Lipofectamine, as described in section 2.4.2.2, 24 hours after seeding. Cells were washed once with HBSS and coverslips were placed in a microscope chamber containing HBSS. eYFP images were taken before treatment and at 15 min intervals following addition of agonist. Images were acquired on a ZEISS Axio Observer.Z1 microscope fitted with a spinning disk structured illumination Viva Tome, using narrow band 490/20 nm excitation and 536/40 nm emission and a 63x oil-immersion Plan-Apochromat objective, and captured on an Axiocam MRm charge-coupled device camera. Images were optically sectioned using AxioVision software (ZEISS).

2.6.4.2 ArrayScan quantitative internalisation assay

Receptor internalisation was quantitatively assessed using ArrayScan high content analysis. Cells were seeded at 4 x 10^4 cells/well in poly-D-lysine coated black-walled, clear-bottomed 96-well plates and incubated overnight at 37°C. Culture medium was replaced with serum-free medium containing agonist concentrations in triplicate. Cells were incubated with agonist for 45 min, then washed once with PBS and fixed with 3.7% (w/v) paraformaldehyde for 1 hour at room temperature. Fixed cells were washed three times with PBS, then stained with 10 µg/mL Hoechst 33342 for 30 min at room temperature protected from light. Cells were washed 3x with PBS before acquiring eYFP and DAPI images using a Cellomics ArrayScan II high content imager. Internalisation was quantified using an algorithm designed to identify the number of individual 'endosomal recycling compartments' in the eYFP channel, which was normalised against cell number using the Hoechst 33342 signal in the DAPI channel.

2.6.5 Actin cytoskeleton staining

To assess GPR35-mediated effects on actin cytoskeletal rearrangement, F-actin was stained with tetramethylrhodamine B isothiocyanate (TRITC)-labelled phalloidin. Cells were seeded at 0.5–1 x 10^5 cells/well on poly-D-lysine-coated 22 mm round coverslips in 6-well plates and incubated for at least 48 hours at 37°C to recover normal morphology after seeding. Cells were treated with agonist/antagonist, then washed twice with PBS and fixed with 3.7% (w/v) paraformaldehyde for 20 min at room temperature. Fixed cells were washed twice with PBS, permeabilised with 0.1% (v/v) Triton X-100 in PBS for 20 min at room temperature and blocked with 0.5% (w/v) bovine serum albumin (BSA) in PBS for 1 hour at 37°C. Cells were washed twice with PBS and stained with 5 µg/mL phalloidin-TRITC (Sigma-Aldrich) in PBS for 1 hour at room temperature protected from light. Cells were washed three times with PBS and coverslips were mounted onto glass slides using Immu-Mount (Fisher Scientific). Images were acquired on a ZEISS Axio Observer.Z1 microscope fitted with a spinning disk structured illumination Viva Tome, using a 40x oil-immersion Plan-Apochromat objective. Emission at 610 nm was imaged using an Axiocam MRm charge-coupled device camera. Images were optically sectioned using AxioVision software (ZEISS).

2.7 Immunoblotting

2.7.1 Sample preparation

2.7.1.1 Whole-cell lysates

Cells were seeded in 6-well plates and cultured until confluent, then stimulated with the relevant ligand(s). To lyse, cells were washed twice with ice-cold PBS and immediately lysed with 200 µL/well RIPA buffer containing cOmplete™ EDTA-free Protease Inhibitor Cocktail (Roche) (and PhosSTOP™ Phosphatase Inhibitor Cocktail (Roche) if immunoblotting for phosphoproteins). Lysates were passed 5x through a 25 gauge needle, rotated at 4°C for 30 min and then subjected to centrifugation at 20,000 x *g* for 10 min at 4°C to remove debris.

2.7.1.2 Membrane and cytosolic fractions

Cells were seeded in 10 cm dishes and cultured until confluent. Cells were washed once with ice-cold PBS and detached by scraping into 2–3 mL ice-cold PBS, then subjected to centrifugation at 1750 x *g* for 5 min at 4°C. Cell pellets were incubated at – 80°C for at least 30 min. Thawed pellets were resuspended in 1 mL TE buffer containing cOmplete™ EDTA-free Protease Inhibitor Cocktail (Roche) and homogenised by passing 50 x in a Dounce homogeniser and passing 5 x through a 25 gauge needle. Homogenate was subjected to centrifugation at 500 x *g* for 5 min at 4°C to remove cell debris. Supernatants were carefully collected and subjected to centrifugation at 100,000 x *g* for 60 min at 4°C. For cytosolic fractions, supernatant was collected. For membrane fractions, membrane pellets were resuspended in 400 µL TE buffer containing protease inhibitors and passed 5x through a 25 gauge needle.

2.7.1.3 Determination of protein concentration

Protein concentrations of samples for immunoblotting were determined by bicinchoninic assay (BCA), using a standard curve of 0.2–2 µg/µL BSA. 10 µL of sample or standard was added to a clear 96-well plate. Proteoquant BCA Reagent B (Expedeon) was diluted 1:50 in Proteoquant BCA Reagent A (Expedeon) and 200 µL/well added to the samples. The plate was incubated at 37°C for 15 min before reading the absorbance at 562 nm on a POLARStar Omega

(BMG Labtech). Sample concentrations were interpolated from the standard curve. Samples were diluted to 1 µg/µL, then aliquoted and stored at − 20°C.

2.7.2 SDS-PAGE and protein transfer

Protein samples were separated by sodium dodecyl sulphate polyacrylamide gel electrophoresis (SDS-PAGE). Samples were denatured by adding 2 x Laemmli buffer and incubating at 65°C for 10 min. 10–30 µg protein/well was loaded onto BOLT® 4–12% Bis-Tris Plus Gels (Life Technologies) or NuPAGE® Novex® 4–12% Bis-Tris Gels (Life Technologies). Gels were run in NuPAGE® MOPS SDS Running Buffer (Life Technologies) at 200 V for 30–50 min. Proteins were transferred from the gel onto nitrocellulose membrane using a wet transfer system. Proteins were transferred in transfer buffer at 35 V for 90 min.

2.7.3 Probing and detection

2.7.3.1 Probing for chemiluminescent detection (GPR35-HA)

GPR35-HA was detected using chemiluminescence. Membranes were blocked in 5% (w/v) BSA for 1 hour at room temperature or overnight at 4°C, then incubated for 1 hour at room temperature with rat anti-HA High Affinity (Roche) at 1:1000 dilution in TBS with 0.5% (v/v) NP-40, 10% (v/v) goat serum and 5% (w/v) BSA. Membranes were washed 5 x 5 min in TBS with 0.5% (v/v) NP-40, then incubated for 1 hour at room temperature with HRP-goat anti-rat IgG (Sigma-Aldrich) at 1:5000 dilution in the same buffer. Membranes were washed 5 x 5 min in TBS with 0.5% (v/v) NP-40, and bands were detected using Immobilon Western Chemiluminescent HRP Substrate (Millipore).

2.7.3.2 Probing for fluorescent detection

All other proteins were detected using fluorescent detection on a LI-COR® Odyssey system. Antibodies used are detailed in Table 2-4. Membranes were blocked in LI-COR Blocking Buffer (PBS) (or (TBS) for phosphoproteins) for 1 hour at room temperature, then incubated with primary antibody in blocking buffer with 0.2% (v/v) Tween-20 overnight at 4°C. Membranes were washed 5 x 5 min with PBS or TBS with 0.1% (v/v) Tween-20, then incubated with IRDye® fluorescently labelled secondary antibody in blocking buffer with 0.2% (v/v)

Tween-20 for 1 hour at room temperature protected from light. Membranes were washed 5 x 5 min with PBS or TBS with 0.1% (v/v) Tween-20, then imaged on a LI-COR Odyssey using the 700 nm and 800 nm channels.

Table 2-4 Antibodies used in immunofluorescent immunoblotting

Antibody	Supplier	Dilution
Primary antibodies		
Anti-HA High Affinity (rat)	Roche	1:1000
Monoclonal anti-FLAG M2 (mouse)	Sigma-Aldrich	1:1000
Gα12 Antibody (S-20) (rabbit)	Santa Cruz Biotechnology	1:1000
Gα13 Antibody (A-20) (rabbit)	Santa Cruz Biotechnology	1:1000
β-arrestin-1 (D8O3J) rabbit mAb	Cell Signaling Technology	1:1000
β-arrestin-2 (CD16D9) rabbit mAb	Cell Signaling Technology	1:1000
Anti-β-tubulin mouse monoclonal	Sigma-Aldrich	1:500
Secondary antibodies		
IRDye 800CW Goat anti-Rat IgG*	LI-COR	1:10000
IRDye 680RD Goat anti-Mouse IgG*	LI-COR	1:15000
IRDye 800CW Donkey anti-Rabbit IgG*	LI-COR	1:10000
IRDye 680RD Donkey anti-Rabbit IgG*	LI-COR	1:10000

*When multiplexing, IRDye 800CW was used to detect the lower abundance protein i.e. G protein or β-arrestin and IRDye 680RD was used to detect the loading control.

2.8 Mass spectrometry

2.8.1 Sample preparation

Flp-In T-REx-293 GPR35-HA cells were seeded in 10 x T150 flasks and grown until confluent, then GPR35-HA expression was induced by adding 100 ng/mL doxycycline and incubating overnight at 37°C. Cells were washed once with Krebs/HEPES buffer containing 1.18 μM KH_2PO_4 , and incubated in this buffer for 90 min at 37°C. After stimulating with 100 μM zaprinast for 5 min at 37°C, the cells were harvested in 1 mL/flask PBS containing 1 mM EDTA. Cells were subjected to centrifugation at 1000 x *g* for 5 min and the cell pellet was resuspended in 10 mL TE buffer containing cOmplete EDTA-free Protease Inhibitor Cocktail (Roche) and PhosSTOP™ Phosphatase Inhibitor Cocktail (Roche). Cells were homogenised by sonication and the homogenate subjected to centrifugation at 40,000 x *g* at 4°C. The membrane pellet was solubilised in 5 mL TBS containing 1% (v/v) NP-40 plus protease and phosphatase inhibitor cocktails and incubated on ice for 1 hour. After centrifugation at 20,000 x *g* for 20 min at

4°C, the supernatant was diluted 1:1 in TBS, and GPR35-HA was immunoprecipitated using anti-HA affinity matrix (Roche). The sample was incubated with 100 µL affinity matrix suspension with rotation overnight at 4°C. After extensive washing with TBS containing 0.5% (v/v) NP-40 followed by a final wash with TBS containing 500 mM NaCl, GPR35-HA was eluted from the matrix by adding 100 µL Laemmli buffer. The sample was resolved by SDS-PAGE on 10% Bis-Tris acrylamide gels. Gels were exposed to X-ray film overnight at − 80°C. GPR35-HA bands were excised by overlaying the exposed film, and the gel pieces were washed 3 x 15 min with 100 mM triethylammonium bicarbonate (TEAB). Disulfide bonds were reduced and alkylated by incubation with 10 mM DTT in 50 mm TEAB at 60°C for 30 min followed by 100 mM iodoacetamide in 50 mm TEAB at room temperature for 30 min protected from light. Gel slices were dehydrated by washing 3 x 15 min in 50 mM TEAB with 50% (v/v) acetonitrile and 1 x 15 min in 100% acetonitrile, then resuspended in 50 mM TEAB with 10% (v/v) acetonitrile and incubated overnight at 37°C with 1 µg sequencing grade trypsin. The resulting tryptic peptides were extracted by vortexing three times with 50 mM TEAB with 50% (v/v) acetonitrile and pooling the washes. Peptides were dried and resuspended in 30 µL 0.1% (v/v) trifluoroacetic acid and the pH adjusted to <2 with 1% (v/v) trifluoroacetic acid.

2.8.2 Mass spectrometry

Mass spectrometry was carried out by Dr. Andrew Bottrill at the University of Leicester Proteomics Facility. Samples were analysed as described previously (Butcher et al., 2014). LC-MS/MS was carried out using an LTQ Orbitrap mass spectrometer (Thermo Fisher Scientific). A reverse-phase trapping column (0.3 mm inner diameter x 1 mm) containing 5 µm C_{18} 300 Å Acclaim PepMap medium (Dionex) was loaded with the tryptic peptides at high flow rate. Peptides were eluted through a reverse phase capillary column (75 µm inner diameter x 150 mm) containing Symmetry C_{18} 100 Å medium (Waters) that was self-packed using a high pressure packing device (Proxeon Biosystems) (Butcher et al., 2014).

2.8.3 Mass spectrometry data analysis

Spectra were searched against the UniProtKB/Swiss-Prot database using Mascot software (Matrix Science Ltd.) with peptide tolerance set to 5 ppm and the MS/MS tolerance set to 0.6 Da. Fixed modifications were set as carbamidomethylcysteine with variable modifications of phosphoserine, phosphothreonine, phosphotyrosine, and oxidized methionine. The enzyme was set to trypsin/Pro, and up to two missed cleavages were allowed. Spectra of phosphorylated peptides were manually inspected to verify phosphorylated residues using Scaffold software (Proteome Software).

2.9 Experimental animals

2.9.1 Maintenance of experimental animals

Animals were housed under 12 hour light/dark cycles (0700–1900 light, 1900–0700 dark) at ambient temperature and were maintained on normal chow (Rat and Mouse No. 1 maintenance diet, Special Diet Services). All animals used for experimental procedures were adult males. All procedures were conducted in accordance with the Animals (Scientific Procedures) Act 1986 under project licence 60/4286, held by Dr. Delyth Graham (University of Glasgow).

2.9.2 GPR35 knockout (KO) mouse

2.9.2.1 Breeding

A colony of GPR35 KO mice was established at the University of Glasgow in 2014. Animals were obtained from the Genomics Institute of the Novartis Research Foundation, San Diego. An inbred colony of homozygous (HO) KO animals was maintained to supply female HO KO breeders. F1 hemizygous (HE) offspring were generated by breeding HO KO females with C57BL/6 males (Charles River). HO wild type (WT) and KO littermates (F2 offspring) were generated by breeding F1 HE males with F1 HE females. All experimental procedures were carried out on male F2 HO littermates.

2.9.2.2 Genotyping

Genotypes were determined by end-point PCR on genomic DNA extracted from ear notches. DNA was extracted using the DNeasy® Blood and Tissue Kit (QIAGEN) as per the manufacturer's instructions. Briefly, tissue was digested with proteinase K overnight at 56°C, lysed by the addition of lysis buffer and passed through a DNeasy Mini spin column by centrifuging at 6000 x *g* for 1 min. The column was washed once with a guanidine hydrochloride-containing buffer and once with an ethanol-containing buffer. DNA was eluted in 50 µL nuclease-free water. Fragments of wild type mGPR35 and the knockout construct were amplified by PCR using the following primers:

mGPR35 Forward:
5' ATCGCATGCACCAGTGGACAGAGAC 3'
Neo Forward:
5' GACGAGTTCTTCTGAGGGGATCGATC 3'
mGPR35 Reverse:
5' GGTCCACAGCAATGGCAGTGACCAG 3'

20 µL PCR reactions were set up using the following components:

- 1 x HotStarTaq® PCR Buffer (QIAGEN) (contains 1.5 mM $MgCl_2$)
- 2 mM MgCl2 (3.5 mM total)
- 1.6 mM (0.4 mM each) dNTP mix
- 0.3 µM each primer
- 50 ng genomic DNA
- 2.5 units HotStarTaq DNA Polymerase (QIAGEN)

Reaction mixtures were subjected to thermal cycling using the following conditions:

1.	Preheating	94°C	15 min
2.	Denaturing	94°C	30 sec
3.	Annealing	60°C	30 sec
4.	Extension	72°C	45 sec
5.	Repeat steps 2–4 (x 34)		
6.	Final extension	72°C	5 min
7.	Hold	4°C	∞

The presence of the WT and KO PCR products was assessed by agarose gel electrophoresis (section 2.3.7).

2.9.3 Stroke-prone spontaneously hypertensive rat (SHRSP)

An inbred colony of SHRSP, originally obtained from the Department of Anatomy and Cell Biology at the University of Michigan, has been maintained in-house at the University of Glasgow since 1991 (Dominiczak et al., 1993).

2.10 *In vivo* procedures

2.10.1 Experimental design

Group numbers for blood pressure measurements were based on historical systolic blood pressure recordings in male SHRSP rats of 196.6 ± 10.2 (standard deviation) mmHg. For 80% power and $\alpha = 0.05$, 8 animals per group were required to detect a biologically meaningful difference of 15 mmHg. For the Ang II infusion model, the blood pressure difference was expected to be approximately 20 mmHg and so the group size was reduced to 6. Animals were randomly allocated into treatment groups by an independent observer and the experimenter was blinded to treatments until after analysis was performed. If telemetry readings were outside of the physiological blood pressure range (due to technical error such as displacement of the probe) at any time over the duration of the study period, the entire dataset for that animal was excluded prior to unblinding.

2.10.2 Surgical procedures

Recovery surgery was carried out under aseptic conditions, and animals were anaesthetised with 1 L/min 2.5% isoflurane and 1.5 L/min medical O_2 throughout the procedure. Fur was removed from the incision area using clippers, and the skin was sterilised with Betadine povidone-iodine solution or Vetasept chlorhexidine solution. Following recovery surgery, animals were weighed and recovered in a 32°C hot box until fully conscious, and monitored daily by weighing to assess post-operative health.

2.10.3 Blood pressure monitoring by telemetry

2.10.3.1 Telemetry probe implantation in the mouse

PhysioTel® PA-C10 pressure transmitters (DSI) were surgically implanted into 12-13-week old mice, with the transmitter positioned subcutaneously on the right shoulder and the catheter inserted into the left carotid artery, as previously described (Huetteman and Bogie, 2009). The transmitters were calibrated to verify accuracy to within 3 mmHg before implantation. With the animal in a prone position, a 10 mm incision was made on the right shoulder and a subcutaneous pocket made towards the flank by blunt dissection. The transmitter was positioned in the pocket and the animal placed in a supine position to make the second incision. A vertical 15 mm midline incision was made in the neck, and a Luer-Lock needle was used to tunnel the catheter under the skin towards the incision. The remainder of the procedure was performed under 16x magnification. The mandibular glands were separated to expose the trachea, and the left carotid artery was isolated by blunt dissection. The artery was permanently ligated with 5-0 Mersilk suture (Ethicon) at the bifurcation of the internal and external branches. The suture was retracted towards the head of the mouse, and a second length of suture was placed approximately 10 mm below the first and retracted towards the tail to occlude blood flow. A third suture was positioned between the first and second and tied loosely, to be secured around the catheter after insertion. A 30-gauge needle was bent to approximately 100° with the bevel facing up, and used to puncture the ventral wall of the artery. Right-angled forceps were used to lift the wall at the puncture site in order to insert the catheter. Once inserted, the middle suture

was tightened around the artery and catheter, and the tension on the caudal suture was released to allow advancement of the catheter towards the transverse aorta. The caudal suture was tied around the artery and catheter, and finally the cranial suture was released and used to tie a final knot around the catheter at the point of ligation. Both incisions were sutured using 4-0 coated Vicryl absorbable suture (Ethicon) and the animal administered with analgesic (5 mg/kg carprofen) by subcutaneous injection.

2.10.3.2 Telemetry probe implantation in the rat

PhysioTel PA-C40 pressure transmitters (DSI) were surgically implanted into 8–9-week old rats, with the transmitter positioned intraperitoneally and the catheter inserted into the abdominal aorta, as previously described (Huetteman and Bogie, 2009). The transmitters were calibrated to verify accuracy to within 3 mmHg before implantation. A vertical 30 mm midline incision was made in the abdomen, and the intestines positioned outside the peritoneum on sterile, PBS-soaked gauze. The remainder of the procedure was performed under 10x magnification. A length of 5-0 Mersilk suture was positioned under the aorta approximately 20 mm above the common iliac bifurcation, and retracted towards the head to occlude blood flow. A 30-gauge needle was bent to approximately 100° with the bevel facing up, and used to puncture the ventral wall of the artery. Right-angled forceps were used to lift the wall at the puncture site in order to insert the catheter and advance it towards the heart. The insertion site was sealed using hemostatic gauze and Vetbond tissue adhesive. The intestines were replaced into the peritoneum and the transmitter was secured by suturing to the abdominal wall whilst closing the muscle layer using non-absorbable 4-0 Ethilon suture (Ethicon). The skin was sutured with 4-0 coated Vicryl, and the animal was administered with analgesic (5 mg/kg carprofen) by subcutaneous injection.

2.10.3.3 Data recording and analysis

Following a 7-day recovery period, transmitters were remotely switched on and measurements of systolic blood pressure, diastolic blood pressure, heart rate and activity (an arbitrary measure of locomotion) were recorded using the Dataquest IV Telemetry System (DSI). Measurements were recorded every 5 min

for the duration of the study. These were used to calculate daily and nightly means based on the 12-hour light/dark cycle in order to show diurnal variation, or converted into 24-hour means.

2.10.4 Blood pressure monitoring by tail cuff plethysmography

Non-invasive tail cuff plethysmography was used to measure systolic blood pressure in 6–8-week old SHRSP. Rats were trained by taking several mock measurements before commencing the study. Rats were placed at 30°C for 15 min prior to the procedure, and the procedure was carried out on a heat mat to encourage vasodilation. Rats were restrained by hand to minimise distress, and an inflatable cuff with a built-in piezoceramic transducer was positioned at the base of the tail. Approximately 10 readings were taken in each session. Outlying readings were discarded and the mean of the remaining readings was taken.

2.10.5 Echocardiography

M-mode echocardiography was used to assess cardiac function in mice, as described by Ram et al. (Ram et al., 2011). M-mode echocardiographic images were obtained using a Siemens Acuson Sequoia 512 ultrasound unit with an 18LS probe set at a frequency of 14 MHz. Animals were anaesthetised with 1 L/min 1.5% isoflurane and 1.5 L/min medical O2 throughout the procedure. Animals were placed in a supine position on a heat mat and fur was removed from the chest area using clippers. Ultrasound gel was applied to the probe and M-mode images obtained on the longitudinal axis just above the papillary muscle. Left ventricular dimensions during systole and diastole were measured using ImageJ software, as shown in Figure 2-1. Measurements were taken from nine separate cardiac cycles over three different images. Fractional shortening (FS), end systolic volume (ESV), end diastolic volume (EDV) and ejection fraction (EF) were calculated using the following equations:

$$FS\ (\%) = ((LVEDD - LVESD)/LVEDD) \times 100$$

$$ESV\ (mL) = (7/(2.4 + LVESD)) \times LVESD^3$$

$$EDV\ (mL) = (7/(2.4 + LVEDD)) \times LVEDD^3$$

$$EF\ (\%) = ((EDV - ESV)/EDV) \times 100$$

Where LVEDD = left ventricular end diastolic dimension and LVESD = left ventricular end systolic dimension. ESV and EDV were derived using the Teichholz method (Teichholz et al., 1976).

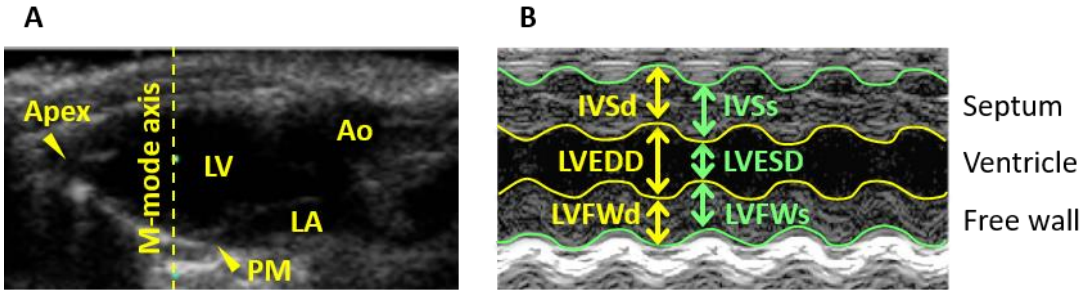

Figure 2-1 Measuring LV dimensions using M-mode echocardiography (A) Longitudinal B-mode image showing visible heart regions (LV = left ventricle; LA = left atrium; Ao = aorta; PM = papillary muscle) and the axis used to generate 1-dimensional M-mode images. **(B)** M-mode image showing dimensions measured (IVSd = intraventricular septum in diastole; IVSs = intraventricular septum in systole; LVEDD = left ventricular end diastolic dimension; LVESD = left ventricular end systolic dimension; LVFWd = left ventricular free wall in diastole; LVFWs = left ventricular free wall in systole.)

2.10.6 Subcutaneous infusion of Ang II

Ang II was administered by subcutaneous infusion using ALZET® micro-osmotic pumps (Model 1002, Charles River). Treatment commenced at 13–14 weeks of age (seven days after telemetry implantation) and continued for two weeks until sacrifice. Angiotensin II human (Sigma-Aldrich) was dissolved in water and sterilised by passing through a 0.2 µm filter. Pumps were filled with the appropriate concentration of Ang II to deliver a dose of 400 ng/kg/min (24 µg/kg/hour) at a flow rate of 0.25 µL/hour. After filling as per the manufacturer's instructions, pumps were primed in sterile saline overnight at 37°C. Pumps were subcutaneously implanted on the left flank (the opposite side to telemetry apparatus) under aseptic conditions. A 10 mm incision was made

below the left shoulder and a large subcutaneous pocket made towards the flank by blunt dissection. The pump was inserted into the pocket, then the incision was sutured with 4-0 coated Vicryl and the animal administered with analgesic (5 mg/kg carprofen) by subcutaneous injection.

2.10.7 Oral administration of amlexanox

Amlexanox was dissolved in DMSO to a stock concentration of 20 mM. Daily dosing commenced at six weeks of age and continued for six weeks until sacrifice. Treated animals received a daily dose of 2.5 mg/kg/day in highly palatable egg custard baby food. Control animals received an equivalent volume of DMSO in egg custard baby food.

2.11 Wire myography

2.11.1 Isolation and mounting

Aortas and mesenteric arteries were isolated from experimental animals for use in wire myography. Aortas and mesenteries were collected at sacrifice under terminal anaesthesia and placed immediately into ice-cold PSS. Fat and connective tissue was removed and 2 mm lengths of vessel were dissected in PSS under a dissecting microscope. For mesenteric arteries, only second or third order vessels with a diameter <200 μm were used. Vessels were mounted onto 40 μm (aortas) or 25 μm (mesenteric arteries) wires on a four-channel multi myograph system (DMT), as originally described by Mulvany and Halpern (Mulvany and Halpern, 1977). Following mounting, vessels were equilibrated in PSS at 37°C for 30 min.

2.11.2 Normalisation

The transmural pressure of mesenteric arteries was normalised using Laplace's law ($T = r_i \times P$, where T = wall tension, r_i = internal radius and P = transmural pressure), using successive stretches of the vessel to create a standard curve of internal circumference against wall tension. The internal circumference was adjusted to 90% of that required to produce a transmural pressure of 100 mmHg or 13.3 kPa, thereby putting the vessel under passive, but not active, tension (Angus and Wright, 2000). Aortas were not normalised, but placed under a fixed

tension of 1 g (9.81 mN). Following the normalisation process, vessels were allowed to equilibrate at 37°C for a further 60 min.

2.11.3 Wake-up protocol

To stimulate maximal contraction, vessels were subjected to a K^+-mediated 'wake-up' protocol prior to stimulating with the chosen ligand. After draining the PSS, KPSS was added to the bath and wall tension recorded for at least 1 min before washing three times with PSS and allowing to return to baseline tension, then repeating the process. Following wake-up, vessels were equilibrated in PSS at 37°C for 30 min.

2.11.4 Data recording and analysis

After normalisation and wake-up, vessels were treated with the appropriate ligands by adding cumulatively to the bath, allowing the wall tension to plateau for 2–3 min between each addition. Wall tension was recorded in mN using LabChart software (ADInstruments). Traces were analysed using LabChart Reader software (ADInstruments), using the maximum peak or minimum trough after each addition and subtracting the mean baseline reading to obtain change in force (ΔF) in mN. For mesenteric arteries, change in active effective pressure (AEP) was calculated using the following equation:

$$\Delta AEP\ (kPa) = (\Delta F/w)\ /\ (ID_1/2) \times 100$$

Where F = force (mN), w = wall length (mm) and ID_1 = working internal diameter after normalisation (μm). For aortas, contraction was plotted as percentage of the maximum response to K^+.

2.12 Histology

2.12.1 Fixation

Tissues were harvested at sacrifice under terminal anaesthesia and placed immediately into 10% (v/v) formalin for 24 hours. Rat tissues were sliced transversely after 24 hours and placed back into 10% formalin for a further

24 hours. Following fixation, tissues were washed in PBS and stored in 50% (v/v) ethanol at 4°C until use.

2.12.2 Paraffin embedding and sectioning

Tissues were processed for paraffin embedding using a Shandon™ Excelsior™ tissue processor (Thermo Scientific), then embedded in paraffin wax. All tissues were embedded on the transverse axis. 3–5 µm sections were cut on a microtome and baked onto silane-treated microscope slides at 50°C overnight.

2.12.3 Deparaffinisation and dehydration

Prior to staining, sections were deparaffinised in Histoclear for 2 x 7 min, then rehydrated by incubating for 7 min each in 100% ethanol, 95% (v/v) ethanol and 70% (v/v) ethanol.

2.12.4 Wheat-germ agglutinin (WGA) staining

WGA was used to stain sialic acid and *N*-acetylglucosaminyl residues in cardiomyocyte cell membranes in order to measure cardiomyocyte hypertrophy (Huet and Garrido, 1972). Following deparaffinisation and dehydration, 5 µM heart (left ventricle + septum) sections were washed in running tap water for 5 min. Antigen retrieval was performed by microwaving in pre-heated 10 mM sodium citrate solution (pH 6) with 0.1% (v/v) Tween-20 for 10 min. Following antigen retrieval, sections were cooled to room temperature before blocking in 1% (v/v) goat serum + 5% (w/v) BSA for 1 hour at room temperature. Sections were then incubated with 10 µg/mL WGA conjugated to Alexa Fluor 555 (Molecular Probes) (diluted in blocking solution) for 1 hour at room temperature protected from light. Sections were washed for 2 x 5 min in PBS protected from light, then mounted with ProLong® Gold anti-fade reagent with DAPI (Molecular Probes) and dried overnight at room temperature before imaging. DAPI and Alexa Fluor 555 images were taken with a x40 objective on an Olympus BX40 microscope using a QImaging QICAM Fast 1394 camera. The experimenter was blinded to treatment groups during imaging and analysis. Four fields of view showing cardiomyocytes in transverse orientation were taken from each section. Cardiomyocyte width (the longest axis of a transversely-orientated cardiomyocyte) was measured using ImageJ software. Approximately 50 cells

from each field of view were measured, using a grid system to minimise bias, meaning a mean cardiomyocyte width for each animal was calculated from >200 measurements.

2.12.5 Picro-sirius red staining

Picro-sirius red was used to stain collagen fibres in heart and kidney tissue as a measure of cardiac and renal fibrosis. Following deparaffinisation and dehydration, 3 µm heart (left ventricle + septum) and kidney sections were incubated for 5 min in distilled water. Nuclei were stained by incubating in Weigert's hematoxylin (Sigma-Aldrich) for 10 min, then sections were washed in running tap water for 10 min. Sections were stained with picro-sirius red (0.1% (w/v) sirius red in saturated picric acid solution (both Sigma-Aldrich)) for 90 min. Sections were washed 2 x 3 min in acidified water (0.01 N HCl), then vigorously shaken to remove water before dehydrating in 100% ethanol for 3 min. Sections were cleared in Histoclear for 2 x 7 min, mounted in DPX mountant and dried overnight at room temperature. Images were taken with a x40 objective on an Olympus BX41 microscope using a QImaging Go-3 camera. The experimenter was blinded to treatment groups during imaging and analysis. For hearts, six fields of view were taken. For kidneys, eight fields of view (four interstitial and four perivascular) were taken. Fibrosis was quantified by measuring the proportion of red pixels using Image-Pro Plus software (Media Cybernetics).

2.12.6 Hematoxylin and eosin (H&E) staining

Hematoxylin and eosin was used to stain nuclei and cytoplasm in order to visualise the gross morphology of blood vessels. Following deparaffinisation and dehydration, 5 µm aorta or carotid artery sections were incubated for 5 min in distilled water. Sections were stained with Harris hematoxylin (CellPath) for 2 min, then washed in running tap water for 5 min. Sections were incubated in 70% (v/v) ethanol for 1 min, then stained with Eosin Y (CellPath) for 3 min. Sections were washed in 95% (v/v) ethanol for 2 x 30 sec, then dehydrated in 100% ethanol for 2 x 5 min. Sections were cleared in Histoclear for 2 x 5 min, mounted in DPX mountant and dried overnight at room temperature. Images showing the whole vessel were taken with a x4 (aortas) or x10 (carotid arteries) objective on an Olympus BX41 microscope using a QImaging Go-3 camera. The

experimenter was blinded to treatment groups during imaging and analysis. Total and lumen areas were measured using ImageJ software and used to calculate medial area (total area − lumen area) and wall-to-lumen ratio (total area − lumen area/lumen area).

2.13 Gene expression analysis

2.13.1 Tissue harvest and lysis

2.13.1.1 Heart and kidney tissue lysis

Animal tissues were snap frozen in liquid nitrogen at sacrifice and stored at − 80°C. To lyse, 30–50 mg of tissue was transferred to an RNase-free microcentrifuge tube along with 700 µL QIAzol® (QIAGEN) and two 3 mm tungsten carbide beads. Tissues were homogenised for 2 x 1 min in a QIAGEN TissueLyser.

2.13.1.2 Aorta tissue lysis

The entire thoracic aorta was snap frozen in liquid nitrogen at sacrifice and stored at − 80°C. For disruption, the aorta was cooled in liquid nitrogen and crushed to a fine powder using a mortar and pestle cooled on dry ice. The resulting powder was lysed by the addition of QIAGEN RTL buffer containing 1% (v/v) ß-mercaptoethanol, and homogenised using a QIAshredder spin column (QIAGEN) by applying to the column and subjecting to centrifugation at 16,000 x *g* for 2 min.

2.13.2 RNA extraction

2.13.2.1 RNA extraction from heart and kidney tissue

RNA extraction was performed immediately following tissue lysis using the miRNeasy® Mini Kit (QIAGEN) as per the manufacturer's instructions. Briefly, homogenate was mixed with chloroform and subjected to centrifugation at 12,000 x *g* for 15 min at 4°C. The aqueous phase containing RNA was collected and mixed with 100% ethanol, then applied to an RNeasy Mini spin column and subjected to centrifugation at 8000 x *g* for 15 sec at room temperature. The flow-through was discarded and the column was washed with guanidine-

containing stringent wash buffer. On-column DNA digestion was performed using the RNase-free DNase Set (QIAGEN) as per the manufacturer's instructions. The column was then washed again with stringent wash buffer, then washed twice with mild wash buffer, centrifuging for 2 min after the final wash to remove residual ethanol. RNA was eluted in 30 µL nuclease-free water.

2.13.2.2 RNA extraction from aorta tissue

RNA extraction was performed immediately following tissue lysis using the RNeasy Fibrous Tissue Mini Kit (QIAGEN) as per the manufacturer's instructions. Briefly, homogenate was incubated with proteinase K (supplied in kit at unknown concentration) at 55°C for 10 min and cleared by centrifugation at 10 000 x *g* for 3 min. The supernatant was applied to an RNeasy Mini spin column and subjected to DNase digestion and washing as detailed in section 2.13.2.1.

2.13.2.3 Determination of RNA concentration

RNA concentration was determined by measuring absorbance at 260 nm using a NanoDrop spectrophotometer. RNA purity was assessed using the A_{230}/A_{260} and A_{260}/A_{280} ratios, with ratios of 2–2.2 considered pure. RNA was stored at – 80°C until use.

2.13.3 Reverse Transcription (RT)

1 µg of RNA was reverse transcribed to cDNA using TaqMan® Reverse Transcription Reagents (Life Technologies). 20 µL reactions were set up in 96-well PCR plates using the following components:

- 1 x RT Buffer
- 5.5 mM $MgCl_2$
- 2 mM (0.5 mM each) dNTP mix
- 2.5 µM Random hexamers
- 8 units RNase Inhibitor
- 25 units MultiScribe™ RT
- 200–1000 ng RNA

Reaction mixtures were incubated in a thermal cycler using the following conditions:

1.	Annealing	25°C	10 min
2.	Extension	48°C	30 min
3.	Inactivation	95°C	5 min
4.	4°C	∞	

cDNA was stored at − 20°C until use.

2.13.4 Quantitative Real-Time PCR (qRT-PCR)

qRT-PCR was performed using Applied Biosystems TaqMan® Gene Expression Assays (Life Technologies) containing a pair of unlabelled PCR primers and a TaqMan probe which binds downstream of the forward primer and carries a fluorescent label on the 5' end and a minor groove binder and non-fluorescent quencher on the 3' end. The assays used are detailed in Table 2-5. 10 µL reactions were set up in triplicate in 384-well MicroAmp® Optical PCR plates (Life Technologies) using the following components:

- 1 x TaqMan Universal Master Mix II, no UNG (Life Technologies)
- 1 x TaqMan Assay
- 100 ng cDNA (2 µL RT product)

Table 2-5 Taqman gene expression assays

Gene	Assay	Label
Gpr35	Mm01973686_s1	FAM
Agtr1a	Mm00616371_m1	FAM
Ppib	Mm00478295_m1	FAM

Plates were read on a QuantStudio™ Flex Real-Time PCR System (Thermo Fisher Scientific) using the fluorescence channel appropriate to the probe. Reaction mixtures were subjected to thermal cycling using the following conditions:

1.	Preheating	95°C	10 min
2.	Denaturing	95°C	15 sec
3.	Annealing	60°C	1 min
4.	Repeat steps 2–3 (x40)		

Comparative cycle threshold (C_T) values were obtained using QuantStudio Flex software (Thermo Fisher Scientific).

2.13.5 qRT-PCR data analysis

C_T values were compared with a suitable housekeeper gene (run in parallel) to generate ΔC_T values (ΔC_T = C_T of housekeeper − C_T of gene of interest). These were analysed using the $2^{-\Delta\Delta CT}$ method (Livak and Schmittgen, 2001) in which ΔC_T values are compared with that of an appropriate control to generate $\Delta\Delta C_T$ values and relative quantification (RQ) values ($RQ = 2^{-\Delta\Delta CT}$). Standard errors are expressed as RQ_{min} ($RQ_{min} = 2^{-(\Delta\Delta CT + SEM)}$) and RQ_{max} ($RQ_{max} = 2^{-(\Delta\Delta CT - SEM)}$).

2.14 Statistical analysis

Statistical analyses were carried out using Graphpad Prism software. Data were assumed to be normally distributed, and were therefore compared using parametric tests; either two-tailed unpaired student's t test (for two groups) or one-way analysis of variance (ANOVA; for three or more groups). For densitometry measurements (phosphorylation studies), normal distribution of datasets was verified prior to ANOVA using the Shapiro-Wilk test (performed using Microsoft Excel). Tukey's post-test was used for multiple comparisons. Hemodynamic measurements made by telemetry were compared using two-way repeated measures ANOVA (basal GPR35 knockout study and amlexanox SHRSP study) or student's t test on the slope of the linear regression calculated for individual animals (Ang II infusion study).

Chapter 3 G protein- and β-arrestin-mediated responses to GPR35 stimulation

3.1 Introduction

As discussed in section 1.2, any one GPCR can couple to multiple cytoplasmic mediators that each feed into different signalling pathways. As a result of this heterogeneity, GPCR signal transduction is regulated on several different levels, which must be well understood if a receptor is to be pursued as a therapeutic target. Determining the intracellular signalling mechanisms involved in GPR35 function will be key to elucidating its role in the cardiovascular system and to assessing its potential as a therapeutic target.

Agonist-dependent phosphorylation of receptor intracellular domains is an important component of GPCR signalling that is now known to have profound effects on the desensitisation of G protein signalling, the internalisation and recycling of the receptor and the capacity of the receptor to promote G protein-independent signalling (section 1.2) (Innamorati et al., 1998, Ren et al., 2005, Nobles et al., 2011). Phosphorylation of GPCRs at serine and threonine residues can potentially occur on any part of the intracellular domain, but receptors are most commonly phosphorylated on the third intracellular loop and/or the C-terminal tail (Tobin et al., 2008). Furthermore, the precise locations of the phosphorylated residues can influence downstream signalling and receptor function (Nobles et al., 2011, Prihandoko et al., 2016). Very little is known about the capacity of GPR35 to undergo agonist-dependent phosphorylation and what effect this might have on signalling responses such as the recruitment of ß-arrestin and subsequent receptor internalisation. This chapter describes investigations into the agonist-dependent phosphorylation of GPR35 and how this defines the outcomes of GPR35 activation. The subsequent generation of a phosphorylation-deficient mutant (PDM) form of the receptor enabled further evaluation of the contribution of agonist-dependent phosphorylation to downstream responses to GPR35 activation.

Besides phosphorylation, the coupling specificity of a particular GPCR clearly has a major impact on its downstream cellular effects. Selective inhibition or deletion of individual G proteins has therefore proven valuable in elucidating the

pathways and functional consequences associated with individual GPCRs. However, in the absence of selective pharmacological inhibitors, genetic manipulation is sometimes the only option, and this can be difficult and costly when relying on animal models. Recently, however, HEK293-derived cell lines that are CRISPR-edited to eliminate expression of individual G proteins and arrestins (generated by Asuka Inoue, Tohoku University, Japan) have been made available to the GPCR research community. These cell lines provide a novel, practical, cell-based model with which to address questions about GPCR signalling and functional selectivity, and were used in the present study to investigate the contributions of $G\alpha_{12/13}$ and ß-arrestin-1/2 to GPR35-mediated cellular responses.

3.1.1 Aims

The aims of this chapter were to:

- Determine whether GPR35 undergoes agonist-dependent phosphorylation
- Assess species- and agonist-specific differences in this phosphorylation
- Determine the region(s) and specific sites at which this phosphorylation occurs
- Assess the contributions of these phosphorylation sites to $G_{12/13}$- and ß-arrestin-mediated GPR35 signalling
- Assess the contributions of phosphorylation, $G_{12/13}$ and ß-arrestin-1/2 to GPR35-mediated cellular responses.

3.2 Results

3.2.1 Investigating agonist-dependent phosphorylation of GPR35

Butcher et al. have reported on radiolabelling- and mass spectrometry-based methods for identifying phosphorylated residues on GPCRs, which they have successfully used to identify phosphorylation sites for a number of GPCRs (Butcher et al., 2014, Butcher et al., 2011a, Butcher et al., 2011b). These techniques require affinity purification of the receptor from cell lysates using a C-terminal haemagglutinin (HA) epitope tag. In order to utilise these methods to study agonist-dependent phosphorylation of GPR35, it was therefore necessary to generate an HA-tagged GPR35 construct and stably transfect it into HEK293 cells in preparation for subsequent studies. To investigate potential species differences in GPR35 phosphorylation, these studies were performed with human, mouse and rat GPR35. HA-tagged human (h), mouse (m) and rat (r) GPR35 constructs (hGPR35-HA, mGPR35-HA and rGPR35-HA) were generated and stably transfected under a doxycycline-inducible promoter into a HEK293-derived cell line. Doxycycline-inducible, homogeneous cell-surface expression of the tagged receptors was confirmed by immunocytochemistry (Figure 3-1).

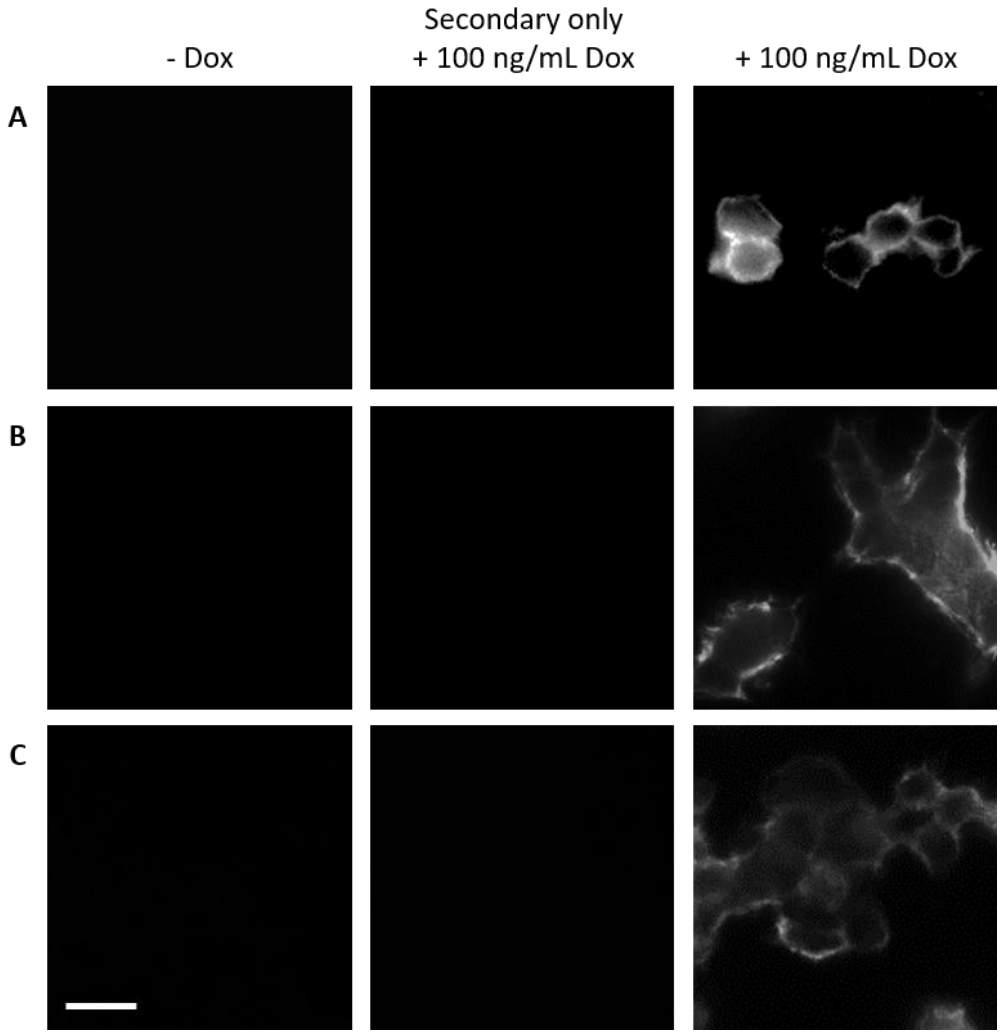

Figure 3-1 GPR35-HA stable cell lines express GPR35-HA at the cell surface Anti-HA immunocytochemistry showing (A) hGPR35-HA, (B) mGPR35-HA and (C) rGPR35-HA expression at the cell surface. Expression of the constructs was induced by incubating with doxycycline (Dox) overnight at 37°C. Scale bar = 20 µm.

Synthetic ligands of GPR35 have varying potencies and efficacies, which sometimes differ between the human, mouse and rat orthologues (Table 1-3 and Table 1-4). To determine potential species- and agonist-specific differences in phosphorylation level, [^{32}P]-orthophosphate labelling was used to assess GPR35 phosphorylation in response to a range of synthetic ligands with various pharmacological properties and species selectivities (Figure 3-2 A). hGPR35-HA, mGPR35-HA and rGPR35-HA all underwent agonist-induced phosphorylation in line with predictions based on reported pharmacological findings (Figure 3-2 B-D). Notably, zaprinast induced a strong phosphorylation of all three species orthologues, while pre-treatment with the antagonist CID-2745687 abolished zaprinast-induced phosphorylation in the human orthologue only (Figure 3-2 B), supporting previous reports that this antagonist is highly human-selective

(Jenkins et al., 2012). Pamoic acid, doxantrazole and amlexanox induced a significantly lower level of phosphorylation at the human orthologue than zaprinast (Figure 3-2 B), in line with reports that these compounds act as partial agonists at hGPR35 in ß-arrestin recruitment assays (Jenkins et al., 2012, MacKenzie et al., 2014). Pamoic acid, which is reported to be a human-selective partial agonist, also displayed selectivity towards hGPR35 in this assay, as it did not induce any phosphorylation of the mouse or rat orthologues (Figure 3-2 C-D) (Jenkins et al., 2012).

As well as demonstrating ligand and species differences in phosphorylation, these hGPR35 autoradiographs and immunoblots demonstrate a previously unknown feature of GPR35. While the rodent orthologues both resolved in SDS-PAGE as an apparently single polypeptide with a molecular mass of approximately 50 kDa (Figure 3-2 C-D), hGPR35 appeared to resolve as two separate polypeptides with molecular masses of approximately 40 and 60 kDa (Figure 3-2 A). All of the orthologues resolved at a higher molecular mass than the native mass of 34 kDa. Interestingly, the higher molecular mass human GPR35 variant appeared to be less abundant in the immunoblot, but there was no difference in intensity in the autoradiograph. This suggests that the higher molecular mass species is more efficiently phosphorylated than the lower molecular mass counterpart.

A

Ligand	Properties
Zaprinast	Full agonist
CID-2745687	Competitive antagonist, human-selective
Pamoic acid	Partial agonist, human-selective
Doxantrazole	Partial agonist (human), full agonist (rodent)
Amlexanox	Partial agonist

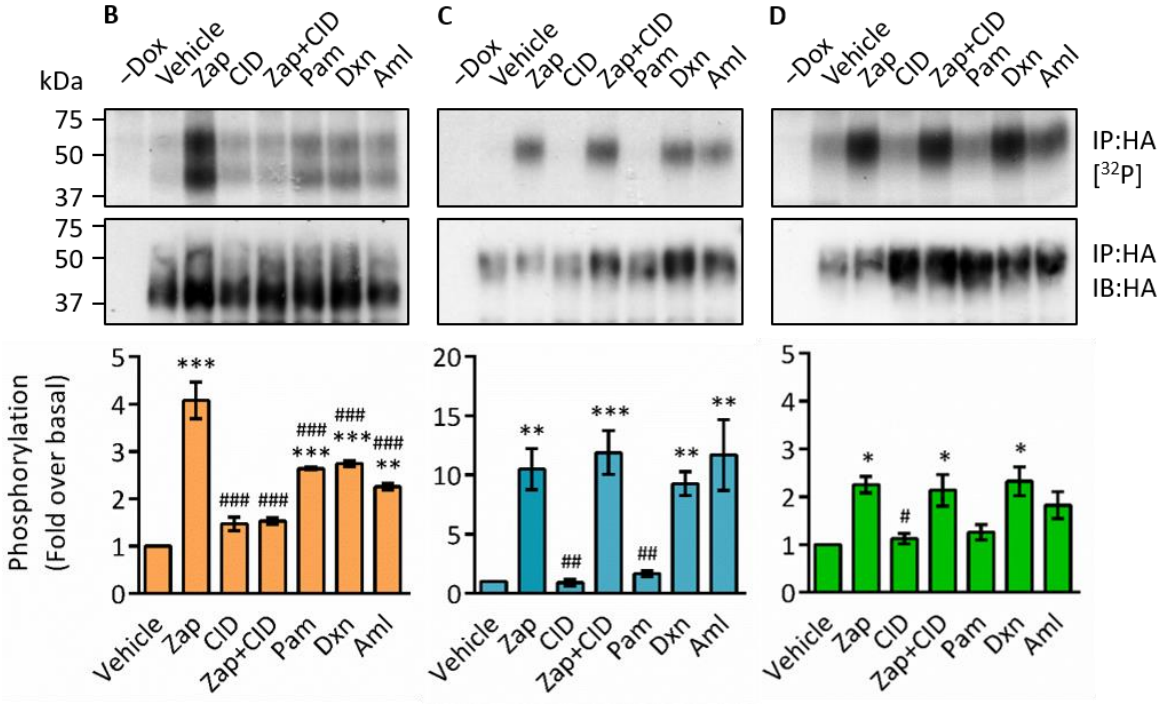

Figure 3-2 Human, mouse and rat GPR35 undergo agonist-dependent phosphorylation
(A) Ligands tested and their notable pharmacological properties. **(B, C, D)** Representative autoradiographs (top panels) and anti-HA immunoblots (IB) (bottom panels) showing [^{32}P] incorporation into **(B)** hGPR35-HA, **(C)** mGPR35-HA or **(D)** rGPR35-HA immunoprecipitates (IP). Cells were stimulated with the indicated agonists for 5 min prior to lysis. Antagonist-treated cells (CID and Zap+CID) were preincubated with antagonist for 15 min prior to stimulation with agonist. Quantification shows mean fold change of [^{32}P] incorporation over vehicle-treated cells, measured by densitometric analysis of autoradiographs from n = 3 independent experiments +/- SEM. **p*<0.05, ***p*<0.01, ****p*<0.001 compared with vehicle; #*p*<0.05, ##*p*<0.01, ###*p* <0.001 compared with zaprinast in one-way ANOVA with Tukey's multiple comparisons post-test. (Dox = doxycycline; Zap = 100 µM zaprinast; CID = 10 µM CID-2745687; Pam = 100 nM pamoic acid; Dxn = 100 µM doxantrazole; Aml = 100 µM amlexanox.)

GPR35 has previously been reported to have different glycosylation states (Jenkins et al., 2011). To determine whether the different molecular mass bands observed in the phospholabelling experiments represented differentially glycosylated GPR35 species, human and mouse GPR35-HA were treated with *N*-glycosidase F and resolved by SDS-PAGE (Figure 3-3). Treatment with the glycosidase caused a decrease in molecular mass of both orthologues to match the predicted native mass of 34 kDa, indicating that mGPR35-HA is processed to make one predominant glycosylated species, whereas hGPR35-HA is processed

into two differentially glycosylated forms. The more heavily *N*-glycosylated hGPR35 species was less abundant, but more efficiently phosphorylated (Figure 3-2 B).

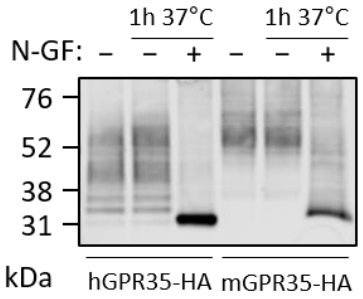

Figure 3-3 Human and mouse GPR35-HA are differentially *N*-glycosylated Anti-HA immunoblot of hGPR35-HA- and mGPR35-HA-expressing cell lysates in their glycosylated states or following treatment with N-GF (N-GF = *N*-glycosidase F).

Agonist-dependent GPCR phosphorylation, and specifically the location of the phosphorylated residues, has been shown to influence the signalling and functional outcomes of GPCR activation (Nobles et al., 2011, Prihandoko et al., 2016). Therefore, having determined that GPR35 is phosphorylated in response to agonist, it was of interest to investigate the location(s) of this phosphorylation in order to compare GPR35 with other GPCRs. Mass spectrometry was performed on tryptic peptides generated from affinity-purified hGPR35-HA to map the precise phosphorylation sites following stimulation with 100 μM zaprinast (Figure 3-4). Five serine and threonine phosphorylation sites were identified, all of which were located in the helix 8/C-terminal tail region. These five residues comprised all of the serine and threonine residues present in these regions, including one residue (S294) that is substituted for arginine in 48% of the population as the result of a SNP that has been associated with cardiovascular disease (Figure 1-2) (Sun et al., 2008). Notably, phosphorylation of S300 and S303, which are present in the same tryptic peptide, was observed both individually and in tandem, indicating that multiple sites on hGPR35 can be phosphorylated simultaneously.

AA	B Ions	Y Ions
E	130.1	1598.8
F	277.1	1469.7
Q	405.2	1322.6
E	534.2	1194.6
A	605.3	1065.5
S+80	772.3	994.5
A	843.3	827.5
L	956.4	756.5
A	1027.4	643.4
V	1126.5	572.3
A	1197.5	473.3
P	1294.6	402.2
S	1381.6	305.2
A	1452.6	218.2
K	1598.8	147.1

AA	B Ions	Y Ions
E	130.1	1598.8
F	277.1	1469.7
Q	405.2	1322.6
E	534.2	1194.6
A	605.3	1065.5
S	692.3	994.5
A	763.3	827.5
L	876.4	756.5
A	947.5	643.4
V	1046.5	572.3
A	1117.6	473.3
P	1214.6	402.2
S+80	1381.6	305.2
A	1452.6	218.1
K	1598.8	147.1

AA	B Ions	Y Ions
A	72.0	2673.1
H	209.1	2602.2
K	337.2	2465.0
S+80	504.2	2336.9
Q	632.3	2169.9
D	747.3	2041.9
S+80	914.3	1926.8
L	1027.4	1759.8
C+57	1187.4	1646.7
V	1286.5	1486.7
T	1387.5	1387.6
L	1500.6	1286.6
A	1571.6	1173.5
Y	1743.7	1102.5
P	1831.8	939.4
Y	1994.8	842.4
D	2109.8	679.3
V	2208.9	564.3
P	2306.0	465.2
D	2421.0	368.2
Y	2584.1	253.1
A	2673.1	90.1

AA	B Ions	Y Ions
A	72.0	2593.1
H	209.1	2522.1
K	337.2	2385.0
S	424.2	2256.9
Q	552.3	2169.9
D	667.3	2041.9
S	754.4	1926.8
L	867.4	1839.8
C+57	1027.5	1726.7
V	1126.5	1566.7
T+80	1307.6	1467.6
L	1420.6	1286.6
A	1491.7	1173.5
Y	1654.7	1102.5
P	1751.8	939.4
Y	1914.9	842.4
D	2029.9	679.3
V	2128.9	564.3
P	2226.0	465.2
D	2341.0	368.2
Y	2504.1	253.1
A	2593.1	90.1

Peptide	Peptide prob.	Phospho-residue
(K)EFQEApSALAVAPSAKAHK(-)	100%	S287
(K)EFQEASALAVAPpSAKAHK(-)	96%	S294
(K)AHKpSQDSLCVTLAYPYDVPDYA(-)	86%	S300
(K)AHKSQDpSLCVTLAYPYDVPDYA(-)	100%	S303
(K)AHKpSQDpSLCVTLAYPYDVPDYA(-)	89%	S300/S303
(K)AHKSQDSLCVpTLAYPYDVPDYA(-)	96%	T307

Figure 3-4 LC-MS/MS identifies five phosphorylation sites in the hGPR35 C-terminal tail following zaprinast stimulation Fragmentation tables associated with phosphorylated peptides. All theoretical ions are shown, and those identified in the analysis are highlighted in green. Phosphorylated residues are highlighted in red. Peptide prob. indicates percentage probability of a correct peptide based on the discriminant score; both are generated by Scaffold software. HA = haemagglutinin.

Serine and threonine residues present in the ICLs were included in the peptide coverage from the mass spectrometry analysis, but no phosphorylation of these sites was observed. Thus, phosphorylation of hGPR35 appears to occur exclusively on the C-terminal tail. To test this hypothesis, a potentially 'phosphorylation-deficient' mutant (PDM) of hGPR35-HA was generated, where each of the five identified phosphorylation sites was mutated to alanine (Figure 3-5 A). In order to determine whether the rodent GPR35 orthologues are also exclusively phosphorylated in the C-terminal tail region, a mGPR35 PDM, with all serine and threonine residues in the C-terminal tail mutated to alanine, was also generated (Figure 3-5 A). The mutant constructs were stably transfected into a doxycycline-inducible HEK293 cell line, and doxycycline-inducible, cell-surface expression of the tagged receptors was confirmed by immunocytochemistry (Figure 3-5 B-C).

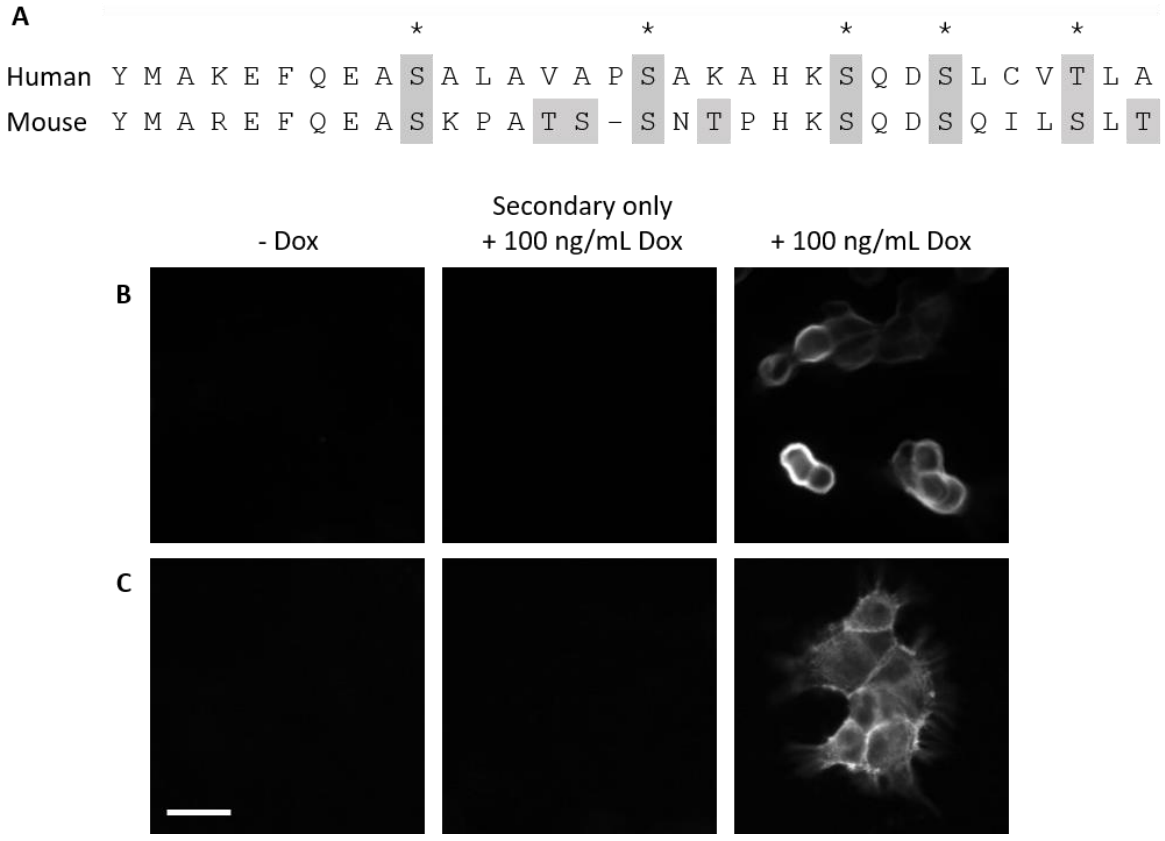

Figure 3-5 GPR35(PDM)-HA stable cell lines express GPR35(PDM)-HA at the cell surface
(A) PDM mutagenesis strategy. Residues highlighted in grey were mutated to alanine. Residues marked with an asterisk are those found to be phosphorylated in LC-MS/MS. **(B,C)** Anti-HA immunocytochemistry showing **(B)** human and **(C)** mouse GPR35(PDM)-HA expression at the cell surface. Expression of the constructs was induced by incubating with doxycycline (Dox) overnight at 37°C. Scale bar = 20 μm.

The human and mouse GPR35 phosphorylation-deficient mutants did not undergo detectable phosphorylation following zaprinast stimulation (Figure 3-6). The amount of the human mutant protein in the immunoprecipitate was much lower than that of the wild type counterpart (Figure 3-6 A). This was due to reduced viability of the mutant-expressing cell line, which may in itself be a meaningful finding as it suggests phosphorylation-deficient GPR35 might confer a survival defect. However, there was a detectable level of the mutant protein compared with the uninduced (−Dox) control cells (Figure 3-5 B and Figure 3-6 A), and no difference in [^{32}P] incorporation between the vehicle- and zaprinast-treated cells (Figure 3-6). It was therefore concluded that neither human nor mouse GPR35 phosphorylation-deficient mutant was phosphorylated in response to agonist, and that GPR35 is exclusively phosphorylated at sites within the C-terminal tail.

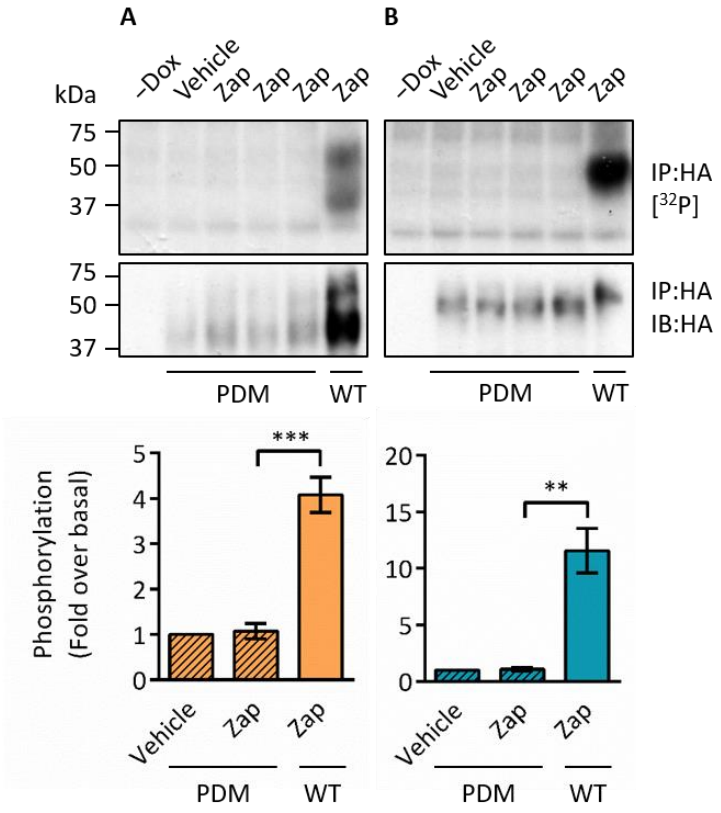

Figure 3-6 Human and mouse GPR35 phosphorylation-deficient mutants do not undergo agonist-dependent phosphorylation Representative autoradiographs (top panels) and anti-HA immunoblots (bottom panels) showing [^{32}P] incorporation into **(A)** human or **(B)** mouse wild type (WT) or phosphorylation-deficient mutant (PDM) GPR35-HA immunoprecipitates. Cells were stimulated with 100 μM zaprinast (Zap) for 5 min prior to lysis. Quantification shows mean fold change of [^{32}P] incorporation over vehicle-treated cells, measured by densitometric analysis of autoradiographs from n = 3 independent experiments +/- SEM. **p<0.01, ***p<0.001 in one-way ANOVA with Tukey's multiple comparisons post-test. (Dox = doxycycline.)

3.2.2 The effects of GPR35 phosphorylation on G protein and β-arrestin recruitment

For many GPCRs, agonist-dependent phosphorylation within the C-terminal tail region causes alterations in the binding of cytoplasmic signalling proteins, most commonly leading to increased recruitment of ß-arrestin (Innamorati et al., 1998, Ren et al., 2005, Nobles et al., 2011). In order to determine the impact of phosphorylation on ß-arrestin-2 recruitment to GPR35, the contribution of each of the individual phosphorylation sites in human GPR35 identified by mass spectrometry (Figure 3-4) was assessed using site-directed mutagenesis in combination with a BRET-based ß-arrestin-2 recruitment assay (Figure 3-7). This assay utilises two constructs: ß-arrestin-2 fused with *Renilla* luciferase (RLuc) as a BRET donor, and a GPCR with a C-terminal eYFP tag as a BRET acceptor (section 2.6.2). Human GPR35-eYFP BRET acceptor constructs were generated in which each serine or threonine phosphorylation site (Figure 3-7 A) was mutated to alanine either individually or simultaneously to prevent phosphorylation. When HEK293 cells expressing these constructs and the BRET donor ß-arrestin-2-RLuc were stimulated with zaprinast, each mutation appeared to have a different impact on ß-arrestin-2 recruitment, as demonstrated by decreases in the maximal BRET response compared with the wild type receptor sequence (Figure 3-7 B-C). Every mutation except S294A significantly reduced maximal ß-arrestin-2 recruitment, with S303A having the greatest individual effect. In the phosphorylation-deficient mutant, with all identified phosphorylation sites removed, BRET was reduced to almost baseline levels. A cell-surface ELISA against the N-terminal FLAG epitope tag demonstrated that all mutants were efficiently trafficked to the cell membrane (Figure 3-7 D), suggesting that this lack of ß-arrestin-2 recruitment is due to alterations in GPR35 post-translational regulation and not simply a lack of expression at the cell surface.

Since the S303A mutation appeared to have the greatest effect on ß-arrestin recruitment, and this phosphorylation site exists within a cluster of serine and threonine residues that is conserved between the human and rodent orthologues (Figure 3-9 A), two double mutants (S300A/S303A and S303A/T307A) were made to determine whether these phosphorylation sites are a minimum requirement for ß-arrestin-2 recruitment. While the S300A/S303A double mutant did not show

a significant reduction in ß-arrestin-2 recruitment compared with the S303A single-site mutant, the S303A/T307A double mutant had a significantly impaired capacity for ß-arrestin-2 recruitment compared with either of the single-site mutants. Furthermore, this double mutation was sufficient to reduce BRET to the level of the fully phosphorylation-deficient mutant (Figure 3-7 B-C), suggesting that phosphorylation of at least one of these two residues is necessary for ß-arrestin-2 recruitment to GPR35 following zaprinast stimulation.

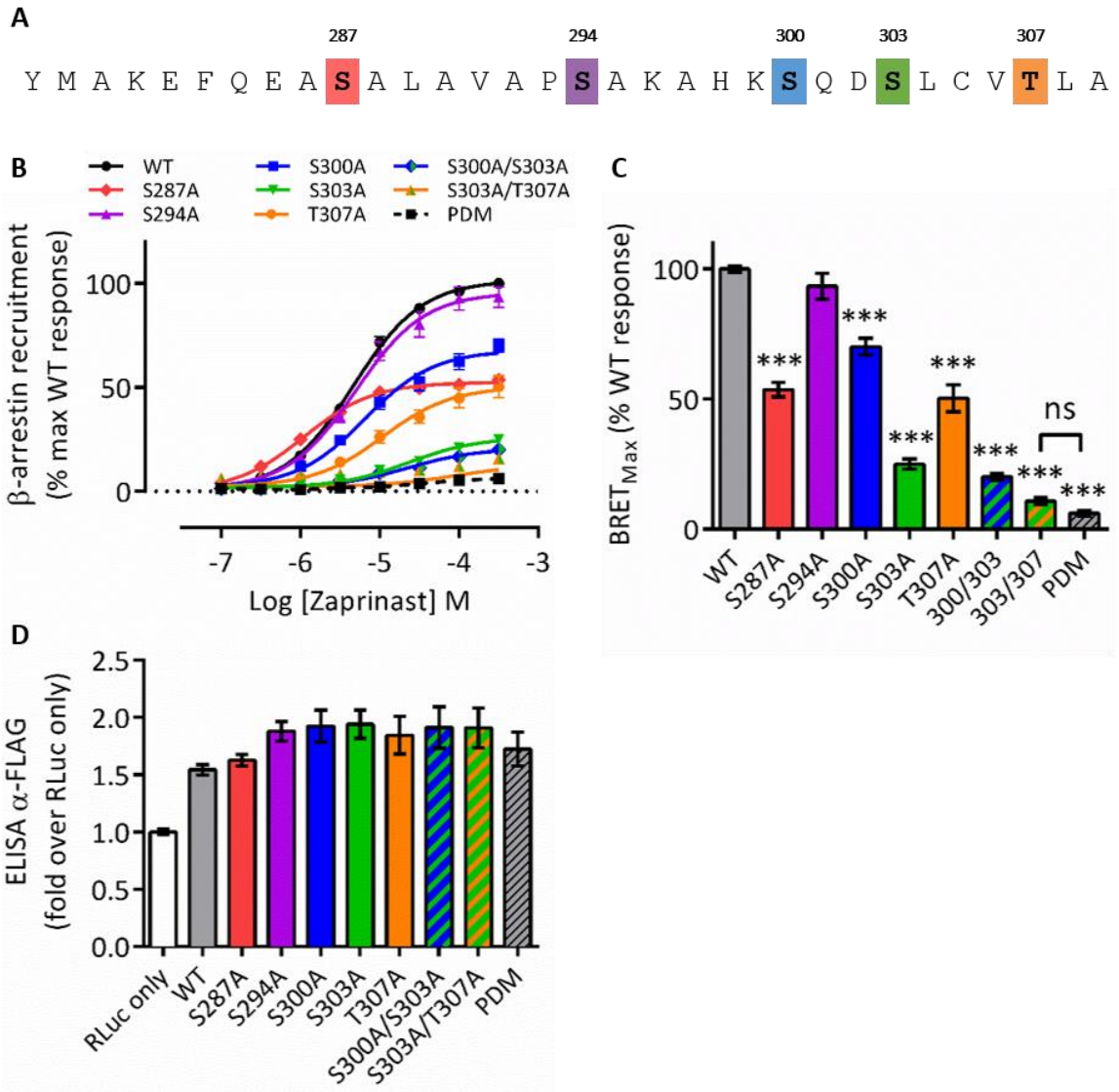

Figure 3-7 Phosphorylation sites in the hGPR35 C-terminal tail are required for β-arrestin-2 recruitment (A) Amino acid residues mutated to alanine in the hGPR35 BRET sensors. **(B)** Zaprinast concentration-response curves for hGPR35 wild type (WT) and serine to alanine mutants. **(C)** Maximal BRET stimulated by zaprinast treatment. **(D)** Anti-FLAG ELISA showing cell-surface expression of hGPR35-eYFP mutants co-transfected with β-arrestin-2-RLuc compared with cells transfected with β-arrestin-2-RLuc only. All data are means pooled from n = 3 independent experiments performed in triplicate +/- SEM. ***p<0.001 compared with WT; ns = not significant in one-way ANOVA with Tukey's multiple comparisons post-test. BRET = bioluminescence resonance energy transfer; ELISA = enzyme-linked immunosorbent assay; PDM = phosphorylation-deficient mutant.

To investigate the possibility that different phosphorylation sites play a role in responses to different agonists, the same mutant sensors were tested in response to stimulation by two partial agonists, pamoic acid and amlexanox (Figure 3-8 B). While the rank order of $BRET_{Max}$ for the different mutants was broadly similar with these agonists compared with zaprinast (Figure 3-7), there were some notable differences in the responses. S294A had a significant effect on ß-arrestin-2 recruitment induced by the partial agonists, although this mutant still retained 75–80% of the wild type response (Figure 3-8). With pamoic acid as the stimulus, both of the double mutantions reduced BRET to the level of the phosphorylation-deficient mutant (Figure 3-8 A-B). With amlexanox, the phosphorylation-deficient mutant retained a low level of ß-arrestin-2 recruitment (23% of the wild type response); however, the S303A mutation alone was sufficient to reduce ß-arrestin-2 recruitment to the level of the phosphorylation-deficient mutant (Figure 3-8 C-D).

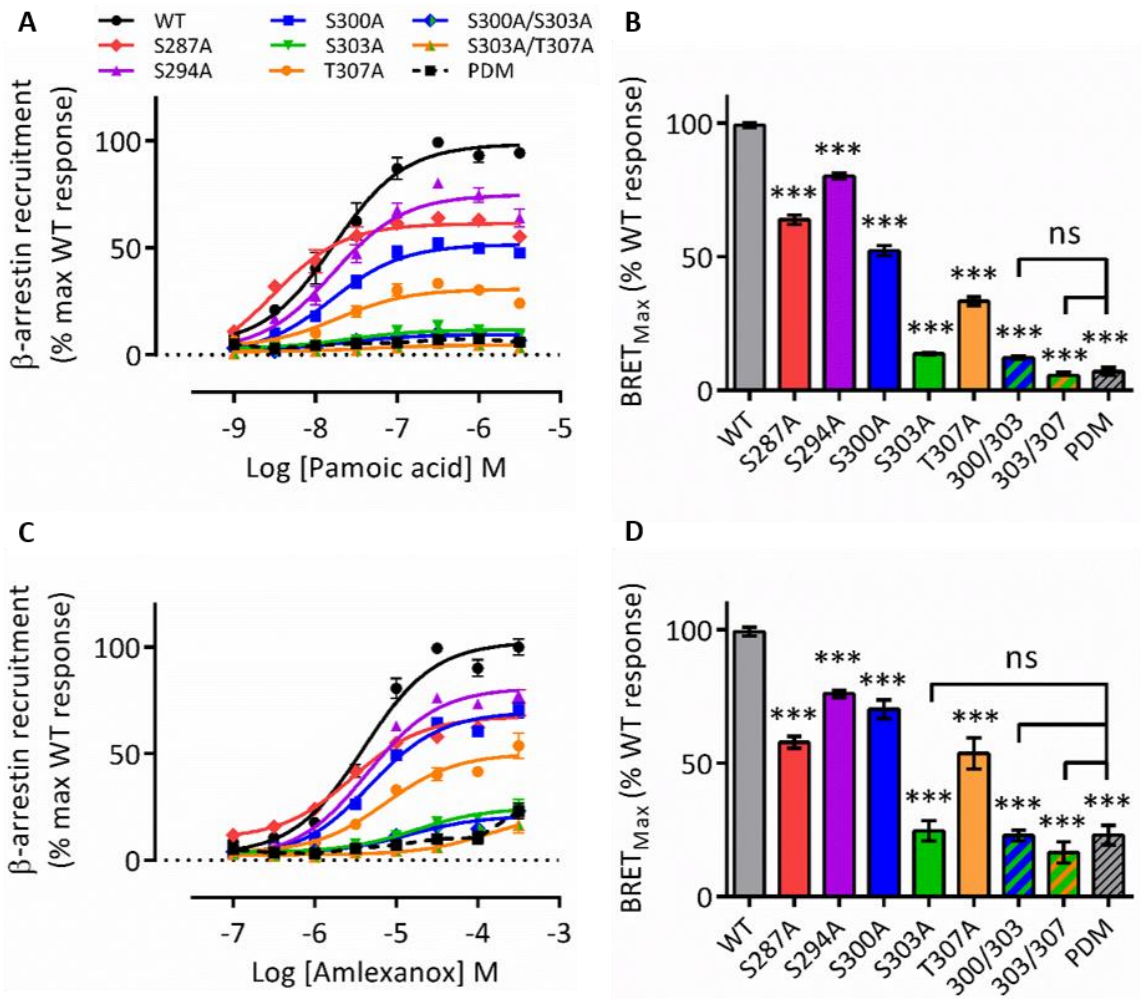

Figure 3-8 The impact of hGPR35 phosphorylation sites on β-arrestin-2 recruitment is dependent on the type of agonist (A and C) Concentration-response curves of **(A)** pamoic acid and **(C)** amlexanox for hGPR35 wild type (WT) and serine to alanine mutants. **(B and D)** Maximal BRET stimulated by **(B)** pamoic acid and **(D)** amlexanox treatment. All data are means pooled from n = 3 independent experiments performed in triplicate +/- SEM. ***p<0.001 compared with WT; ns = not significant in one-way ANOVA with Tukey's multiple comparisons post-test. BRET = bioluminescence resonance energy transfer; ELISA = enzyme-linked immunosorbent assay; PDM = phosphorylation-deficient mutant.

To investigate whether the phosphorylation sites that impacted ß-arrestin-2 recruitment to human GPR35 have similar importance in the rodent orthologues, equivalent BRET sensor serine/threonine to alanine mutants of mouse and rat GPR35 were tested (Figure 3-9). Since the rodent orthologues have substantially more serine and threonine residues in their C-terminal tails than the human orthologue, their phosphorylation sites were grouped into four clusters that correspond to the hGPR35 phosphorylation sites as identified by mass spectrometry (Figure 3-9 A). Similarly to hGPR35, with both mGPR35 and rGPR35, mutating all of the sites simultaneously reduced zaprinast-induced ß-arrestin-2 recruitment to almost baseline levels (Figure 3-9 B-E). Mutant A, with a mutation at a serine corresponding to hGPR35 S287, did not have

impaired ß-arrestin-2 recruitment, and in fact appeared to show enhanced potency and efficacy of the zaprinast-mediated response for rGPR35 (Figure 3-9 B-E). Mutant B, with mutations in a cluster corresponding to hGPR35 S294, had unaltered ß-arrestin-2 recruitment for mGPR35 but slightly impaired ß-arrestin-2 recruitment for rGPR35. Mutant C, with mutations in the conserved 'SQDS' motif equivalent to hGPR35 S300/S303, was unable to recruit ß-arrestin-2, with BRET reduced to the level of the phosphorylation-deficient mutants for both mGPR35 and rGPR35. Mutant D, with mutations in a cluster at the extreme C-terminus corresponding to hGPR35 T307, had moderately impaired ß-arrestin recruitment. Once again, all mutants were efficiently trafficked to the cell surface of HEK293 cells (Figure 3-9 F-G). These results suggest that, similarly to human GPR35, the S303-equivalent sites in mouse and rat GPR35 are essential for ß-arrestin-2 recruitment, whereas the T307-equivalent cluster makes a significant contribution, but is not essential.

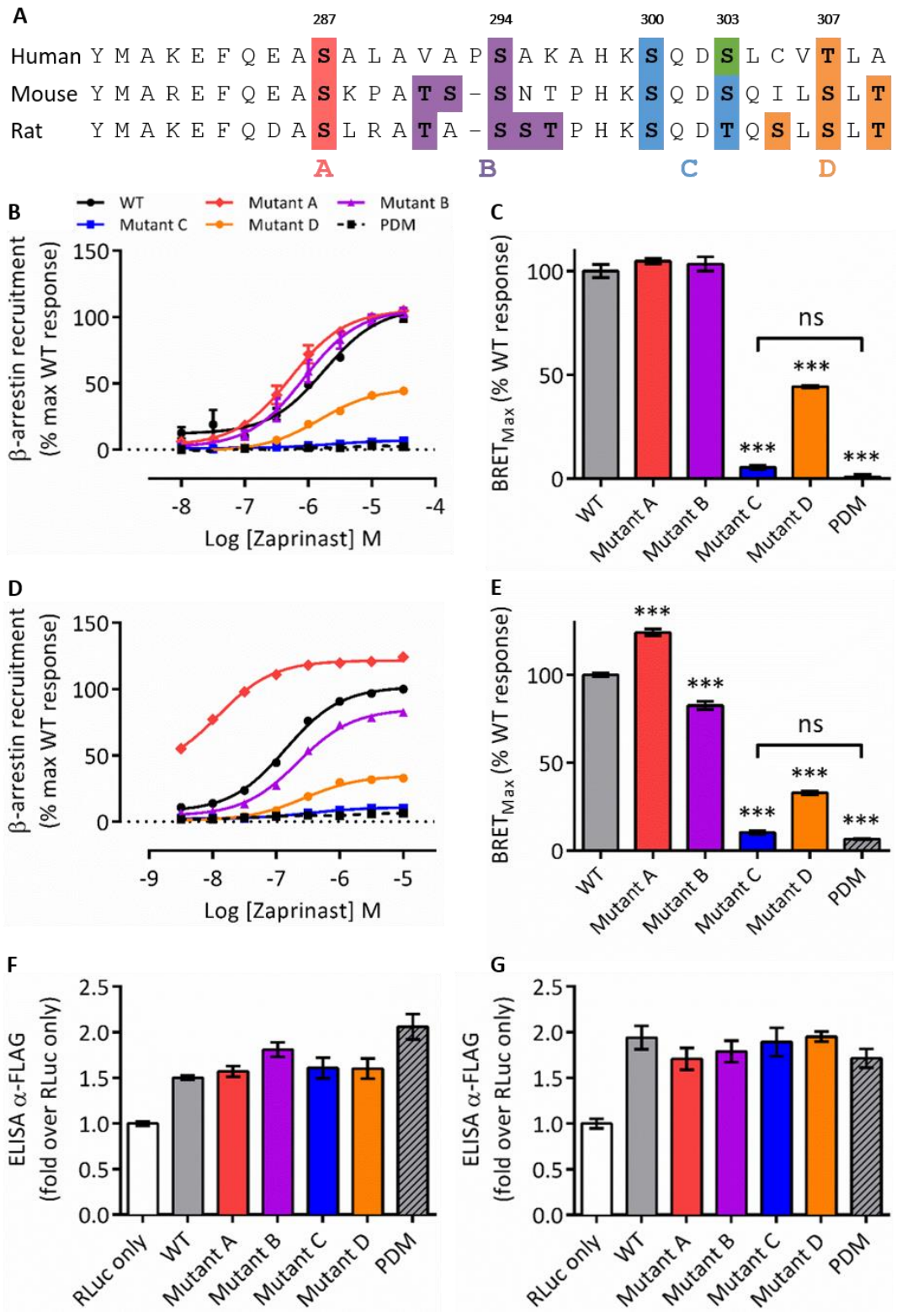

Figure 3-9 The impact of GPR35 phosphorylation sites on β-arrestin-2 recruitment is similar for different species orthologues (A) Amino acid residues mutated to alanine in the mGPR35 and rGPR35 BRET sensors. **(B and D)** Zaprinast concentration-response curves for **(B)** mGPR35 and **(D)** rGPR35 wild type (WT) and serine to alanine mutants. **(C and E)** Maximal BRET of **(C)** mGPR35 and **(E)** rGPR35 stimulated by zaprinast treatment. **(F and G)** Anti-FLAG ELISA showing cell-surface expression of **(F)** mGPR35-eYFP and **(G)** rGPR35-eYFP mutants co-transfected with β-arrestin-RLuc, compared with cells transfected with β-arrestin-RLuc only. All data are means pooled from n = 3 independent experiments performed in triplicate +/- SEM. ***p<0.001 compared with WT; ns = not significant in one-way ANOVA with Tukey's multiple comparisons post-test. BRET = bioluminescence resonance energy transfer; ELISA = enzyme-linked immunosorbent assay; PDM = phosphorylation-deficient mutant.

While these detailed insights into the molecular determinants of ß-arrestin-2 recruitment to GPR35 are important in understanding context-dependent differences in GPR35 signalling, an additional aim of this work was to understand the downstream consequences of these differences, whether they are mediated by G proteins or ß-arrestins and how differences in these multiple signals affect the cellular response. The phosphorylation-deficient mutant of human GPR35 was used to address this question, as it cannot recruit ß-arrestin and is therefore potentially a G protein-biased form of GPR35. However, before using this mutant in further studies, it was necessary to determine whether it retained the ability to recruit G protein. An unbiased approach to investigating G protein recruitment, which uses GPCR/Gα peptide intramolecular BRET sensors in HEK293 cells (Malik et al., 2013), has previously been utilised to show that of all the G proteins that couple to GPR35, $G\alpha_{13}$ is recruited with the greatest efficacy (Mackenzie, A.E., Hudson, B. and Milligan, G., unpublished data). Therefore, a GPR35(PDM)/$G\alpha_{13}$ intramolecular BRET sensor and an equivalent GPR35(PDM)/no peptide control sensor were constructed to investigate the effects of the C-terminal tail phosphorylation site mutations on G protein recruitment to GPR35 (Figure 3-10 A). The phosphorylation-deficient mutant was indeed able to couple to $G\alpha_{13}$ peptide; moreover, removing the phosphorylation sites enhanced both the potency and the efficacy of the response to zaprinast compared with the wild type sensor (Figure 3-10 B and C).

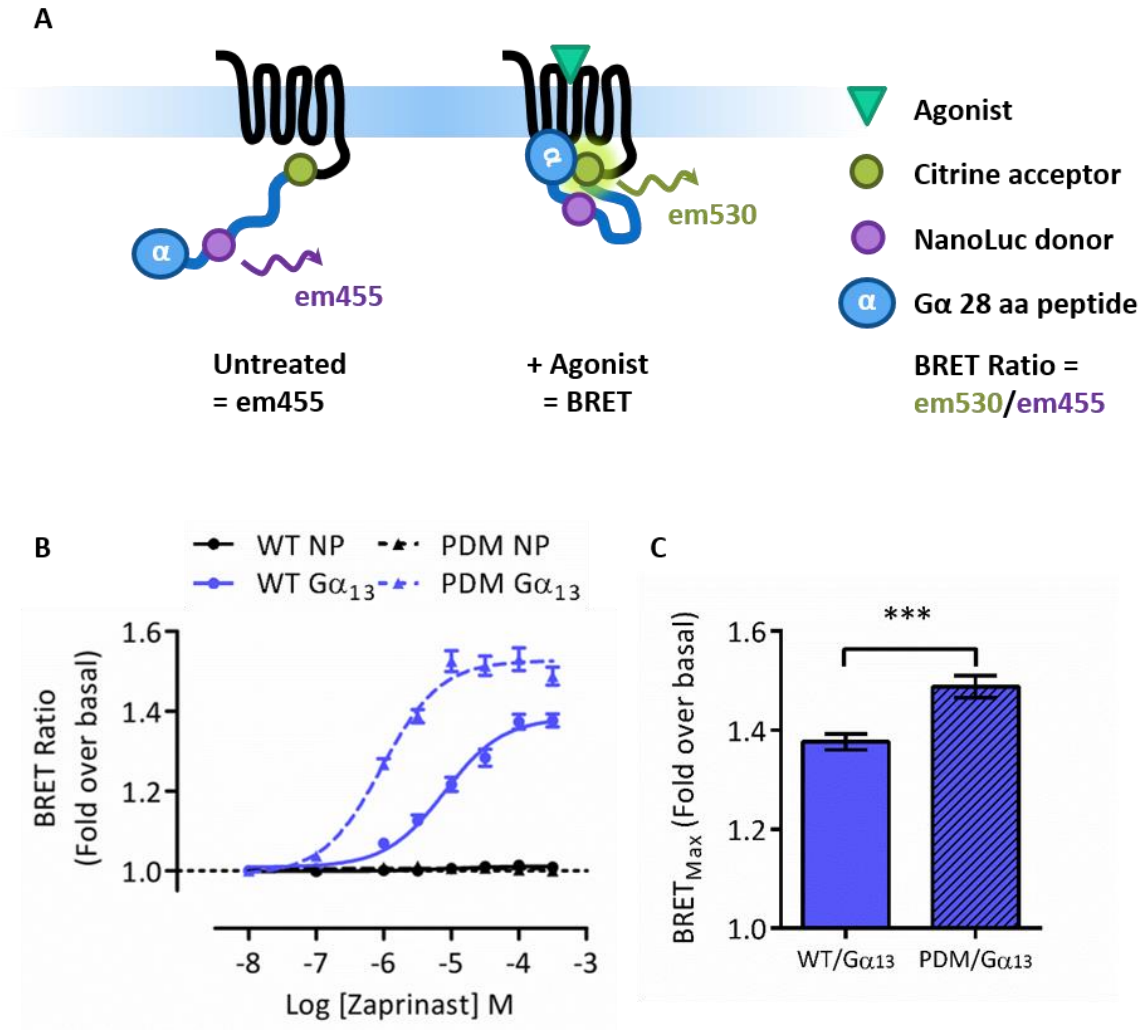

Figure 3-10 Human GPR35 phosphorylation-deficient mutant retains the ability to couple to $G\alpha_{13}$ (A) Schematic representation of intramolecular BRET sensor constructs (em = emission wavelength in nm). **(B)** Zaprinast concentration-response curves for hGPR35 no peptide (NP) or $G\alpha_{13}$ 28 amino acid peptide (G_{13}) intramolecular BRET sensors; curves for wild type (WT) and phosphorylation-deficient mutant (PDM) are shown. **(C)** Maximal BRET stimulated by zaprinast treatment. All data are means pooled from n = 3 independent experiments performed in triplicate +/- SEM. ****p*<0.001 compared with WT in two-tailed unpaired student's t test. BRET = bioluminescence resonance energy transfer.

In order to investigate whether this effect of C-terminal tail mutations also occurs in response to different agonists, the intramolecular BRET sensors were also tested with the partial agonists pamoic acid and amlexanox (Figure 3-11). As with zaprinast, the potency and efficacy of the response was significantly higher for the phosphorylation-deficient mutant than for the wild type sensor when either pamoic acid or amlexanox was used to induce G protein recruitment (Figure 3-11 A-D). Notably, the effect of the mutations on maximal BRET was amplified with the partial agonists (Figure 3-11 B and D), resulting in an efficacy comparable to that of zaprinast (Figure 3-11 E).

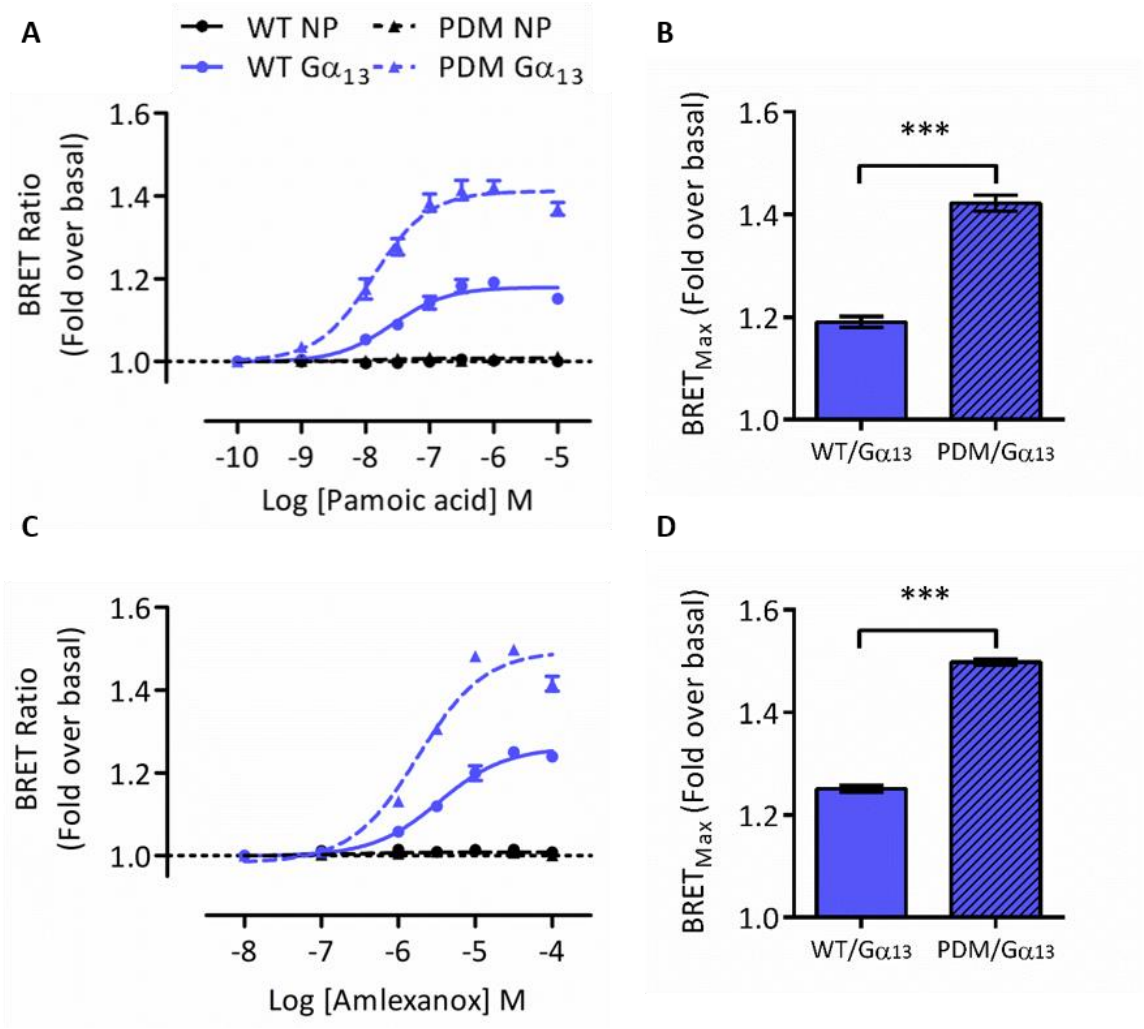

Figure 3-11 A phosphorylation-deficient GPR35 mutant is able to recruit $G\alpha_{13}$ with full efficacy in response to partial agonists (A and C) Concentration-response curves of **(A)** pamoic acid and **(C)** amlexanox for hGPR35 no peptide (NP) or $G\alpha_{13}$ intramolecular BRET sensors; curves for wild type (WT) and phosphorylation-deficient mutant (PDM) are shown. **(B and D)** Maximal BRET stimulated by **(B)** pamoic acid and **(D)** amlexanox treatment. All data are means pooled from n = 3 independent experiments performed in triplicate +/- SEM. ***p<0.001 compared with WT in two-tailed unpaired student's t test. BRET = bioluminescence resonance energy transfer.

3.2.3 Investigating G protein- and β-arrestin-mediated aspects of GPR35 signalling

Previous studies on GPR35 have resulted in a basic understanding of its coupling profile and some of its downstream effects (Figure 1-6) (Divorty et al., 2015). However, these have not been studied in detail and some of our knowledge of the pathways involved is based on assumptions. Linking specific cellular effects of GPR35 with cytoplasmic mediators, particularly G proteins and ß-arrestins, will be key to utilising this receptor as a drug target, especially with regard to the potential development of biased ligands as therapeutics.

The contributions of phosphorylation, $G\alpha_{13}$ and ß-arrestins to downstream responses elicited by GPR35 agonists were evaluated using CRISPR-edited HEK293 cell lines deficient in the relevant signalling proteins. In order to investigate GPR35-specific signalling in these cells, it was necessary to stably transfect the relevant CRISPR-edited 'knockout' cell lines with GPR35 (Figure 3-12). Both wild type and phosphorylation-deficient FLAG-GPR35-eYFP constructs were transfected into the parental cell line (hereafter referred to as parental + WT or parental + PDM), and the wild type construct was transfected into the $G\alpha_{12/13}$ knockout ($G_{12/13}$ KO) and ß-arrestin-1/2 knockout (Arr KO) cell lines (hereafter referred to as $G_{12/13}$ KO + WT or Arr KO + WT). The clonal cell lines generated were manually screened for homogeneous GPR35 expression at the cell surface based on their eYFP fluorescence.

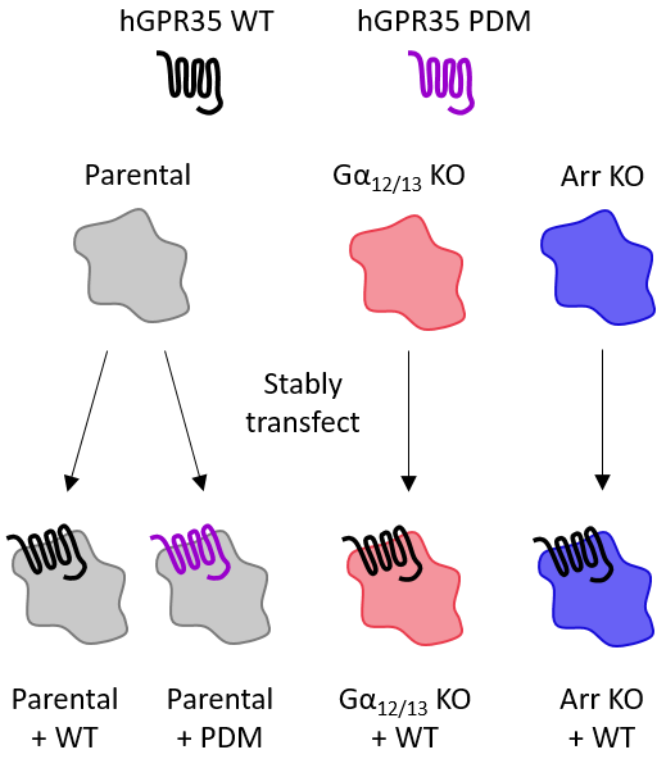

Figure 3-12 Schematic representation of modified GPR35-expressing cell lines. CRISPR-edited $G\alpha_{12/13}$ or β-arrestin-1/2 'knockout' (KO) cell lines (or the parental, non-edited cell line) were stably transfected with FLAG-hGPR35-eYFP wild type (WT) or phosphorylation-deficient mutant (PDM).

Prior to using these modified cell lines in subsequent studies, the absence of the relevant proteins and the expression of GPR35 were confirmed by immunoblotting (Figure 3-13). $G\alpha_{12}$, $G\alpha_{13}$, ß-arrestin-1, ß-arrestin-2 and FLAG-GPR35 were all detectable in the transfected parental cell lines, although $G\alpha_{12}$

appeared to be present at a lower level in the parental + GPR35 PDM cells compared with the other lines (Figure 3-13). $G\alpha_{12}$ and $G\alpha_{13}$ were absent and ß-arrestin-1, ß-arrestin-2 and FLAG-GPR35 were present in both $G_{12/13}$ KO + WT clones. Due to the lower levels of the ß-arrestins in $G_{12/13}$ KO + WT clone 3, $G_{12/13}$ KO + WT clone 2 was selected for use in the subsequent studies. ß-arrestin-1 was absent and $G\alpha_{12}$, $G\alpha_{13}$ and FLAG-GPR35 were present in both Arr KO + WT clones. A faint signal was observed for ß-arrestin-2 in these cell lines – however, due to the absence of ß-arrestin-1, this band could not indicate contamination of the KO cell line by parental cells. It is likely that this observation was the result of non-specific activity of the antibody, but even if ß-arrestin-2 was present in these cells, it was at a significantly reduced level compared with the parental cells. Since FLAG-GPR35 was poorly expressed in Arr KO + WT clone 5, Arr KO + WT clone 6 was selected for use in the subsequent studies.

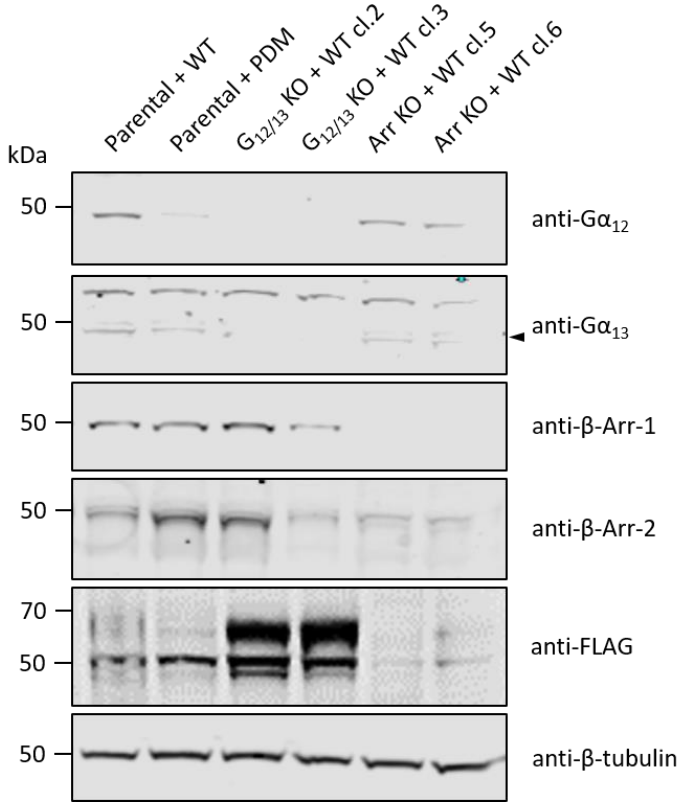

Figure 3-13 Immunoblot analysis confirms identities of stably transfected CRISPR-edited knockout cell lines. Membrane fractions ($G\alpha_{12}$, $G\alpha_{13}$, FLAG) or cytosolic fractions (β-Arr-1, β-Arr-2, β-tubulin) of CRISPR-edited and GPR35-transfected cell lysates were immunoblotted for G protein, β-arrestin or FLAG-GPR35. As transfectants were clonally selected, different clones (cl.) of the knockout cell lines were assessed. Images are representative of n = 2 individual experiments. WT = FLAG-hGPR35-eYFP wild type; PDM = FLAG-hGPR35-eYFP phosphorylation-deficient mutant; Arr = arrestin.

Having generated the CRISPR-edited, stably transfected cell lines, the aim of the study was to characterise signalling responses to GPR35 stimulation in these cells. Receptor internalisation is by far the best-characterised ß-arrestin-mediated response to GPCR activation (Luttrell and Lefkowitz, 2002), and so the manner in which this process is triggered by GPR35 stimulation was investigated.

The GPR35 internalisation response was qualitatively examined by live-cell confocal microscopy (Figure 3-14). In the absence of agonist, GPR35 was homogeneously expressed at the cell surface in all cell lines. In the parental + WT cells, wild type GPR35 was rapidly internalised in response to zaprinast treatment, with GPR35-eYFP visibly internalised into endocytic vesicles after 15 min (Figure 3-14). After 45 min, the majority of wild type receptor was present in the intracellular endocytic compartment. This was also the case in the $G_{12/13}$ KO + WT cell line, except that peak internalisation appeared to be

reached after only 30 min. In the parental + PDM cells, some vesicles were visible after 15 min, but were substantially fewer in number than in the wild type cell line, with the majority of receptor remaining at the plasma membrane over 45 min. In the Arr KO + WT cell line, no zaprinast-induced internalisation of GPR35 could be detected (Figure 3-14).

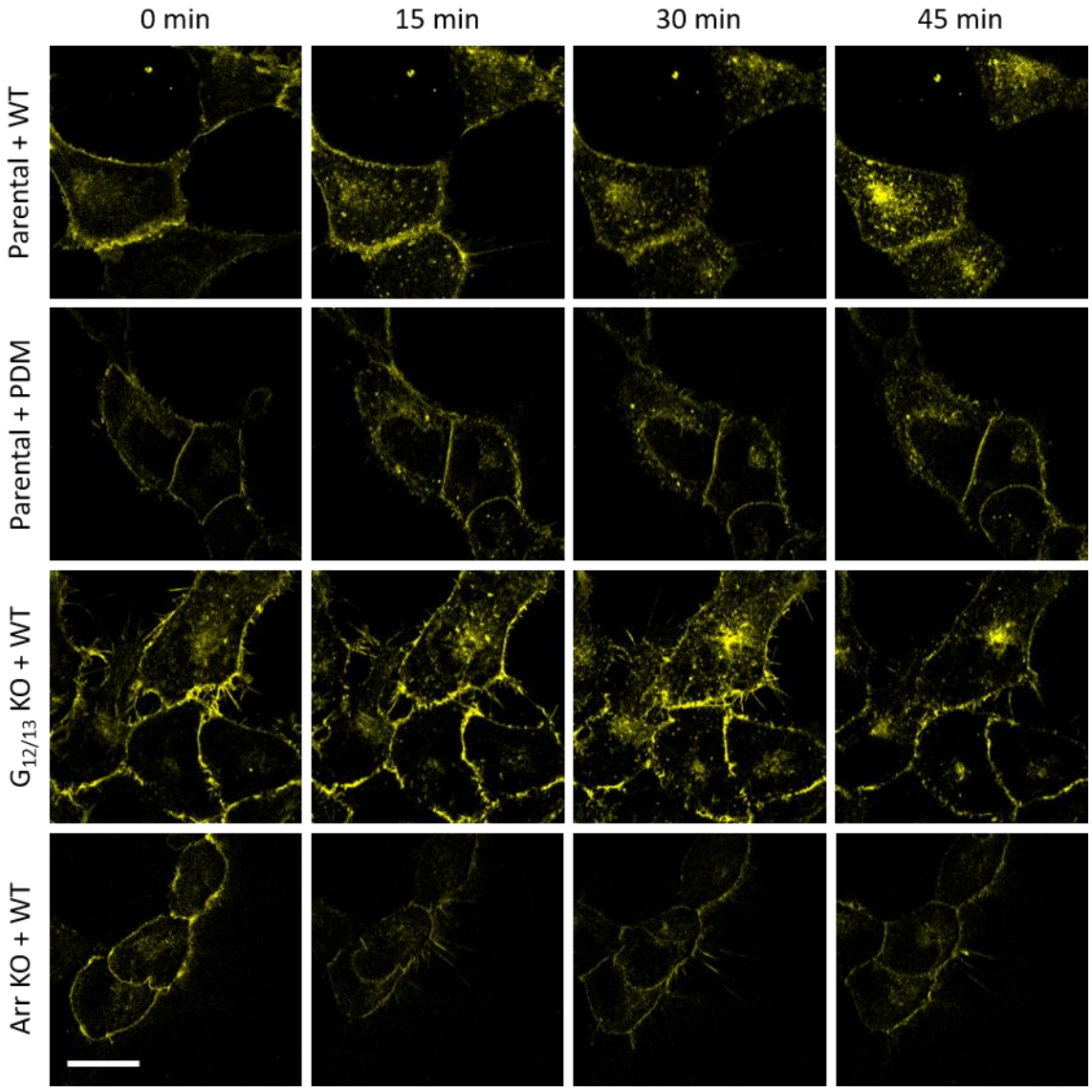

Figure 3-14 Both GPR35 phosphorylation and β-arrestin are required for zaprinast-induced GPR35 internalisation Internalisation of GPR35-eYFP was qualitatively assessed by live-cell confocal microscopy. Cells were stimulated with 100 μM zaprinast for 45 min and imaged at the time points indicated. Images are representative of n = 3 independent experiments. Scale bar = 20 μm. WT = FLAG-hGPR35-eYFP wild type; PDM = FLAG-hGPR35-eYFP phosphorylation-deficient mutant.

Although qualitatively assessing GPR35 internalisation provides useful insights, a more accurate understanding of internalisation events requires quantitative analysis. The Arrayscan high-content imaging system was used to quantify GPR35

internalisation in the modified cell lines in order to build on the qualitative observations (Figure 3-15). This method uses an algorithm designed to identify the number of individual internalised vesicles in the eYFP channel, which is normalised against cell number using a nuclear stain. A zaprinast concentration-response curve (Figure 3-15 A-B) demonstrated that while little or no internalisation was detected in the parental + PDM or Arr KO + WT cells, the maximal internalisation in the $G_{12/13}$ KO + WT cells was significantly greater than that in the parental + WT cells. This was also apparent in a time-course of internalisation, which showed that GPR35 was internalised at a steady rate over 40–50 min in both the parental + WT cells and the $G_{12/13}$ KO + WT cells (Figure 3-15 C).

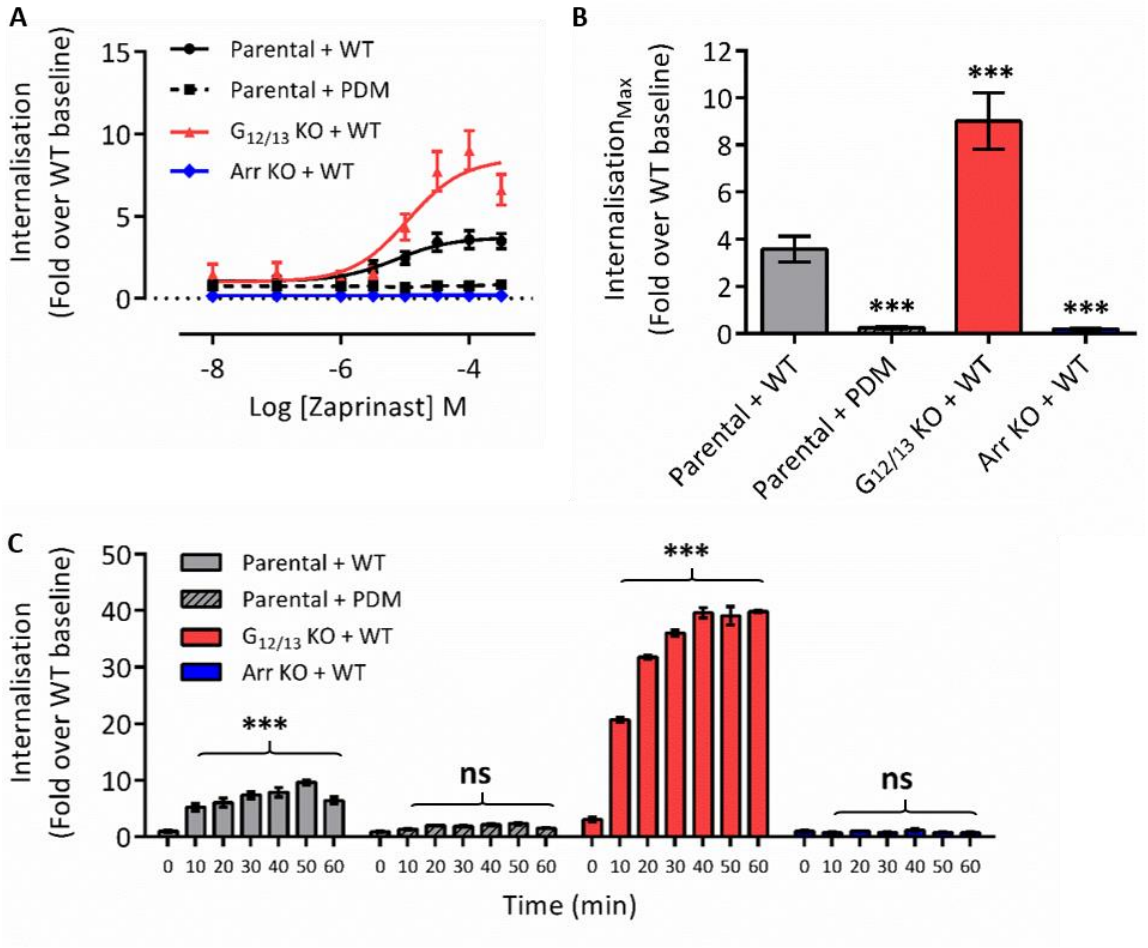

Figure 3-15 GPR35 phosphorylation, β-arrestin and $G\alpha_{12/13}$ all influence the efficacy of the GPR35 internalisation response (A) Concentration-response curves of GPR35-eYFP internalisation after 45 min zaprinast treatment in modified cell lines. **(B)** Maximal GPR35 internalisation after 45 min zaprinast treatment. **(C)** Time course of GPR35 internalisation stimulated by 100 μM zaprinast. **(A–B)** Data are means pooled from n = 3 independent experiments performed in triplicate +/- SEM; **(C)** Data are representative of n = 2 independent experiments performed in triplicate +/- SEM. ***p<0.001 compared with **(B)** Parental + WT or **(C)** 0 min in one-way ANOVA.

These data suggest that ß-arrestin-1/2 are essential for agonist-induced GPR35 internalisation to occur (Figure 3-14 and Figure 3-15). This conclusion is consistent with the current belief that the ß-arrestins are the primary regulators of GPCR internalisation (Goodman et al., 1996, Laporte et al., 1999). However, a potential criticism of this finding is that the Arr KO cells express a much lower level of FLAG-GPR35 (Figure 3-13) and thus are potentially less sensitive to zaprinast, which could account for the lack of internalisation response observed. To address this, ß-arrestin-2 was transfected into the Arr KO cells in an attempt to 'rescue' the internalisation phenotype (Figure 3-16). Transient transfection of Arr KO + GPR35 WT cells with ß-arrestin-2-mCherry, but not the empty vector pcDNA3, resulted in rapid internalisation of GPR35-eYFP in response to zaprinast (Figure 3-16), which was similar to that observed in the parental + GPR35 WT cell line (Figure 3-14). Even cells with relatively weak expression of ß-arrestin-2-mCherry rapidly internalised GPR35-eYFP, suggesting that modest amounts of ß-arrestin-2 are sufficient to induce internalisation of GPR35. These findings further support the conclusion that a lack of ß-arrestin prevents agonist-induced internalisation of GPR35.

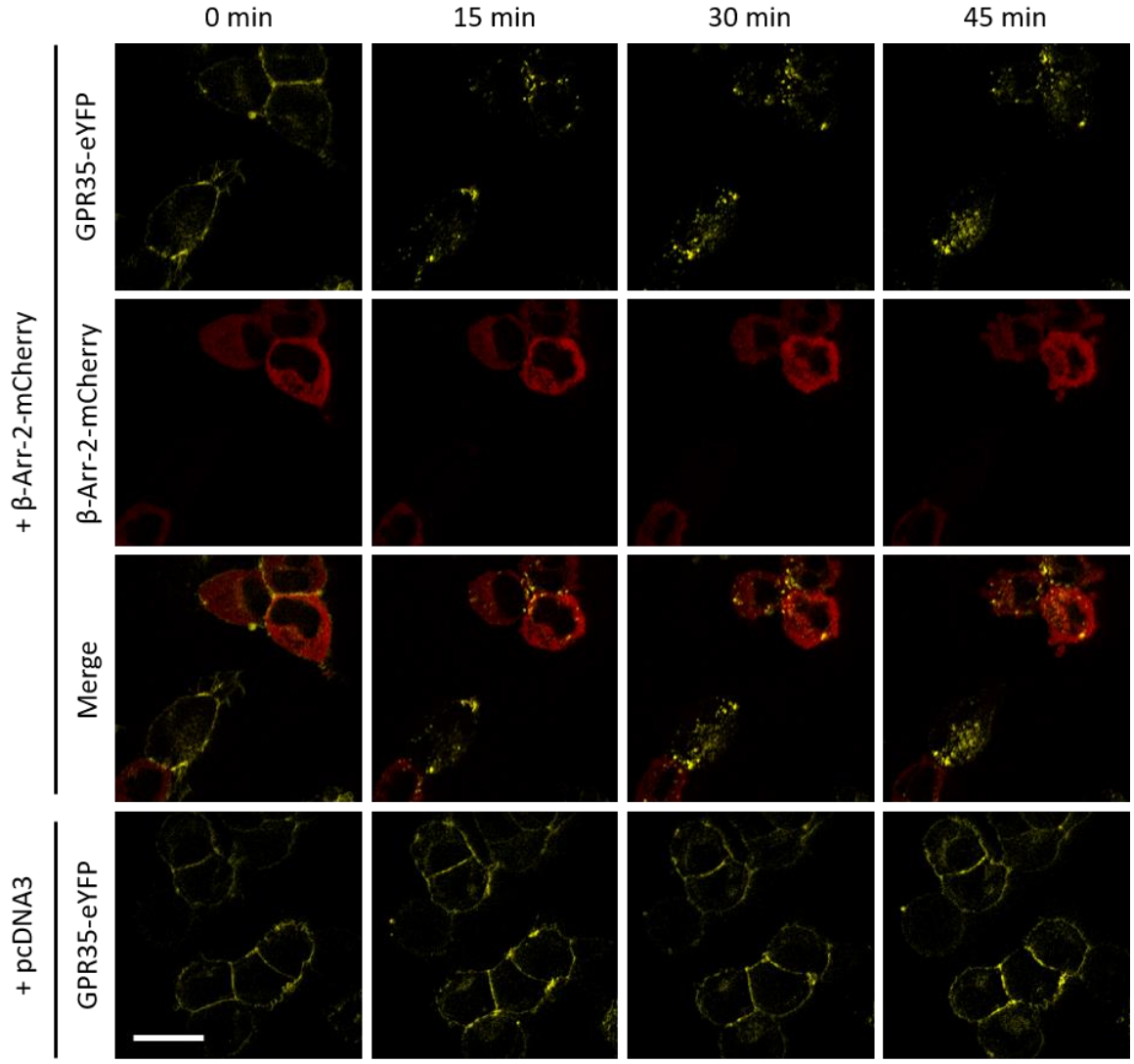

Figure 3-16 Transfection of Arr KO + WT cells with β-arrestin-2-mCherry rescues the internalisation phenotype Arr KO cells expressing wild type GPR35-eYFP cells were transiently transfected with β-arrestin-2-mCherry or the empty vector pcDNA3. Cells were stimulated with 100 µM zaprinast for 45 min and imaged at the time points indicated. Scale bar = 20 µm.

After establishing the role of ß-arrestin in GPR35 internalisation, $G\alpha_{12/13}$-mediated downstream responses were examined to establish what role this aspect of GPR35 signalling might have in the regulation of cellular processes. Since $G\alpha_{12/13}$ signalling is often associated with changes in cell morphology *via* reorganisation of the actin cytoskeleton (Gohla et al., 1999, Schappi et al., 2014), the distribution of actin was examined in the modified cell lines using TRITC-labelled phalloidin to stain filamentous (F)-actin (Figure 3-17). Substantial differences were observed in the actin distribution between the parental and knockout cell lines even before they were stably transfected with GPR35 (Figure 3-17, left-hand panels). The untransfected parental cells formed a relatively regular monolayer, with the cell edges clearly defined by F-actin

staining at the periphery of the cytoplasm. The untransfected $G_{12/13}$ KO cells, however, had a much less ordered distribution of F-actin, with many short, disordered filaments distributed throughout the cytoplasm. The untransfected Arr KO cells were more similar to the parental cells, but with enriched F-actin at cell-cell contacts.

Next, the GPR35-expressing cell lines were examined to determine the effect of agonist stimulation on F-actin distribution. An unexpected finding was that transfection with wild type GPR35 alone (without agonist stimulation) was sufficient to induce changes in actin cytoskeletal organisation in the parental cells (Figure 3-17, middle panels). These cells had a more spread-out morphology, and showed formation of some ordered stress fibres. This was also observed in the Arr KO + WT cell line, but not in the $G_{12/13}$ KO + WT cell line, suggesting that these changes were mediated by $G\alpha_{12/13}$.

The effects of GPR35 activation on actin distribution were examined by stimulating the modified cells with zaprinast for 30 min (Figure 3-17, right-hand panels). In the parental + WT cells, zaprinast stimulation led to the formation of an increased number of actin fibres which were ordered into bundles. This effect was also observed in the Arr KO + WT cells. It was not observed in the parental + PDM cells, but this appeared to be due to shrinking and apoptosis of the cells. It is possible that this cytotoxic effect was related to the prolonged and unregulated activity of GPR35 in these cells, especially considering that the protein expression level of GPR35 was found to be much greater in these cells than in the Arr KO + WT cell line (Figure 3-13). Zaprinast stimulation had no effect on actin distribution in the $G_{12/13}$ KO + WT cells, supporting the hypothesis that GPR35 stimulates reorganisation of the actin cytoskeleton *via* $G\alpha_{12/13}$.

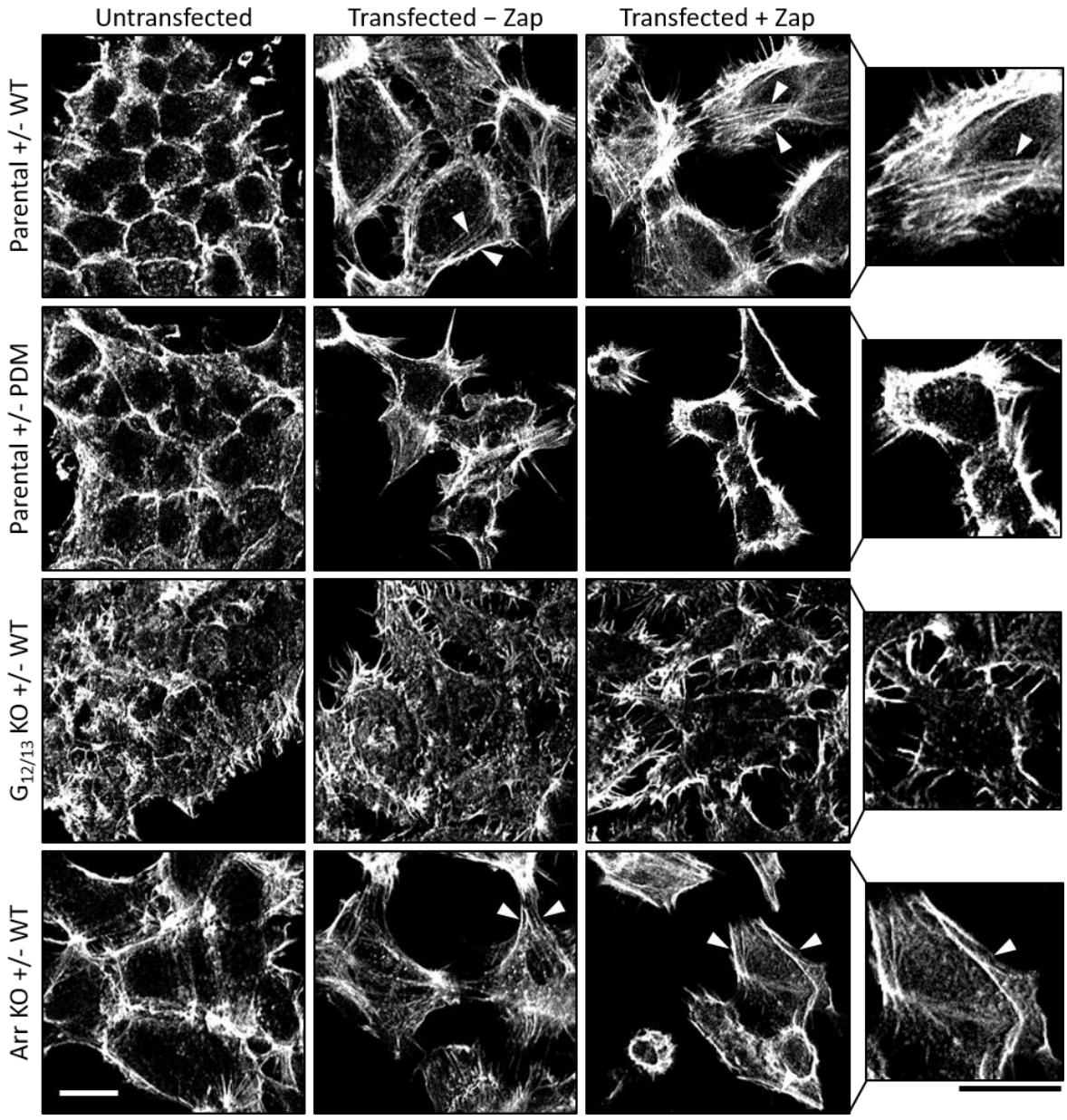

Figure 3-17 GPR35 promotes $G\alpha_{12/13}$-mediated formation of F-actin stress fibres Modified cell lines were stained for F-actin using TRITC-phalloidin. Cells were untreated (left- hand and middle panels) or stimulated for 30 min with 100 μM zaprinast (right-hand panels). Examples of stress fibres are indicated by white arrowheads. Scale bars = 20 μm.

The observation that transfection of the parental cells with WT GPR35 was sufficient to cause some actin reorganisation suggests that constitutive activity of GPR35, or the presence of a GPR35 agonist in the culture medium, might influence the actin cytoskeleton. To determine whether the observed changes to the cytoskeleton in untreated cells were mediated by GPR35 overexpression, the modified cell lines were cultured with the GPR35 inverse agonist ML-145 prior to staining (Figure 3-18). In all of the cell lines except $G_{12/13}$ KO + WT, culturing the GPR35-expressing cells in ML-145 altered the actin distribution so that it resembled that of the equivalent untransfected cells. This further supports the

hypothesis that GPR35 overexpression is sufficient to induce reorganisation of the actin cytoskeleton.

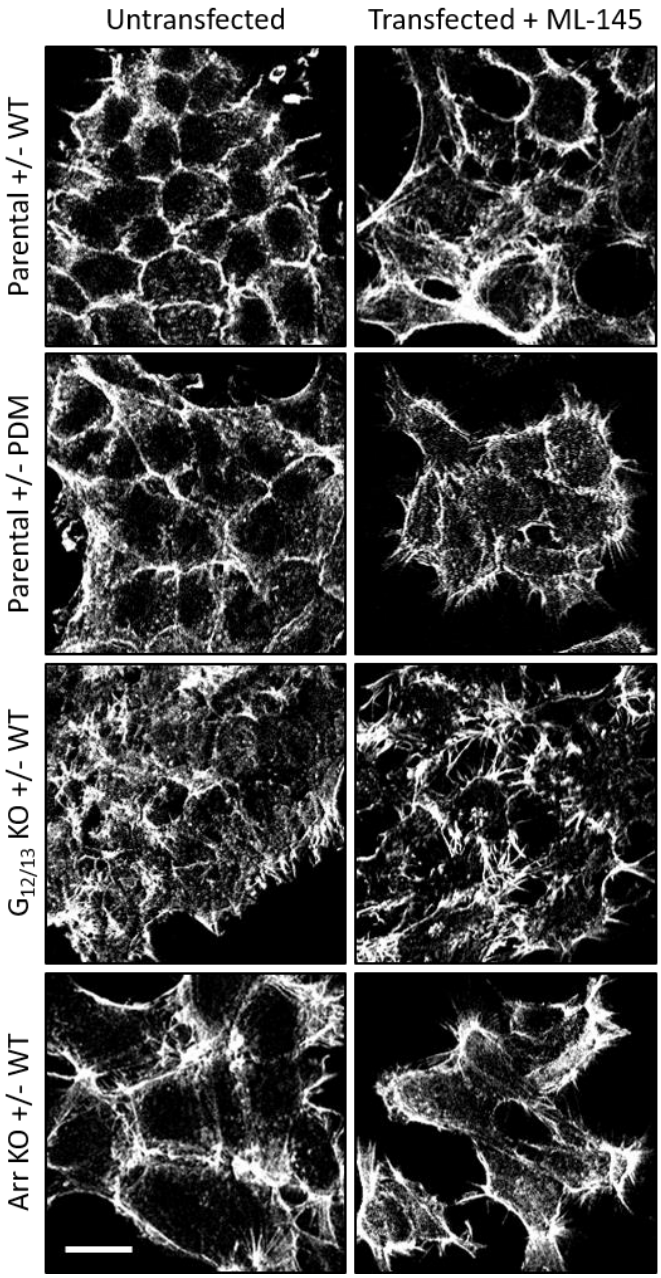

Figure 3-18 ML-145 inhibits changes to the actin cytoskeleton induced by GPR35 overexpression Modified cell lines were cultured for 24 hours in normal maintenance medium (right-hand panels) or in normal maintenance medium + 1 μM ML-145 (left-hand panels) and then stained for F-actin using TRITC-phalloidin. Scale bar = 20 μm.

3.3 Discussion

3.3.1 Agonist-dependent phosphorylation of GPR35

The large majority of GPCRs have potential phosphorylation sites in their intracellular domains, and for several receptors these have been confirmed experimentally by radioisotope labelling, mass spectrometry and/or phosphorylation site-specific antibodies (Butcher et al., 2011a, Nobles et al., 2011, Butcher et al., 2014, Bouzo-Lorenzo et al., 2016). This study is the first to investigate agonist-dependent phosphorylation of GPR35 and its downstream consequences. The data reported here show that, like many other GPCRs, GPR35 undergoes agonist-dependent phosphorylation. The extent of this phosphorylation differs depending on the agonist and the species orthologue in a manner that reflects the relative efficacies and species selectivities of the different agonists determined in pharmacological assays. Most commonly, these pharmacological assays are based on measuring ß-arrestin recruitment (Jenkins et al., 2012, Southern et al., 2013, MacKenzie et al., 2014). Therefore, the ability of agonists to induce phosphorylation of GPR35 can be said to correlate with their efficacy with regard to the recruitment of ß-arrestin. This association has been further investigated in this chapter, and the findings are discussed below.

While phosphorylation is often assumed to link directly with ß-arrestin recruitment and subsequent functional consequences, several therapeutically important GPCRs, such D_1R, D_2R, $ß_2AR$ and $5\text{-}HT_{2C}R$, can be constitutively phosphorylated by certain GRKs independently of agonist stimulation (Butcher et al., 2014, Li et al., 2015). This does not appear to be the case for human or mouse GPR35, as little or no constitutive phosphorylation of hGPR35 could be detected in radiolabelling assays. However, the rat orthologue did appear to incorporate some [^{32}P]-orthophosphate in the absence of agonist stimulation, resulting in a smaller fold-change in response to agonist than that observed for hGPR35 or mGPR35. This might be explained by the fact that rGPR35 has more potential phosphorylation sites (serine and threonine residues) in its C-terminal tail than either hGPR35 or mGPR35, and that phosphorylation resulting from constitutive GRK activity is therefore amplified. However, it is not known whether this would occur *in vivo* and/or have a significant effect on endogenous

GPR35 function. This is something that should be considered when generalising findings from *in vivo* or *ex vivo* rat studies to humans.

The location of phosphorylation sites varies widely between different GPCRs, in line with the diversity of the ICL and C-terminal tail regions within the family. The $ß_2$AR is phosphorylated at 13 sites distributed throughout its ICL3 and C-terminal tail (Nobles et al., 2011), whereas the M_3 muscarinic receptor is heavily phosphorylated at up to 15 sites in its exceptionally long ICL3, but at only one site in its C-terminal tail (Butcher et al., 2011a). Both free fatty acid receptor 4 (FFA_4) and the ghrelin receptor GHSR1a have two distinct clusters of phosphorylation sites occurring in different parts of the C-terminal tail, which differentially regulate downstream signalling (Butcher et al., 2014, Bouzo-Lorenzo et al., 2016, Prihandoko et al., 2016). In the present study, mass spectrometry analysis identified five sites in the hGPR35 C-terminal tail that were phosphorylated following agonist stimulation. Removing these sites by mutating them to alanine eliminated [^{32}P]-orthophosphate incorporation, suggesting that these residues are the principal or only sites of agonist-dependent phosphorylation within GPR35. While these sites do not clearly group into two clusters based on their proximity to each other, as in FFA_4 and GHSR1a, their potential to differentially regulate signalling was explored further in ß-arrestin and $Gα_{13}$ recruitment studies (discussed in section 3.3.2 and 3.3.3).

3.3.1.1 Applications of mass spectrometry-based approaches to studying GPCR phosphorylation

GPCR phosphorylation has been the subject of intense study for decades, and its roles in receptor desensitisation and internalisation have long been appreciated (Benovic et al., 1987, Innamorati et al., 1998, Seibold et al., 2000). However, new paradigms regarding the ability of site-specific phosphorylation to regulate G protein-independent signalling have recently emerged (Tobin et al., 2008, Liggett, 2011). In the past, truncation and mutagenesis studies have highlighted the importance of different 'clusters' of phosphorylation sites in directing cellular responses to the activation of some GPCRs (Innamorati et al., 1998, Orsini et al., 1999, Milasta et al., 2005). However, greater precision is required in order to further dissect the theory of the 'phosphorylation barcode' and determine its impact on signalling. Mass spectrometry-based approaches have

enabled the precise identification of individual phosphorylated residues for a number of receptors of interest (Busillo et al., 2010, Butcher et al., 2011a, Nobles et al., 2011, Butcher et al., 2014, Bouzo-Lorenzo et al., 2016). Applying these approaches to more GPCRs will likely reveal important distinctions in the way different sub-groups of GPCRs are phosphorylated and transduce their signals. For example, based on the findings of the present study, GPR35 appears to fall into a category of receptors that contain multiple short clusters of phosphorylation sites in their C-terminal tails that differentially regulate ß-arrestin recruitment. Whether GPR35 phosphorylation also influences G protein-independent signalling, as it does for GSHR1a and FFA_4, is yet to be determined.

The accuracy afforded by mass spectrometry has facilitated the design of tools such as phosphorylation site mutants and phosphorylation site-specific antibodies for a number of GPCRs, which are now being used to study the impact of differential phosphorylation on signalling (Busillo et al., 2010, Butcher et al., 2011a, Nobles et al., 2011, Prihandoko et al., 2016). Such tools will also be valuable in investigating the true importance of differential phosphorylation *in vivo*. For example, phosphorylation site-specific antibodies have been used to demonstrate differential phosphorylation of M_3R in different mouse tissues (Butcher et al., 2011a). Furthermore, a phosphorylation-deficient M_3R mutant has recently been used to generate a knock-in mouse, which is providing insight into the impact of M_3R phosphorylation on learning and memory *in vivo* (Poulin et al., 2010, Bradley et al., 2016). As detailed phosphorylation profiles are generated and utilised in *in vivo* studies for more GPCRs, the therapeutic potential of targeting this aspect of GPCR signalling will become clear.

3.3.2 β-arrestin recruitment to GPR35

ß-arrestin recruitment has been used extensively in multiple assay formats to identify and characterise ligands of GPR35 (Jenkins et al., 2010, Zhao et al., 2010, Deng et al., 2012, Jenkins et al., 2012, Neetoo-Isseljee et al., 2013, MacKenzie et al., 2014). All of the synthetic agonists of GPR35 identified to date induce ß-arrestin recruitment, and this response has become a reliable and robust measure of GPR35 activation. Furthermore, ß-arrestin recruitment has long been known to have important functional consequences in the transduction

of the GPCR signal, from desensitisation and internalisation to G protein-independent signalling.

Despite ß-arrestin being an important aspect of the cellular response to the vast majority of GPCRs, there does not appear to be a universal binding site to which it is recruited; interactions vary depending on the receptor in question, and are regulated through both conformational changes and covalent modifications. For example, the third intracellular loop is important for ß-arrestin binding to the α_2AR, M_2R and M_3R (Lee et al., 2000, DeGraff et al., 2002, Poulin et al., 2010), whereas a conserved tripeptide motif at the bottom of helix three is essential for ß-arrestin binding to the *N*-formyl peptide receptor (Bennett et al., 2000). However, the largest interface and the most common point of interaction is the receptor C-terminal tail. Phosphorylation of residues in this region enhances ß-arrestin recruitment, as discussed above. For some receptors, small clusters of serine and threonine residues in the C-terminal tail are essential for ß-arrestin recruitment. For example, mutation of three threonines and one serine within the last seven residues of the orexin A receptor leads to a substantial reduction in ß-arrestin recruitment and co-internalisation (Milasta et al., 2005). Similarly, for both GSHR1a and FFA_4, mutation of two or three serine and threonine residues is sufficient to inhibit ß-arrestin recruitment and receptor internalisation (Butcher et al., 2014, Bouzo-Lorenzo et al., 2016). For these receptors, however, different clusters appear to make varying contributions, with clusters closer to the C-terminus having a greater impact on ß-arrestin recruitment.

Having herein identified several phosphorylation sites in the hGPR35 C-terminal tail, the influence of each of these sites on ß-arrestin recruitment was evaluated using a BRET-based ß-arrestin-2 recruitment assay. Of the five phosphorylation sites identified by mass spectrometry, four made a significant contribution to the maximal efficacy of ß-arrestin-2 recruitment regardless of agonist or species orthologue. Individual substitution of these sites had varying degrees of impact on ß-arrestin recruitment in response to zaprinast, inhibiting BRET by between 30% (S300) and 75% (S303). Substituting either all five of the sites or S303 and T307 (the two most C-terminal sites) simultaneously resulted in almost complete inhibition of ß-arrestin recruitment. This suggests that agonist-dependent

phosphorylation of S303, and, to a lesser extent, T307, is necessary for ß-arrestin binding to GPR35. This same hierarchical rank order of sites was observed both with different agonists and at different species orthologues, with S303 having the greatest impact on phosphorylation in response to all three agonists and in all three orthologues. The finding that individual phosphorylation sites make unequal contributions to ß-arrestin recruitment further supports the emerging theory that site-specific phosphorylation, and not merely bulk negative charge, is necessary for ß-arrestin to interact with GPCRs *via* the C-terminal tail. This provides evidence of a 'phosphorylation barcode' for GPR35, and thus highlights the potential capacity for context- or tissue-specific regulation of this receptor. This could have important implications in the search for a function for GPR35, given the diversity of its proposed roles in multiple tissues and physiological systems.

One notable secondary observation from the mutagenesis studies is that S294 substitution does not appear to have a significant effect on ß-arrestin recruitment to human GPR35 in response to a full agonist, despite the fact that phosphorylation of this residue was detected by mass spectrometry. This is surprising, considering S294 is the residue affected by a SNP that has been associated with both IBD and coronary artery disease (Sun et al., 2008, Imielinski et al., 2009, Ellinghaus et al., 2013). One potential explanation for this SNP's association with disease is that it alters GPR35 phosphorylation and thus ß-arrestin recruitment, and thereby dysregulates either desensitisation or G protein-independent signalling. However, this hypothesis is not supported by the findings presented here.

3.3.3 $G\alpha_{13}$ recruitment to GPR35

GPR35 coupling to $G\alpha_{13}$ has previously been demonstrated using both a chimeric $G\alpha_{13}/G\alpha_q$ G protein in a $[Ca2+]_i$ assay and an activation state-sensing GTP-$G\alpha_{13}$ antibody (Jenkins et al., 2011). The construction of a GPR35-$G\alpha_{13}$ intramolecular BRET sensor provided an unbiased and direct method of measuring G protein recruitment to GPR35 without the use of a chimeric G protein (Mackenzie, A.E., Hudson, B. and Milligan, G., unpublished data; and this work). These studies confirmed that $G\alpha_{13}$ is recruited to GPR35 in response to agonist, with a potency comparable to that observed for ß-arrestin recruitment (zaprinast EC_{50} = 7.8 μM

and 4.7 μM, respectively). The present study also assessed the ability of the phosphorylation-deficient GPR35 mutant to recruit $G\alpha_{13}$ using a GPR35(PDM)-$G\alpha_{13}$ sensor. While the mutant did not recruit ß-arrestin-2, it retained the capacity to recruit $G\alpha_{13}$, and in fact did so with enhanced potency and efficacy. This enhancement could reflect a low level of constitutive phosphorylation and/or ß-arrestin recruitment that limits the propensity of wild type GPR35 to couple to $G\alpha_{13}$. However, since the effects of the individual mutations were not assessed here, it is not known whether the sites influencing $G\alpha_{13}$ coupling are the same as those that strongly impact ß-arrestin-2 recruitment. Nonetheless, these findings suggest that constitutive phosphorylation is another potential means by which GPR35 signalling could be regulated in a context-specific manner, although it must be considered that these experiments were carried out in a highly artificial overexpression system, and it is unclear to what extent this might affect signalling *in vivo*.

3.3.4 Internalisation of GPR35

Studies into the internalisation of GPR35 utilised novel, HEK293-derived cell lines that were CRISPR-edited to delete either $G\alpha_{12/13}$ or ß-arrestin-1/2 and stably transfected with GPR35. These cell lines were used as a means of investigating the molecular determinants of GPR35 internalisation. The data presented here show that GPR35 is rapidly internalised in response to agonist stimulation in a phosphorylation- and ß-arrestin-dependent manner. Both the parental cell line expressing phosphorylation-deficient GPR35 and the ß-arrestin-1/2-deficient cell line expressing wild type GPR35 failed to internalise GPR35 in response to zaprinast stimulation in both qualitative and quantitative assays. This finding is consistent with well-documented roles for both GRK-mediated phosphorylation and ß-arrestin in stimulating clathrin-mediated endocytosis (Goodman et al., 1996, Laporte et al., 1999, Seibold et al., 2000, Thomsen et al., 2016). However, although a significant level of internalisation of the phosphorylation-deficient mutant could not be detected in the quantitative assay, live-cell microscopy revealed that a small amount of receptor was internalised into endocytic vesicles in response to zaprinast. This residual response is presumably due to either a low level of phosphorylation at alternative sites within the ICLs, or a low level of phosphorylation-independent ß-arrestin recruitment in these cells. It is important to note that this finding

shows that phosphorylation-deficient and ß-arrestin-deficient cells do not have equivalent phenotypes, and this should be kept in mind in studies in which phosphorylation-deficient mutants are used as 'G protein-biased' receptors.

Another noteworthy observation from these studies is that the magnitude of the internalisation response is significantly greater in the $G\alpha_{12/13}$-deficient cells than in the parental cell line when both express wild type GPR35. This suggests that not only do phosphorylation and ß-arrestin desensitise the G protein response, but conversely, $G\alpha_{12/13}$ has a limiting effect on ß-arrestin-mediated internalisation. Since $G\alpha_{12}$ and $G\alpha_{13}$ are ubiquitously expressed *in vivo* (Wettschureck and Offermanns, 2005), this is unlikely to have implications for endogenous GPR35 regulation. However, it reveals an interesting mechanistic detail that warrants further attention. If this effect occurs with other G proteins with more restricted expression patterns, it has implications for tissue-specific GPCR signalling – namely that the presence or absence of different G proteins could also alter the magnitude of the ß-arrestin-mediated signalling response.

One limitation of these experiments already noted was the inconsistent level of GPR35 expression across the cell lines being compared, particularly the relatively low expression level in the Arr KO + WT cell line. Weak expression of GPR35-eYFP occurred despite attempts to select high-expressing clones based on eYFP fluorescence, and reflects a practical challenge in successfully scaling up clones of this genotype. One possible reason for this is that a high level of GPR35 expression combined with ß-arrestin deficiency confers a selective disadvantage onto the cells. This could be a result of GPR35-mediated G protein signalling driven by the presence of an agonist in the culture medium, which in the absence of ß-arrestin is not desensitised or terminated. Since $G\alpha_{12/13}$ signalling is associated with reduced adhesion and increased migration, a high level of uncontrolled GPR35-$G\alpha_{13}$ signalling would not be conducive to colony selection.

In order to address this limitation and determine whether the lack of internalisation was due to the lack of ß-arrestin or simply the weak GPR35 expression, the Arr KO + WT cells were transiently transfected with ß-arrestin-2 in an attempt to restore the parental phenotype. Re-expression of ß-arrestin-2 was sufficient to enable agonist-induced internalisation of GPR35, which confirms that the internalisation defect was indeed due to a lack of ß-arrestin

and not a result of insufficient GPR35 expression. While this finding was useful as a proof of concept, achieving comparable expression levels of receptor across all the modified cell lines would enable more robust and reliable analysis. The selection process used to generate these cell lines should therefore be optimised to facilitate more reliable screening and selection in the future.

3.3.5 GPR35-mediated effects on the actin cytoskeleton

As well as investigating the typical ß-arrestin-mediated response of internalisation in these modified cell lines, a second aim was to investigate putative G protein-mediated cellular responses. GPR35 overexpression and agonism have been reported to alter the actin cytoskeleton in HEK293 cells as well as in cardiomyocytes and vascular smooth muscle cells, although the precise effect of this on cell morphology is inconsistent between studies (Min et al., 2010, Ronkainen et al., 2014, McCallum et al., 2015). These effects on the cytoskeleton are hypothesised to be due to the coupling of GPR35 to $G\alpha_{13}$; however, $G\alpha_{12/13}$, $G\alpha_{q/11}$, and ß-arrestins have all been shown to be capable of stimulating actin stress fibre formation (Buhl et al., 1995, Vogt et al., 2003, Barnes et al., 2005). The CRISPR-modified cell lines provided a means of determining whether $G\alpha_{12}$ and $G\alpha_{13}$ mediate the previously reported effects of GPR35 on the actin cytoskeleton.

It was immediately obvious that even in the absence of exogenous GPR35 or any intentional stimulus, the untransfected cell lines differed in their actin distribution patterns. This was especially striking in the $G\alpha_{12/13}$ KO cells, which had a very different shape and actin distribution than the parental and Arr KO cell lines. This is perhaps not surprising, considering the known importance of these G proteins in regulating actin dynamics and cell morphology (Gohla et al., 1999, Schappi et al., 2014). The second observation was that transfection of GPR35 alone was sufficient to induce actin fibre formation in cells expressing $G\alpha_{12/13}$ (including those not expressing ß-arrestin-1/2), and that stimulation with zaprinast enhanced this effect. The fact that no actin rearrangement occurred in the $G\alpha_{12/13}$ KO cell line upon either GPR35 transfection or zaprinast stimulation is evidence that these effects of GPR35 are mediated by $G\alpha_{12}$ and/or $G\alpha_{13}$. Furthermore, culturing the cells with the GPR35 inverse agonist ML-145 reversed

the effects of GPR35 overexpression, which further demonstrates that these effects were due to GPR35-dependent signalling.

The fact that GPR35 overexpression alone is sufficient to alter the actin cytoskeleton in HEK293 cells has important implications for its potential roles in the cardiovascular system and CVD. GPR35 expression is induced in the heart during heart failure, and these findings suggest that this could contribute to the cellular remodelling in the heart that drives pathogenesis. (Min et al., 2010, Ronkainen et al., 2014). Furthermore, GPR35 agonism has recently been reported to have similar effects on actin reorganisation in human vascular smooth muscle cells, and so this pathway may also drive vascular remodelling in the development of diseases such as hypertension (McCallum et al., 2015).

$G\alpha_{12}$ and $G\alpha_{13}$ are thought to mediate most of their effects, including those on the actin cytoskeleton, through the activation of Rho-GEFs and the subsequent activation of RhoA and its principal effector, ROCK (Buhl et al., 1995, Worzfeld et al., 2008, Siehler, 2009). Both RhoA and ROCK are known to be highly important in cardiovascular function and pathophysiology, with their activity stimulating vascular smooth muscle contraction, endothelial contractility and cardiac hypertrophy (Takefuji et al., 2012, Hartmann et al., 2015, Huveneers et al., 2015). There is already some evidence to suggest that GPR35 can activate the RhoA pathway in cells of the cardiovascular system – in human vascular smooth muscle cells, GPR35-mediated effects on migration were inhibited by the RhoA pathway inhibitors Y-27632 and Y-16 (McCallum et al., 2015). The findings reported here therefore combine with existing evidence to support an emerging model of GPR35 signalling in the cardiovascular system, whereby GPR35 couples to $G\alpha_{13}$, which activates the RhoA/ROCK pathway in order to regulate the actin cytoskeleton. This in turn influences cardiovascular function by stimulating cardiovascular remodelling and/or vascular contractility.

3.3.5.1 Challenges in studying the GPR35/$G\alpha_{13}$/RhoA signalling axis

Qualitatively assessing the actin cytoskeleton, as described here, is one of a limited number of endpoints that can be used to study the activity of $G\alpha_{12/13}$-coupled receptors such as GPR35. Direct and quantitative second-messenger assays to measure the activation of the $G\alpha_s$, $G\alpha_i$ and $G\alpha_{q/11}$ families have been

available for many years, but measuring $G\alpha_{12/13}$ activation presents unique challenges. Most current methods rely on indirect measurement of downstream signalling outcomes. Assay systems based on measuring RhoA pathway activation, such as RhoA-GTP pull-down assays, have been used with relative success (Ren et al., 1999). However, these techniques carry the caveat that $G\alpha_{12/13}$ is not the only family to activate this pathway, and so they cannot definitively prove $G\alpha_{12/13}$ involvement. To overcome this limitation, such techniques could be combined with methods that selectively eliminate alternative pathways, such as selective inhibitors or 'knockout' cell lines like the ones used in this study. This would be an interesting avenue to pursue in future investigations into the GPR35/$G\alpha_{13}$ pathway. Alternatively, label-free technologies such as dynamic mass redistribution offer an unbiased approach to studying G protein coupling, and could be particularly useful for studying receptors with an atypical coupling profile, such as GPR35 (Schröder et al., 2010). This technology has the added benefit of being non-invasive and therefore applicable to primary cells, enabling the study of GPCR signalling in more physiologically relevant systems than that afforded by existing approaches (Schröder et al., 2011). Such novel techniques hold promise for facilitating the study of challenging or poorly-characterised GPCRs.

3.3.5.2 CRISPR-edited cell lines as a model in which to study GPCR signalling

The findings described in this chapter highlight the potential value of the CRISPR-edited 'knockout' cell lines used in these studies. They demonstrate that the HEK293-derived cell lines can successfully be stably transfected with a GPCR of interest, and that whole-cell responses to receptor activation, such as actin cytoskeleton rearrangement, are altered in such systems. Cell lines deficient in all of the major G proteins and ß-arrestin-1 and -2, as well as combinations thereof, have generously been made freely available to the GPCR research community. A range of these cell lines, including $G\alpha_{q/11}$-deficient cells and the ß-arrestin-1/2-deficient cells used in this work, are already being used to answer a variety of questions by several different groups (Schrage et al., 2015, Alvarez-Curto et al., 2016). These cell lines offer a straightforward approach compared with previously used methods of generating G protein-deficient cell lines, such as isolation from knockout mouse embryos (Vogt et al., 2003). Such genetic

approaches are especially valuable when selective pharmacological inhibitors are not available, as is the case with $G\alpha_{12/13}$. CRISPR-edited G protein-deficient cell lines therefore provide a novel and unique model that can be used to investigate important aspects of GPCR signalling such as coupling specificity and functional selectivity.

The data presented here build on the current understanding of GPR35 signalling, which suggests that $G\alpha_{13}$ and ß-arrestin are the major receptor-coupling proteins responsible for GPR35-mediated effects on the cardiovascular system. These findings provide further insight into the intracellular events that follow agonist binding to GPR35. In addition, these studies have resulted in novel tools with which to further probe GPR35 function.

Chapter 4 Assessing the cardiovascular phenotype of a global GPR35 knockout mouse

4.1 Introduction

Since the generation of the first knockout mouse line in 1989, genetic mouse models have proven to be powerful tools in assigning gene and protein function (Thompson et al., 1989). Knockout mice have become invaluable in the drug discovery process, enabling the identification of targets with physiological significance and, for the most part, accurate prediction of the effects of pharmacological modulation. In a retrospective study into the targets of the 100 best-selling drugs, the knockout mouse phenotype correlated with the therapeutic effect of the drug for the majority of protein targets (Zambrowicz and Sands, 2003). This approach has been applied successfully in order to interrogate the functions and therapeutic target potential of orphan GPCRs, and is particularly useful where a lack of available ligands hinders pharmacological studies (Ahmad et al., 2015). In the case of GPR35, the lack of synthetic antagonists with sufficient affinity at the rodent orthologue (section 1.4.3.2) makes the knockout mouse approach the best method with which to investigate the physiological consequences of blocking or eliminating GPR35 function.

Although *in vitro* studies in cells of the cardiovascular system have suggested roles for GPR35 in the regulation of both cardiac and vascular structure and function (Ronkainen et al., 2014, McCallum et al., 2015), very little is currently known about the effects of GPR35 modulation on the cardiovascular system *in vivo*. The only study to date to report on the phenotype of a GPR35 global knockout mouse detected a significant and considerable 37.5 mmHg increase in systolic blood pressure compared with the wild type background strain, when assessed by Millar catheterisation of the right carotid artery under general anaesthesia (Min et al., 2010). However, this finding was not followed up with any in-depth analysis, despite the fact that it implicates GPR35 as a potential target in the therapeutic control of blood pressure. The same study also assessed heart weight, based on the finding that overexpression of GPR35 in neonatal rat cardiomyocytes led to cellular hypertrophy and reduced viability and may therefore play a role in cardiac remodelling (Min et al., 2010). However, heart weight to body weight ratio was unaffected in the GPR35 knockout mice

compared with the wild type strain. These findings suggest a potential role for GPR35 in the regulation of blood pressure, but fail to provide a comprehensive account of the cardiovascular pathophysiology resulting from an absence of GPR35 expression. This chapter describes more detailed investigations into the cardiovascular phenotype of the GPR35 global knockout mouse model, comprising studies into its haemodynamic properties and the structure and function of cardiovascular end organs (the heart, aorta, mesenteric resistance arteries and kidneys).

Measurement of blood pressure in small animal models has been used extensively in the study of hypertension and related cardiovascular pathologies. There are two common approaches that may be utilised: non-invasive monitoring by means of tail-cuff plethysmography, and invasive monitoring using a fluid-filled intra-arterial catheter (Krege et al., 1995, Mills et al., 2000). While tail-cuff plethysmography has the advantage of being non-invasive, the technique presents challenges with regard to minimising stress artefacts, which can reduce the sensitivity of measurements. Conversely, catheterisation combined with an exteriorised pressure transducer provides very sensitive measurements, but usually requires either long-term restraint or general anaesthesia and so is not considered to be optimally representative of normal physiological conditions (Kramer and Kinter, 2003, Constantinides et al., 2011). However, the development of a radiotelemetry-based approach involving remote transmission of pressure measurements from an implanted catheter and pressure transducer has provided a means of accurately monitoring haemodynamic parameters in conscious, unrestrained animals (Mills et al., 2000, Kramer and Kinter, 2003). Radiotelemetry has therefore become the preferred method for monitoring blood pressure *in vivo*. This technique was used in the present study to monitor blood pressure and other haemodynamic parameters in GPR35 knockout mice, alongside *in vivo* and *ex vivo* assessments of the structure and function of cardiovascular tissues in this model.

4.1.1 Aims

The aims of this chapter were to:

- Accurately assess the effects of global knockout of GPR35 on basal haemodynamic parameters using an implantable radiotelemetry device

- Determine the effects of global knockout of GPR35 on basal cardiovascular function

- Determine the effects of global knockout of GPR35 on the morphology of cardiovascular tissues.

4.1.2 Study design

The purpose of this study was to compare the basal cardiovascular phenotype of a GPR35 knockout mouse with that of the wild type background strain, C57BL/6. Only male animals were used in order to eliminate sex-specific variation. Homozygous wild type and knockout littermates were bred, and were of sufficient body weight to tolerate telemetry probe implantation by 12 weeks of age. Probes were implanted at 12 weeks of age, followed by a 7-day recovery period during which no measurements were taken (Figure 4-1). At 13 weeks of age, cardiac function was assessed by echocardiography, then probes were remotely switched on and haemodynamic parameters were monitored continuously for 7 days, followed by sacrifice and *ex vivo* analysis (Figure 4-1). Blood pressure, heart rate and locomotive activity are all subject to intrinsic circadian rhythms in rodents, and the presence of these rhythms are indicative of normal health and cardiovascular function (Takeda and Maemura, 2011). In order to assess the diurnal variation in the parameters measured, the telemetry data generated in this study were separated into two 12-hour periods representing the dark period (night) and the light period (day). Treatment was followed by sacrifice and *ex vivo* analysis at 14 weeks of age.

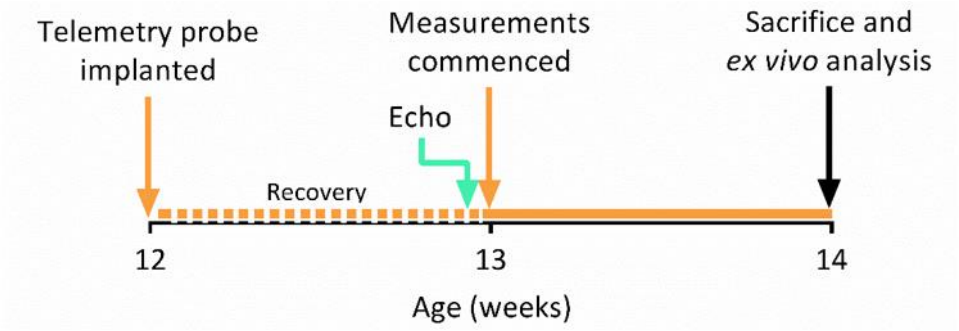

Figure 4-1 GPR35 KO study timeline

4.2 Results

4.2.1 Haemodynamic properties of the GPR35 knockout mouse

Blood pressure and heart rate are two highly regulated haemodynamic indicators of cardiovascular function, which are altered in response to various physiological and pathophysiological stimuli. These parameters, as well as locomotive activity, were assessed in wild type and GPR35 knockout mice using telemetry (Figure 4-2 and Figure 4-3). All of the parameters measured followed normal diurnal rhythms over the light/dark cycle in both wild type and GPR35 knockout mice (Figure 4-2 and Figure 4-3). Neither systolic, diastolic nor mean arterial blood pressure was significantly altered in GPR35 knockout mice compared with wild type mice (Figure 4-2). While systolic, diastolic and mean arterial blood pressure appeared to be higher in the GPR35 knockout mice at certain times during the period of monitoring (for example on day five), these differences were not consistent or significant over the duration of the study when compared using two-way repeated measures ANOVA.

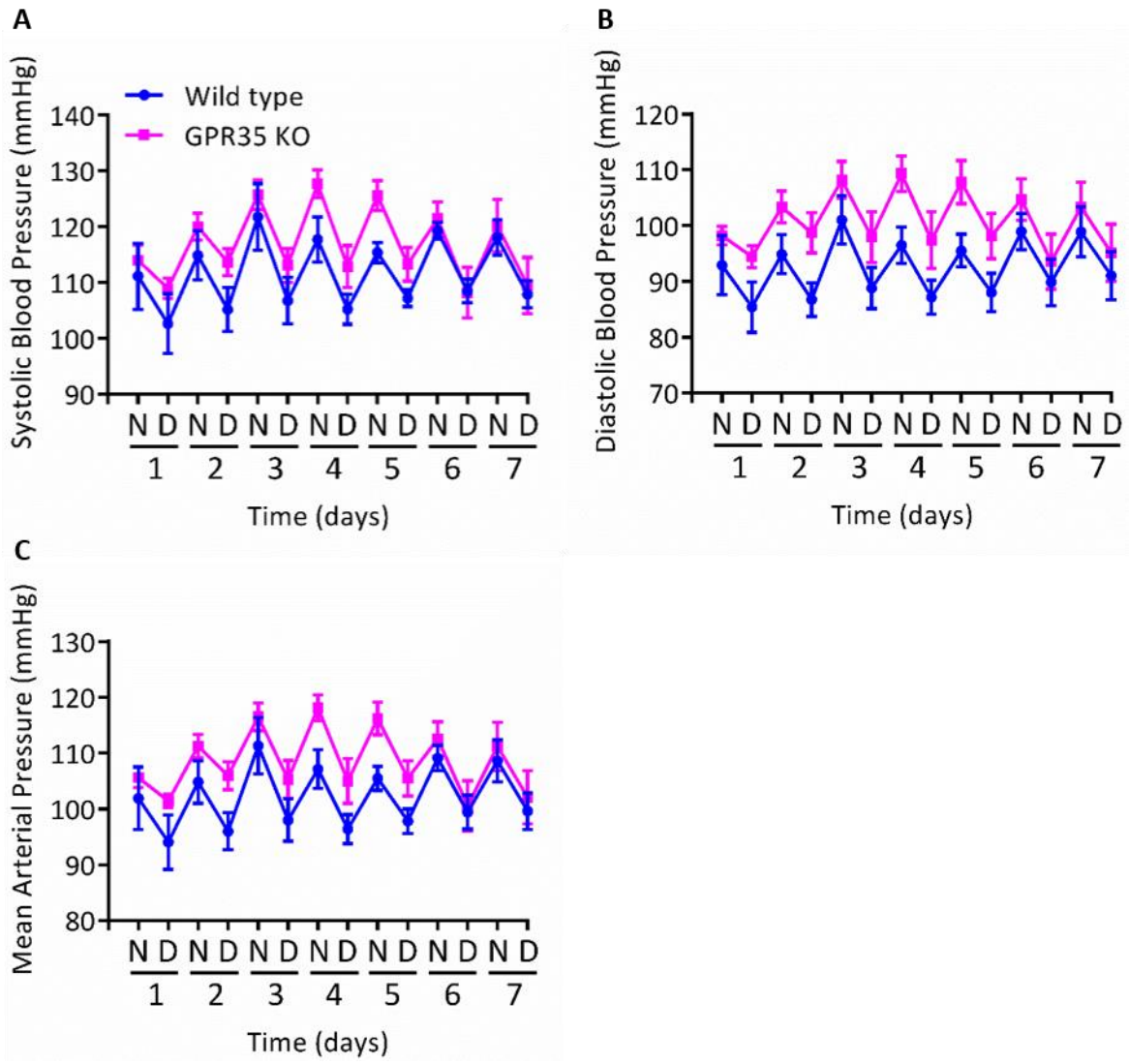

Figure 4-2 Blood pressure is unaltered in GPR35 knockout mice. (A) Systolic blood pressure, **(B)** diastolic blood pressure and **(C)** mean arterial pressure were monitored over seven days using telemetry in wild type (blue circles) and GPR35 knockout (KO) (pink squares) mice. Data are presented as 12-hour means representing night (N) and day (D) periods; mean +/- SEM of n = 6 (wild type) or n = 8 (KO) animals. Data were compared by two-way repeated measures ANOVA, but no significant differences were found.

Similarly to blood pressure, heart rate and locomotive activity were not significantly altered in GPR35 knockout mice compared with wild type mice. Heart rate appeared to be somewhat lower in the GPR35 knockout mice (Figure 4-3 A), but this trend was not significant when compared using two-way repeated measures ANOVA. Activity was also unaltered in the GPR35 knockout mice and followed normal diurnal rhythms in both groups, suggesting that the surgical procedure was well tolerated and that the one-week recovery period was sufficient to ensure an accurate representation of haemodynamic parameters under normal behavioural and physiological conditions (Figure 4-3 B).

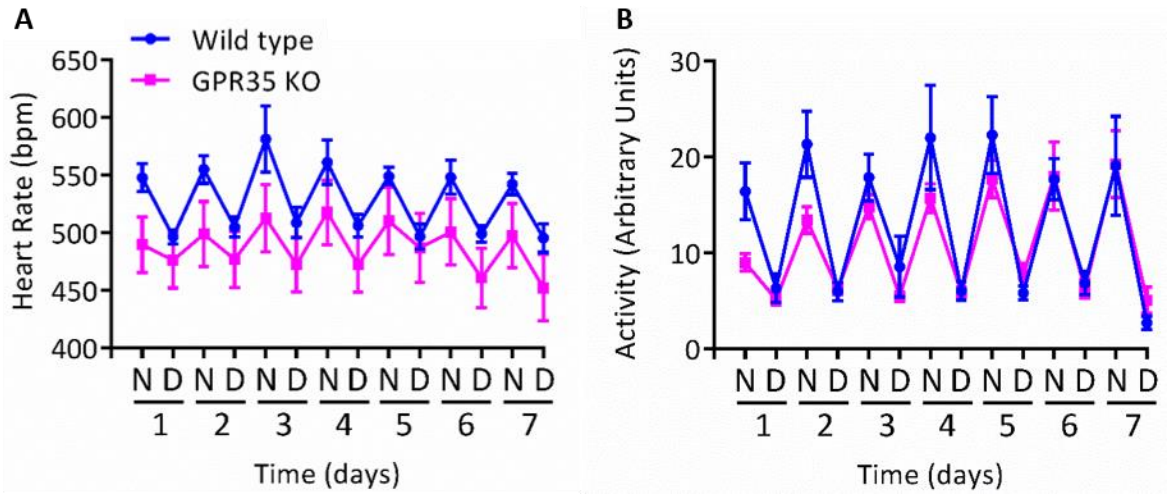

Figure 4-3 Heart rate and locomotive activity are unaltered in GPR35 knockout mice. (A) heart rate (bpm = beats per minute) and **(B)** activity were monitored over seven days using telemetry in wild type (blue circles) and GPR35 knockout (KO) (pink squares) mice. Data are presented as 12-hour means representing night (N) and day (D) periods; mean +/- SEM of n = 6 (wild type) or n = 8 (KO) animals. Data were compared by two-way repeated measures ANOVA, but no significant differences were found.

4.2.2 Cardiovascular function in the GPR35 knockout mouse

In addition to blood pressure and heart rate, measurements of both cardiac and vascular function can be used to assess the state of the cardiovascular system in animal models. Alterations in left ventricular mass and left ventricular systolic function, assessed by echocardiography, are indicative of chronic cardiovascular dysfunction in both rodent models and human disease (Gao et al., 2011, Lam et al., 2011). In the present study, left ventricular mass, diameter and systolic function in wild type and GPR35 knockout mice were assessed *in vivo* by echocardiography, which was performed prior to commencement of telemetry recordings at 13 weeks of age (Figure 4-4). Potential differences in left ventricular structure were assessed by measuring left ventricular end diastolic wall thickness and diameter. Neither left ventricular wall thickness nor left ventricular diameter were significantly altered in GPR35 knockout mice compared with wild type mice (Figure 4-4 B and D). To quantify cardiac contractility, fractional shortening and ejection fraction of the left ventricle were calculated using measurements of the left ventricular end systolic and end diastolic diameters (Figure 4-4 C and D) and volumes (Figure 4-4 F and G) (method described in section 2.10.5). Fractional shortening and ejection fraction were both unaltered in GPR35 knockout mice compared with wild type mice

(Figure 4-4 E and H). Overall, these data suggest that global knockout of GPR35 does not affect cardiac function under basal conditions.

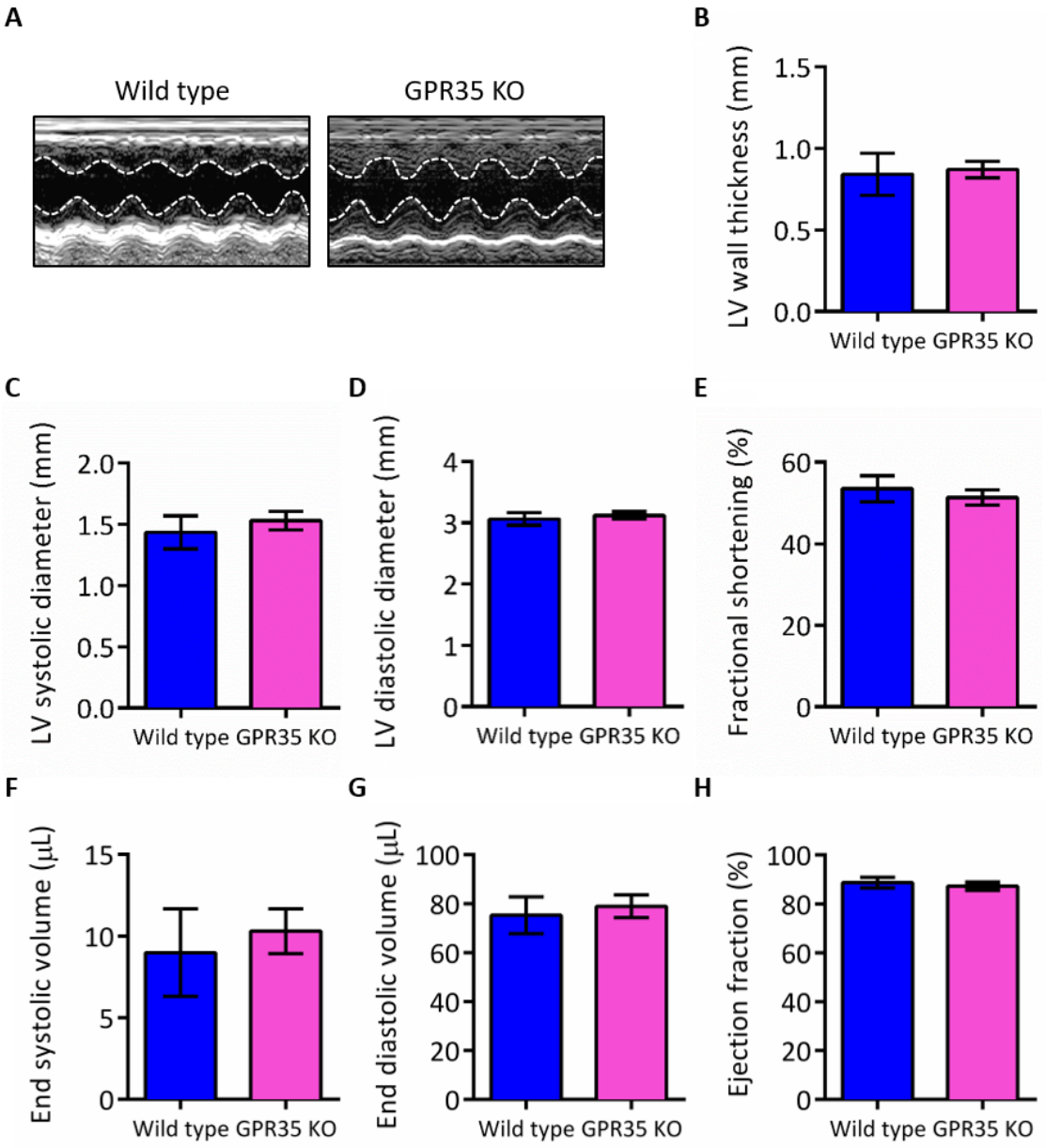

Figure 4-4 Cardiac function is unaltered in GPR35 knockout mice. (A) Representative M-mode echocardiography images taken on the longitudinal axis at the level of the papillary muscle. Scale bar = 3 mm. **(B–H)** Measurements derived from M-mode images: **(B)** end diastolic left ventricular (LV) wall thickness; **(C)** LV systolic diameter; **(D)** LV diastolic diameter; **(E)** fractional shortening of the left ventricle calculated from end systolic and diastolic diameters; **(F)** end systolic volume; **(G)** end diastolic volume; **(H)** ejection fraction calculated from end systolic and diastolic volumes. Data are mean +/- SEM of n = 6 (wild type) or n = 8 (GPR35 KO) animals. Data were compared by two-tailed unpaired t test, but no significant differences were found.

As well as previously being associated with cardiac hypertrophy and dysfunction, GPR35 has recently been reported to stimulate migration of vascular smooth muscle cells and proliferation of vascular endothelial cells, suggesting a possible role in the regulation of vascular function (McCallum et al., 2015). To assess

vasoreactivity in the GPR35 knockout mouse, constriction and relaxation responses of blood vessels from these mice were examined *ex vivo* using wire myography (Figure 4-5).

In small mammals, second- to third-order mesenteric arteries are generally considered to be representative of the small resistance arteries that contribute to peripheral resistance in essential hypertension (Mulvany and Aalkjaer, 1990, Christensen and Mulvany, 2001). Therefore, constriction and relaxation responses of second- to third-order mesenteric arteries from GPR35 knockout mice were investigated (Figure 4-5 A and B). Mesenteric arteries from both wild type and GPR35 knockout mice showed increased intramural active effective pressure in response to noradrenaline, displaying sigmoidal concentration-response curves (Figure 4-5 A). However, mesenteric arteries from GPR35 knockout mice showed no significant differences in the constriction response to noradrenaline compared with those from wild type mice (Figure 4-5 A and E). Mesenteric arteries from both wild type and GPR35 knockout mice that were pre-constricted with 30 μM noradrenaline displayed limited relaxation responses to carbachol, which were not significantly different between the strains (Figure 4-5 B).

Due to the limited relaxation response observed with the mesenteric arteries, wire myography was also performed on aortas in order to accurately assess arterial relaxation responses in GPR35 knockout mice (Figure 4-5 C and D). Aortas were pre-constricted with 1 μM phenylephrine to induce maximal constriction. Maximal constriction to phenylephrine was not significantly different in aortas from GPR35 knockout mice compared with those from wild type mice (Figure 4-5 C). Aortas from both wild type and GPR35 knockout mice showed substantial concentration-dependent relaxation in response to carbachol (Figure 4-5 D). However, aortas from GPR35 knockout mice showed no significant differences in carbachol-induced relaxation compared with those from wild type mice (Figure 4-5 D and E). Overall, these data suggest that GPR35 knockout mice have normal vascular constriction and relaxation responses.

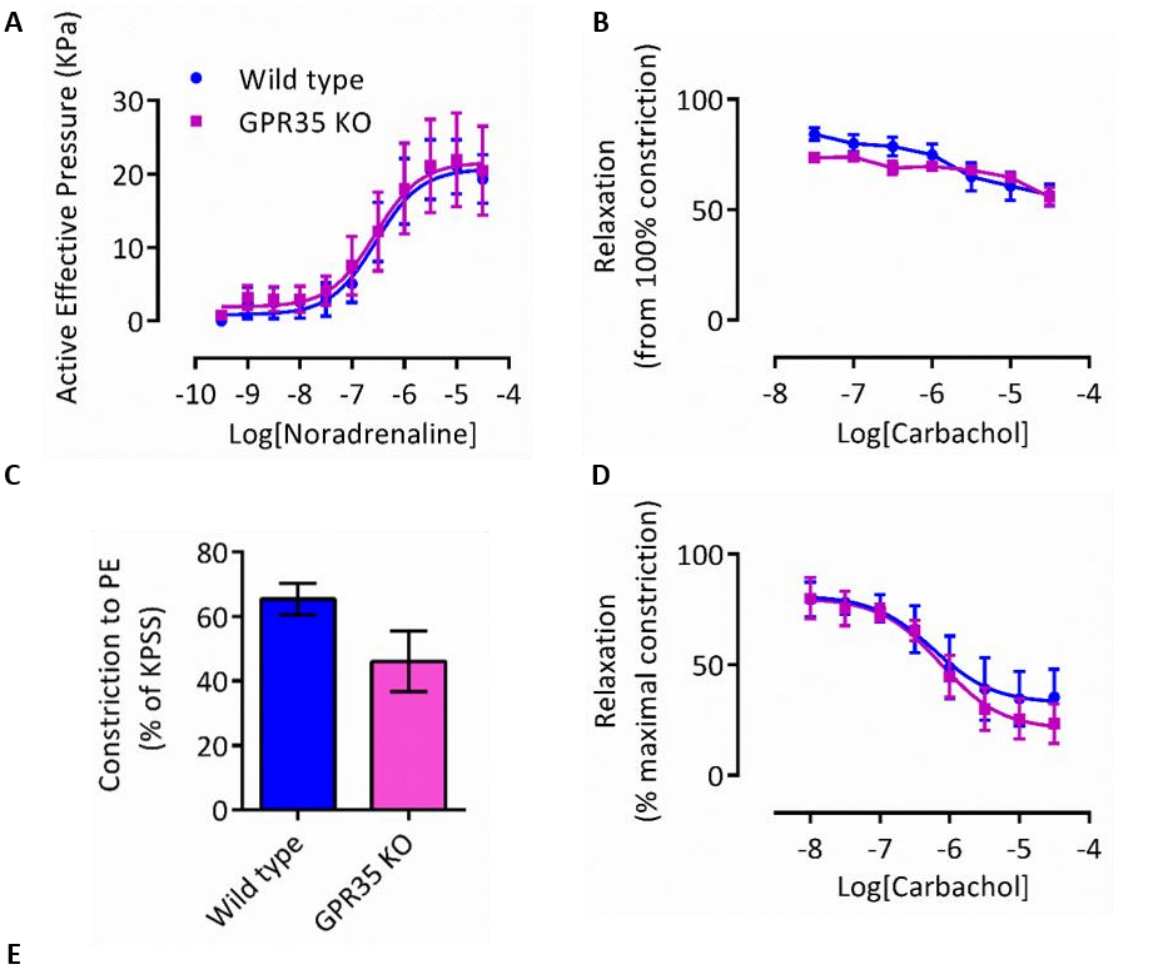

E

Group	pEC_{50}	P value	E_{max}	P value	AUC	P value
Mesenteric arteries: constriction to noradrenaline						
Wild type	6.48 ± 0.143	0.949	21.4 ± 3.64	0.977	261 ± 14.0	0.636
GPR35 KO	6.47 ± 0.121		21.2 ± 6.26		248 ± 3.20	
Aorta: relaxation to carbachol						
Wild type	6.41 ± 0.374	0.519	36.1 ± 10.9	0.322	405 ± 48.2	0.586
GPR35 KO	6.07 ± 0.251		19.7 ± 8.96		366 ± 43.3	

Figure 4-5 Vascular constriction and relaxation responses are unaltered in GPR35 knockout mice. Wire myography was performed on mesenteric arteries **(A, B)** or aortas **(C, D)** of wild type (blue circles) and GPR35 KO (pink squares) mice. **(A)** Constriction concentration-response curves of mesenteric arteries to noradrenaline. **(B)** Relaxation of noradrenaline-constricted mesenteric arteries to carbachol. **(C)** Constriction of aortas to 1 μM phenylephrine (PE). **(D)** Relaxation concentration-response curves of PE-constricted aortas to carbachol. **(E)** Statistical analysis of mean pEC_{50}, E_{max} and area under curve (AUC) from concentration-response curves generated for each individual animal. Curve statistics were compared by two-tailed unpaired t test, but no significant differences were found. Data are mean +/- SEM of n = 4 (mesenteric arteries) or n = 3 (aortas).

4.2.3 Gross morphology of cardiovascular tissues in the GPR35 knockout mouse

Hypertrophy and fibrosis of the heart, blood vessels and kidneys are end-organ indicators of cardiovascular dysfunction. To further investigate potential cardiovascular dysfunction in GPR35 knockout mice, gross morphology of cardiovascular tissues in these mice was examined.

No differences were observed between wild type and GPR35 knockout mice in whole heart or left ventricular mass when normalised to either total body mass or tibia length (Figure 4-6 A and B). The cellular morphology of the myocardium was also unaffected, with no significant alteration in mean cardiomyocyte diameter in GPR35 knockout mice compared with wild type mice (Figure 4-6 C). Wild type and GPR35 knockout mice also had similarly low levels of both perivascular and interstitial cardiac fibrosis, as determined by staining of collagen deposits with picro-sirius red (Figure 4-7). Thus, GPR35 knockout mice appeared to have normal cardiac morphology, with no end-organ damage.

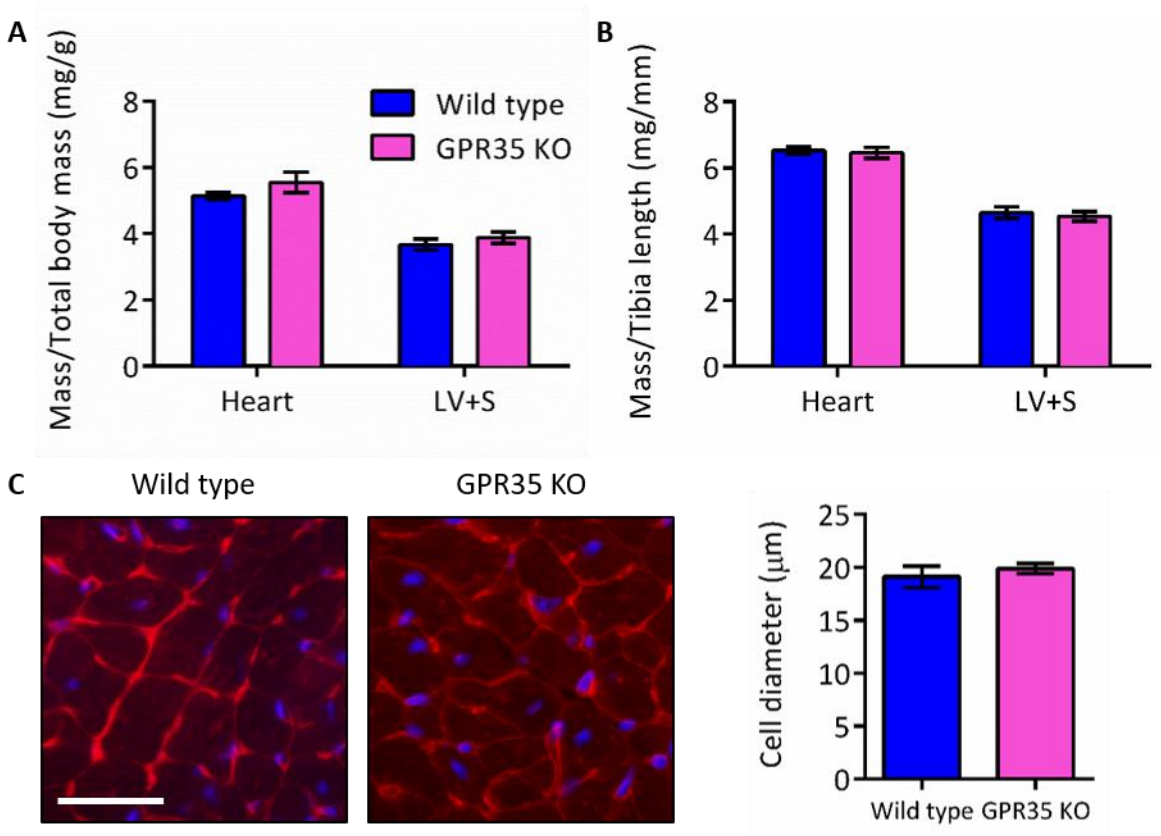

Figure 4-6 Cardiac mass and cardiomyocyte morphology are unaltered in GPR35 knockout mice. (A, B) Whole heart and left ventricle + septum (LV+S) mass were determined at sacrifice and normalised to **(A)** total body mass or **(B)** tibia length. **(C)** Transverse heart sections were stained with fluorescently-tagged wheat germ agglutinin (red) to visualise cardiomyocyte cell membranes, and with DAPI (blue) to visualise nuclei. Cell diameter was quantified by measuring the width of cardiomyocytes orientated on the short axis. Scale bar = 30 µm. Data are mean +/- SEM of n = 8 animals (mass) or n = 5 animals (cell diameter). Data were compared by two-tailed unpaired t test, but no significant differences were found.

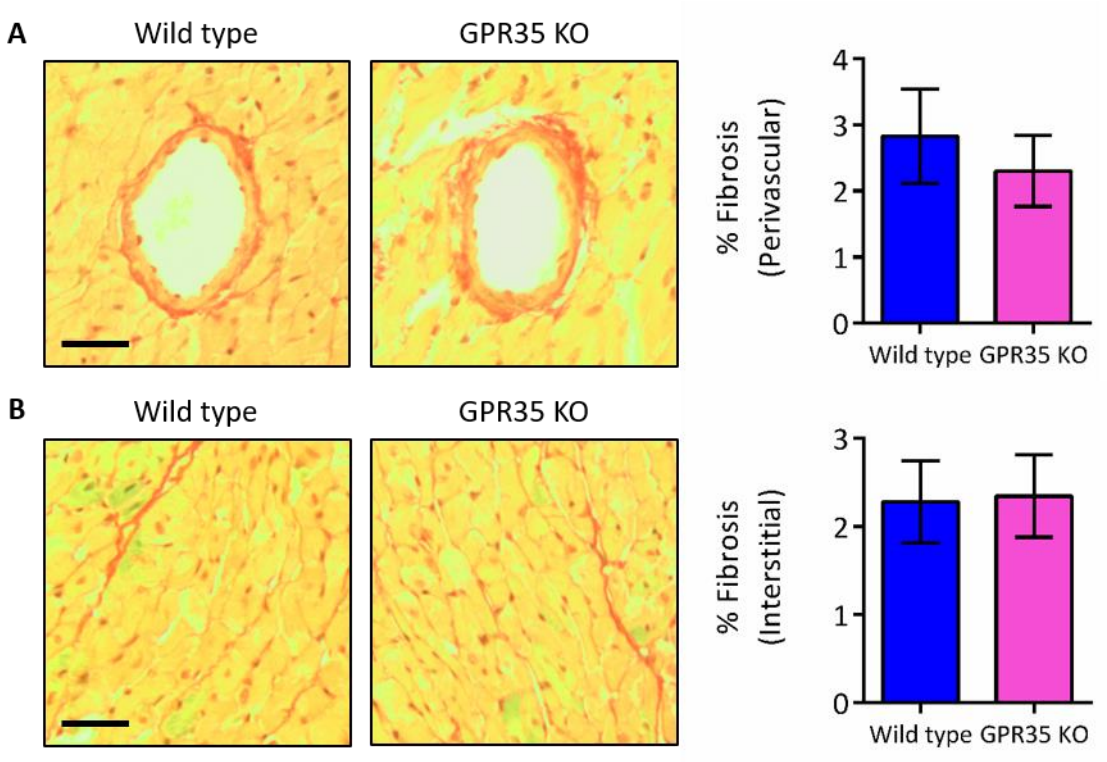

Figure 4-7 Cardiac fibrosis is unaltered in GPR35 knockout mice. Transverse heart sections were stained with picro-sirius red to visualise collagen (red staining). Images of **(A)** perivascular and **(B)** interstitial regions were taken, and percent fibrosis was quantified as percentage of red pixels. Scale bars = 30 μm. Data are mean +/- SEM of n = 5 animals. Data were compared by two-tailed unpaired t test, but no significant differences were found.

Large vessel morphology in GPR35 knockout mice was assessed by staining aortas with hematoxylin and eosin, and potential vascular remodelling was examined by quantifying medial area (Figure 4-8). Aortas from both wild type and GPR35 knockout mice had healthy morphology, and no significant difference in medial area was observed (Figure 4-8).

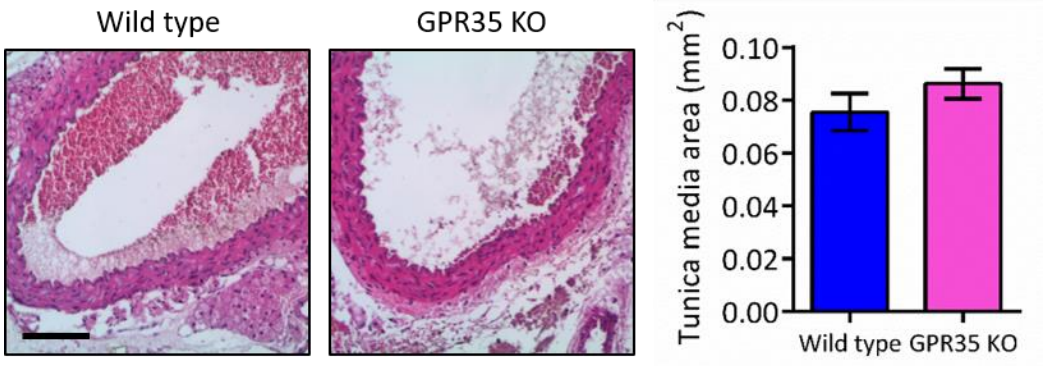

Figure 4-8 Vascular morphology is unaltered in GPR35 knockout mice. Transverse aorta sections were stained with hematoxylin and eosin to visualise vascular morphology, and tunica media area was quantified by measuring the smooth muscle layer (bright pink staining). Scale bar = 100 μm. Data are mean +/- SEM of n = 5 animals. Data were compared by two-tailed unpaired t test, but no significant difference was found.

Since renal dysfunction and injury are secondary outcomes of cardiovascular dysfunction, renal mass and fibrosis in GPR35 knockout mice were also assessed (Figure 4-9). No differences in average kidney mass were observed between wild type and GPR35 knockout mice when normalised to either total body weight or tibia length (Figure 4-9 A and B). Levels of both interstitial and perivascular fibrosis were not significantly altered in GPR35 knockout mice compared with wild type mice (Figure 4-9 C and D). Thus, GPR35 knockout mice displayed normal renal morphology, which is indicative of normal blood pressure regulation and cardiovascular function.

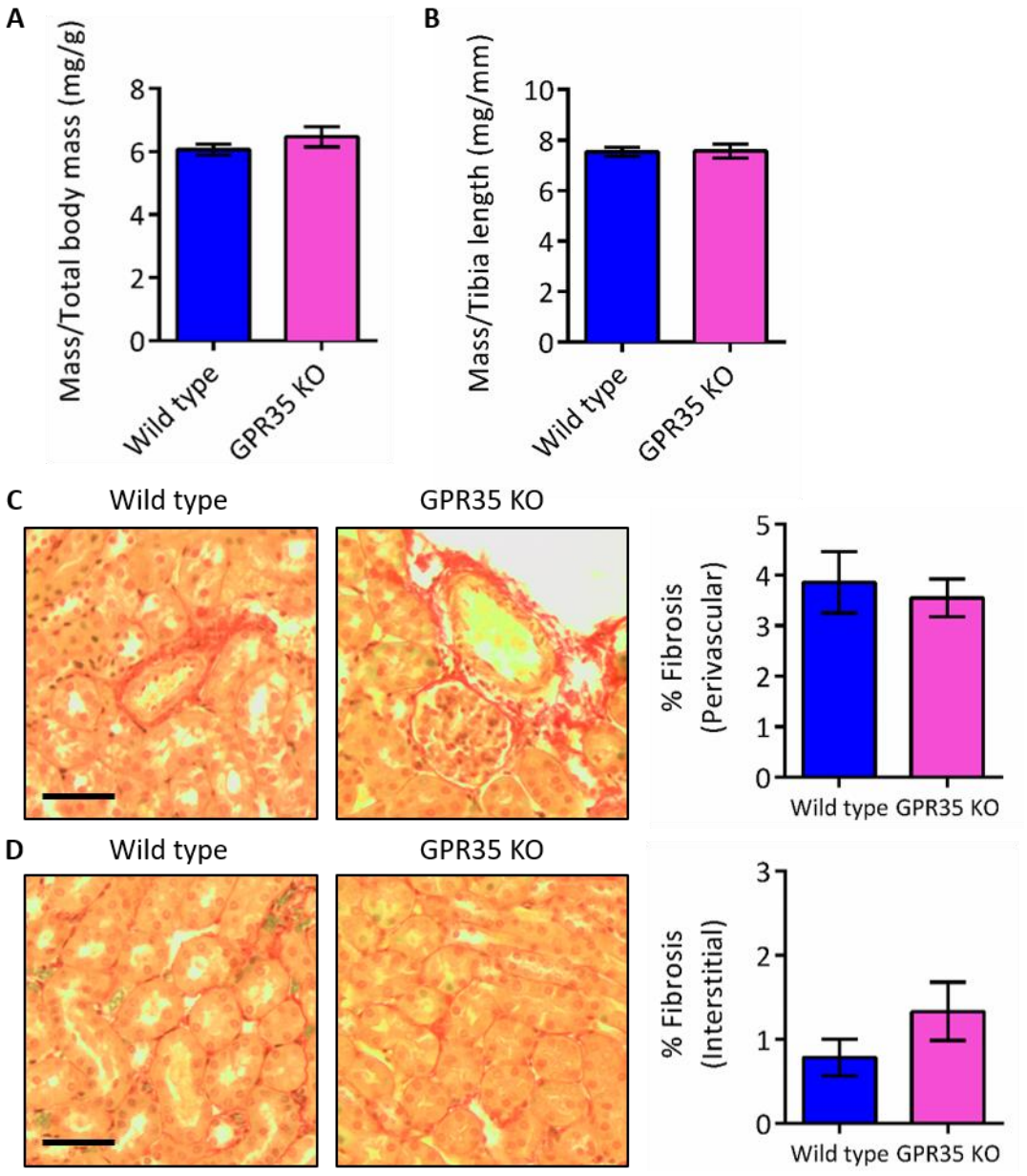

Figure 4-9 Renal mass and fibrosis are unaltered in GPR35 knockout mice. (A, B) Average kidney mass was determined at sacrifice and normalised to **(A)** total body mass or **(B)** tibia length. **(C, D)** Transverse kidney sections were stained with picro-sirius red to visualise collagen (red staining). Images of **(C)** interstitial and **(D)** perivascular regions were taken, and percent fibrosis was quantified as percentage of red pixels. Scale bars = 50 μm. Data are mean +/- SEM of n = 8 animals (mass) or n = 5 animals (fibrosis). Data were compared by two-tailed unpaired t test, but no significant differences were found.

4.3 Discussion

4.3.1 GPR35 knockout mice have normal haemodynamic properties

The aim of this chapter was to characterise the basal cardiovascular phenotype of a global GPR35 knockout mouse. The data presented here demonstrate that there are no significant differences in haemodynamic parameters, cardiac function, vascular contractility or cardiac, vascular or renal morphology in GPR35 knockout mice when compared with the wild type background strain. These findings support the conclusion that GPR35 knockout mice have a normal cardiovascular phenotype, and therefore GPR35 does not play a significant role in the homeostatic regulation of the cardiovascular system.

The lack of a blood pressure phenotype in the GPR35 knockout mouse was particularly surprising, since Min *et al*. previously reported that they found the mean systolic blood pressure of this strain to be 37.5 mmHg higher than that of wild type littermates (Min et al., 2010). This is a substantial and physiologically meaningful difference, and formed part of the rationale for carrying out the present study. However, the finding was not replicated here. There are several reasons why these two studies might have had such different outcomes, stemming from the fact that they employed two very different methods of measuring blood pressure. The first used Millar catheterisation to record haemodynamic parameters at a single time point under terminal anaesthesia, whereas in the present study, blood pressure was monitored continuously for 7 days. These differing approaches may account for the different conclusions reached in a number of ways. Blood pressure is highly variable throughout the 24-hour light/dark cycle, with mean arterial pressure in mice varying by up to 15 mmHg between light and dark periods and up to 40 mmHg over a whole 24-hour period (Van Vliet et al., 2003). Furthermore, these variations are highly correlated with locomotive activity (Van Vliet et al., 2003). Therefore, the time of day that measurements are taken, and how active the animal is, can strongly impact the result obtained. For these reasons, continuous monitoring by telemetry over hours and/or days leads to considerably less statistical variation and a more accurate depiction of haemodynamic parameters than single-point readings (Van Vliet et al., 2006). However, irrespective of 24-hour variation, the

present study did detect differences in mean arterial pressure of up to 11 mmHg between wild type and GPR35 knockout mice in certain 12-hour periods. While the source of this day-to-day variation is unclear, this was not significant over the 7-day duration of the study. A similar pattern was observed for heart rate, with the heart rate of GPR35 knockout mice being up to 69 bpm lower than that of wild type mice during night-time periods, but not significantly different overall. This further emphasises the importance of monitoring haemodynamic parameters over time to gain a more accurate and physiologically representative understanding of cardiovascular regulation in mouse models. It is possible that deletion of GPR35 makes these mice more sensitive to transient environmental or metabolic influences on blood pressure and heart rate, since these parameters appear to be less stable from day to day in GPR35 knockout mice than in wild type mice. However, the study was conducted in multiple batches of animals, with recordings taking place over several different 7-day periods with different start days, so this instability is not due to any specific event (such as human disturbance on a particular day). The differences appear to be more pronounced during night-time (active) periods, which may reflect greater day/night blood pressure variability in GPR35 knockout mice. More detailed studies into the effects of GPR35 on blood pressure variability could yield further insight into this possible scenario.

Besides the limitations of a single-point blood pressure measurement, an additional caveat to the previous study was that measurements were taken while the animals were under anaesthesia (although the anaesthetic agent and dose used are not reported) (Min et al., 2010). Isoflurane anaesthesia, which is frequently used in such studies, has previously been shown to have a significant effect on mean arterial pressure, as have the injectable agents ketamine/xylazine and pentobartital sodium (Janssen et al., 2004, Constantinides et al., 2011). For an uncharacterised strain such as the GPR35 knockout mouse, it is not possible to rule out the prospect that the blood pressure difference observed by Min *et al*. was due to differences in the reaction to the anaesthesia, rather than an overall difference in physiological blood pressure, especially since it was the only cardiovascular parameter assessed. Telemetry provides the opportunity to obtain blood pressure readings in the complete absence of anaesthetic agents and after a suitable recovery period

following surgery. Therefore, it is possible to have greater confidence in the conclusion of the present study: that blood pressure is not significantly altered in GPR35 knockout mice.

A limitation of this study, and a possible explanation for the lack of blood pressure effect observed, is that only one age range of mice was studied. All mice were between 12 and 14 weeks of age, the youngest age at which telemetry probes could be implanted. It is conceivable that pathological changes could become apparent in older animals. Min et al. do not report the age range of the mice used in their study (Min et al., 2010). To address this limitation, it would be necessary to repeat the study in aged mice.

4.3.2 GPR35 knockout mice have normal cardiovascular function

In addition to blood pressure and heart rate, several other parameters were assessed in the GPR35 knockout mouse in order to achieve a comprehensive basal characterisation of its cardiovascular phenotype. Echocardiographic assessment of left ventricular global systolic function found no differences in either fractional shortening or ejection fraction in the GPR35 knockout mice compared with the wild type strain. Since GPR35 expression in the heart has been linked to adverse cardiac remodelling, and heterologous overexpression of GPR35 has been shown to drive cardiomyocyte hypertrophy, one might expect GPR35 knockout mice to have altered cardiac mass or structure (Min et al., 2010, Ronkainen et al., 2014). However, cardiac mass and cardiomyocyte morphology were found to be comparable to that of wild type mice. An obvious explanation for this is that GPR35 expression has thus far only been detected in the heart under pathophysiological conditions. Moreover, it has been shown to be upregulated in the heart in response to hypoxia-inducible factor 1 activation and following coronary artery ligation or trans-aortic constriction (TAC), suggesting that its expression may only be induced after the onset of disease (Ronkainen et al., 2014). This would explain the lack of effect observed in the heart under basal conditions. However, this raises the query of whether GPR35 fulfils a protective or pathological role in the progression of adverse remodelling and heart failure. These processes can be modelled using surgical techniques such as TAC or by inducing hypertension through various means (Takefuji et al.,

2012). Assessing the effects of such procedures in the GPR35 knockout mouse would therefore be a particularly interesting avenue to pursue in order to answer this question.

As in the heart, global knockout of GPR35 also had no detectable effect on vascular function or morphology in this study. Neither constriction nor endothelium-dependent dilation was altered in the aortae or mesenteric resistance arteries of GPR35 knockout mice. This suggests that GPR35 does not contribute to vascular contractility under basal conditions. GPR35 expression has been detected in primary cell cultures of vascular endothelial cells and vascular smooth muscle cells; however, it has not been detected directly in vascular tissue (McCallum et al., 2015). A potential role of GPR35 in the vasculature *in vivo* therefore remains undefined, but, as in the heart, it may be necessary to induce disease for any GPR35-mediated effects to manifest.

4.3.3 A normal phenotype does not prove a lack of function

A lack of abnormal phenotype in a knockout mouse is not an uncommon occurrence – it has been estimated that some 10–15% of knockout mice generated display no discernible phenotypic alteration (although publication bias makes such estimates very broad) (Barbaric et al., 2007). There are several explanations for a knockout mouse not displaying an anticipated phenotype. There may truly be no effect of removing the gene due to the phenomenon of genetic redundancy, where a different gene is capable of performing the function of the absent gene. In particular, global constitutive knockout mice like the one used in this study allow for upregulation of functionally compensatory genes that can mask the phenotypic effect of the knockout (Rudnicki et al., 1992, Nedvetzki et al., 2004). However, a more likely explanation for an apparent lack of abnormal phenotype in any given knockout mouse is that differences in physiology are present, but are not detected using the specific screening tools or outcomes used in the study. In this case, large-scale, unbiased functional screens of knockout mouse phenotypes that broadly cover the various therapy areas might prove useful in identifying gene functions and novel therapeutic targets. This approach has been used successfully to identify novel genes involved in processes such as platelet function, bone remodelling and neuropathic pain, to name but a few (Tang et al., 2010, Bassett et al., 2012,

White et al., 2013, Kostich et al., 2016). However, despite their value, these screens can still fail to identify any alteration. An alternative explanation for a lack of abnormal phenotype in these cases is that the abnormality may only become evident under certain environmental or physiological conditions. In such cases, a more focused and in-depth approach, such as the use of disease models to imitate altered physiological conditions, is required. Any of these explanations might apply to the GPR35 knockout mouse, and the lack of phenotypic alteration in cardiovascular function observed in this study should not be construed as a definitive lack of function.

Does the apparent absence of a role in basal cardiovascular regulation suggest that GPR35 is not a potential therapeutic target in CVD? On the contrary, this finding may in fact strengthen its value, given the existing evidence for an association between GPR35 and CVD. If a gene is benign under normal conditions, but is upregulated and active under pathophysiological conditions, it is likely to have more specific on-target effects than a gene that is ubiquitously and/or constitutively expressed. This potential for increased specificity is one factor that makes orphan GPCRs attractive drug targets. Moreover, in 2003, Zambrowicz and Sands argued that many of the most successful drug targets (which have not changed substantially in the last 14 years) do not directly cause disease, but constitute molecular ‘switches’ that bring about a change in physiology that has the desired therapeutic effect (Zambrowicz and Sands, 2003). This suggests that even though GPR35 modulation has no apparent influence on cardiovascular regulation in healthy mice, its role and therapeutic value may become evident when disease is induced. This reasoning gives rise to the conclusion that there is a need to determine the effects of GPR35 deficiency in CVD models, which forms the basis of the following chapter.

Chapter 5 Cardiovascular effects of angiotensin II infusion in a global GPR35 knockout mouse

5.1 Introduction

Following the studies described in the previous chapter, it was concluded that GPR35 knockout mice have normal blood pressure regulation or cardiovascular function under basal conditions. However, several previous studies have demonstrated effects of GPR35 in cells and tissues of the cardiovascular system (section 1.4.6.5). Some of these studies, particularly those reporting on *in vivo* effects in rodents and humans, have provided evidence for roles of GPR35 within pathophysiological contexts. Min et al. reported that GPR35 expression in heart tissue was higher in patients with heart failure compared with healthy control subjects (Min et al., 2010). Similarly, Ronkainen et al. reported increased cardiac expression of GPR35 in response to hypoxia and in *in vivo* rodent models of myocardial infarction and heart failure (Ronkainen et al., 2014). These findings suggest that GPR35 expression is induced in cardiovascular tissues under pathophysiological conditions, and so its role in the cardiovascular system may only manifest during cardiovascular disease. It remains unclear whether this induction of GPR35 contributes to the pathogenesis of disease, or whether it is an adaptive mechanism conferring a protective effect. Although several studies have investigated the effects of heterologous overexpression of GPR35 in cells of the cardiovascular system or GPR35 upregulation *in vivo*, the consequences of reduced GPR35 activity on the development of cardiovascular dysfunction have not been examined. In order to address this, an Ang II infusion model of hypertension and cardiovascular end-organ damage was used to determine the effects of global GPR35 deficiency on blood pressure regulation and cardiovascular function in the context of cardiovascular stress.

Long-term exposure to elevated levels of Ang II is known to have various pathological effects on the cardiovascular system *in vivo*. These include increased vascular tone and blood pressure, which lead to vascular inflammation and remodelling, accelerated development of atherosclerosis and cardiac hypertrophy and injury following chronic exposure (Weiss et al., 2001, Crowley et al., 2006, Qi et al., 2011, Lima et al., 2016). Due to its systemic and wide-ranging effects in the cardiovascular system, chronic infusion of Ang II in rodents

has been used extensively as a model for hypertension and cardiovascular disease (Weiss et al., 2001, Lu et al., 2015, Regan et al., 2015, Takayanagi et al., 2015, Lima et al., 2016).

The dose of Ang II used in rodent studies is critical in achieving the required pathophysiological outcomes for a specific model. High doses of Ang II induce abdominal aortic aneurysm, and high infusion rates are frequently used in studies that attempt to model this pathology (Lu et al., 2015). However, the high doses used in this model are intrinsically associated with a significant risk of mortality caused by spontaneous rupture of the aneurysm, typically within the first week of treatment (Cao et al., 2010). Conversely, low infusion rates can model specific cardiovascular pathologies such as heart failure with preserved ejection fraction without inducing a pressor response (Regan et al., 2015). Intermediate doses of 400–1000 ng/kg/min for two to six weeks are typically used to induce a moderate-to-severe increase in blood pressure (20–50 mmHg), along with the associated pathological outcomes in end organs such as the heart and kidney (Crowley et al., 2006, Moore et al., 2015, Takayanagi et al., 2015). This chapter describes the effects of 2-week infusion of a low pressor dose of Ang II on the cardiovascular characteristics of both wild type and GPR35 knockout mice.

5.1.1 Aims

The aims of this chapter were to:

- Establish an Ang II infusion model in GPR35 knockout mice

- Accurately assess the effects of Ang II infusion on haemodynamic parameters in wild type and GPR35 knockout mice using an implantable telemetry device

- Determine the effects of Ang II infusion on cardiovascular function in wild type and GPR35 knockout mice

- Determine the effects of Ang II infusion on cardiovascular end-organ damage in wild type and GPR35 knockout mice

5.1.2 Study design

The purpose of this study was to compare the effects of 2-week Ang II infusion on blood pressure and cardiovascular function in the GPR35 knockout mouse, compared with those in the wild type background strain, C57BL/6. Since it was hypothesised that GPR35 knockout mice would have an exacerbated response to Ang II infusion, it was necessary to use as low a dose as possible to prevent mortalities due to abdominal aortic aneurysm. In order to be able to detect a response to Ang II infusion with minimal risk of mortality in the GPR35 knockout mice, a low pressor dose of 400 ng/kg/min of Ang II was used to induce a moderate blood pressure increase.

Only male animals were used in order to eliminate sex-specific variation. Homozygous wild type and knockout littermates were bred, and were of sufficient body weight to tolerate telemetry probe implantation by 12 weeks of age. Probes were implanted at 12 weeks of age, followed by a 7-day recovery period during which no measurements were taken. At 13 weeks of age, cardiac function was assessed by echocardiography, then osmotic minipumps containing water or Ang II were implanted subcutaneously. Following minipump implantation, probes were remotely switched on and haemodynamic parameters were monitored continuously for 14 days (Figure 5-1). Blood pressure, heart rate and locomotive activity are all subject to intrinsic circadian rhythms in rodents, and the presence of these rhythms are indicative of normal health and cardiovascular function (Takeda and Maemura, 2011). In order to assess the diurnal variation in the parameters measured, the telemetry data generated in this study were separated into two 12-hour periods representing the dark period (night) and the light period (day). After 2 weeks of monitoring and infusion, a second echocardiographic assessment of cardiac function was performed, followed by sacrifice and *ex vivo* analysis at 15 weeks of age (Figure 5-1).

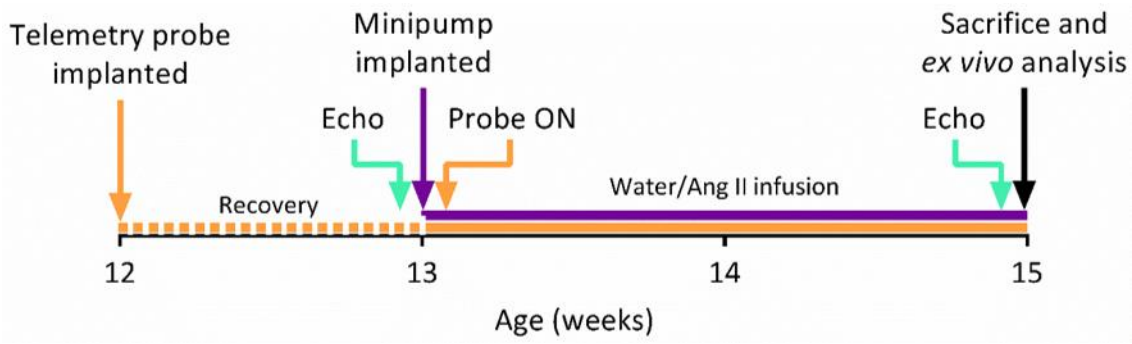

Figure 5-1 GPR35 KO Ang II infusion study timeline

5.2 Results

5.2.1 Effects of Ang II infusion on haemodynamic properties in wild type and GPR35 knockout mice

In order to assess the effects of Ang II infusion on blood pressure and heart rate in wild type and GPR35 knockout mice, haemodynamic parameters were monitored using an implantable telemetry system during 2-week infusion of either water or Ang II. One mortality occurred in the GPR35 knockout Ang II treatment group, which was confirmed by post-mortem examination to be due to a ruptured abdominal aortic aneurysm. Data from this animal were excluded from all analyses.

All of the parameters measured followed normal diurnal rhythms over the light/dark cycle in all treatment groups (Figure 5-2 through Figure 5-5). In wild type mice, Ang II infusion induced a steady and moderate increase in blood pressure of approximately 20 mmHg over the 2-week period (Figure 5-2). This increase had a delayed onset, only becoming apparent from day nine of infusion onwards. At day 14 (following 2-week infusion), Ang II-infused mice had significantly higher systolic, diastolic and mean arterial blood pressures than water-infused mice (Figure 5-2 A, C and E). Overall, the change in blood pressure over time (calculated from the slope of the linear regression over 14 days) was significantly greater for wild type mice infused with Ang II than those infused with water, with a mean increase of 1.42±0.39 mmHg/day versus −0.13±0.20 mmHg/day in systolic blood pressure, 1.24±0.27 mmHg/day versus 0.11±0.15 mmHg in diastolic blood pressure and 1.29±0.33 mmHg/day versus −0.03±0.17 mmHg/day in mean arterial pressure (Figure 5-2 B, D and F). In GPR35 knockout mice, no differences between Ang II- and water-infused mice were observed in either blood pressure on day 14 or change over time, with a mean increase in mean arterial pressure of 0.58±0.35 mmHg/day in water-infused mice and 0.12±0.24 mmHg/day in Ang II-infused mice (Figure 5-3).

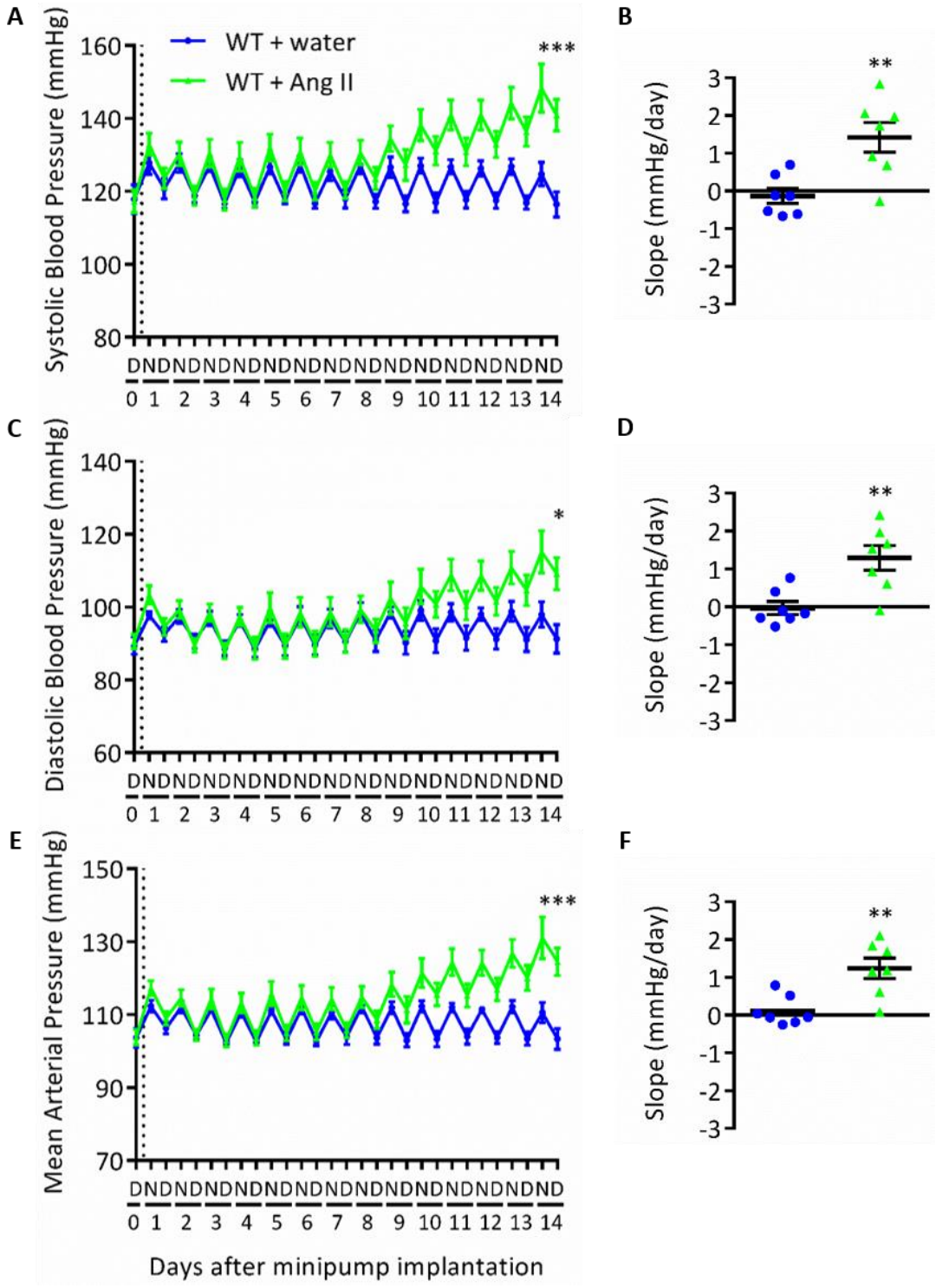

Figure 5-2 Wild type mice develop Ang II-induced hypertension (A, B) Systolic, **(C, D)** diastolic and **(E, F)** mean arterial blood pressure were monitored in wild type (WT) mice infused with either water or Ang II over 2 weeks. Baseline measurements were taken on day 0 prior to minipump implantation (indicated by dotted line). **(A, C, E)** Data are presented as 12-hour means representing night (N) and day (D) periods of n = 7 animals +/- SEM; **p*<0.05, ****p*<0.001 in two-tailed unpaired t test on day 14. **(B, D, F)** Change over 14 days was compared by two-tailed unpaired t-test on the slope of the linear regression (mmHg/day) for each individual animal, ***p*<0.01.

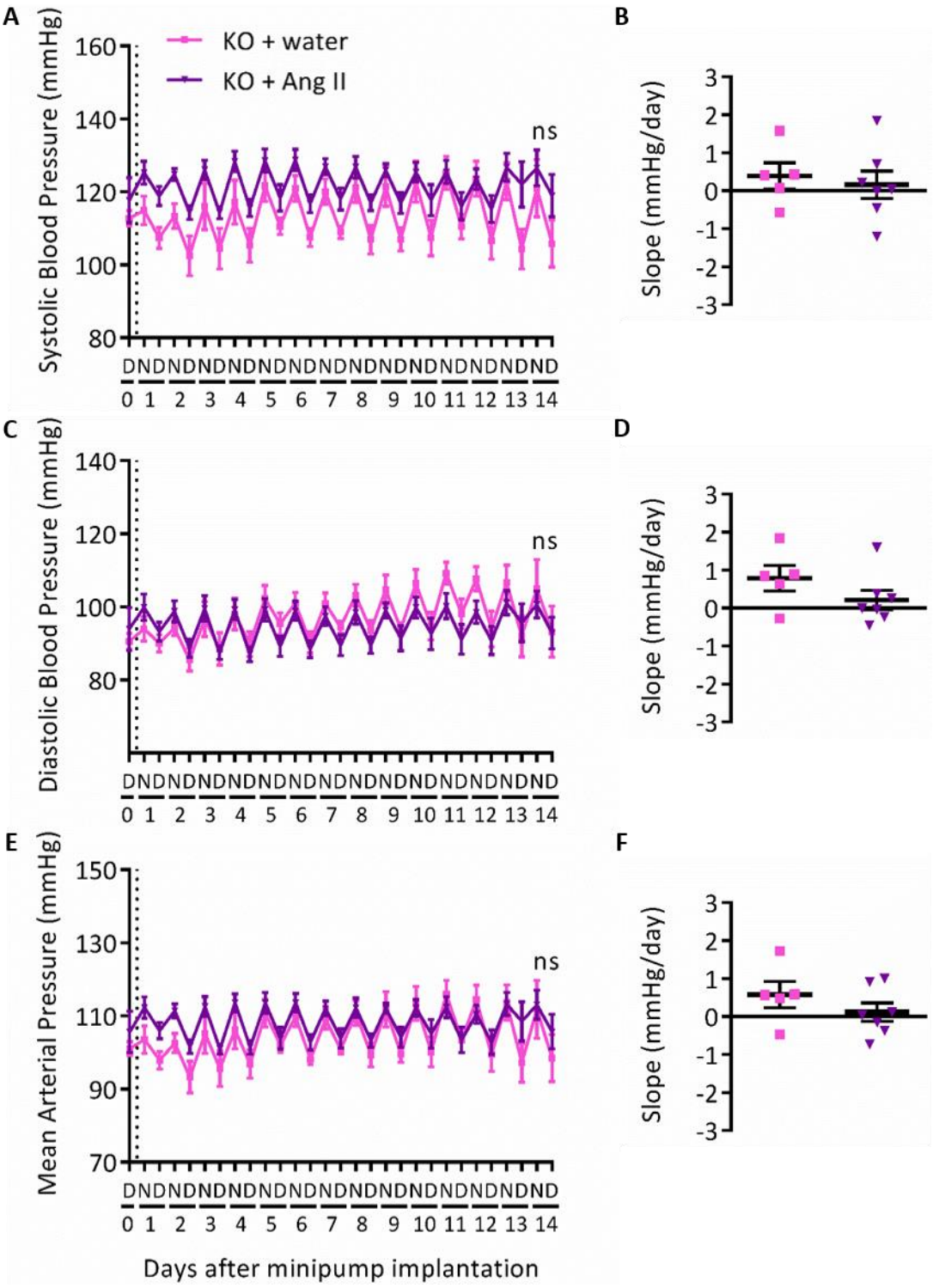

Figure 5-3 GPR35 knockout mice are resistant to AngII-induced hypertension (A, B) Systolic, **(C, D)** diastolic and **(E, F)** mean arterial blood pressure were monitored in GPR35 knockout (KO) mice infused with either water or Ang II over 2 weeks. Baseline measurements were taken on day 0 prior to minipump implantation (indicated by dotted line). **(A, C, E)** Data are presented as 12-hour means representing night (N) and day (D) periods of n = 5 (KO + water) or n = 7 (KO + Ang II) animals +/- SEM; ns = not significant in two-tailed unpaired t test on day 14. **(B, D, F)** Change over 14 days was compared by two-tailed unpaired t-test on the slope of the linear regression (mmHg/day) for each individual animal, but no significant differences were found.

Heart rate and locomotive activity were also monitored by telemetry (Figure 5-4 and Figure 5-5). In wild type mice, there was no significant difference in heart rate on day 14 in Ang II-infused mice compared with water-infused mice (Figure 5-4 A). In GPR35 knockout mice, heart rate on day 14 was significantly higher in Ang II-infused mice than in water-infused mice (508±13 bpm versus 453±17 bpm) (Figure 5-5 A). However, the change over time was not significantly different; heart rate decreased over time in all treatment groups, with a mean decrease of 2.34±0.80 bpm/day and 2.11±1.28 bpm/day in water- and Ang II-infused wild type mice and 3.27±0.70 bpm/day and 0.93±0.89 bpm/day in water- and Ang II-infused GPR35 knockout mice, respectively (Figure 5-4 B and D and Figure 5-5 B and D). No significant differences in activity were observed between the water and Ang II treatment groups in either wild type mice (Figure 5-4 C and D) or GPR35 knockout mice (Figure 5-5 C and D). Activity followed normal diurnal rhythms in all treatment groups (Figure 5-4 C and Figure 5-5 C), suggesting that the surgical procedures were well tolerated.

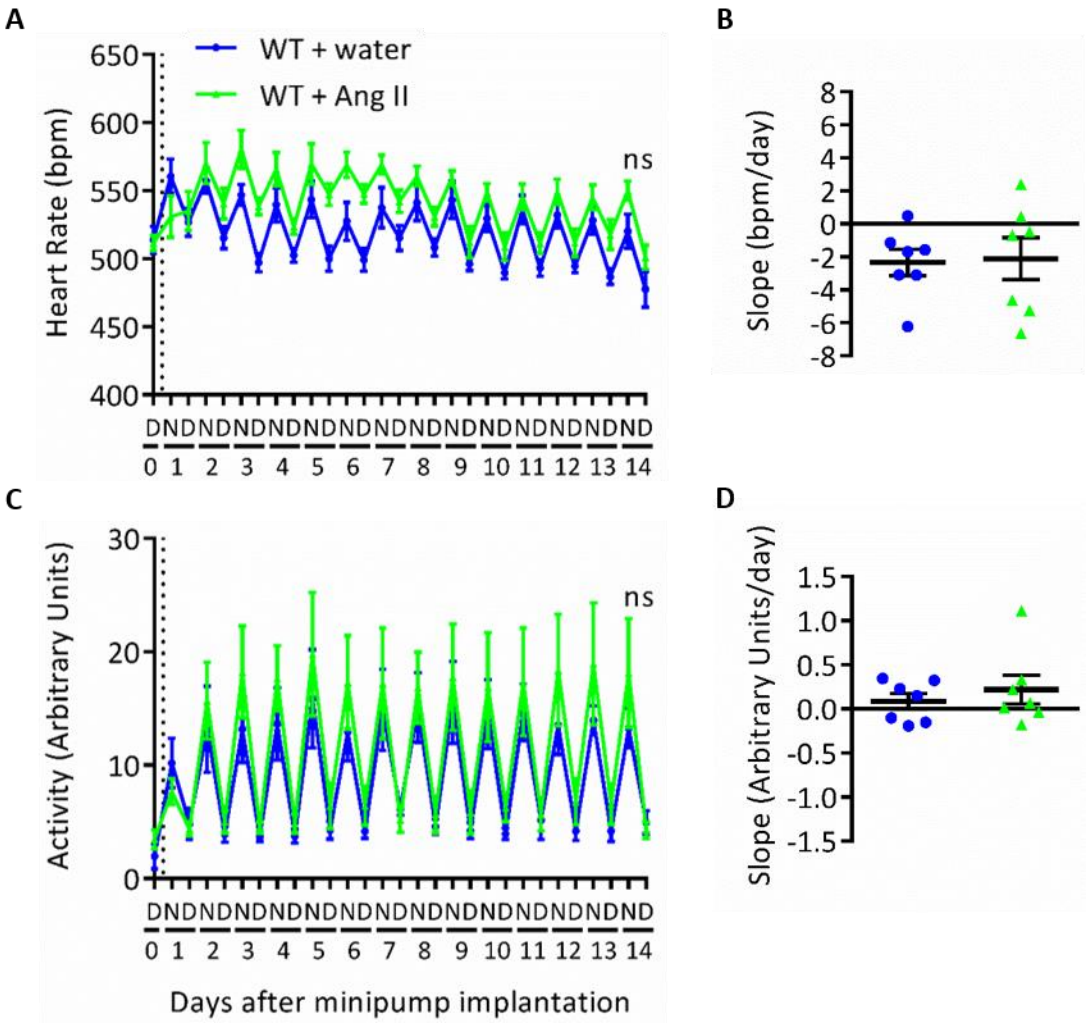

Figure 5-4 Ang II infusion does not affect heart rate or activity in wild type mice (A, B) Heart rate in beats per minute (bpm) and **(C, D)** activity were monitored in wild type (WT) mice infused with either water or Ang II over 2 weeks. Baseline measurements were taken on day 0 prior to minipump implantation (indicated by dotted line). **(A, C)** Data are presented as 12-hour means representing night (N) and day (D) periods; mean +/- SEM of n = 7 animals; ns = not significant in two-tailed unpaired t test on day 14. **(B, D)** Change over 14 days was compared by two-tailed unpaired t-test on the slope of the linear regression (bpm/day or arbitrary units/day) for each individual animal, but no significant differences were found (ns = not significant).

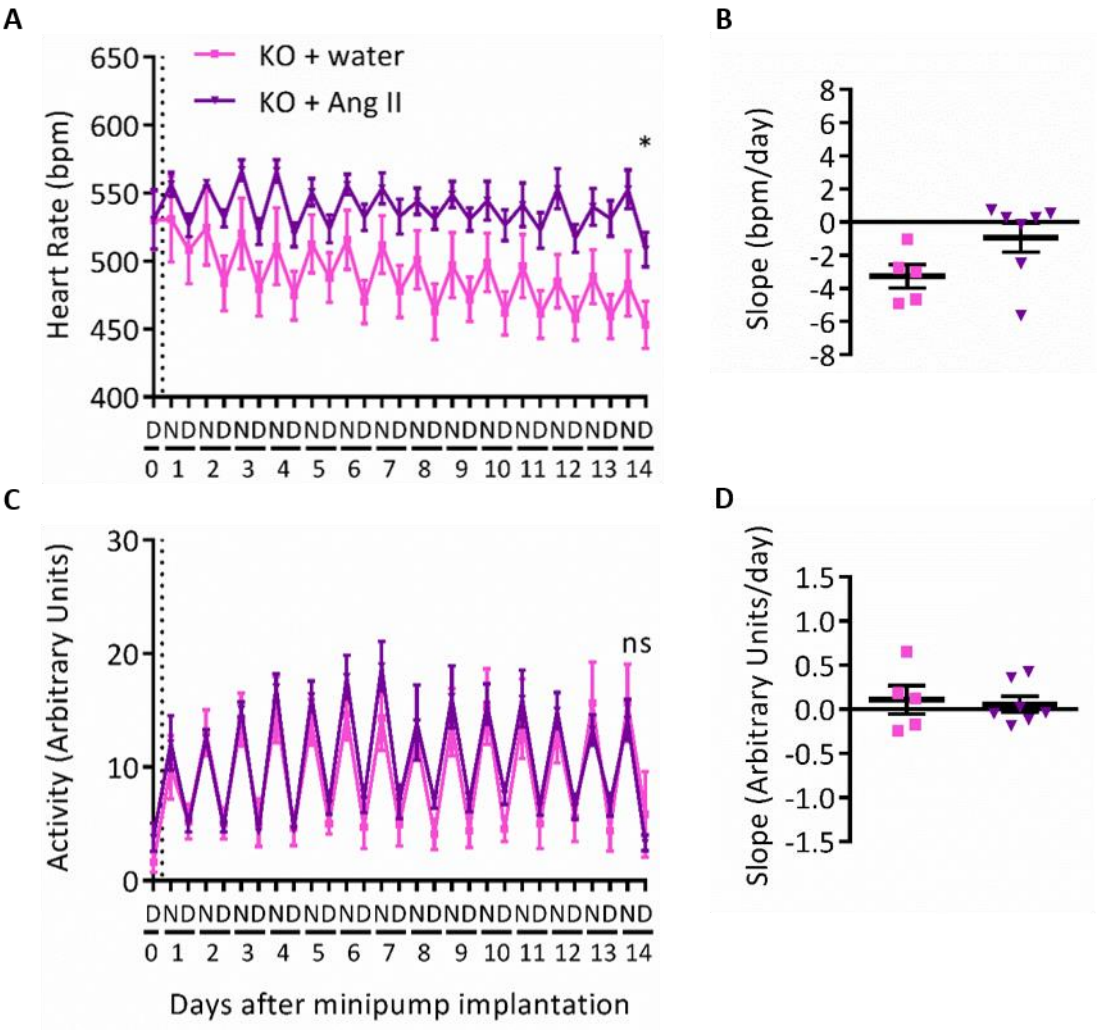

Figure 5-5 Ang II infusion does not affect heart rate or activity in GPR35 knockout mice
(A, B) Heart rate in beats per minute (bpm) and **(C, D)** activity were monitored in GPR35 knockout (KO) mice infused with either water or Ang II over 2 weeks. Baseline measurements were taken on day 0 prior to minipump implantation (indicated by dotted line). **(A, C)** Data are presented as 12-hour means representing night (N) and day (D) periods; mean +/- SEM of n = 5 (KO + water) or n = 7 (KO + Ang II) animals; *p<0.05, ns = not significant in two-tailed unpaired t test on day 14. **(B, D)** Change over 14 days was compared by two-tailed unpaired t-test on the slope of the linear regression (bpm/day or arbitrary units/day) for each individual animal, but no significant differences were found.

5.2.2 Effects of Ang II infusion on cardiovascular function in wild type and GPR35 knockout mice

In addition to inducing hypertension, chronic Ang II infusion has previously been shown to lead to alterations in cardiovascular function that mimic those associated with cardiovascular disease (Regan et al., 2015, Lima et al., 2016, Takayanagi et al., 2016). Cardiac and vascular function in wild type and GPR35 knockout mice subjected to Ang II infusion were investigated using *in vivo* and *ex vivo* methods, as described in Chapter 4.

Cardiac function was assessed by echocardiography on day 0, prior to minipump implantation, and on day 14, following two weeks of infusion and prior to sacrifice. In wild type mice, left ventricular wall thickness and diameter were not different on day 14 compared with day 0 after either water or Ang II infusion (Figure 5-6 B–D). However, both fractional shortening and ejection fraction were significantly reduced on day 14 compared with day 0 (by 6.3±2.2% and 5.0±1.8%, respectively; both $p<0.05$) in wild type mice infused with Ang II (Figure 5-6 E and H). The changes in fractional shortening and ejection fraction in Ang II-infused mice were significant when compared with those in water-infused mice (+0.4±1.6% and +0.3±1.2%, respectively; both $p<0.05$) (Figure 5-7).

In GPR35 knockout mice, none of the echocardiographic measurements taken, including fractional shortening and ejection fraction, were significantly different on day 14 compared with day 0 (Figure 5-8). The changes in fractional shortening and ejection fraction were close to 0% in both water- and Ang II-infused GPR35 knockout mice, and were not significantly different between groups (Figure 5-9). Thus, 2-week Ang II infusion led to significantly reduced fractional shortening and ejection fraction in wild type mice, but not in GPR35 knockout mice (Figure 5-7 and Figure 5-9).

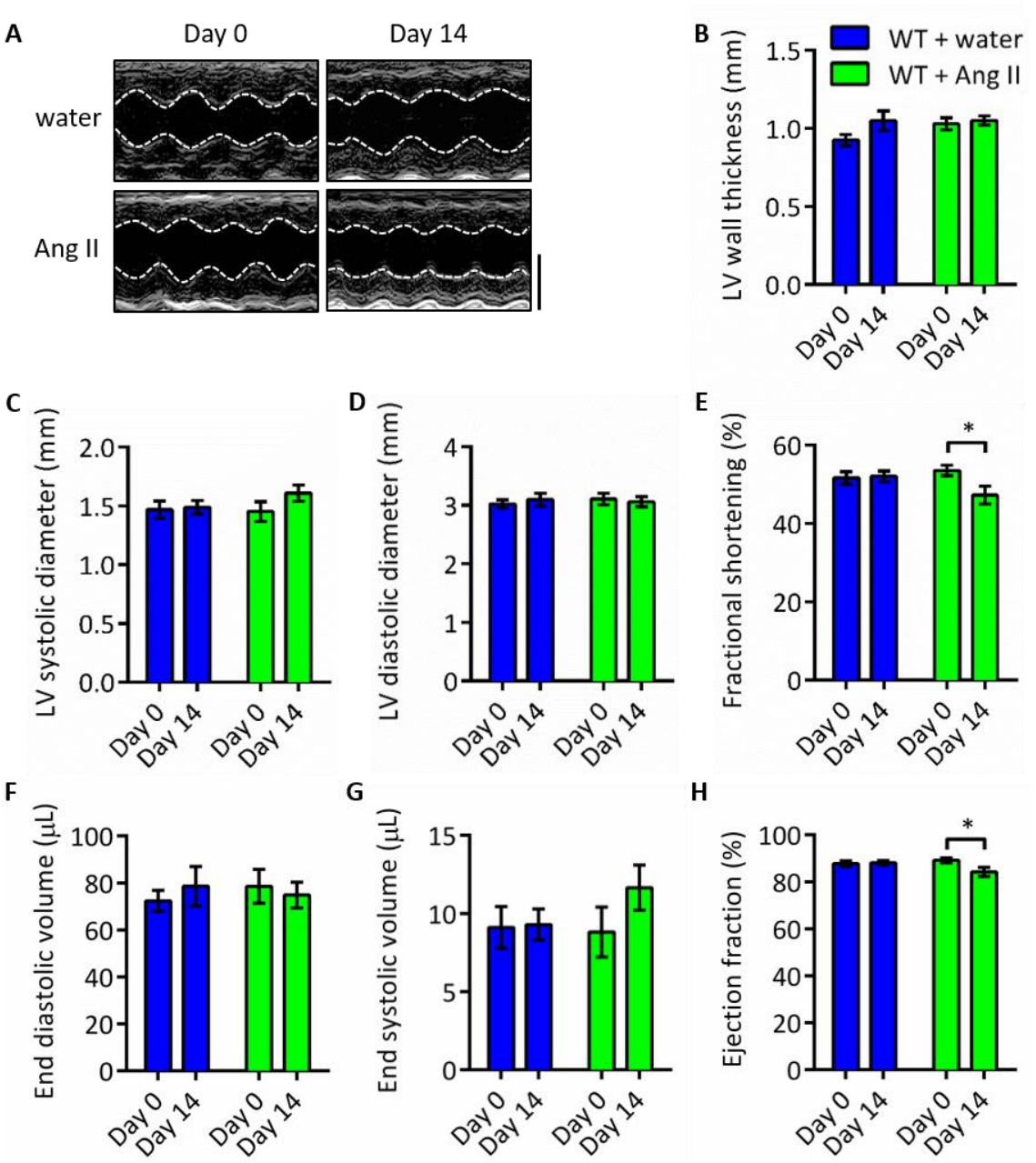

Figure 5-6 Fractional shortening and ejection fraction are significantly reduced in wild type mice following 2-week Ang II-infusion (A) Representative M-mode echocardiography images taken on the longitudinal axis at the level of the papillary muscle from wild type (WT) mice. Scale bar = 3 mm. **(B–H)** Measurements taken from M-mode images: **(B)** end diastolic left ventricular (LV) wall thickness; **(C)** end systolic and **(D)** end daistolic LV diameter; **(E)** fractional shortening of the left ventricle calculated from end systolic and diastolic diameters; **(F)** end systolic and **(G)** end diastolic volume; **(H)** ejection fraction calculated from end systolic and diastolic volumes. Data are mean +/- SEM of n = 8 (water) or n = 6 (Ang II) animals. *p<0.05 in two-tailed paired t test (day 0 vs. day 14).

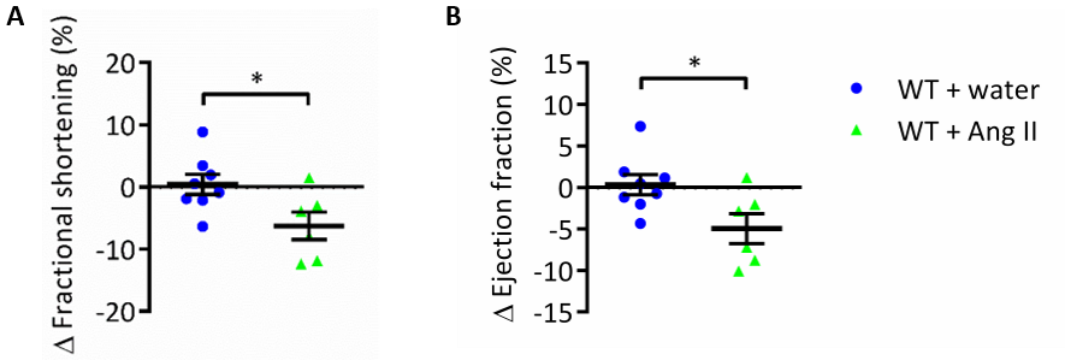

Figure 5-7 Two-week Ang II infusion leads to impaired cardiac function in wild type mice
Change in **(A)** fractional shortening and **(B)** ejection fraction of wild type (WT) mice following 2-week infusion of water (blue circles) or Ang II (green triangles). *p<0.05 in two-tailed unpaired t-test.

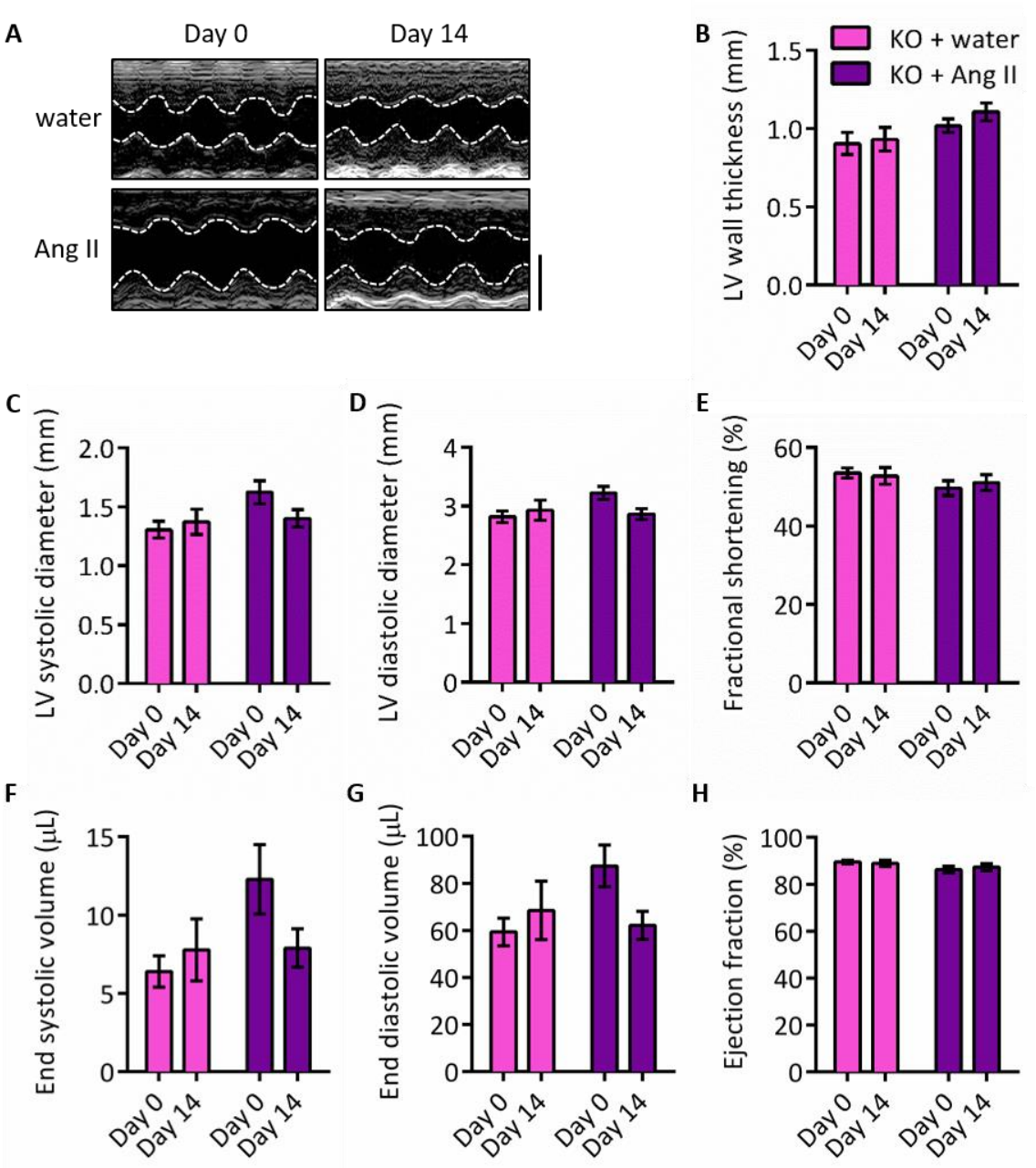

Figure 5-8 Echocardiographic measurements are not affected by 2-week Ang II-infusion in GPR35 knockout mice (A) Representative M-mode echocardiography images taken on the longitudinal axis at the level of the papillary muscle from GPR35 knockout (KO) mice. Scale bar = 3 mm. **(B–H)** Measurements taken from M-mode images: **(B)** end diastolic left ventricular (LV) wall thickness; **(C)** end systolic and **(D)** end daistolic LV diameter; **(E)** fractional shortening of the left ventricle calculated from end systolic and diastolic diameters; **(F)** end systolic and **(G)** end diastolic volume; **(H)** ejection fraction calculated from end systolic and diastolic volumes. Data are mean +/- SEM of n = 6 animals. Data were compared by two-tailed paired t test (day 0 vs. day 14), but no significant differences were found.

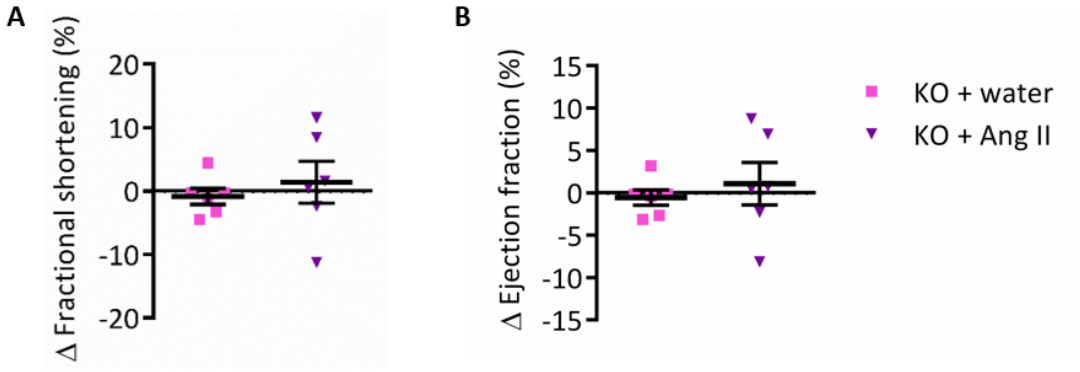

Figure 5-9 GPR35 knockout mice are resistant to Ang II-induced impairment of cardiac function Change in **(A)** fractional shortening and **(B)** ejection fraction of GPR35 knockout (KO) mice following 2-week infusion of water (pink squares) or Ang II (purple triangles). Data were compared by two-tailed unpaired t-test, but no significant differences were found.

To assess the effects of 2-week Ang II infusion on vasoreactivity in wild type and GPR35 knockout mice, constriction and relaxation responses of mesenteric arteries from water- and Ang II-infused mice were examined *ex vivo* by wire myography (Figure 5-10 and Figure 5-11). Mesenteric arteries from both wild type and GPR35 knockout mice infused with either water or Ang II showed increased intramural active effective pressure in response to noradrenaline, displaying sigmoidal concentration-response curves (Figure 5-10 A and B). Although mesenteric arteries from the Ang II-infused mice showed a trend towards increased maximal constriction for both wild type and GPR35 knockout strains, this was found not to be statistically significant (Figure 5-10 C). Mesenteric arteries from all treatment groups showed relaxation in response to carbachol when pre-constricted with 30 μM noradrenaline, displaying sigmoidal concentration-response curves (Figure 5-11 A and B). However, relaxation responses were observed only in a small proportion of vessels. Vessels that did not relax in response to carbachol were excluded from the analysis, leading to significantly reduced group sizes; therefore, statistical analysis could not be performed on the relaxation curves. However, Ang II-infused mice showed a trend towards reduced maximal relaxation for both wild type and GPR35 knockout strains (Figure 5-11 C). Overall, the combined findings for constriction and relaxation responses suggest a trend towards increased tone and stiffness of resistance vessels from Ang II-infused mice for both wild type and GPR35 knockout strains. Therefore, it was concluded that global knockout of GPR35 has no effect on vascular function in the context of Ang II-induced hypertension.

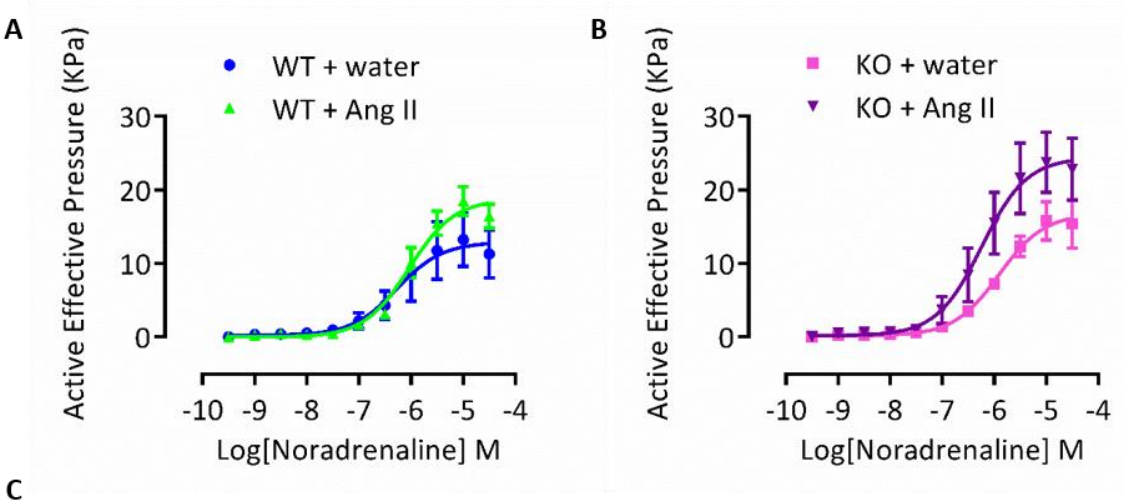

C

Group	pEC_{50}	P value	E_{max}	P value	AUC	P value
Mesenteric arteries: constriction to noradrenaline						
WT + water	6.14 ± 0.122	0.461	12.6 ± 3.58	0.226	29.1 ± 9.75	0.665
WT + Ang II	6.03 ± 0.073		16.4 ± 1.68		34.0 ± 4.49	
KO + water	5.96 ± 0.121	0.205	16.1 ± 3.10	0.371	31.5 ± 4.66	0.156
KO + Ang II	6.27 ± 0.176		23.5 ± 4.30		54.3 ± 12.1	

Figure 5-10 Vascular constriction responses are not affected by 2-week Ang II infusion in either wild type or GPR35 knockout mice Constriction concentration-response curves to noradrenaline of mesenteric arteries from **(A)** wild type (WT) or **(B)** GPR35 knockout (KO) mice following 2-week infusion with water or Ang II. **(C)** Statistical analysis of mean pEC_{50}, E_{max} and area under curve (AUC) from concentration-response curves generated for each individual animal. Curve statistics were compared by two-tailed unpaired t test, but no significant differences were found. Data are mean +/- SEM of n = 5 animals.

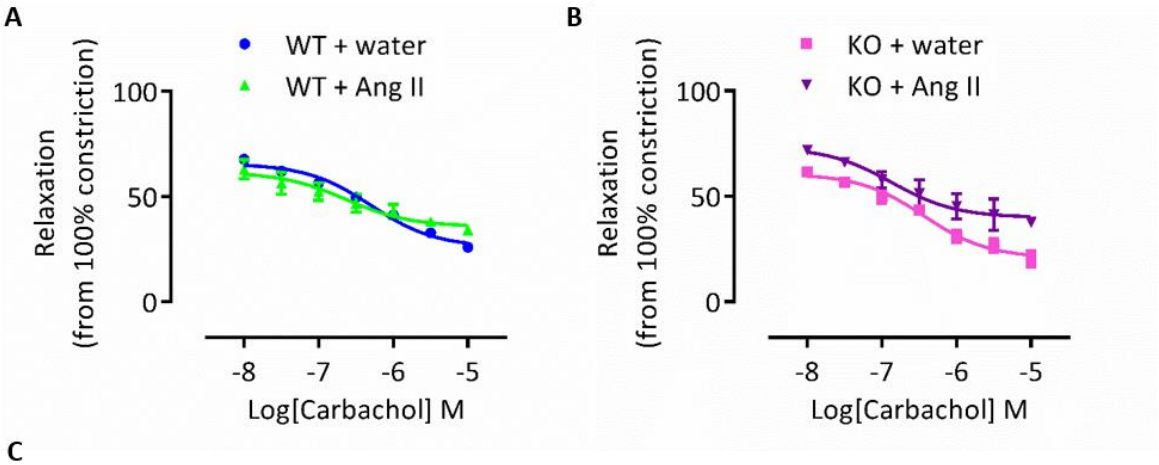

C

Group	pEC_{50}	P value	E_{max}	P value	AUC	P value
Mesenteric arteries: relaxation to carbachol						
WT + water	6.30	-	26.0	-	216	-
WT + Ang II	6.65 ± 0.225		35.5 ± 0.155		220 ± 12.9	
KO + water	6.44 ± 0.028	-	20.6 ± 3.69	-	188 ± 12.1	-
KO + Ang II	6.95 ± 0.135		41.8 ± 6.27		208 ± 15.2	

Figure 5-11 Vascular relaxation responses are not affected by 2-week Ang II infusion in either wild type or GPR35 knockout mice Relaxation concentration-response curves to carbachol of mesenteric arteries from **(A)** wild type (WT) or **(B)** GPR35 knockout (KO) mice following 2-week infusion with water or Ang II. **(C)** Mean pEC_{50}, E_{max} and area under curve (AUC) from concentration-response curves generated for each individual animal. Curve statistics could not be statistically compared due to insufficient group sizes. All data are mean +/- SEM of n = 2 animals (n = 1 for WT + water).

5.2.3 Effects of Ang II infusion on gross morphology of cardiovascular tissues in wild type and GPR35 knockout mice

Ang II infusion has previously been shown to cause significant pathophysiological remodelling in cardiovascular tissues (Qi et al., 2011, Takayanagi et al., 2016). In order to assess Ang II-induced remodelling and end-organ damage in wild type and GPR35 knockout mice, gross morphology of the hearts, carotid arteries and kidneys of Ang II-infused mice was examined.

In this study, Ang II infusion did not significantly affect whole heart or left ventricular mass in either wild type or GPR35 knockout mice (Figure 5-12 A–D). There was also no detectable induction of hypertrophy at the cellular level, with no significant increase in cardiomyocyte diameter observed in either strain (Figure 5-12 E). Cardiac fibrosis was similarly unaffected, with no significant increase in either perivascular or interstitial fibrosis induced by Ang II in wild type or GPR35 knockout mice (Figure 5-13).

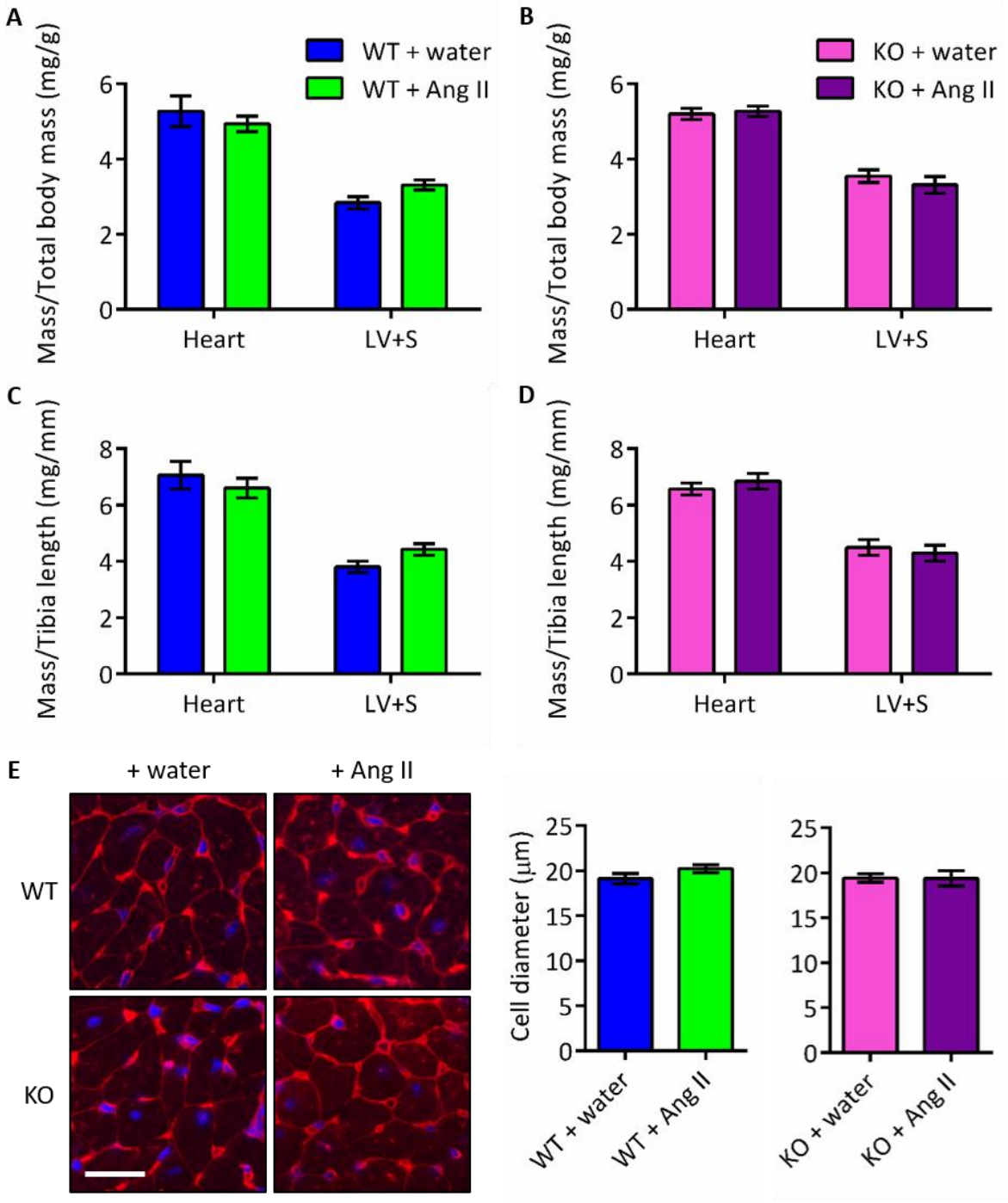

Figure 5-12 Cardiac mass and cardiomyocyte morphology are not affected by 2-week Ang II infusion in either wild type or GPR35 knockout mice (A–D) Whole heart and left ventricle + septum (LV+S) mass of wild type (WT) **(A, C)** and GPR35 knockout (KO) **(B, D)** mice were determined at sacrifice and normalised to total body mass **(A, B)** or tibia length **(C, D)**. **(E)** Transverse heart sections were stained with fluorescently-tagged wheat germ agglutinin (red) to visualise cardiomyocyte cell membranes, and with DAPI (blue) to visualise nuclei. Cell diameter was quantified by measuring the width of cardiomyocytes orientated on the short axis. Scale bar = 20 µm. Data are mean +/- SEM of n = 7 animals (mass) or n = 5 animals (cardiomyocyte size). Data were compared by two-tailed unpaired t test, but no significant differences were found.

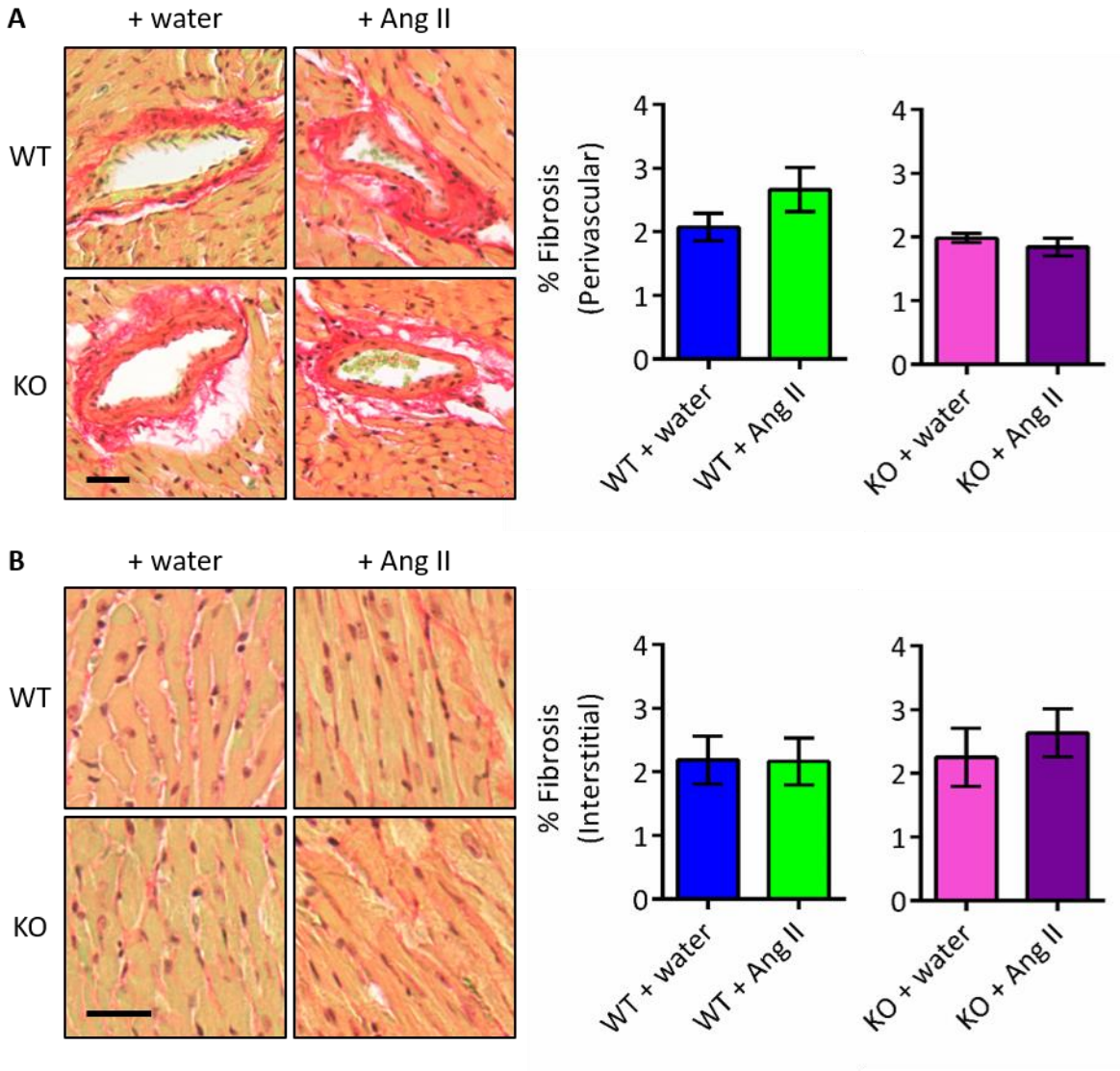

Figure 5-13 Cardiac fibrosis is not affected by 2-week Ang II infusion in either wild type or GPR35 knockout mice Transverse heart sections were stained with picro-sirius red to visualise collagen (red staining). Images of **(A)** perivascular and **(B)** interstitial regions were taken, and percent fibrosis was quantified as percentage of red pixels. Scale bar = 30 μm. Data are mean +/- SEM of n = 5 animals. Data were compared by two-tailed unpaired t test, but no significant differences were found.

Large vessel morphology was assessed by staining carotid arteries with hematoxylin and eosin. Vascular morphology was unaffected by Ang II infusion, with no difference in medial area induced by Ang II infusion in either wild type or knockout mice (Figure 5-14).

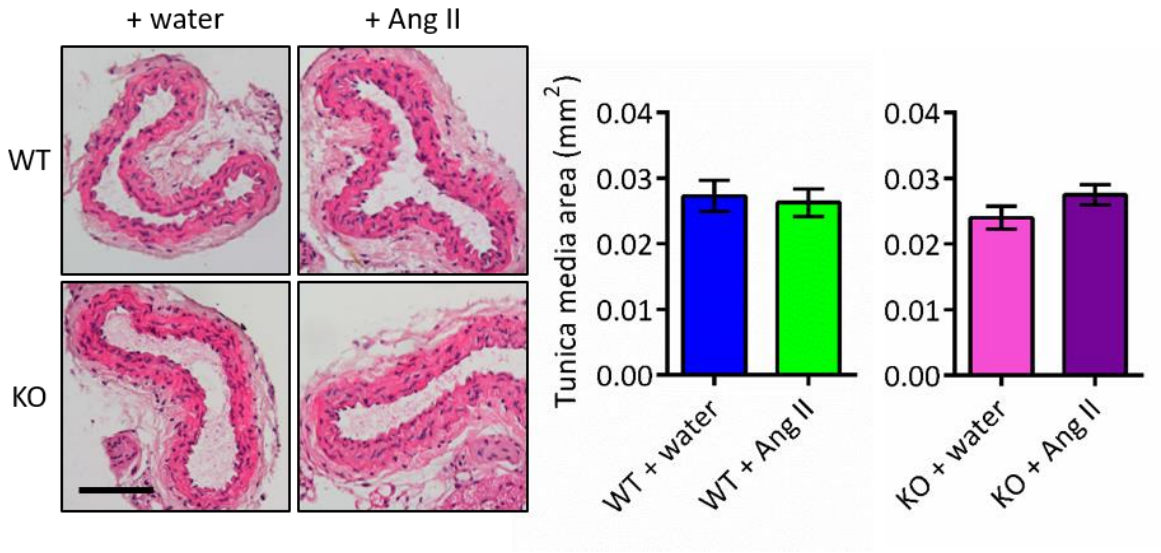

Figure 5-14 Vascular morphology is not affected by 2-week Ang II infusion in either wild type or GPR35 knockout mice Transverse carotid artery sections were stained with hematoxylin and eosin to visualise vascular morphology, and tunica media area was quantified by measuring the smooth muscle layer (bright pink staining). Scale bar = 100 μm. Data are mean +/- SEM of n = 4 animals. Data were compared by two-tailed unpaired t test, but no significant difference was found.

The effects of Ang II infusion on renal hypertrophy and fibrosis were also assessed. As in the heart, no significant differences in renal mass were observed (Figure 5-15). There were also no detectable effects of Ang II infusion on either perivascular or insterstitial fibrosis in the kidneys of either wild type or GPR35 knockout mice (Figure 5-16).

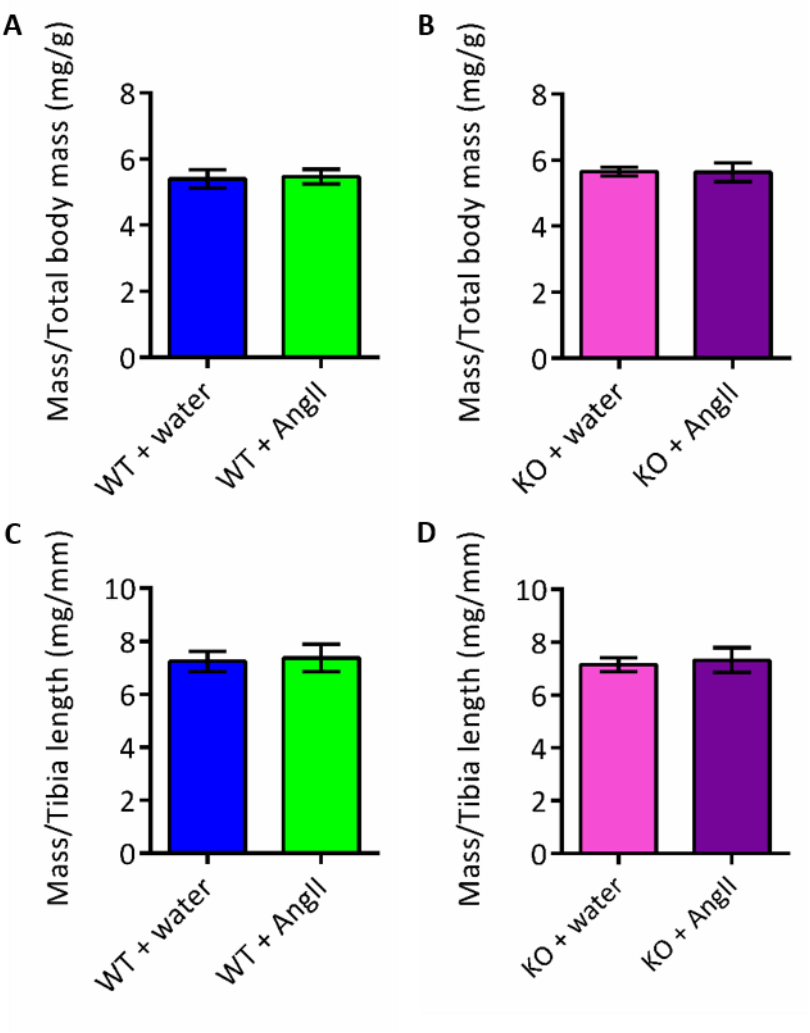

Figure 5-15 Renal mass is not affected by 2-week Ang II infusion in either wild type or GPR35 knockout mice Average kidney mass of wild type (WT) **(A, C)** and GPR35 knockout (KO) **(B, D)** mice were determined at sacrifice and normalised to total body mass **(A, B)** or tibia length **(C, D)**. Data are mean +/- SEM of n = 7 animals. Data were compared by two-tailed unpaired t test, but no significant differences were found.

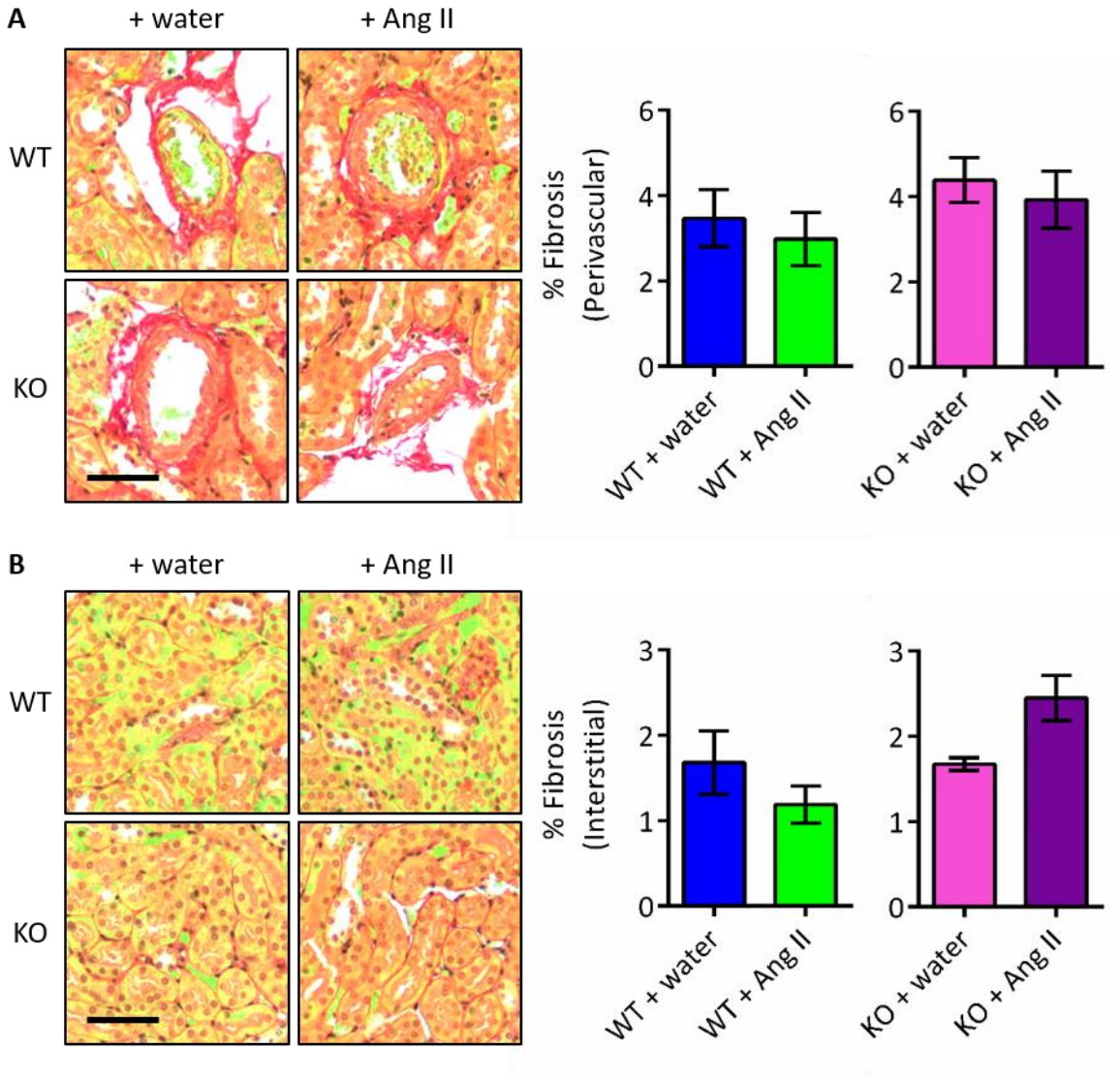

Figure 5-16 Renal fibrosis is not affected by 2-week Ang II infusion in either wild type or GPR35 knockout mice Transverse kidney sections were stained with picro-sirius red to visualise collagen (red staining). Images of **(A)** interstitial and **(B)** perivascular regions were taken, and percent fibrosis was quantified as percentage of red pixels. Scale bars = 50 µm. Data are mean +/- SEM of n = 5 animals. Data were compared by two-tailed unpaired t test, but no significant differences were found.

5.2.4 Effects of Ang II infusion on receptor gene expression in wild type and GPR35 knockout mice

One potential explanation for the finding that GPR35 knockout mice are resistant to Ang II-induced hypertension is that the AT_1R is downregulated in these mice. This possibility was investigated by quantifying $AT_{1a}R$ mRNA (*Agtr1a*) expression in cardiovascular tissues of wild type and GPR35 knockout mice using qRT-PCR analysis (Figure 5-17 A). *Agtr1a* mRNA was detected in heart, aorta and kidney tissue of water-infused wild type mice (C_T values of 24.4, 30.8 and 24.6, respectively) and GPR35 knockout mice (C_T values of 24.0, 31.3 and 25.1,

respectively). *Agtr1a* expression in these tissues was not affected by Ang II infusion in either wild type or GPR35 knockout mice. However, significantly higher expression was detected in the heart tissue of untreated GPR35 knockout mice compared with untreated wild type mice (Figure 5-17 A).

Based on previous reports that GPR35 is upregulated in the heart in some cardiovascular pathologies, *Gpr35* expression in cardiovascular tissues of wild type mice subjected to 2-week infusion of water or Ang II was also assessed (Figure 5-17 B) (Min et al., 2010, Ronkainen et al., 2014). *Gpr35* mRNA was detected in heart, aorta and kidney tissue of water-infused wild type mice (C_T values of 32.4, 33.1 and 35.4, respectively); however, no significant increase in *Gpr35* expression in response to Ang II infusion was observed (Figure 5-17 B).

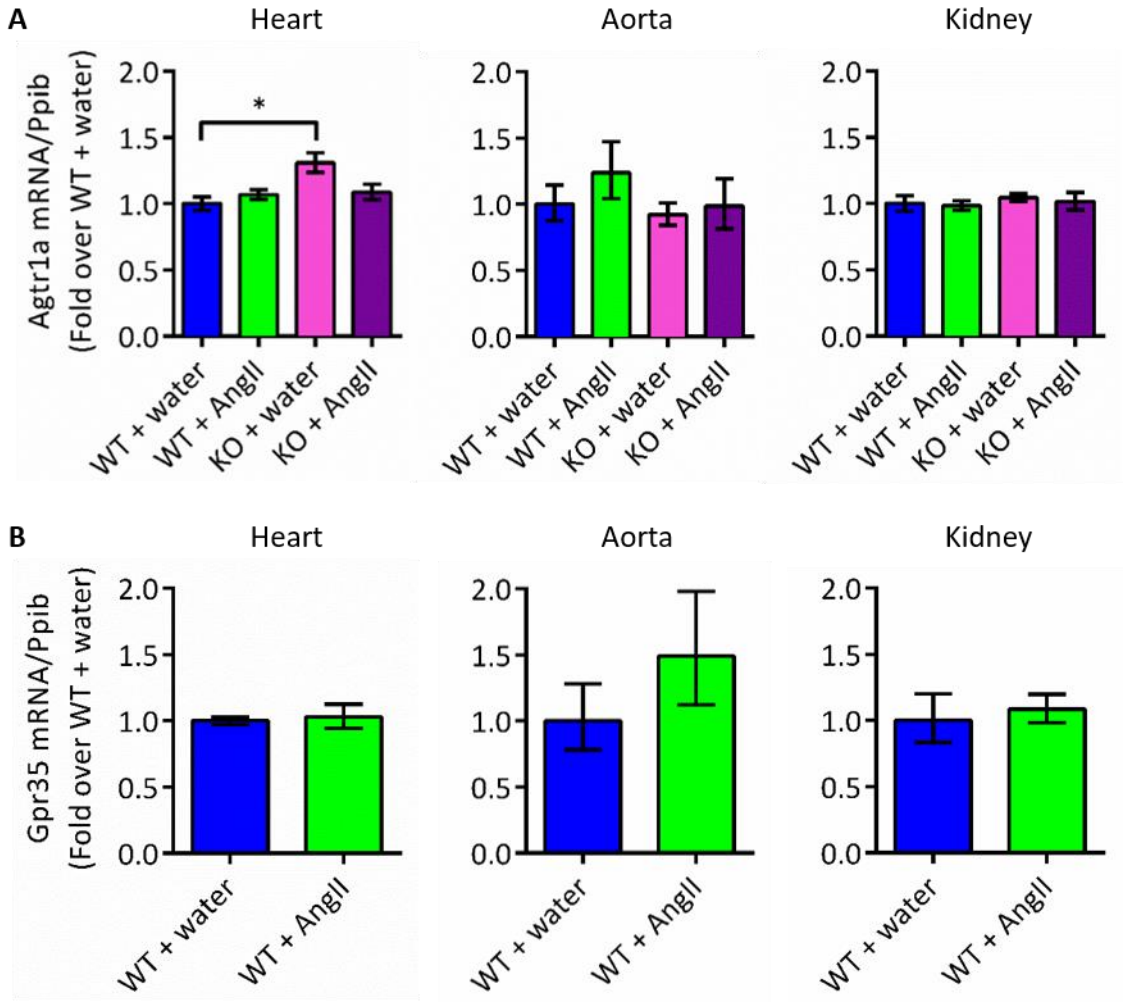

Figure 5-17 *Agtr1a* and *Gpr35* gene expression are not affected by 2-week Ang II infusion in either wild type or GPR35 knockout mice (A) *Agtr1a* gene expression relative to *Ppib* in wild type (WT) and GPR35 knockout (KO) mice subjected to 2-week infusion of water or Ang II. **(B)** *Gpr35* gene expression relative to *Ppib* in WT mice subjected to 2-week infusion of water or Ang II. Data are mean +RQmax/-RQmin of n = 4 animals. Data were compared by one-way ANOVA with Tukey's multiple comparisons post-test (A) or two-tailed unpaired t test (B); *p<0.05.

5.3 Discussion

5.3.1 Low-dose Ang II infusion leads to hypertension in wild type mice

Ang II infusion in mice has been used in many studies investigating different aspects of cardiovascular pathophysiology, including aortic aneurysm, hypertension and heart failure (Weiss et al., 2001, Lu et al., 2015, Regan et al., 2015, Lima et al., 2016, Takayanagi et al., 2016). The cardiovascular effects of Ang II infusion vary depending on the infusion rate or dose of Ang II and the duration of infusion. In this study, C57BL/6 mice were infused with a low pressor dose of 400 ng/kg/min Ang II for two weeks. Blood pressure began to increase after 8 days, and a modest increase in blood pressure of approximately 20 mmHg was observed after two weeks. This is a slower onset and less drastic increase than has been reported previously, with doses of 490 ng/kg/min inducing a 40 mmHg increase within 3 days, and 1000 ng/kg/min inducing a 50 mmHg increase within 5 days, as measured by either radiotelemetry or tail-cuff plethysmography (Crowley et al., 2006, Moore et al., 2015). The modest Ang II blood pressure response observed in this study is most likely a result of the slightly lower dose used, which was a necessary measure to take in order to minimise the risk of mortality in the event that GPR35 knockout mice had an exacerbated response to Ang II. However, this difference in outcome may also reflect strain- or facility-specific differences in the Ang II response. Many of these studies use wild type animals as littermate controls for transgenic or knockout animals, meaning they are highly inbred and therefore not identical to the generic background strain. There is also potential variation in the procedures associated with preparing the Ang II and osmotic minipumps, as well as the blood pressure measurements themselves. Caution should therefore be taken when comparing the results of different studies, and high internal validity should be the priority when interpreting the results of a particular study.

As well as an increase in blood pressure, 2-week Ang II infusion also led to impaired left ventricular systolic function in wild type mice. Although no concomitant increase in cardiac mass or cardiomyocyte hypertrophy was observed, this observation is indicative of the pathological cardiac remodelling and cardiac dysfunction associated with chronic hypertension. Similarly to the

Ang II blood pressure response, the extent of left ventricular systolic dysfunction observed following Ang II infusion varies between different studies (González et al., 2015, Glenn et al., 2015, Khan et al., 2015). However, the modest decreases in fractional shortening and ejection fraction observed in this study were statistically significant when compared with changes over two weeks in water-infused control mice. Although this is probably not a clinically meaningful alteration, it is suggestive of the initiation of pathophysiological processes, and is sufficient to serve as a wild type control against which to compare responses in the GPR35 knockout mouse.

Unlike blood pressure and cardiac function, the remaining endpoints (vascular reactivity; cardiac, vascular and renal morphology; cardiac and renal fibrosis; and *Atgr1a* mRNA expression) were not significantly altered by two-week Ang II infusion in wild type mice at the selected dose. These parameters have all previously been reported to undergo changes in response to infusion of slightly higher doses of Ang II (Moore et al., 2015, Takayanagi et al., 2015, Mikolajczyk et al., 2016). This suggests that a dose of 400 ng/kg/min over two weeks is not sufficient to induce detectable changes in all cardiovascular end organs; rather, this dose results in an intermediate phenotype characterised by moderately increased blood pressure and mild cardiac dysfunction, without associated end-organ damage.

Gpr35 mRNA expression in the heart, aorta and kidney of wild type mice was also not significantly altered by 2-week Ang II infusion. *Gpr35* expression in the heart has previously been reported to increase in response to coronary artery ligation or TAC in mouse models (Ronkainen et al., 2014). The data reported here suggest that this is an effect specific to models of severe cardiac injury or remodelling, and that the modest blood pressure and cardiac changes observed in this study were not sufficient to induce a detectable increase in *Gpr35* expression. However, *Gpr35* mRNA was detected in all three tissues in both water- and Ang II-infused wild type mice. Low levels of *Gpr35* expression in the heart and in primary vascular cells have been reported previously, and the findings presented here corroborate these reports (Taniguchi et al., 2006, McCallum et al., 2015).

5.3.2 GPR35 knockout mice are resistant to the effects of low-dose Ang II infusion

Due to a previous report suggesting that GPR35 knockout mice have increased blood pressure (Min et al., 2010), the hypothesis of this study was that GPR35 knockout mice are more sensitive to the effects of Ang II on the cardiovascular system. However, the data presented here demonstrate the opposite – GPR35 knockout mice were resistant to the Ang II-induced increase in blood pressure and impairment of cardiac function observed in wild type mice. The changes in systolic, diastolic and mean arterial blood pressure over the 2-week infusion period were not significantly different in Ang II-infused mice compared with water-infused mice, whereas Ang II-infused wild type mice underwent increases of approximately 20 mmHg. Left ventricular fractional shortening and ejection fraction were similarly unaltered, with no significant differences between water- and Ang II-infused GPR35 knockout mice after 14 days, compared with significant differences of >6% in wild type mice.

Given how little is known about the *in vivo* function of GPR35, there are many possible explanations for the lack of an Ang II response in the GPR35 knockout mouse. The fact that the Ang II response was completely abolished in these animals, rather than merely attenuated, suggests an important role for GPR35 in Ang II-mediated signalling – perhaps more important than was previously supposed, given its orphan status. The simplest explanation for this is that GPR35 directly interacts with the Ang II signalling axis, for example by acting as a co-receptor with the AT_1R. The AT_1R is known to heterodimerise with a wide range of other Class A GPCRs, including dopamine D_1R, ß-ARs, cannabinoid receptor 1 and purinergic $P2Y_6$ receptor (Zeng et al., 2003, Barki-Harrington et al., 2003, Rozenfeld et al., 2011, Nishimura et al., 2016). These interacting GPCRs alter AT_1R signalling, either by stabilising the active AT_1R conformation or by biasing the receptor to signal through a particular (sometimes atypical) G protein. Genetic deletion of the $P2Y_6$ receptor has been shown to attenuate Ang II-induced effects on blood pressure and vascular function, and direct evidence for $P2Y_6/AT_1R$ interaction has been reported (Nishimura et al., 2016). It is therefore possible to speculate that the similar effect on blood pressure in the present study are due to GPR35 interacting with AT_1R. This has not been investigated previously, but would be relatively straightforward to test *in vitro*

using classical techniques for studying protein-protein interactions or one of many techniques that have been developed to probe GPCR oligomerisation (Marsango et al., 2015, Nakamura et al., 2016).

An alternative explanation for the findings reported here is that GPR35 interacts with Ang II-mediated blood pressure regulation indirectly through its effects on other pathways. Previous studies linking GPR35 with inflammation (section 1.4.6.3) provide another potential means by which GPR35 might alter Ang II-induced effects on the cardiovascular system. GPR35 expression has been detected on both lymphocytes and several myeloid cells, as well as in vascular endothelial cells (Wang et al., 2006, Yang et al., 2010, Fallarini et al., 2010, McCallum et al., 2015). In addition, studies with GPR35 agonists have suggested possible roles in proinflammatory cytokine release, macrophage recruitment and leukocyte arrest onto the vascular endothelium (Barth et al., 2009, Fallarini et al., 2010, Maravillas-Montero et al., 2015). Vascular inflammation is now recognised as an important factor in the development of Ang II-induced hypertension and associated end-organ damage (McMaster et al., 2015, Wenzel et al., 2016). Various immune cells, including T cells, monocytes and natural killer cells, are recruited to vascular and perivascular tissues in response to Ang II infusion, and the resulting inflammation contributes to the vascular dysfunction that leads to hypertension (Guzik et al., 2007, Wenzel et al., 2011, Kossmann et al., 2013, Mikolajczyk et al., 2016). Therefore, the apparent requirement for GPR35 in Ang II-induced hypertension may in fact be due to a role in driving vascular inflammation, rather than a direct effect in vascular cells. This is an interesting possibility that has not previously been explored, and these findings could be followed up with future studies into the effects of GPR35 on markers of vascular inflammation in models of hypertension.

The finding that GPR35 knockout mice are protected from Ang II-induced impairment of cardiac function could be due to either direct effects in the myocardium or the absence of a blood pressure effect to initiate remodelling. However, previous studies demonstrating the induction of GPR35 expression in the heart during pathological cardiac remodelling suggest it has a direct function in this tissue (Min et al., 2010, Ronkainen et al., 2014). It is possible that GPR35 has independent functions in the development of hypertension (*via* effects on

the vasculature) and during cardiac remodelling and heart failure (*via* effects in the heart).

Regardless of the physiological mechanism underlying the roles of GPR35 in Ang II-induced hypertension and impaired cardiac function, the findings of this study suggest a pathological role for GPR35 in the development of CVD. Given previous reports that GPR35 couples selectively to $G\alpha_{13}$ and regulates actin reorganisation in both cardiomyocytes and vascular smooth muscle cells, these cardiovascular effects of GPR35 are likely mediated by the $G\alpha_{13}$/RhoA/ROCK pathway. Although the conclusion of this study conflicts with the previous blood pressure study in GPR35 knockout mice, existing evidence of pathological roles for $G\alpha_{13}$/RhoA/ROCK signalling in the cardiovascular system provide a rationale for the finding that GPR35 knockout mice are protected from CVD (Wirth et al., 2008, Surma et al., 2011, Takefuji et al., 2012).

5.3.3 Is GPR35 a viable therapeutic target in hypertension?

Although the mechanism by which inactivation of GPR35 attenuates Ang II-induced hypertension remains unclear, the findings presented here suggest that targeting GPR35 could be a novel approach by which to therapeutically control blood pressure. The most obvious application of this would be to use GPR35 antagonists to treat hypertension. It will therefore be necessary to test whether pharmacological manipulation of GPR35 activity can alter the development of hypertension in *in vivo* models of CVD. A study investigating pharmacological agonism of GPR35 in a rat model of hypertension is described in the following chapter.

The lack of antagonists with affinity for rodent GPR35 orthologues will make investigating the therapeutic potential of GPR35 antagonism challenging. Ongoing screening efforts (supported by novel bioinformatic approaches to ligand identification as well as an improved understanding of the mechanisms of species selectivity) may yet yield equipotent GPR35 antagonists that will enable such studies (Ngo et al., 2016a, MacKenzie et al., 2014). However, a number of alternative approaches could also be explored in order to address this challenge. For example, blocking monoclonal antibodies, rather than small-molecule inhibitors, are an alternative means by which to inhibit GPCRs *in vivo*. In

particular, novel, single-domain ‘nanobodies’ derived from those that naturally occur in camelids are currently being pursued as experimental and therapeutic tools with which to alter GPCR function (Mujić-Delić et al., 2014, Manglik et al., 2016). These have been successfully used to antagonise GPCRs (particularly chemokine receptors) both *in vitro* and *in vivo*, and thus provide a possible alternative to small molecule ligands with which to block GPR35 function (Maussang et al., 2013, Griffiths et al., 2016).

In lieu of suitable molecules for blocking the rodent GPR35 orthologue, novel approaches may be used that enable *in vivo* testing of the existing human-selective antagonists. ‘Humanised’ mice, in which the human receptor orthologue is knocked in either globally or to specific tissues, are already being used in GPCR research to answer a range of challenging questions (Tello et al., 2013, Jun et al., 2014, Robinson et al., 2015). A humanised GPR35 knock-in mouse is currently being developed, and will enable the effects of pharmacological antagonism of GPR35 to be assessed *in vivo* for the first time. This, along with a better understanding of the physiological roles of GPR35, will reveal its true potential as a pharmacological target in CVD.

Chapter 6 Cardiovascular effects of a GPR35 agonist in the stroke-prone spontaneously hypertensive rat

6.1 Introduction

The findings described in the previous two chapters suggest that although a global deficiency of GPR35 has no effect on the basal regulation of cardiovascular function, it does attenuate some of the pathological outcomes of chronic cardiovascular stress. This implies a role for GPR35 in the development and progression of cardiovascular dysfunction in disease. These conclusions led to the hypothesis that, if GPR35 deficiency attenuates cardiovascular dysfunction, then increased GPR35 activity would exacerbate it. This hypothesis is explored in this chapter. Furthermore, in order to assess the therapeutic potential of GPR35 as a pharmacological target in CVD, it is important to establish whether its activity can be pharmacologically modulated *in vivo*. To address this question, it was of interest to determine the effects of pharmacological agonism of GPR35 *in vivo*, within the physiological context of CVD. This chapter describes the cardiovascular effects of long-term administration of a GPR35 agonist in a rodent model of CVD.

The stroke-prone spontaneously hypertensive rat (SHRSP) is a well-characterised genetic model of cerebrovascular disease and essential hypertension that has been used extensively in the study of cardiovascular pathologies including stroke, hypertension and end-organ damage (Yamori and Horie, 1977, Jacob et al., 1991, Rocha et al., 1998, Flores-Munoz et al., 2012, McLachlan et al., 2014). The SHRSP model is an inbred strain isolated from Wistar-Kyoto rats, which begins to develop high blood pressure at 4–7 weeks of age and demonstrates moderate-to-severe hypertension (>200 mmHg) by 10–12 weeks of age (Yamori and Horie, 1977, Christiansen et al., 2002). It is therefore a highly useful model in which to study the progression of cardiovascular dysfunction from an early age, without the need for exogenous interventions such as salt-loading. The mechanisms of hypertension in the SHRSP are polygenic and are still not fully understood, although a large number of genetic studies have identified several loci that contribute to the hypertensive phenotype (Jacob et al., 1991, Graham et al., 2007, Yamamoto et al., 2013). Similarly to human essential hypertension

(also a complex polygenic condition), blockade of the renin-angiotensin-aldosterone system is effective in reducing blood pressure and end-organ damage in this model (Flores-Munoz et al., 2012, McLachlan et al., 2014). These similarities between the SHRSP and human essential hypertension make it an ideal model in which to study the potential role of GPR35 in hypertension and cardiovascular pathophysiology.

As discussed previously (section 1.4.3.1), a number of synthetic agonists with efficacy at the rat GPR35 orthologue have now been identified (Jenkins et al., 2010, Southern et al., 2013, MacKenzie et al., 2014). The partial agonist amlexanox is among the most potent of these in ß-arrestin recruitment assays (EC_{50} = 23 nM (MacKenzie et al., 2014)), and has previously been shown to have good oral bioavailability and pharmacokinetic properties (Khandwala et al., 1997, Southern et al., 2013). For these reasons, amlexanox was selected as the agonist for this study. Amlexanox is a mast cell stabiliser first developed and used clinically in Japan as an anti-inflammatory and anti-allergic agent (Makino et al., 1987, Bell, 2005). It is currently used as a topical anti-inflammatory treatment for aphthous ulcers (marketed as Aphthasol®), but has been shown to have clinical efficacy both as a topical treatment and as an oral tablet (Bell, 2005, Meng et al., 2009). A pharmacokinetic study of the 5% oral paste in humans showed sufficient gastrointenstinal absorption to reach serum concentrations of up to 120 ng/mL (402 nM) from a single dose of 100 mg, and a half-life of 3.5 hours (Khandwala et al., 1997).

Amlexanox is not a novel drug, and as such it has several known targets other than GPR35. It binds with high affinity to the non-canonical IκB kinases (IKKs) IKK-ε and TANK-binding kinase-1 (TBK-1), which are associated with obesity and insulin resistance (Reilly et al., 2013). It inhibits these kinases with an IC_{50} of 1–2 μM, and has been shown to stimulate increased fat metabolism, increased insulin sensitivity and weight loss in obese mice at doses of 25–50 mg/kg/day (Reilly et al., 2013). In addition, amlexanox has recently been reported to inhibit GRK5 with an IC_{50} of 13 μM (Homan et al., 2014). However, the potency of amlexanox at these alternative targets is in the micromolar range – at least 100-fold lower than the concentrations required to activate rat GPR35 (MacKenzie et al., 2014). Therefore, careful dosing should limit potential off-

target effects mediated by these kinases in *in vivo* studies in the SHRSP. This chapter describes an *in vivo* study into the cardiovascular effects of amlexanox treatment in the SHRSP.

6.1.1 Aims

The aims of this chapter were to:

- Accurately assess the effects of amlexanox treatment on haemodynamic parameters in the SHRSP using an implantable telemetry device

- Determine the effects of amlexanox treatment on cardiovascular end-organ damage in the SHRSP

- Assess potential off-target effects of amlexanox on fat metabolism in the SHRSP

6.1.2 Study design

The dose of amlexanox used in this study was critical in minimising potential off-target effects of the treatment. It has been reported that oral doses of 25–50 mg/kg/day are sufficient to achieve serum concentrations of >5 μM in mice (Reilly et al., 2013). Therefore, an oral dose of 2.5 mg/kg/day was estimated to be required for a serum concentration of approximately 500 nM, which would achieve maximum efficacy at GPR35 without inhibiting other, lower-potency targets. To minimise stress artefacts in blood pressure measurements, amlexanox was administered orally in food. Control animals received an equivalent volume of vehicle (DMSO) in the same manner.

In this study, amlexanox was administered to SHRSP in order to determine the effects of GPR35 agonist on blood pressure and end-organ damage in a model of essential hypertension. Only male animals were used in order to eliminate sex-specific variation. Oral administration of vehicle or amlexanox commenced at 6 weeks of age and continued daily for 6 weeks (Figure 6-1). The body weight of animals limits the age at which telemetry probes can be safely implanted; therefore systolic blood pressure was monitored by tail-cuff plethysmography prior to treatment and weekly for the first 3 weeks of treatment. At 9–10 weeks

of age, telemetry probes were implanted and haemodynamic parameters were monitored continuously by telemetry for the following 3 weeks of treatment (Figure 6-1). In order to assess the diurnal variation in the parameters measured, the telemetry data generated in this study were separated into two 12-hour periods representing the dark period (night) and the light period (day). Treatment was followed by sacrifice and *ex vivo* analysis at 12 weeks of age.

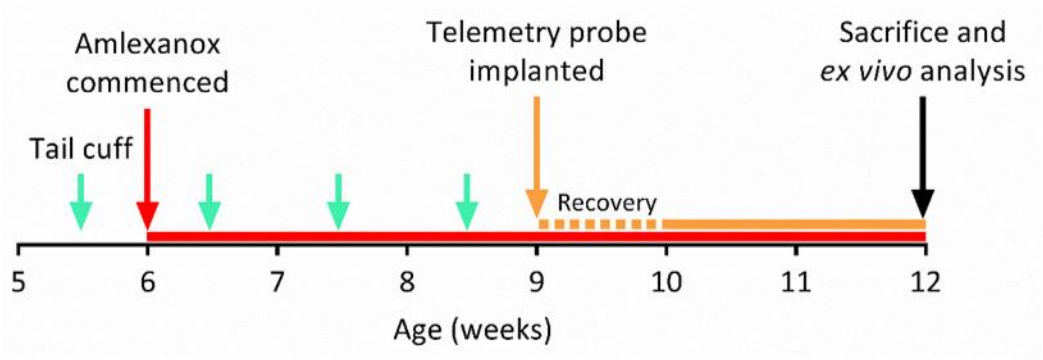

Figure 6-1 SHRSP amlexanox study timeline

6.2 Results

6.2.1 Effects of amlexanox treatment on haemodynamic properties in the SHRSP

Blood pressure and other haemodynamic parameters were monitored in conscious SHRSP over six weeks of amlexanox administration (Figure 6-2 and Figure 6-3). All parameters followed normal diurnal rhythms over the light/dark cycle in both vehicle-treated and amlexanox-treated SHRSP (Figure 6-2 and Figure 6-3). Systolic blood pressure measured by tail-cuff plethysmography was not significantly different between the groups at day 0 prior to commencement of treatment (Figure 6-2 A). Systolic blood pressure increased over weeks 1–3 of treatment, but was not significantly different between the groups during this time (Figure 6-2 A). However, by the commencement of telemetry recordings at week 4 (9–10 weeks of age), systolic blood pressure in both groups reached a plateau that was significantly higher in amlexanox-treated SHRSP than in vehicle-treated animals, by a difference of approximately 12.5 mmHg (Figure 6-2 A). Mean arterial pressure was also significantly higher in amlexanox-treated SHRSP, whereas diastolic blood pressure showed a trend towards being higher but was not significantly different according to statistical analysis (Figure 6-2 B).

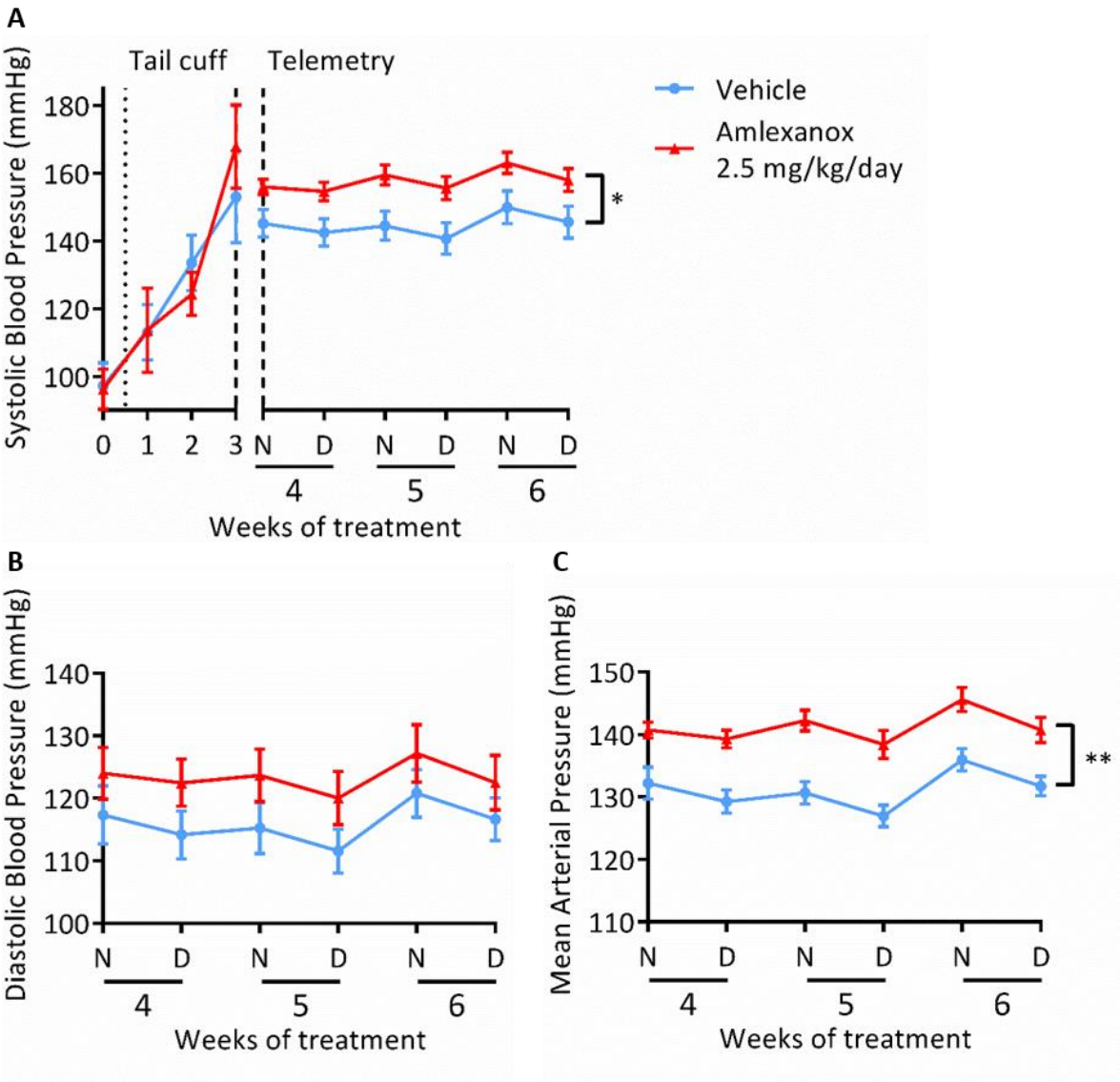

Figure 6-2 Blood pressure is significantly increased by amlexanox treatment in SHRSP (A) Systolic blood pressure, **(B)** diastolic blood pressure and **(C)** mean arterial pressure were monitored over six weeks **(A)** or three weeks **(B, C)** in SHRSP treated with vehicle (blue circles) or 2.5 mg/kg/day amlexanox (red triangles) using tail-cuff plethysmography and/or telemetry. Tail-cuff data are presented as weekly averages of 24-hour means and telemetry data are presented as weekly averages of 12-hour means representing night (N) and day (D) periods; mean +/- SEM of n = 8 animals. *p<0.05, **p<0.01 in two-way repeated measures ANOVA.

Heart rate and locomotive activity were also monitored by telemetry during weeks 4–6 of amlexanox treatment (Figure 6-3). No significant differences in either heart rate or activity were observed between vehicle-treated and amlexanox-treated SHRSP (Figure 6-3). Activity was subject to normal diurnal rhythms in both groups, suggesting the surgical procedure was well tolerated and the haemodynamic parameters observed are representative of those under normal behavioural conditions (Figure 6-3 B).

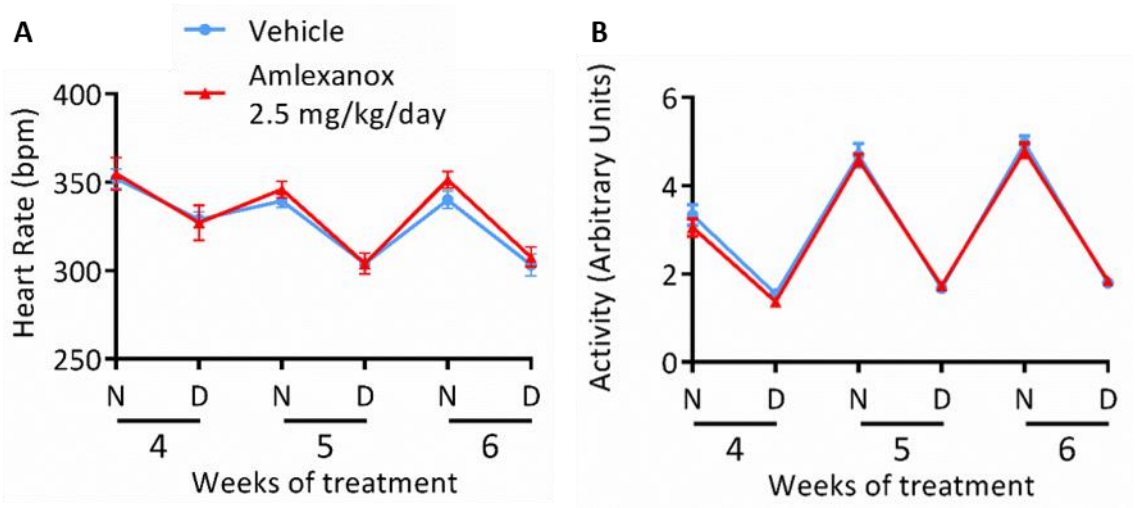

Figure 6-3 Heart rate and locomotive activity are not affected by amlexanox treatment in SHRSP (A) Heart rate in beats per minute (bpm) and **(B)** locomotive activity were monitored over three weeks in SHRSP treated with vehicle (blue circles) or 2.5 mg/kg/day amlexanox (red triangles) using telemetry. Data are presented as weekly averages of 12-hour means representing night (N) and day (D) periods; mean +/- SEM of n = 8 animals. Data were compared by two-way repeated measures ANOVA, but no significant differences were found.

6.2.2 Effects of amlexanox treatment on cardiovascular end-organ damage in the SHRSP

The SHRSP is known to have increased levels of cardiovascular end-organ damage such as pathological cardiac remodelling and fibrosis (Flores-Munoz et al., 2012, McLachlan et al., 2014). In order to determine whether amlexanox treatment exacerbates these markers of advanced cardiovascular damage, gross morphology of the heart and kidney in amlexanox-treated SHRSP was examined.

Both whole heart and left ventricular mass were significantly increased in amlexanox-treated SHRSP when normalised to total body mass (Figure 6-4 A). Increases were also observed when normalised to tibia length, although this difference was only statistically significant for left ventricular mass and not whole heart mass (Figure 6-4 B). There was a trend towards increased cardiomyocyte diameter, although the difference observed was small and not statistically significant (Figure 6-4 C). Overall, these data suggest that amlexanox treatment exacerbated gross cardiac hypertrophy in the SHRSP.

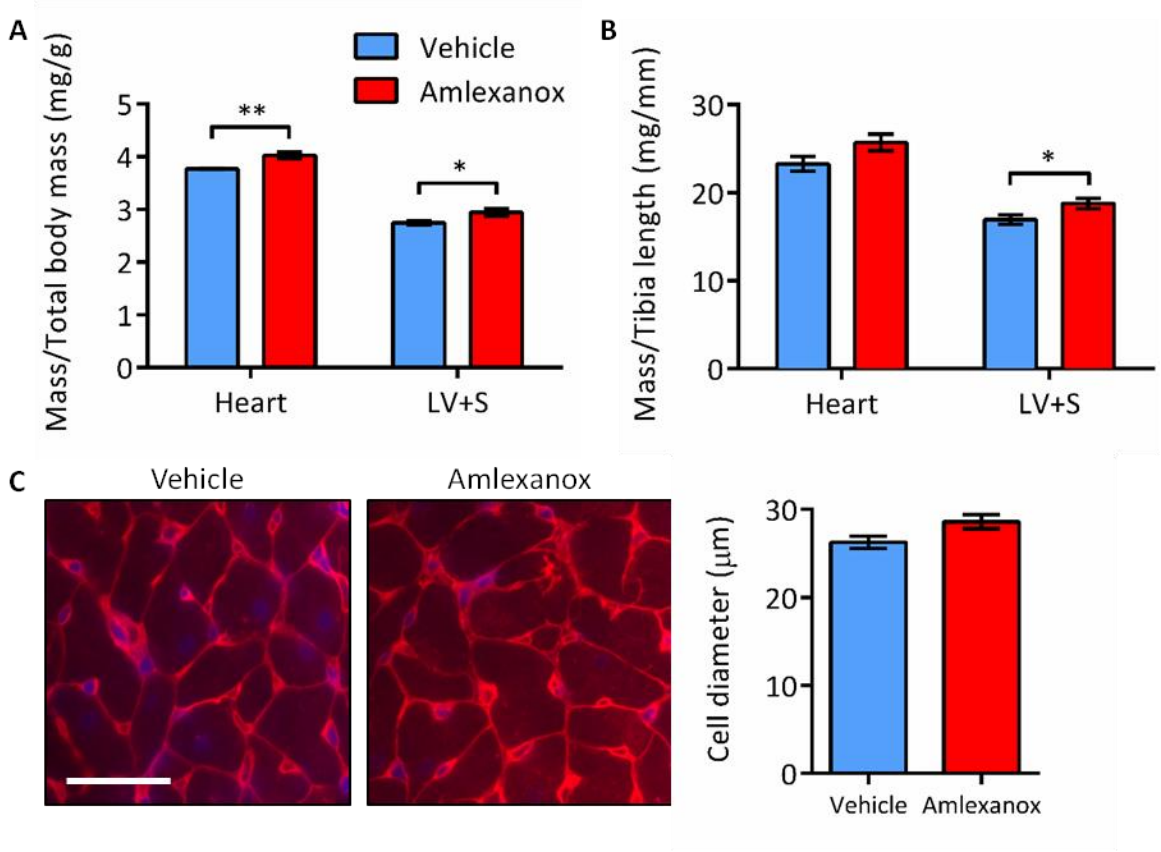

Figure 6-4 Cardiac mass is significantly increased by amlexanox treatment in SHRSP (A, B) Whole heart and left ventricle + septum (LV+S) mass were determined at sacrifice and normalised to **(A)** total body mass or **(B)** tibia length. **(C)** Transverse heart sections were stained with fluorescently-tagged wheat germ agglutinin (red) to visualise cardiomyocyte cell membranes, and with DAPI (blue) to visualise nuclei. Cell diameter was quantified by measuring the width of cardiomyocytes orientated on the short axis. Scale bar = 50 µm. Data are mean +/- SEM of n = 8 animals (mass) or n = 5 animals (cardiomyocyte size). *p<0.05, **p<0.01 in two-tailed unpaired t test.

Cardiac fibrosis is another marker of cardiac dysfunction that is present under basal conditions in the SHRSP (Flores-Munoz et al., 2012, McLachlan et al., 2014). However, amlexanox treatment did not have a significant effect on either perivascular or interstitial fibrosis in the SHRSP myocardium (Figure 6-5).

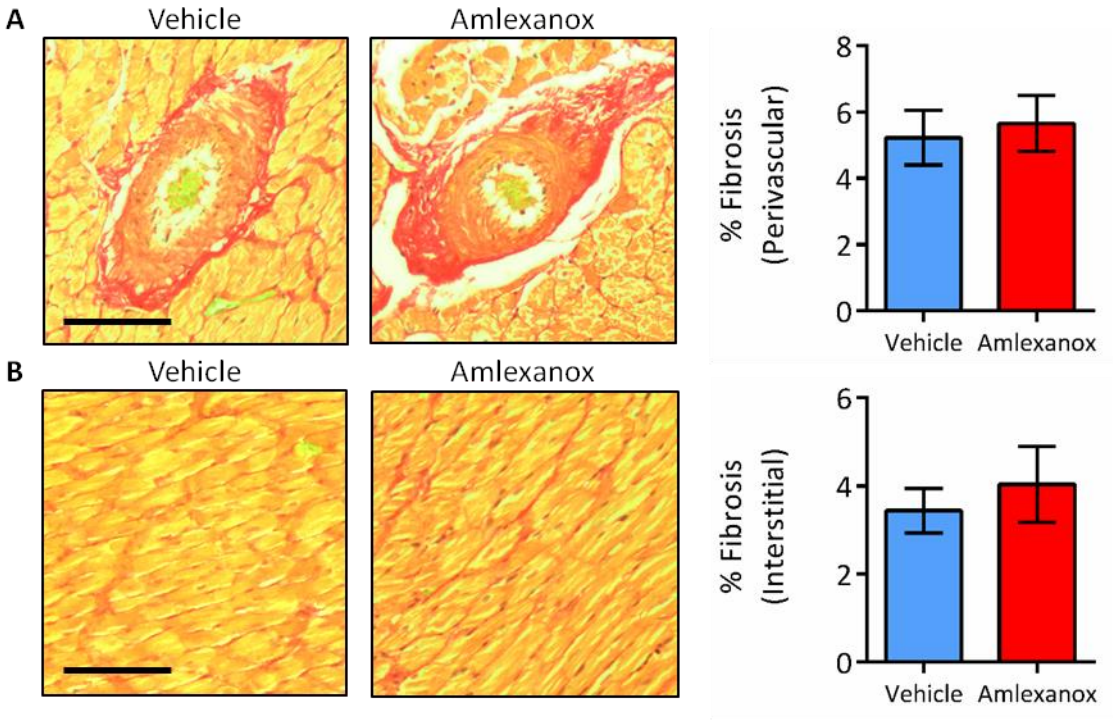

Figure 6-5 Cardiac fibrosis is not affected by amlexanox treatment in the SHRSP Transverse heart sections were stained with picro-sirius red to visualise collagen (red staining). Images of **(A)** perivascular and **(B)** interstitial regions were taken, and percent fibrosis was quantified as percentage of red pixels. Scale bars = 100 µm. Data are mean +/- SEM of n = 5 animals. Data were compared by two-tailed unpaired t test, but no significant differences were found.

In order to determine the effects of amlexanox on end-organ damage in the kidney, renal mass and fibrosis were assessed (Figure 6-6). No differences in average kidney mass were observed between vehicle-treated and amlexanox-treated SHRSP when normalised to either total body weight or tibia length (Figure 6-6 A and B). Perivascular fibrosis in the kidney was significantly increased in amlexanox-treated SHRSP (Figure 6-6 C). Interstitial fibrosis was very low in both groups, and was not affected by amlexanox treatment (Figure 6-6 D).

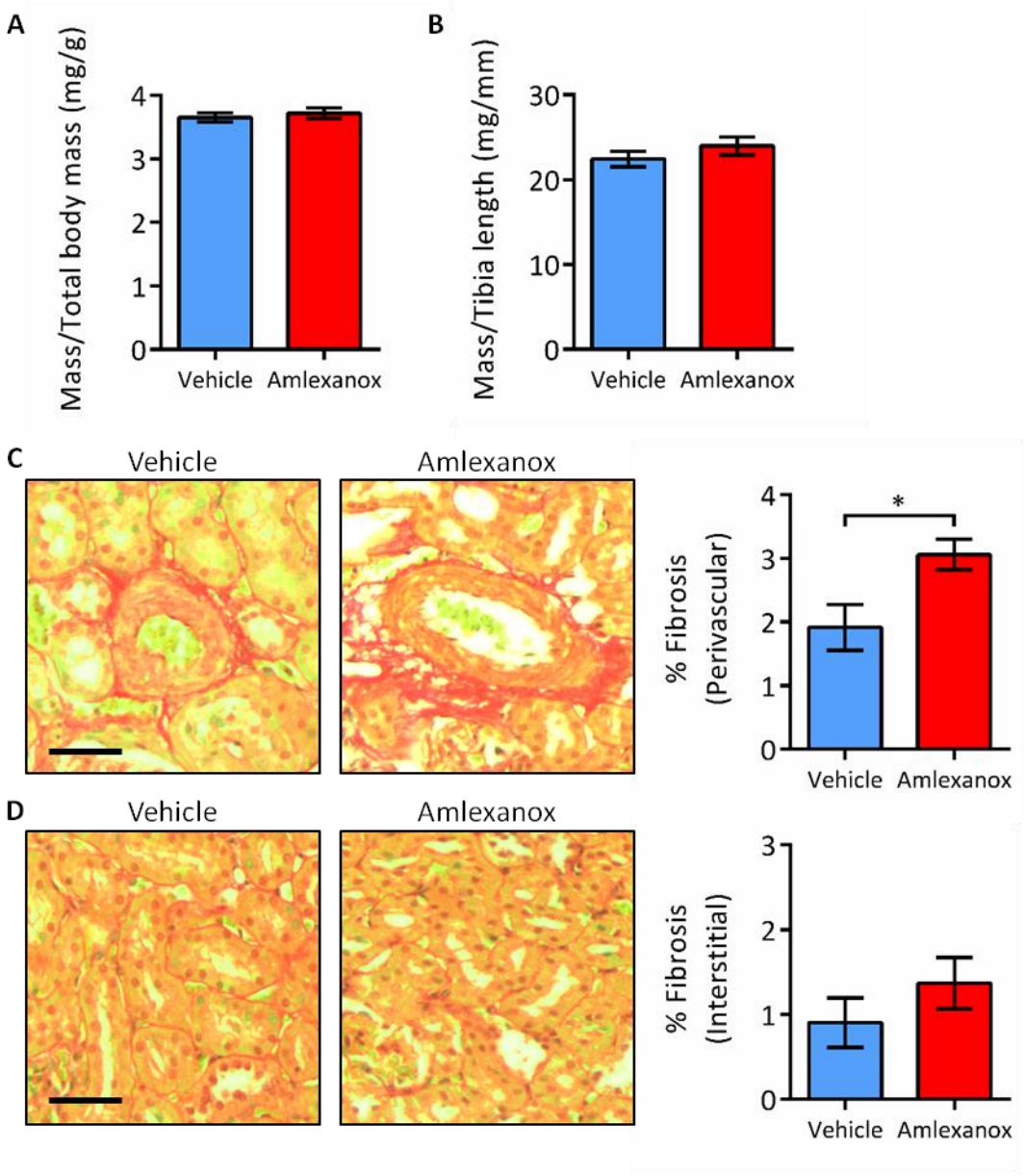

Figure 6-6 Renal perivascular fibrosis is significantly increased by amlexanox treatment in the SHRSP (A, B) Average kidney mass was determined at sacrifice and normalised to **(A)** total body mass or **(B)** tibia length. **(C, D)** Transverse kidney sections were stained with picro-sirius red to visualise collagen (red staining). Images of **(C)** interstitial and **(D)** perivascular regions were taken, and percent fibrosis was quantified as percentage of red pixels. Scale bars = 50 μm. Data are mean +/- SEM of n = 8 animals (mass) or n = 5 animals (fibrosis). *p<0.05 in two-tailed unpaired t test.

6.2.3 Effects of amlexanox treatment on fat metabolism in the SHRSP

Higher doses of amlexanox have previously been shown to reduce both total body mass and body fat mass in mouse models of genetic and diet-induced obesity through the inhibition of the alternative targets IKK-ε and TBK-1 (Reilly et al., 2013). In order to address the possibility that the findings described in this chapter are due to inhibition of non-GPR35 targets, potential effects of

amlexanox treatment on body weight and fat pad mass in the SHRSP were assessed (Figure 6-7). Total body mass was not affected by amlexanox treatment (Figure 6-7 A). No significant differences in either retroperitoneal or epididymal fat pad mass were observed between vehicle-treated and amlexanox-treated SHRSP, whether normalised to total body mass or tibia length (Figure 6-7 B). These data suggest that the low dose of amlexanox used in this study was not sufficient to induce detectable off-target effects on fat metabolism in the SHRSP.

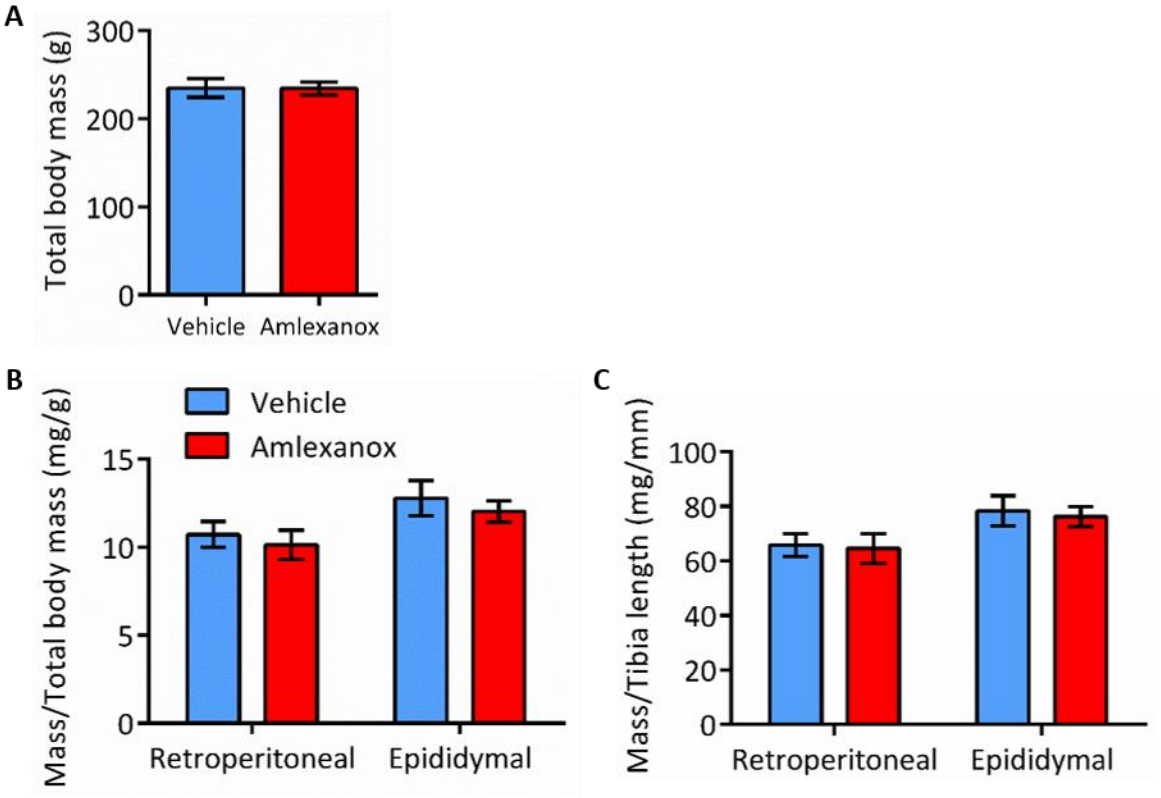

Figure 6-7 Body mass and fat pad mass are not affected by amlexanox treatment in the SHRSP (A) Total body mass and **(B, C)** retroperitoneal and epididymal fat pad mass were determined at sacrifice, and fat pad mass was normalised to either **(B)** total body mass or **(C)** tibia length. Data are mean +/- SEM of n = 8 animals. Data were compared by two-tailed unpaired t test, but no significant differences were found.

6.3 Discussion

6.3.1 Amlexanox induces increased blood pressure and end-organ damage in SHRSP

The findings presented here show that oral administration of the GPR35 agonist amlexanox leads to increased blood pressure and cardiovascular end-organ damage in the SHRSP, a rat model of essential hypertension. After 6 weeks of treatment, systolic blood pressure was approximately 12.5 mm/Hg higher in amlexanox-treated animals than in vehicle-treated animals. In a clinical setting, blood pressure differences of this magnitude have a significant effect on the risk of cardiovascular events, complications and all-cause mortality (Ettehad et al., 2016). In addition, this blood pressure-raising effect was sufficient to induce increases in cardiac mass and perivascular fibrosis in the kidney, both of which are indicators of cardiovascular stress and early markers of pathological remodelling in the SHRSP (Graham et al., 2004, Hultström, 2012). This suggests that pharmacological agonism of GPR35 exacerbates pre-existing CVD, indicating a pathological role for GPR35 in the development of hypertension and associated end-organ damage.

The mean blood pressure of the 10–12 week-old SHRSPs used in this study was considerably lower than that reported for the original SHRSP strain (Yamori and Horie, 1977). This discrepancy can be explained by differences in the techniques used to measure blood pressure as well as colony-specific genetic and phenotypic variation. The SHRSP colony at the University of Glasgow, which has been bred in-house for over 20 years, has previously been reported to have milder hypertension than the original strain, with systolic blood pressures of 140–160 mmHg at 10–12 weeks of age (Flores-Munoz et al., 2012, McLachlan et al., 2014). The blood pressures observed in this study are in line with these previous reports, which suggests that the blood pressure values were recorded accurately.

Although a significant difference in blood pressure was observed after telemetry probe implantation and recovery (10–12 weeks of age), this difference was not evident in younger SHRSP when systolic blood pressure was measured by tail-cuff plethysmography (6–9 weeks of age). It is not clear whether this is due to a lag

between the commencement of amlexanox treatment and the increase in blood pressure, or the lower sensitivity of the tail-cuff method. Nonetheless, this study further supports the view that radiotelemetry is a sensitive method capable of detecting relatively small differences in blood pressure, in spite of the limitation that it can only be used in small animals after they have reached a certain size threshold (Kramer and Kinter, 2003). Once again, the rapid restoration of diurnal rhythms in haemodynamic parameters and locomotive activity suggest that the telemetry probe implantation procedure was well tolerated.

6.3.2 Are the effects of amlexanox on SHRSP mediated by GPR35?

A limitation of this study is that amlexanox is known to act at several targets other than GPR35 (Reilly et al., 2013, Homan et al., 2014). Therefore, it is not possible to ascertain that these effects on the cardiovascular system are specifically mediated by GPR35. However, the study was designed to minimise off-target effects of amlexanox by using a dose that would lead to serum levels that were sufficient to activate GPR35 (EC_{50} = 23 nM (MacKenzie et al., 2014)) but not the alternative targets (IC_{50} = 1–13 μM (Reilly et al., 2013, Homan et al., 2014)). In addition, body mass and fat pad mass were measured at the end of the study in order to monitor potential off-target effects at IKK-ε and TBK1, which have previously been associated with increased fat metabolism in mice. Although higher doses of amlexanox have previously been shown to increase fat metabolism in obese mice (Reilly et al., 2013), no detectable effects of amlexanox on fat metabolism were observed in this study, with similar epididymal and retroperitoneal fat pad masses in vehicle- and amlexanox-treated animals following six weeks of treatment. However, this is a very basic assessment of fat metabolism, and more in-depth investigation would be required to confirm that the effect on blood pressure was not mediated by these kinases. For example, it would be informative to determine whether fat pad mass, weight gain and expression of lipid metabolism-associated genes are altered by this lower dose of amlexanox in rats fed a high-fat diet.

Amlexanox is also an inhibitor of GRK5, which is known to be expressed and play important roles in cardiovascular tissues (Hullmann et al., 2016). However, previous studies show that GRK5 activity is associated with increased blood

pressure and severe cardiac hypertrophy (Keys et al., 2005, Hullmann et al., 2014). In particular, it has been demonstrated to have GPCR-independent effects on hypertrophic gene expression which drive pathological hypertrophy and the progression of heart failure (Traynham et al., 2015). Therefore, off-target inhibition of GRK5 by amlexanox would potentially have had the opposite effects to those observed in this study. Furthermore, the potency of amlexanox at rat GPR35 is approximately 1000-fold greater than at GRK5 (Homan et al., 2014, MacKenzie et al., 2014). These factors make it very unlikely that the increased blood pressure and end-organ damage observed here are due to amlexanox-mediated inhibition of GRK5.

In most *in vivo* agonist studies, it is customary to validate findings by blocking the observed effects of the agonist with a pharmacological antagonist. However, as discussed in previous chapters, the human-selective nature of available GPR35 antagonists makes this approach impossible using existing tools. An alternative approach would be to determine whether these effects also occur in the absence of GPR35 expression using the GPR35 knockout mouse. However, like many GPR35 ligands, amlexanox also displays significant species selectivity, and is approximately 10-fold less potent at the mouse orthologue than at the rat orthologue (Milligan group, unpublished data). Therefore, a higher dose would be required to achieve equivalent efficacy in mice, which would increase the likelihood of off-target effects. Furthermore, the findings discussed in Chapters 4 and 5 suggest that pre-existing CVD is necessary for GPR35-mediated effects to be observed. Therefore, a CVD model such as Ang II infusion would have to be used alongside agonist administration in the knockout mouse, which would introduce additional variables.

In lieu of suitable methods for blocking amlexanox agonism at GPR35, confidence in the GPR35-specific nature of these findings could be improved by replicating the results with different GPR35 agonists. However, most of the available agonists are either not potent enough to be used safely *in vivo* or have known alternative targets that are likely to influence cardiovascular function – for example, one of the first-discovered and most frequently used GPR35 agonists, zaprinast, is a PDE5 inhibitor with low micromolar potency, which has cGMP-mediated effects on vascular and myocardial contraction (Mohan et al.,

1996, Medina et al., 2000, Ziolo et al., 2003). Since this study commenced, the novel GPR35 agonists lodoxamide and bufrolin – also mast cell stabilisers – have been reported to have comparable potency to amlexanox at rat GPR35, and have also been shown to be equipotent at the rat and human orthologues (MacKenzie et al., 2014). These agonists could be used in the SHRSP to determine whether other GPR35 agonists have similar effects to amlexanox on blood pressure and end-organ damage. However, little is known about the oral bioavailability and pharmacokinetic properties of these agonists, and it will be necessary to characterise these properties if lodoxamide and bufrolin are to be used in future *in vivo* studies.

6.3.3 Possible mechanisms of GPR35-mediated effects of amlexanox in the SHRSP

Although the present study did not investigate the precise mechanism by which GPR35 might exert its effects on cardiovascular function, the observed pathological effects of amlexanox (and presumably GPR35) in the SHRSP are consistent with the current understanding of GPR35 signalling. Previous reports, as well as the findings presented in Chapter 3, suggest that GPR35 alters cell size, shape and differentiation state *via* its activation of $G\alpha_{13}$ and the RhoA/ROCK pathway (Jenkins et al., 2011, Ronkainen et al., 2014, McCallum et al., 2015). Although increases in vascular tone and basal regulation of blood pressure are primarily mediated by $G\alpha_{q/11}$-coupled receptors such as the AT_1R and endothelin-1 receptors, these GPCRs often also couple to $G\alpha_{12/13}$. Whilst $G\alpha_{12/13}$ are not required for basal regulation of blood pressure, they have been shown to play a major role in the development of cardiovascular dysfunction. For example, the pathophysiological effects of TAC-induced heart failure and Ang II-induced hypertension have been shown to be $G\alpha_{13}$-dependent and mediated by RhoA (Takefuji et al., 2012). Similarly, Wirth et al. demonstrated that salt-induced hypertension is dependent on both $G\alpha_{12/13}$ and their effector, the Rho-GEF LARG (Wirth et al., 2008). Therefore, GPR35-mediated activation of $G\alpha_{13}$ and the RhoA/ROCK pathway in cardiovascular tissues is a reasonable explanation for the effects of amlexanox in SHRSP reported here.

Although this proposed signalling mechanism can account for the effects of GPR35 agonism on blood pressure and end-organ damage, it is not clear whether

the effects observed in this study are due to GPR35 activity in the heart, vasculature or other tissues. Once again, these results suggest both a direct effect of GPR35 on blood pressure, and end-organ damage in cardiovascular tissues, which may be secondary to the increase in blood pressure or due to independent GPR35 activity in these tissues. As discussed in section 5.3.2, the current understanding of GPR35 function in the cardiovascular system suggests it may make independent contributions to the regulation of both vascular function and cardiac hypertrophy, either through modulation of signalling in vascular cells and cardiomyocytes or through indirect effects on vascular inflammation *via* its expression on immune cells (Wang et al., 2006, Yang et al., 2010, Fallarini et al., 2010). More detailed investigation of the effects of GPR35 in different cell types will be necessary in order to determine the specific functions of GPR35 in different tissues.

6.3.4 The therapeutic potential of GPR35 in CVD

The finding that pharmacological agonism of GPR35 exacerbates pre-existing CVD suggests that, conversely, antagonism of GPR35 could be a novel therapeutic strategy to combat CVD. The next logical step in these studies will be to test whether antagonism or inactivation of GPR35 can prevent or reverse the development of hypertension and its associated end-organ damage. The SHRSP is an ideal model in which to investigate this, due to the early age at which hypertension begins to develop, and the model's similarities with human hypertension (discussed in section 6.1). However, once again, a lack of suitable pharmacological tools means this is currently not possible. A variety of alternative approaches, as discussed in section 5.3.3, will hopefully circumvent this issue and enable the value of GPR35 as a therapeutic target in CVD to be assessed.

Chapter 7 Final discussion

The aims of this work were to investigate GPR35 signalling *in vitro*, examine the role of GPR35 in the cardiovascular system, and determine the contribution of GPR35 to cardiovascular pathophysiology in a relevant model, in order to evaluate the potential of GPR35 as a therapeutic target in CVD. Each of these aims was addressed by the studies described in the preceding chapters. This chapter summarises the main conclusions of this thesis and their implications.

Although GPR35 has been the subject of *in vitro* studies for several years, previous work has primarily focused on identifying ligands and coupling partners, and relatively little is known about its influence on downstream signalling and cellular responses. The studies described in Chapter 3 add to the existing knowledge of GPR35 signalling, identifying previously unknown aspects of the molecular and cellular responses to GPR35 activation and providing a rationale for how this receptor influences the cardiovascular system. The findings demonstrate the role of agonist-dependent phosphorylation in the regulation of different cellular outcomes of GPR35 activation. Mutagenesis studies established how different phosphorylation sites in the GPR35 C-terminal tail contribute to ß-arrestin recruitment, and provide additional evidence for the 'phosphorylation barcode' hypothesis (Tobin et al., 2008, Liggett, 2011). This offers a potential explanation for how GPR35 appears to have several different coupling profiles and physiological functions, depending on which tissue or cell type is being studied.

Although GPR35 has previously been shown to couple to $G\alpha_{13}$ (Jenkins et al., 2011), the experiments described in Chapter 3 are the first to directly demonstrate that this coupling leads to reorganisation of the actin cytoskeleton in HEK293 cells. Reorganisation of the actin cytoskeleton in cardiomyocytes has previously been linked to GPR35 overexpression and function (Min et al., 2010, Ronkainen et al., 2014). Therefore, GPR35/$G\alpha_{13}$-mediated activation of the RhoA/ROCK pathway, either in cardiomyocytes or in vascular cells, is likely to be responsible for GPR35-mediated effects on the cardiovascular system. This is further supported by the findings presented in Chapter 5, which suggest that knocking out GPR35 has protective effects similar to those of cardiomyocyte-

and vascular smooth muscle-specific knockout of $G\alpha_{12/13}$ (Wirth et al., 2008, Takefuji et al., 2012).

The main limitation of the existing studies investigating GPR35 signalling (both in this thesis and in the wider literature) is that they have mostly been conducted in artificial cell culture models such as HEK293 cells. Although the simplicity and ubiquity of these models provide a convenient means by which to study basic aspects of GPCR signalling, they are not representative of normal physiological function. Therefore, it should now be a priority to translate some of these studies into more physiologically relevant contexts, such as primary cell models, to determine whether findings are applicable *in vivo*. This is particularly important for GPR35, as it has been shown to have very different functions in different tissues; for example, it is thought to couple to $G\alpha_{i/o}$ in DRG neurons, but $G\alpha_{13}$ in vascular smooth muscle cells (Ohshiro et al., 2008, McCallum et al., 2015). Therefore, observations made in HEK293 cells may not necessarily be generalisable to the different cell types in which GPR35 is expressed. Developing a better understanding of how GPR35 signals in primary cells of the cardiovascular system (and in other physiological systems) will be critical in assessing its role in CVD and its potential as a therapeutic target.

In addition to a large number of *in vitro* studies on GPR35 signalling, a number of studies have investigated the functions of GPR35 *in vivo*, primarily focusing on its proposed role in the peripheral nervous system and pain transduction (Cosi et al., 2011, Resta et al., 2016). However, these studies were based on administration of the GPR35 agonists kynurenic acid and zaprinast, which are known to have alternative targets (ionotropic glutamate receptors and PDE5, respectively (Medina et al., 2000, Schwarcz et al., 2012)), and do not directly demonstrate GPR35 involvement. The *in vivo* studies described in Chapters 4, 5 and 6 investigate the role of GPR35 in a different physiological system: the cardiovascular system. Although existing reports have suggested roles for GPR35 in both hypertension and heart failure (Min et al., 2010, Ronkainen et al., 2014), the actual consequences of GPR35 activity (or lack thereof) had not previously been investigated in detail. The studies described here demonstrate a role for GPR35 in CVD using multiple approaches: the GPR35 knockout mouse, two different models of CVD and a GPR35 agonist study. Taken together, these

findings show that although GPR35 does not appear to be important in basal cardiovascular regulation, it plays an important role in the development of CVD. The data demonstrate that a lack of GPR35 expression in the GPR35 knockout mouse prevents the development of Ang II-induced hypertension and associated cardiac dysfunction (Chapter 5), whereas increased GPR35 activity through pharmacological agonism in the SHRSP exacerbates pre-existing hypertension and associated end-organ damage (Chapter 6). These findings indicate that GPR35 activity is involved in the pathophysiological processes contributing to the development of CVD.

Despite investigating the effects of GPR35 deficiency on various aspects of the cardiovascular system, the GPR35 knockout mouse studies were not successful in determining a mechanism for the apparent pathological influence of GPR35. For example, knocking out GPR35 does not appear to impact directly on vascular reactivity either under basal conditions or in the early stages of hypertension development. However, based on existing evidence and the *in vitro* studies described in Chapter 3, it seems likely that a GPR35/$G\alpha_{13}$/RhoA/ROCK signalling pathway is involved. However, a number of alternative mechanisms, such as crosstalk with the other GPCRs or effects on vascular inflammation through actions in immune cells, could potentially explain the pathological function of GPR35 in CVD. Future work should aim to determine which of these mechanisms is responsible for the role of GPR35 in the development of CVD, or whether multiple mechanisms are involved.

A major limitation of these *in vivo* studies is the lack of validation using a GPR35 antagonist. Before GPR35 can be pursued as a therapeutic target, it will be necessary to confirm that the effects seen here are specifically due to the actions of GPR35. As discussed in Chapters 5 and 6, novel technologies such as humanised mice and blocking antibodies will soon provide a means to antagonise GPR35 *in vivo*. Future research should therefore focus on establishing the therapeutic benefit of GPR35 antagonism in models of CVD.

The overall aim of this work – to assess the therapeutic potential of GPR35 in CVD – is driven by the shortcomings of current therapies for hypertension and heart failure. As discussed in Chapter 1, these diseases remain a major health burden despite decades of research and many existing therapies (Campbell et

al., 2016, Hunt et al., 2009). Most of the existing therapies are based on modulation of either the renin-angiotensin system or the adrenergic system, and are usually used in combinations of between two and five different drugs from different classes (Williams et al., 2004, Hunt et al., 2009). However, a significant problem is that many patients are intolerant or unresponsive to these combinations; 20–30% of patients with hypertension are estimated to be resistant to treatment (Calhoun et al., 2008, Eirin et al., 2016). Therefore, the identification of novel therapeutic targets in distinct receptor systems has the potential to add to and/or improve upon the existing repertoire of treatments. The findings reported here suggest that GPR35 is indeed a potential novel therapeutic target in CVD, and that GPR35 antagonists might be used to combat hypertension and/or associated diseases caused by pathological cardiac remodelling.

In addition to the pro-hypertensive actions of GPR35 shown in this work, previous reports have demonstrated that GPR35 is upregulated in the heart both in heart failure patients and in an animal model of heart failure (Min et al., 2010, Ronkainen et al., 2014), suggesting that GPR35 and its endogenous agonist play a direct role in pathological cardiac remodelling. Therefore, similarly to the use of AT_1R biased agonists, targeting GPR35 may have a dual benefit in the treatment of heart failure – both countering systemic hypertension and acting directly on the heart to prevent remodelling. Investigating the progression of pathological cardiac remodelling in the absence of GPR35 activity (either in the GPR35 knockout mouse or with antagonists, when they become available) could reveal enhanced therapeutic potential for GPR35.

In this work, GPR35 knockout mice were found to have a similar phenotype to $G\alpha_{13}$ cardiomyocyte-specific knockout mice in terms of resistance to Ang II-induced cardiac remodelling (Takefuji et al., 2012). Assuming that the pathological effects of GPR35 are indeed mediated by the $G\alpha_{13}$/RhoA/ROCK pathway, targeting these downstream mediators may be an alternative approach to modulating GPR35 function. ROCK has previously been proposed as a therapeutic target in CVD, and the approved ROCK inhibitor fasudil prevents hypertension-induced cardiac and vascular remodelling, as well as many other cardiovascular pathologies, in animal models (Higashi et al., 2003,

Phrommintikul et al., 2008, Surma et al., 2011). However, ROCK is very widely expressed, and while this may contribute to its many apparent therapeutic benefits, GPR35 is a much more specific and therefore preferable target. Further investigation of the links between GPR35 function and RhoA/ROCK activation in the cardiovascular system may reveal additional therapeutic opportunities.

Although the findings reported here focus on GPR35 as a therapeutic target in CVD, it is important to consider the other proposed physiological functions of this receptor, of which there are many (discussed in section 1.4.6). GPR35 has been implicated in a range of processes, from pain transduction to gastrointestinal inflammation (Divorty et al., 2015, Mackenzie and Milligan, 2015), and these other potential functions mean that administering a GPR35 antagonist in a therapeutic setting would potentially have on-target effects that are unintended or undesirable. However, since the roles of GPR35 in other tissues are far from being well defined, it is impossible to predict such effects. Therefore, any future antagonist studies with a view to using GPR35 as a therapeutic target should include detailed investigation not just of cardiovascular function, but of other processes potentially affected by modulation of GPR35 activity. Furthermore, the role of the endogenous agonist must be considered – the levels of the endogenous agonist in the circulation and in relevant tissues in the disease state, and its affinity for GPR35, will determine whether an antagonist is therapeutically effective. Though these studies have not shed further light on the potential endogenous agonist(s) of GPR35, it is hoped that further advances in elucidating the function of this orphan receptor might provide insight on this matter.

An additional lesson to be learned from the findings of these studies is that the function of an orphan receptor may not be immediately obvious, but it may be revealed under the appropriate conditions. The findings of Chapter 4 suggested that the GPR35 knockout mouse has normal cardiovascular function, but a pathophysiological role was revealed after inducing hypertension. This approach may be useful in investigating the other proposed functions of GPR35; for example, if attempting to confirm a suggested role in inflammatory bowel disease, it may be worthwhile to assess the phenotype of the GPR35 knockout

mouse under basal conditions and in a chemically-induced disease model such as dextran sodium sulphate-induced colitis (Wirtz et al., 2007). This applies not just to GPR35, but to the other >120 non-olfactory orphan GPCRs with unknown physiological functions (Davenport et al., 2013, Alexander et al., 2015). Expression patterns might provide a useful starting point; however, a lack of expression also does not definitively prove a lack of function. The role of GPR35 in CVD was not immediately obvious from its expression pattern, as the receptor appears to be poorly expressed in cardiovascular tissues until the onset of disease. Alternatively, as with GPR35, clues to the function of orphan receptors might be found in genetic disease associations. It is important to continue searching for orphan receptor functions, using both conventional and novel approaches, in order to fully exploit the therapeutic value of the GPCR superfamily.

Although years of research have failed to find a definitive function for GPR35, recent work has led to significant advances in our understanding of its pharmacology, signalling and physiology. Several studies using *in vivo* models have highlighted its physiological importance and therapeutic potential in a range of diseases. It will be interesting to discover whether its diverse roles – in inflammation, nociception and cardiovascular dysfunction – turn out to have a common mechanism. Alongside physiological studies, multiple screening efforts and thorough pharmacological characterisation have resulted in the development of a large and varied repertoire of tool compounds. These, in combination with novel experimental approaches, will facilitate future studies of GPR35 function; however, there is a need to move the focus away from artificial models towards physiologically and clinically relevant contexts. This will enable assessment of the true translational value of GPR35 as a therapeutic target, and hopefully lead to novel treatment strategies for chronic diseases.

References

AHMAD, R., WOJCIECH, S. & JOCKERS, R. 2015. Hunting for the function of orphan GPCRs - beyond the search for the endogenous ligand. *British Journal of Pharmacology,* 172**,** 3212-28.

ALEXANDER, S. P., DAVENPORT, A. P., KELLY, E., MARRION, N., PETERS, J. A., BENSON, H. E., FACCENDA, E., PAWSON, A. J., SHARMAN, J. L., SOUTHAN, C., DAVIES, J. A. & COLLABORATORS, C. 2015. The Concise Guide to PHARMACOLOGY 2015/16: G protein-coupled receptors. *British Journal of Pharmacology,* 172**,** 5744-869.

ALVAREZ-CURTO, E., INOUE, A., JENKINS, L., RAIHAN, S. Z., PRIHANDOKO, R., TOBIN, A. B. & MILLIGAN, G. 2016. Targeted Elimination of G proteins and Arrestins Defines their Specific Contributions to both Intensity and Duration of G protein-Coupled Receptor Signalling. *Journal of Biological Chemistry*.

ANDRADAS, C., BLASCO-BENITO, S., CASTILLO-LLUVA, S., DILLENBURG-PILLA, P., DIEZ-ALARCIA, R., JUANES-GARCÍA, A., GARCÍA-TABOADA, E., HERNANDO-LLORENTE, R., SORIANO, J., HAMANN, S., WENNERS, A., ALKATOUT, I., KLAPPER, W., ROCKEN, C., BAUER, M., ARNOLD, N., QUINTANILLA, M., MEGÍAS, D., VICENTE-MANZANARES, M., URIGÜEN, L., GUTKIND, J. S., GUZMÁN, M., PÉREZ-GÓMEZ, E. & SÁNCHEZ, C. 2016. Activation of the orphan receptor GPR55 by lysophosphatidylinositol promotes metastasis in triple-negative breast cancer. *Oncotarget*, 7, 47565-75.

ANGUS, J. A. & WRIGHT, C. E. 2000. Techniques to study the pharmacodynamics of isolated large and small blood vessels. *Journal of Pharmacological and Toxicological Methods,* 44**,** 395-407.

BALLESTEROS, J. A. & WEINSTEIN, H. 1995. Integrated methods for the construction of three-dimensional models and computational probing of structure-function relations in G protein-coupled receptors. *Methods in Neurosciences,* 25 366-428.

BARBARIC, I., MILLER, G. & DEAR, T. N. 2007. Appearances can be deceiving: phenotypes of knockout mice. *Briefings in Functional Genomics and Proteomics,* 6**,** 91-103.

BARKI-HARRINGTON, L., LUTTRELL, L. M. & ROCKMAN, H. A. 2003. Dual inhibition of beta-adrenergic and angiotensin II receptors by a single antagonist: a functional role for receptor-receptor interaction in vivo. *Circulation,* 108**,** 1611-8.

BARNES, W. G., REITER, E., VIOLIN, J. D., REN, X. R., MILLIGAN, G. & LEFKOWITZ, R. J. 2005. ß-Arrestin 1 and Gαq/11 coordinately activate RhoA and stress fiber formation following receptor stimulation. *Journal of Biological Chemistry,* 280**,** 8041-50.

BARTH, M. C., AHLUWALIA, N., ANDERSON, T. J., HARDY, G. J., SINHA, S., ALVAREZ-CARDONA, J. A., PRUITT, I. E., RHEE, E. P., COLVIN, R. A. & GERSZTEN, R. E.

2009. Kynurenic acid triggers firm arrest of leukocytes to vascular endothelium under flow conditions. *Journal of Biological Chemistry,* 284**,** 19189-95.

BASSETT, J. H., GOGAKOS, A., WHITE, J. K., EVANS, H., JACQUES, R. M., VAN DER SPEK, A. H., RAMIREZ-SOLIS, R., RYDER, E., SUNTER, D., BOYDE, A., CAMPBELL, M. J., CROUCHER, P. I., WILLIAMS, G. R. & PROJECT, S. M. G. 2012. Rapid-throughput skeletal phenotyping of 100 knockout mice identifies 9 new genes that determine bone strength. *PLoS Genetics,* 8**,** e1002858.

BELL, J. 2005. Amlexanox for the treatment of recurrent aphthous ulcers. *Clinical Drug Investigation,* 25**,** 555-66.

BENNETT, T. A., MAESTAS, D. C. & PROSSNITZ, E. R. 2000. Arrestin binding to the G protein-coupled N-formyl peptide receptor is regulated by the conserved "DRY" sequence. *Journal of Biological Chemistry,* 275**,** 24590-24594.

BENOVIC, J. L., KÜHN, H., WEYAND, I., CODINA, J., CARON, M. G. & LEFKOWITZ, R. J. 1987. Functional desensitization of the isolated beta-adrenergic receptor by the beta-adrenergic receptor kinase: potential role of an analog of the retinal protein arrestin (48-kDa protein). *Proceedings of the National Academy of Sciences of the United States of America,* 84**,** 8879-82.

BERGQUIST, A., MONTGOMERY, S. M., BAHMANYAR, S., OLSSON, R., DANIELSSON, A., LINDGREN, S., PRYTZ, H., HULTCRANTZ, R., LÖÖF, L. A., SANDBERG-GERTZÉN, H., ALMER, S., ASKLING, J., EHLIN, A. & EKBOM, A. 2008. Increased risk of primary sclerosing cholangitis and ulcerative colitis in first-degree relatives of patients with primary sclerosing cholangitis. *Clinical Gastroenterology and Hepatology,* 6**,** 939-43.

BERLINGUER-PALMINI, R., MASI, A., NARDUCCI, R., CAVONE, L., MARATEA, D., COZZI, A., SILI, M., MORONI, F. & MANNAIONI, G. 2013. GPR35 activation reduces Ca2+ transients and contributes to the kynurenic acid-dependent reduction of synaptic activity at CA3-CA1 synapses. *PLoS One,* 8**,** e82180.

BERS, D. M. 2008. Calcium cycling and signaling in cardiac myocytes. *Annual Review in Physiology,* 70**,** 23-49.

BISPING, E., WAKULA, P., POTESER, M. & HEINZEL, F. R. 2014. Targeting cardiac hypertrophy: toward a causal heart failure therapy. *Journal of Cardiovascular Pharmacology,* 64**,** 293-305.

BOND, R. A. & IJZERMAN, A. P. 2006. Recent developments in constitutive receptor activity and inverse agonism, and their potential for GPCR drug discovery. *Trends in Pharmacological Sciences,* 27**,** 92-6.

BOUZO-LORENZO, M., SANTO-ZAS, I., LODEIRO, M., NOGUEIRAS, R., CASANUEVA, F. F., CASTRO, M., PAZOS, Y., TOBIN, A. B., BUTCHER, A. J. & CAMIÑA, J. P. 2016. Distinct phosphorylation sites on the ghrelin receptor, GHSR1a, establish a code that determines the functions of ß-arrestins. *Scientific Reports,* 6**,** 22495.

BRADLEY, S. J., WIEGMAN, C. H., IGLESIAS, M. M., KONG, K. C., BUTCHER, A. J., PLOUFFE, B., GOUPIL, E., BOURGOGNON, J. M., MACEDO-HATCH, T., LEGOUILL, C., RUSSELL, K., LAPORTE, S. A., KÖNIG, G. M., KOSTENIS, E., BOUVIER, M., CHUNG, K. F., AMRANI, Y. & TOBIN, A. B. 2016. Mapping physiological G protein-coupled receptor signaling pathways reveals a role for receptor phosphorylation in airway contraction. *Proceedings of the National Academy of Sciences of the United States of America,* 113**,** 4524-9.

BRISCOE, C. P., TADAYYON, M., ANDREWS, J. L., BENSON, W. G., CHAMBERS, J. K., EILERT, M. M., ELLIS, C., ELSHOURBAGY, N. A., GOETZ, A. S., MINNICK, D. T., MURDOCK, P. R., SAULS, H. R., SHABON, U., SPINAGE, L. D., STRUM, J. C., SZEKERES, P. G., TAN, K. B., WAY, J. M., IGNAR, D. M., WILSON, S. & MUIR, A. I. 2003. The orphan G protein-coupled receptor GPR40 is activated by medium and long chain fatty acids. *Journal of Biological Chemistry,* 278**,** 11303-11.

BRÄUNER-OSBORNE, H., WELLENDORPH, P. & JENSEN, A. A. 2007. Structure, pharmacology and therapeutic prospects of family C G-protein coupled receptors. *Current Drug Targets,* 8**,** 169-84.

BUHL, A. M., JOHNSON, N. L., DHANASEKARAN, N. & JOHNSON, G. L. 1995. Gα12 and Gα13 stimulate Rho-dependent stress fiber formation and focal adhesion assembly. *Journal of Biological Chemistry,* 270**,** 24631-4.

BUNZOW, J. R., VAN TOL, H. H., GRANDY, D. K., ALBERT, P., SALON, J., CHRISTIE, M., MACHIDA, C. A., NEVE, K. A. & CIVELLI, O. 1988. Cloning and expression of a rat D2 dopamine receptor cDNA. *Nature,* 336**,** 783-7.

BURCHFIELD, J. S., XIE, M. & HILL, J. A. 2013. Pathological ventricular remodeling: mechanisms: part 1 of 2. *Circulation,* 128**,** 388-400.

BUSILLO, J. M., ARMANDO, S., SENGUPTA, R., MEUCCI, O., BOUVIER, M. & BENOVIC, J. L. 2010. Site-specific phosphorylation of CXCR4 is dynamically regulated by multiple kinases and results in differential modulation of CXCR4 signaling. *Journal of Biological Chemistry,* 285**,** 7805-17.

BUTCHER, A. J., HUDSON, B. D., SHIMPUKADE, B., ALVAREZ-CURTO, E., PRIHANDOKO, R., ULVEN, T., MILLIGAN, G. & TOBIN, A. B. 2014. Concomitant action of structural elements and receptor phosphorylation determines arrestin-3 interaction with the free fatty acid receptor FFA4. *Journal of Biological Chemistry,* 289**,** 18451-65.

BUTCHER, A. J., PRIHANDOKO, R., KONG, K. C., MCWILLIAMS, P., EDWARDS, J. M., BOTTRILL, A., MISTRY, S. & TOBIN, A. B. 2011a. Differential G-protein-coupled receptor phosphorylation provides evidence for a signaling bar code. *Journal of Biological Chemistry,* 286**,** 11506-18.

BUTCHER, A. J., TOBIN, A. B. & KONG, K. C. 2011b. Examining site-specific GPCR phosphorylation. *Methods in Molecular Biology,* 746**,** 237-49.

CALEBIRO, D., NIKOLAEV, V. O., GAGLIANI, M. C., DE FILIPPIS, T., DEES, C., TACCHETTI, C., PERSANI, L. & LOHSE, M. J. 2009. Persistent cAMP-signals triggered by internalized G-protein-coupled receptors. *PLoS Biology,* 7**,** e1000172.

CALHOUN, D. A., JONES, D., TEXTOR, S., GOFF, D. C., MURPHY, T. P., TOTO, R. D., WHITE, A., CUSHMAN, W. C., WHITE, W., SICA, D., FERDINAND, K., GILES, T. D., FALKNER, B., CAREY, R. M. & COMMITTEE, A. H. A. P. E. 2008. Resistant hypertension: diagnosis, evaluation, and treatment: a scientific statement from the American Heart Association Professional Education Committee of the Council for High Blood Pressure Research. *Circulation,* 117**,** e510-26.

CAMPBELL, N. R., KHALSA, T., LACKLAND, D. T., NIEBYLSKI, M. L., NILSSON, P. M., REDBURN, K. A., ORIAS, M., ZHANG, X. H., BURRELL, L., HORIUCHI, M., POULTER, N. R., PRABHAKARAN, D., RAMIREZ, A. J., SCHIFFRIN, E. L., TOUYZ, R. M., WANG, J. G., WEBER, M. A., EXECUTIVE:, W. H. L., EXECUTIVE:, I. S. O. H., ORGANIZATION, W. S., FEDERATION, I. D., REHABILITATION, I. C. O. C. P. A. & NEPHROLOGY, I. S. O. 2016. High Blood Pressure 2016: Why Prevention and Control Are Urgent and Important. The World Hypertension League, International Society of Hypertension, World Stroke Organization, International Diabetes Foundation, International Council of Cardiovascular Prevention and Rehabilitation, International Society of Nephrology. *Journal of Clinical Hypertension (Greenwich),* 18**,** 714-7.

CAO, R. Y., AMAND, T., FORD, M. D., PIOMELLI, U. & FUNK, C. D. 2010. The Murine Angiotensin II-Induced Abdominal Aortic Aneurysm Model: Rupture Risk and Inflammatory Progression Patterns. *Frontiers in Pharmacology,* 1**,** 9.

CAPOTE, L. A., MENDEZ PEREZ, R. & LYMPEROPOULOS, A. 2015. GPCR signaling and cardiac function. *European Journal of Pharmacology,* 763**,** 143-8.

CHOBANIAN, A. V., BAKRIS, G. L., BLACK, H. R., CUSHMAN, W. C., GREEN, L. A., IZZO, J. L., JONES, D. W., MATERSON, B. J., OPARIL, S., WRIGHT, J. T., ROCCELLA, E. J., JOINT NATIONAL COMMITTEE ON PREVENTION, D., EVALUATION, AND TREATMENT OF HIGH BLOOD PRESSURE. NATIONAL HEART, L.NG, AND BLOOD INSTITUTE & COMMITTEE, N. H. B. P. E. P. C. 2003. Seventh report of the Joint National Committee on Prevention, Detection, Evaluation, and Treatment of High Blood Pressure. *Hypertension,* 42**,** 1206-52.

CHOI, J. W., HERR, D. R., NOGUCHI, K., YUNG, Y. C., LEE, C. W., MUTOH, T., LIN, M. E., TEO, S. T., PARK, K. E., MOSLEY, A. N. & CHUN, J. 2010. LPA receptors: subtypes and biological actions. *Annual Reviews in Pharmacology and Toxicology,* 50**,** 157-86.

CHRISTENSEN, K. L. & MULVANY, M. J. 2001. Location of resistance arteries. *Journal of Vascular Research,* 38**,** 1-12.

CHRISTIANSEN, R. E., ROALD, A. B., TENSTAD, O. & IVERSEN, B. M. 2002. Renal hemodynamics during development of hypertension in young spontaneously hypertensive rats. *Kidney and Blood Pressure Research,* 25**,** 322-8.

CHUNG, K. Y., RASMUSSEN, S. G., LIU, T., LI, S., DEVREE, B. T., CHAE, P. S., CALINSKI, D., KOBILKA, B. K., WOODS, V. L. & SUNAHARA, R. K. 2011. Conformational changes in the G protein Gs induced by the ß2 adrenergic receptor. *Nature,* 477**,** 611-5.

CLAPHAM, D. E. & NEER, E. J. 1997. G protein beta gamma subunits. *Annual Review of Pharmacology and Toxicology,* 37**,** 167-203.

COHN, J. N., FERRARI, R. & SHARPE, N. 2000. Cardiac remodeling--concepts and clinical implications: a consensus paper from an international forum on cardiac remodeling. Behalf of an International Forum on Cardiac Remodeling. *Journal of the American College of Cardiology,* 35**,** 569-82.

CONSTANTINIDES, C., MEAN, R. & JANSSEN, B. J. 2011. Effects of isoflurane anesthesia on the cardiovascular function of the C57BL/6 mouse. *ILAR Journal,* 52**,** e21-31.

COSI, C., MANNAIONI, G., COZZI, A., CARLÀ, V., SILI, M., CAVONE, L., MARATEA, D. & MORONI, F. 2011. G-protein coupled receptor 35 (GPR35) activation and inflammatory pain: Studies on the antinociceptive effects of kynurenic acid and zaprinast. *Neuropharmacology,* 60**,** 1227-31.

CROWLEY, S. D., GURLEY, S. B., HERRERA, M. J., RUIZ, P., GRIFFITHS, R., KUMAR, A. P., KIM, H. S., SMITHIES, O., LE, T. H. & COFFMAN, T. M. 2006. Angiotensin II causes hypertension and cardiac hypertrophy through its receptors in the kidney. *Proceedings of the National Academy of Sciences of the United States of America,* 103**,** 17985-90.

DAIBER, A., STEVEN, S., WEBER, A., SHUVAEV, V. V., MUZYKANTOV, V. R., LAHER, I., LI, H., LAMAS, S. & MÜNZEL, T. 2016. Targeting vascular (endothelial) dysfunction. *British Journal of Pharmacology,* [Epub ahead of print], doi:10.1111/bph.13517.

DAVENPORT, A. P., ALEXANDER, S. P., SHARMAN, J. L., PAWSON, A. J., BENSON, H. E., MONAGHAN, A. E., LIEW, W. C., MPAMHANGA, C. P., BONNER, T. I., NEUBIG, R. R., PIN, J. P., SPEDDING, M. & HARMAR, A. J. 2013. International Union of Basic and Clinical Pharmacology. LXXXVIII. G protein-coupled receptor list: recommendations for new pairings with cognate ligands. *Pharmacological Reviews,* 65**,** 967-86.

DAVIS, J. O. & FREEMAN, R. H. 1976. Mechanisms regulating renin release. *Physiological Reviews,* 56**,** 1-56.

DEGRAFF, J. L., GUREVICH, V. V. & BENOVIC, J. L. 2002. The third intracellular loop of alpha(2)-adrenergic receptors determines subtype specificity of arrestin interaction. *Journal of Biological Chemistry,* 277**,** 43247-43252.

DENG, H., HU, H. & FANG, Y. 2011. Tyrphostin analogs are GPR35 agonists. *FEBS Letters,* 585**,** 1957-62.

DENG, H., HU, H. & FANG, Y. 2012. Multiple tyrosine metabolites are GPR35 agonists. *Scientific Reports,* 2**,** 373.

DEWIRE, S. M., AHN, S., LEFKOWITZ, R. J. & SHENOY, S. K. 2007. ß-Arrestins and Cell Signaling. *Annual Review of Physiology,* 69**,** 483-510.

DEWIRE, S. M., YAMASHITA, D. S., ROMINGER, D. H., LIU, G., COWAN, C. L., GRACZYK, T. M., CHEN, X. T., PITIS, P. M., GOTCHEV, D., YUAN, C., KOBLISH, M., LARK, M. W. & VIOLIN, J. D. 2013. A G protein-biased ligand at the μ-opioid receptor is potently analgesic with reduced gastrointestinal and respiratory dysfunction compared with morphine. *Journal of Pharmacology and Experimental Therapeutics,* 344**,** 708-17.

DIVORTY, N., MACKENZIE, A. E., NICKLIN, S. A. & MILLIGAN, G. 2015. G protein-coupled receptor 35: an emerging target in inflammatory and cardiovascular disease. *Frontiers in Pharmacology,* 6**,** 41.

DOMINICZAK, A. F., MCLAREN, Y., KUSEL, J. R., BALL, D. L., GOODFRIEND, T. L., BOHR, D. F. & REID, J. L. 1993. Lateral diffusion and fatty acid composition in vascular smooth muscle membrane from stroke-prone spontaneously hypertensive rats. *American Journal of Hypertension,* 6**,** 1003-8.

EBERINI, I., DANIELE, S., PARRAVICINI, C., SENSI, C., TRINCAVELLI, M. L., MARTINI, C. & ABBRACCHIO, M. P. 2011. In silico identification of new ligands for GPR17: a promising therapeutic target for neurodegenerative diseases. *Journal of Computer Aided Molecular Design,* 25**,** 743-52.

EIRIN, A., TEXTOR, S. C. & LERMAN, L. O. 2016. Emerging concepts for patients with treatment-resistant hypertension. *Trends in Cardiovascular Medicine*.

ELLINGHAUS, D., FOLSERAAS, T., HOLM, K., ELLINGHAUS, E., MELUM, E., BALSCHUN, T., LAERDAHL, J. K., SHIRYAEV, A., GOTTHARDT, D. N., WEISMÜLLER, T. J., SCHRAMM, C., WITTIG, M., BERGQUIST, A., BJÖRNSSON, E., MARSCHALL, H. U., VATN, M., TEUFEL, A., RUST, C., GIEGER, C., WICHMANN, H. E., RUNZ, H., STERNECK, M., RUPP, C., BRAUN, F., WEERSMA, R. K., WIJMENGA, C., PONSIOEN, C. Y., MATHEW, C. G., RUTGEERTS, P., VERMEIRE, S., SCHRUMPF, E., HOV, J. R., MANNS, M. P., BOBERG, K. M., SCHREIBER, S., FRANKE, A. & KARLSEN, T. H. 2013. Genome-wide association analysis in primary sclerosing cholangitis and ulcerative colitis identifies risk loci at GPR35 and TCF4. *Hepatology,* 58**,** 1074-83.

ETTEHAD, D., EMDIN, C. A., KIRAN, A., ANDERSON, S. G., CALLENDER, T., EMBERSON, J., CHALMERS, J., RODGERS, A. & RAHIMI, K. 2016. Blood pressure lowering for prevention of cardiovascular disease and death: a systematic review and meta-analysis. *The Lancet,* 387**,** 957-67.

FALLARINI, S., MAGLIULO, L., PAOLETTI, T., DE LALLA, C. & LOMBARDI, G. 2010. Expression of functional GPR35 in human iNKT cells. *Biochemical and Biophysical Research Communications,* 398**,** 420-5.

FARGIN, A., RAYMOND, J. R., LOHSE, M. J., KOBILKA, B. K., CARON, M. G. & LEFKOWITZ, R. J. 1988. The genomic clone G-21 which resembles a beta-adrenergic receptor sequence encodes the 5-HT1A receptor. *Nature,* 335**,** 358-60.

FELKER, G. M., BUTLER, J., COLLINS, S. P., COTTER, G., DAVISON, B. A., EZEKOWITZ, J. A., FILIPPATOS, G., LEVY, P. D., METRA, M., PONIKOWSKI, P., SOERGEL, D. G., TEERLINK, J. R., VIOLIN, J. D., VOORS, A. A. & PANG, P. S. 2015. Heart failure therapeutics on the basis of a biased ligand of the angiotensin-2 type 1 receptor. Rationale and design of the BLAST-AHF study (Biased Ligand of the Angiotensin Receptor Study in Acute Heart Failure). *JACC Heart Failure,* 3**,** 193-201.

FLORES-MUNOZ, M., WORK, L. M., DOUGLAS, K., DENBY, L., DOMINICZAK, A. F., GRAHAM, D. & NICKLIN, S. A. 2012. Angiotensin-(1-9) attenuates cardiac fibrosis in the stroke-prone spontaneously hypertensive rat via the angiotensin type 2 receptor. *Hypertension,* 59**,** 300-7.

FORREST, C. M., YOUD, P., KENNEDY, A., GOULD, S. R., DARLINGTON, L. G. & STONE, T. W. 2002. Purine, kynurenine, neopterin and lipid peroxidation levels in inflammatory bowel disease. *Journal of Biomedical Science,* 9**,** 436-42.

FREDRIKSSON, R., LAGERSTRÖM, M. C., LUNDIN, L. G. & SCHIÖTH, H. B. 2003. The G-protein-coupled receptors in the human genome form five main families. Phylogenetic analysis, paralogon groups, and fingerprints. *Molecular Pharmacology,* 63**,** 1256-72.

GAO, S., HO, D., VATNER, D. E. & VATNER, S. F. 2011. Echocardiography in Mice. *Current Protocols in Mouse Biology,* 1**,** 71-83.

GARLAND, S. L. 2013. Are GPCRs still a source of new targets? *Journal of Biomolecular Screening,* 18**,** 947-66.

GIMENEZ, L. E., KOOK, S., VISHNIVETSKIY, S. A., AHMED, M. R., GUREVICH, E. V. & GUREVICH, V. V. 2012. Role of receptor-attached phosphates in binding of visual and non-visual arrestins to G protein-coupled receptors. *Journal of Biological Chemistry,* 287**,** 9028-40.

GLENN, D. J., CARDEMA, M. C., NI, W., ZHANG, Y., YEGHIAZARIANS, Y., GRAPOV, D., FIEHN, O. & GARDNER, D. G. 2015. Cardiac steatosis potentiates angiotensin II effects in the heart. *American Journal of Physiology Heart and Circulatory Physiology,* 308**,** H339-50.

GOHLA, A., OFFERMANNS, S., WILKIE, T. M. & SCHULTZ, G. 1999. Differential involvement of Gα12 and Gα13 in receptor-mediated stress fiber formation. *Journal of Biological Chemistry,* 274**,** 17901-7.

GOHLA, A., SCHULTZ, G. & OFFERMANNS, S. 2000. Role for G(12)/G(13) in agonist-induced vascular smooth muscle cell contraction. *Circulation Research,* 87**,** 221-7.

GOMES, I., AYOUB, M. A., FUJITA, W., JAEGER, W. C., PFLEGER, K. D. & DEVI, L. A. 2016. G Protein-Coupled Receptor Heteromers. *Annual Reviews in Pharmacology and Toxicology,* 56**,** 403-25.

GONZÁLEZ, G. E., RHALEB, N. E., D'AMBROSIO, M. A., NAKAGAWA, P., LIU, Y., LEUNG, P., DAI, X., YANG, X. P., PETERSON, E. L. & CARRETERO, O. A. 2015. Deletion of interleukin-6 prevents cardiac inflammation, fibrosis and dysfunction without affecting blood pressure in angiotensin II-high salt-induced hypertension. *Journal of Hypertension,* 33**,** 144-52.

GOODMAN, O. B., KRUPNICK, J. G., SANTINI, F., GUREVICH, V. V., PENN, R. B., GAGNON, A. W., KEEN, J. H. & BENOVIC, J. L. 1996. β-arrestin acts as a clathrin adaptor in endocytosis of the beta(2)-adrenergic receptor. *Nature,* 383**,** 447-450.

GRAHAM, D., HAMILTON, C., BEATTIE, E., SPIERS, A. & DOMINICZAK, A. F. 2004. Comparison of the effects of omapatrilat and irbesartan/hydrochlorothiazide on endothelial function and cardiac hypertrophy in the stroke-prone spontaneously hypertensive rat: sex differences. *Journal of Hypertension,* 22**,** 329-37.

GRAHAM, D., MCBRIDE, M. W., GAASENBEEK, M., GILDAY, K., BEATTIE, E., MILLER, W. H., MCCLURE, J. D., POLKE, J. M., MONTEZANO, A., TOUYZ, R. M. & DOMINICZAK, A. F. 2007. Candidate genes that determine response to salt in the stroke-prone spontaneously hypertensive rat: congenic analysis. *Hypertension,* 50**,** 1134-41.

GRASSI, G., MARK, A. & ESLER, M. 2015. The sympathetic nervous system alterations in human hypertension. *Circulation Research,* 116**,** 976-90.

GRIFFITHS, K., DOLEZAL, O., CAO, B., NILSSON, S. K., SEE, H. B., PFLEGER, K. D., ROCHE, M., GORRY, P. R., POW, A., VIDUKA, K., LIM, K., LU, B. G., CHANG, D. H., MURRAY-RUST, T., KVANSAKUL, M., PERUGINI, M. A., DOGOVSKI, C., DOERFLINGER, M., ZHANG, Y., PARISI, K., CASEY, J. L., NUTTALL, S. D. & FOLEY, M. 2016. i-bodies, Human Single Domain Antibodies That Antagonize Chemokine Receptor CXCR4. *Journal of Biological Chemistry,* 291**,** 12641-57.

GU, J. L., MÜLLER, S., MANCINO, V., OFFERMANNS, S. & SIMON, M. I. 2002. Interaction of Gα(12) with Gα(13) and Gα(q) signaling pathways. *Proceedings of the National Academy of Sciences of the United States of America,* 99**,** 9352-7.

GUO, J., WILLIAMS, D. J., PUHL, H. L. & IKEDA, S. R. 2008. Inhibition of N-type calcium channels by activation of GPR35, an orphan receptor, heterologously expressed in rat sympathetic neurons. *Journal of Pharmacology and Experimental Therapeutics,* 324**,** 342-51.

GUREVICH, E. V., GAINETDINOV, R. R. & GUREVICH, V. V. 2016. G protein-coupled receptor kinases as regulators of dopamine receptor functions. *Pharmacological Research,* 111**,** 1-16.

GUZIK, T. J., HOCH, N. E., BROWN, K. A., MCCANN, L. A., RAHMAN, A., DIKALOV, S., GORONZY, J., WEYAND, C. & HARRISON, D. G. 2007. Role of the T cell in the

genesis of angiotensin II induced hypertension and vascular dysfunction. *Journal of Experimental Medicine,* 204**,** 2449-60.

HAMANN, J., AUST, G., ARAÇ, D., ENGEL, F. B., FORMSTONE, C., FREDRIKSSON, R., HALL, R. A., HARTY, B. L., KIRCHHOFF, C., KNAPP, B., KRISHNAN, A., LIEBSCHER, I., LIN, H. H., MARTINELLI, D. C., MONK, K. R., PEETERS, M. C., PIAO, X., PRÖMEL, S., SCHÖNEBERG, T., SCHWARTZ, T. W., SINGER, K., STACEY, M., USHKARYOV, Y. A., VALLON, M., WOLFRUM, U., WRIGHT, M. W., XU, L., LANGENHAN, T. & SCHIÖTH, H. B. 2015. International Union of Basic and Clinical Pharmacology. XCIV. Adhesion G protein-coupled receptors. *Pharmacological Reviews,* 67**,** 338-67.

HAMILTON, M. A., STEVENSON, L. W., LUU, M. & WALDEN, J. A. 1990. Altered thyroid hormone metabolism in advanced heart failure. *Journal of the American College of Cardiology,* 16**,** 91-5.

HARRIS, D. M., COHN, H. I., PESANT, S. & ECKHART, A. D. 2008. GPCR signalling in hypertension: role of GRKs. *Clinical Science (London),* 115**,** 79-89.

HARTMANN, S., RIDLEY, A. J. & LUTZ, S. 2015. The Function of Rho-Associated Kinases ROCK1 and ROCK2 in the Pathogenesis of Cardiovascular Disease. *Frontiers in Pharmacology,* 6**,** 276.

HEYNEN-GENEL, S., DAHL, R., SHI, S., SAUER, M., HARIHARAN, S., SERGIENKO, E., DAD, S., CHUNG, T. D., STONICH, D., SU, Y., CARON, M., ZHAO, P., ABOOD, M. E. & BARAK, L. S. 2010. Selective GPR35 Antagonists - Probes 1 & 2. *Probe Reports from the NIH Molecular Libraries Program* [Online].

HEYNEN-GENEL, S. S. S. M.-B.-F.-S. P., FONT-FAMILY:"TIMES NEW ROMAN", S., ROMAN", M.-F.-F.-F. T. N., MSO-FAREAST-LANGUAGE:JA">, DAHL, R., SHI, S., SAUER, M., HARIHARAN, S., SERGIENKO, E., DAD, S., CHUNG, T. D., STONICH, D., SU, Y., ZHAO, P., CARON, M., ABOOD, M. E., BARAK, L. & S. 2011. Selective GPR35 Antagonists - Probe 3. *Probe Reports from the NIH Molecular Libraries Program* [Online].

HIGASHI, M., SHIMOKAWA, H., HATTORI, T., HIROKI, J., MUKAI, Y., MORIKAWA, K., ICHIKI, T., TAKAHASHI, S. & TAKESHITA, A. 2003. Long-term inhibition of Rho-kinase suppresses angiotensin II-induced cardiovascular hypertrophy in rats in vivo: effect on endothelial NAD(P)H oxidase system. *Circulation Research,* 93**,** 767-75.

HIGASHIJIMA, T., FERGUSON, K. M., STERNWEIS, P. C., SMIGEL, M. D. & GILMAN, A. G. 1987. Effects of Mg2+ and the beta gamma-subunit complex on the interactions of guanine nucleotides with G proteins. *Journal of Biological Chemistry,* 262**,** 762-6.

HOMAN, K. T., WU, E., CANNAVO, A., KOCH, W. J. & TESMER, J. J. 2014. Identification and characterization of amlexanox as a G protein-coupled receptor kinase 5 inhibitor. *Molecules,* 19**,** 16937-49.

HOUSLAY, M. D. & BAILLIE, G. S. 2005. ß-arrestin-recruited phosphodiesterase-4 desensitizes the AKAP79/PKA-mediated switching of beta2-adrenoceptor signalling to activation of ERK. *Biochemical Society Transactions,* 33**,** 1333-6.

HUET, C. & GARRIDO, J. 1972. Ultrastructural visualization of cell-coat components by means of wheat germ agglutinin. *Experimental Cell Research,* 75**,** 523-7.

HUETTEMAN, D. A. & BOGIE, H. 2009. Direct blood pressure monitoring in laboratory rodents via implantable radio telemetry. *Methods in Molecular Biology,* 573**,** 57-73.

HULLMANN, J., TRAYNHAM, C. J., COLEMAN, R. C. & KOCH, W. J. 2016. The expanding GRK interactome: Implications in cardiovascular disease and potential for therapeutic development. *Pharmacological Research,* 110**,** 52-64.

HULLMANN, J. E., GRISANTI, L. A., MAKAREWICH, C. A., GAO, E., GOLD, J. I., CHUPRUN, J. K., TILLEY, D. G., HOUSER, S. R. & KOCH, W. J. 2014. GRK5-mediated exacerbation of pathological cardiac hypertrophy involves facilitation of nuclear NFAT activity. *Circulation Research,* 115**,** 976-85.

HULTSTRÖM, M. 2012. Development of structural kidney damage in spontaneously hypertensive rats. *Journal of Hypertension,* 30**,** 1087-91.

HUNT, S. A., ABRAHAM, W. T., CHIN, M. H., FELDMAN, A. M., FRANCIS, G. S., GANIATS, T. G., JESSUP, M., KONSTAM, M. A., MANCINI, D. M., MICHL, K., OATES, J. A., RAHKO, P. S., SILVER, M. A., STEVENSON, L. W. & YANCY, C. W. 2009. 2009 focused update incorporated into the ACC/AHA 2005 Guidelines for the Diagnosis and Management of Heart Failure in Adults: a report of the American College of Cardiology Foundation/American Heart Association Task Force on Practice Guidelines: developed in collaboration with the International Society for Heart and Lung Transplantation. *Circulation,* 119**,** e391-479.

HUVENEERS, S., DAEMEN, M. J. & HORDIJK, P. L. 2015. Between Rho(k) and a hard place: the relation between vessel wall stiffness, endothelial contractility, and cardiovascular disease. *Circulation Research,* 116**,** 895-908.

IMIELINSKI, M., BALDASSANO, R. N., GRIFFITHS, A., RUSSELL, R. K., ANNESE, V., DUBINSKY, M., KUGATHASAN, S., BRADFIELD, J. P., WALTERS, T. D., SLEIMAN, P., KIM, C. E., MUISE, A., WANG, K., GLESSNER, J. T., SAEED, S., ZHANG, H., FRACKELTON, E. C., HOU, C., FLORY, J. H., OTIENO, G., CHIAVACCI, R. M., GRUNDMEIER, R., CASTRO, M., LATIANO, A., DALLAPICCOLA, B., STEMPAK, J., ABRAMS, D. J., TAYLOR, K., MCGOVERN, D., SILBER, G., WROBEL, I., QUIROS, A., BARRETT, J. C., HANSOUL, S., NICOLAE, D. L., CHO, J. H., DUERR, R. H., RIOUX, J. D., BRANT, S. R., SILVERBERG, M. S., TAYLOR, K. D., BARMUDA, M. M., BITTON, A., DASSOPOULOS, T., DATTA, L. W., GREEN, T., GRIFFITHS, A. M., KISTNER, E. O., MURTHA, M. T., REGUEIRO, M. D., ROTTER, J. I., SCHUMM, L. P., STEINHART, A. H., TARGAN, S. R., XAVIER, R. J., LIBIOULLE, C., SANDOR, C., LATHROP, M., BELAICHE, J., DEWIT, O., GUT, I., HEATH, S., LAUKENS, D., MNI, M., RUTGEERTS, P., VAN GOSSUM, A., ZELENIKA, D., FRANCHIMONT, D., HUGOT, J. P., DE VOS, M., VERMEIRE, S., LOUIS, E., CARDON, L. R., ANDERSON, C. A.,

DRUMMOND, H., NIMMO, E., AHMAD, T., PRESCOTT, N. J., ONNIE, C. M., FISHER, S. A., MARCHINI, J., GHORI, J., BUMPSTEAD, S., GWILLAM, R., TREMELLING, M., DELUKAS, P., MANSFIELD, J., JEWELL, D., SATSANGI, J., MATHEW, C. G., PARKES, M., GEORGES, M., DALY, M. J., HEYMAN, M. B., FERRY, G. D., KIRSCHNER, B., LEE, J., ESSERS, J., GRAND, R., STEPHENS, M., et al. 2009. Common variants at five new loci associated with early-onset inflammatory bowel disease. *Nature Genetics,* 41**,** 1335-40.

INNAMORATI, G., SADEGHI, H. M., TRAN, N. T. & BIRNBAUMER, M. 1998. A serine cluster prevents recycling of the V2 vasopressin receptor. *Proceedings of the National Academy of Sciences of the United States of America,* 95**,** 2222-2226.

ITOH, Y., KAWAMATA, Y., HARADA, M., KOBAYASHI, M., FUJII, R., FUKUSUMI, S., OGI, K., HOSOYA, M., TANAKA, Y., UEJIMA, H., TANAKA, H., MARUYAMA, M., SATOH, R., OKUBO, S., KIZAWA, H., KOMATSU, H., MATSUMURA, F., NOGUCHI, Y., SHINOHARA, T., HINUMA, S., FUJISAWA, Y. & FUJINO, M. 2003. Free fatty acids regulate insulin secretion from pancreatic beta cells through GPR40. *Nature,* 422**,** 173-6.

JACOB, H. J., LINDPAINTNER, K., LINCOLN, S. E., KUSUMI, K., BUNKER, R. K., MAO, Y. P., GANTEN, D., DZAU, V. J. & LANDER, E. S. 1991. Genetic mapping of a gene causing hypertension in the stroke-prone spontaneously hypertensive rat. *Cell,* 67**,** 213-24.

JANSSEN, B. J., DE CELLE, T., DEBETS, J. J., BROUNS, A. E., CALLAHAN, M. F. & SMITH, T. L. 2004. Effects of anesthetics on systemic hemodynamics in mice. *American Journal of Physiology Heart and Circulatory Physiology,* 287**,** H1618-24.

JENKINS, L., ALVAREZ-CURTO, E., CAMPBELL, K., DE MUNNIK, S., CANALS, M., SCHLYER, S. & MILLIGAN, G. 2011. Agonist activation of the G protein-coupled receptor GPR35 involves transmembrane domain III and is transduced via Gα(13) and ß-arrestin-2. *British Journal of Pharmacology,* 162**,** 733-748.

JENKINS, L., BREA, J., SMITH, N. J., HUDSON, B. D., REILLY, G., BRYANT, N. J., CASTRO, M., LOZA, M.-I. & MILLIGAN, G. 2010. Identification of novel species-selective agonists of the G-protein-coupled receptor GPR35 that promote recruitment of ß-arrestin-2 and activate Gα(13). *Biochemical Journal,* 432**,** 451-459.

JENKINS, L., HARRIES, N., LAPPIN, J. E., MACKENZIE, A. E., NEETOO-ISSELJEE, Z., SOUTHERN, C., MCIVER, E. G., NICKLIN, S. A., TAYLOR, D. L. & MILLIGAN, G. 2012. Antagonists of GPR35 display high species ortholog selectivity and varying modes of action. *Journal of Pharmacology and Experimental Therapeutics,* 343**,** 683-95.

JONES, A. W. 2016. Perspectives in Drug Development and Clinical Pharmacology: The Discovery of Histamine H1 and H2 Antagonists. *Clinical Pharmacology in Drug Development,* 5**,** 5-12.

JUN, L. S., SHOWALTER, A. D., ALI, N., DAI, F., MA, W., COSKUN, T., FICORILLI, J. V., WHEELER, M. B., MICHAEL, M. D. & SLOOP, K. W. 2014. A novel humanized GLP-1 receptor model enables both affinity purification and Cre-LoxP deletion of the receptor. *PLoS One,* 9**,** e93746.

KATRITCH, V., CHEREZOV, V. & STEVENS, R. C. 2012. Diversity and modularity of G protein-coupled receptor structures. *Trends in Pharmacological Sciences,* 33**,** 17-27.

KEHAT, I., DAVIS, J., TIBURCY, M., ACCORNERO, F., SABA-EL-LEIL, M. K., MAILLET, M., YORK, A. J., LORENZ, J. N., ZIMMERMANN, W. H., MELOCHE, S. & MOLKENTIN, J. D. 2011. Extracellular signal-regulated kinases 1 and 2 regulate the balance between eccentric and concentric cardiac growth. *Circulation Research,* 108**,** 176-83.

KEYS, J. R., ZHOU, R. H., HARRIS, D. M., DRUCKMAN, C. A. & ECKHART, A. D. 2005. Vascular smooth muscle overexpression of G protein-coupled receptor kinase 5 elevates blood pressure, which segregates with sex and is dependent on Gi-mediated signaling. *Circulation,* 112**,** 1145-53.

KHAN, N. S., SONG, C. Y., JENNINGS, B. L., ESTES, A. M., FANG, X. R., BONVENTRE, J. V. & MALIK, K. U. 2015. Cytosolic phospholipase A2α is critical for angiotensin II-induced hypertension and associated cardiovascular pathophysiology. *Hypertension,* 65**,** 784-92.

KHANDWALA, A., VAN INWEGEN, R. G., CHARNEY, M. R. & ALFANO, M. C. 1997. 5% amlexanox oral paste, a new treatment for recurrent minor aphthous ulcers: II. Pharmacokinetics and demonstration of clinical safety. *Oral Surgery, Oral Medicine, Oral Pathology, Oral Radiology,* 83**,** 231-8.

KOLAR, G. R., GROTE, S. M. & YOSTEN, G. L. 2016. Targeting orphan G protein-coupled receptors for the treatment of diabetes and its complications: C-peptide and GPR146. *Journal of Internal Medicine*, 281, 25-40.

KOSSMANN, S., SCHWENK, M., HAUSDING, M., KARBACH, S. H., SCHMIDGEN, M. I., BRANDT, M., KNORR, M., HU, H., KRÖLLER-SCHÖN, S., SCHÖNFELDER, T., GRABBE, S., OELZE, M., DAIBER, A., MÜNZEL, T., BECKER, C. & WENZEL, P. 2013. Angiotensin II-induced vascular dysfunction depends on interferon-γ-driven immune cell recruitment and mutual activation of monocytes and NK-cells. *Arteriosclerosis, Thrombosis, and Vascular Biology,* 33**,** 1313-9.

KOSTENIS, E., WAELBROECK, M. & MILLIGAN, G. 2005. Techniques: promiscuous Gα proteins in basic research and drug discovery. *Trends in Pharmacological Sciences,* 26**,** 595-602.

KOSTICH, W., HAMMAN, B. D., LI, Y. W., NAIDU, S., DANDAPANI, K., FENG, J., EASTON, A., BOURIN, C., BAKER, K., ALLEN, J., SAVELIEVA, K., LOUIS, J. V., DOKANIA, M., ELAVAZHAGAN, S., VATTIKUNDALA, P., SHARMA, V., DAS, M. L., SHANKAR, G., KUMAR, A., HOLENARSIPUR, V. K., GULIANELLO, M., MOLSKI, T., BROWN, J. M., LEWIS, M., HUANG, Y., LU, Y., PIESCHL, R., O'MALLEY, K., LIPPY, J.,

NOURALDEEN, A., LANTHORN, T. H., YE, G., WILSON, A., BALAKRISHNAN, A., DENTON, R., GRACE, J. E., LENTZ, K. A., SANTONE, K. S., BI, Y., MAIN, A., SWAFFIELD, J., CARSON, K., MANDLEKAR, S., VIKRAMADITHYAN, R. K., NARA, S. J., DZIERBA, C., BRONSON, J., MACOR, J. E., ZACZEK, R., WESTPHAL, R., KISS, L., BRISTOW, L., CONWAY, C. M., ZAMBROWICZ, B. & ALBRIGHT, C. F. 2016. Inhibition of AAK1 Kinase as a Novel Therapeutic Approach to Treat Neuropathic Pain. *Journal of Pharmacology and Experimental Therapeutics,* 358**,** 371-86.

KRAMER, K. & KINTER, L. B. 2003. Evaluation and applications of radiotelemetry in small laboratory animals. *Physiological Genomics,* 13**,** 197-205.

KREGE, J. H., HODGIN, J. B., HAGAMAN, J. R. & SMITHIES, O. 1995. A noninvasive computerized tail-cuff system for measuring blood pressure in mice. *Hypertension,* 25**,** 1111-5.

KUC, D., ZGRAJKA, W., PARADA-TURSKA, J., URBANIK-SYPNIEWSKA, T. & TURSKI, W. A. 2008. Micromolar concentration of kynurenic acid in rat small intestine. *Amino Acids,* 35**,** 503-5.

LAM, C. S., LYASS, A., KRAIGHER-KRAINER, E., MASSARO, J. M., LEE, D. S., HO, J. E., LEVY, D., REDFIELD, M. M., PIESKE, B. M., BENJAMIN, E. J. & VASAN, R. S. 2011. Cardiac dysfunction and noncardiac dysfunction as precursors of heart failure with reduced and preserved ejection fraction in the community. *Circulation,* 124**,** 24-30.

LANDER, E. S., LINTON, L. M., BIRREN, B., NUSBAUM, C., ZODY, M. C., BALDWIN, J., DEVON, K., DEWAR, K., DOYLE, M., FITZHUGH, W., FUNKE, R., GAGE, D., HARRIS, K., HEAFORD, A., HOWLAND, J., KANN, L., LEHOCZKY, J., LEVINE, R., MCEWAN, P., MCKERNAN, K., MELDRIM, J., MESIROV, J. P., MIRANDA, C., MORRIS, W., NAYLOR, J., RAYMOND, C., ROSETTI, M., SANTOS, R., SHERIDAN, A., SOUGNEZ, C., STANGE-THOMANN, Y., STOJANOVIC, N., SUBRAMANIAN, A., WYMAN, D., ROGERS, J., SULSTON, J., AINSCOUGH, R., BECK, S., BENTLEY, D., BURTON, J., CLEE, C., CARTER, N., COULSON, A., DEADMAN, R., DELOUKAS, P., DUNHAM, A., DUNHAM, I., DURBIN, R., FRENCH, L., GRAFHAM, D., GREGORY, S., HUBBARD, T., HUMPHRAY, S., HUNT, A., JONES, M., LLOYD, C., MCMURRAY, A., MATTHEWS, L., MERCER, S., MILNE, S., MULLIKIN, J. C., MUNGALL, A., PLUMB, R., ROSS, M., SHOWNKEEN, R., SIMS, S., WATERSTON, R. H., WILSON, R. K., HILLIER, L. W., MCPHERSON, J. D., MARRA, M. A., MARDIS, E. R., FULTON, L. A., CHINWALLA, A. T., PEPIN, K. H., GISH, W. R., CHISSOE, S. L., WENDL, M. C., DELEHAUNTY, K. D., MINER, T. L., DELEHAUNTY, A., KRAMER, J. B., COOK, L. L., FULTON, R. S., JOHNSON, D. L., MINX, P. J., CLIFTON, S. W., HAWKINS, T., BRANSCOMB, E., PREDKI, P., RICHARDSON, P., WENNING, S., SLEZAK, T., DOGGETT, N., CHENG, J. F., OLSEN, A., LUCAS, S., ELKIN, C., UBERBACHER, E., FRAZIER, M., et al. 2001. Initial sequencing and analysis of the human genome. *Nature,* 409**,** 860-921.

LAPORTE, S. A., OAKLEY, R. H., ZHANG, J., HOLT, J. A., FERGUSON, S. S., CARON, M. G. & BARAK, L. S. 1999. The beta2-adrenergic receptor/β-arrestin complex recruits the clathrin adaptor AP-2 during endocytosis. *Proceedings of the National Academy of Sciences of the United States of America,* 96**,** 3712-7.

LARKIN, P. B., SATHYASAIKUMAR, K. V., NOTARANGELO, F. M., FUNAKOSHI, H., NAKAMURA, T., SCHWARCZ, R. & MUCHOWSKI, P. J. 2016. Tryptophan 2,3-dioxygenase and indoleamine 2,3-dioxygenase 1 make separate, tissue-specific contributions to basal and inflammation-induced kynurenine pathway metabolism in mice. *Biochimica et Biophysica Acta,* 1860, 2345-54.

LECCA, D. & ABBRACCHIO, M. P. 2008. Deorphanisation of G protein-coupled receptors: A tool to provide new insights in nervous system pathophysiology and new targets for psycho-active drugs. *Neurochemistry International,* 52**,** 339-51.

LEE, K. B., PTASIENSKI, J. A., PALS-RYLAARSDAM, R., GUREVICH, V. V. & HOSEY, M. M. 2000. Arrestin binding to the M-2 muscarinic acetylcholine receptor is precluded by an inhibitory element in the third intracellular loop of the receptor. *Journal of Biological Chemistry,* 275**,** 9284-9289.

LEVOYE, A., DAM, J., AYOUB, M. A., GUILLAUME, J. L., COUTURIER, C., DELAGRANGE, P. & JOCKERS, R. 2006. The orphan GPR50 receptor specifically inhibits MT1 melatonin receptor function through heterodimerization. *EMBO Journal,* 25**,** 3012-23.

LEVOYE, A. & JOCKERS, R. 2008. Alternative drug discovery approaches for orphan GPCRs. *Drug Discovery Today,* 13**,** 52-8.

LI, L., HOMAN, K. T., VISHNIVETSKIY, S. A., MANGLIK, A., TESMER, J. J., GUREVICH, V. V. & GUREVICH, E. V. 2015. G Protein-coupled Receptor Kinases of the GRK4 Protein Subfamily Phosphorylate Inactive G Protein-coupled Receptors (GPCRs). *Journal of Biological Chemistry,* 290**,** 10775-90.

LI, Z., QIU, Q., GENG, X., YANG, J., HUANG, W. & QIAN, H. 2016. Free fatty acid receptor agonists for the treatment of type 2 diabetes: drugs in preclinical to phase II clinical development. *Expert Opinion on Investigational Drugs,* 25**,** 871-90.

LIGGETT, S. B. 2011. Phosphorylation barcoding as a mechanism of directing GPCR signaling. *Science Signaling,* 4**,** pe36.

LIMA, V. V., ZEMSE, S. M., CHIAO, C. W., BOMFIM, G. F., TOSTES, R. C., CLINTON WEBB, R. & GIACHINI, F. R. 2016. Interleukin-10 limits increased blood pressure and vascular RhoA/Rho-kinase signaling in angiotensin II-infused mice. *Life Sciences,* 145**,** 137-43.

LITOSCH, I. 2016. Decoding Gαq signaling. *Life Sciences,* 152**,** 99-106.

LIU, C., WU, J., ZHU, J., KUEI, C., YU, J., SHELTON, J., SUTTON, S. W., LI, X., YUN, S. J., MIRZADEGAN, T., MAZUR, C., KAMME, F. & LOVENBERG, T. W. 2009. Lactate inhibits lipolysis in fat cells through activation of an orphan G-protein-coupled receptor, GPR81. *Journal of Biological Chemistry,* 284**,** 2811-22.

LIVAK, K. J. & SCHMITTGEN, T. D. 2001. Analysis of relative gene expression data using real-time quantitative PCR and the 2(-Delta Delta C(T)) Method. *Methods,* 25, 402-8.

LOGUE, S. F., GRAUER, S. M., PAULSEN, J., GRAF, R., TAYLOR, N., SUNG, M. A., ZHANG, L., HUGHES, Z., PULITO, V. L., LIU, F., ROSENZWEIG-LIPSON, S., BRANDON, N. J., MARQUIS, K. L., BATES, B. & PAUSCH, M. 2009. The orphan GPCR, GPR88, modulates function of the striatal dopamine system: a possible therapeutic target for psychiatric disorders? *Molecular and Cellular Neuroscience,* 42, 438-47.

LOHSE, M. J. 1993. Molecular mechanisms of membrane receptor desensitization. *Biochimica et Biophysica Acta,* 1179, 171-88.

LU, H., HOWATT, D. A., BALAKRISHNAN, A., MOORLEGHEN, J. J., RATERI, D. L., CASSIS, L. A. & DAUGHERTY, A. 2015. Subcutaneous Angiotensin II Infusion using Osmotic Pumps Induces Aortic Aneurysms in Mice. *Journal of Visualized Experiments*.

LUTTRELL, L. M., FERGUSON, S. S., DAAKA, Y., MILLER, W. E., MAUDSLEY, S., DELLA ROCCA, G. J., LIN, F., KAWAKATSU, H., OWADA, K., LUTTRELL, D. K., CARON, M. G. & LEFKOWITZ, R. J. 1999. ß-arrestin-dependent formation of beta2 adrenergic receptor-Src protein kinase complexes. *Science,* 283, 655-61.

LUTTRELL, L. M. & GESTY-PALMER, D. 2010. Beyond Desensitization: Physiological Relevance of Arrestin-Dependent Signaling. *Pharmacological Reviews,* 62, 305-330.

LUTTRELL, L. M. & LEFKOWITZ, R. J. 2002. The role of ß -arrestins in the termination and transduction of G-protein-coupled receptor signals. *Journal of Cell Science,* 115, 455-65.

LUTTRELL, L. M., MAUDSLEY, S. & BOHN, L. M. 2015. Fulfilling the Promise of "Biased" G Protein-Coupled Receptor Agonism. *Molecular Pharmacology,* 88, 579-588.

LYMPEROPOULOS, A., RENGO, G. & KOCH, W. J. 2013. Adrenergic nervous system in heart failure: pathophysiology and therapy. *Circulation Research,* 113, 739-53.

MACKENZIE, A. E., CALTABIANO, G., KENT, T. C., JENKINS, L., MCCALLUM, J. E., HUDSON, B. D., NICKLIN, S. A., FAWCETT, L., MARKWICK, R., CHARLTON, S. J. & MILLIGAN, G. 2014. The antiallergic mast cell stabilizers lodoxamide and bufrolin as the first high and equipotent agonists of human and rat GPR35. *Molecular Pharmacology,* 85, 91-104.

MACKENZIE, A. E. & MILLIGAN, G. 2015. The emerging pharmacology and function of GPR35 in the nervous system. *Neuropharmacology*.

MAGUIRE, J. J. & DAVENPORT, A. P. 2005. Regulation of vascular reactivity by established and emerging GPCRs. *Trends in Pharmacological Sciences,* 26, 448-54.

MAKINO, H., SAIJO, T., ASHIDA, Y., KURIKI, H. & MAKI, Y. 1987. Mechanism of action of an antiallergic agent, amlexanox (AA-673), in inhibiting histamine release from mast cells. Acceleration of cAMP generation and inhibition of phosphodiesterase. *International Archives of Allergy and Applied Immunology,* 82**,** 66-71.

MALIK, R. U., RITT, M., DEVREE, B. T., NEUBIG, R. R., SUNAHARA, R. K. & SIVARAMAKRISHNAN, S. 2013. Detection of G protein-selective G protein-coupled receptor (GPCR) conformations in live cells. *Journal of Biological Chemistry,* 288**,** 17167-78.

MANGLIK, A., KOBILKA, B. K. & STEYAERT, J. 2016. Nanobodies to Study G Protein-Coupled Receptor Structure and Function. *Annual Reviews in Pharmacology and Toxicology*, 57, 19-37.

MARAVILLAS-MONTERO, J. L., BURKHARDT, A. M., HEVEZI, P. A., CARNEVALE, C. D., SMIT, M. J. & ZLOTNIK, A. 2015. Cutting edge: GPR35/CXCR8 is the receptor of the mucosal chemokine CXCL17. *Journal of Immunology,* 194**,** 29-33.

MARCHESE, A. & TREJO, J. 2013. Ubiquitin-dependent regulation of G protein-coupled receptor trafficking and signaling. *Cellular Signalling,* 25**,** 707-16.

MARSANGO, S., VARELA, M. J. & MILLIGAN, G. 2015. Approaches to Characterize and Quantify Oligomerization of GPCRs. *Methods in Molecular Biology,* 1335**,** 95-105.

MAUDSLEY, S., MARTIN, B. & LUTTRELL, L. M. 2005. The origins of diversity and specificity in g protein-coupled receptor signaling. *Journal of Pharmacology and Experimental Therapeutics,* 314**,** 485-94.

MAUSSANG, D., MUJIĆ-DELIĆ, A., DESCAMPS, F. J., STORTELERS, C., VANLANDSCHOOT, P., STIGTER-VAN WALSUM, M., VISCHER, H. F., VAN ROY, M., VOSJAN, M., GONZALEZ-PAJUELO, M., VAN DONGEN, G. A., MERCHIERS, P., VAN ROMPAEY, P. & SMIT, M. J. 2013. Llama-derived single variable domains (nanobodies) directed against chemokine receptor CXCR7 reduce head and neck cancer cell growth in vivo. *Journal of Biological Chemistry,* 288**,** 29562-72.

MCCALLUM, J. E., MACKENZIE, A. E., DIVORTY, N., CLARKE, C., DELLES, C., MILLIGAN, G. & NICKLIN, S. A. 2015. G-Protein-Coupled Receptor 35 Mediates Human Saphenous Vein Vascular Smooth Muscle Cell Migration and Endothelial Cell Proliferation. *Journal of Vascular Research,* 52**,** 383-95.

MCDONALD, P. H., CHOW, C. W., MILLER, W. E., LAPORTE, S. A., FIELD, M. E., LIN, F. T., DAVIS, R. J. & LEFKOWITZ, R. J. 2000. ß-arrestin 2: a receptor-regulated MAPK scaffold for the activation of JNK3. *Science,* 290**,** 1574-7.

MCLACHLAN, J., BEATTIE, E., MURPHY, M. P., KOH-TAN, C. H., OLSON, E., BEATTIE, W., DOMINICZAK, A. F., NICKLIN, S. A. & GRAHAM, D. 2014. Combined therapeutic benefit of mitochondria-targeted antioxidant, MitoQ10, and angiotensin receptor blocker, losartan, on cardiovascular function. *Journal of Hypertension,* 32**,** 555-64.

MCMASTER, W. G., KIRABO, A., MADHUR, M. S. & HARRISON, D. G. 2015. Inflammation, immunity, and hypertensive end-organ damage. *Circulation Research,* 116**,** 1022-33.

MEDINA, P., SEGARRA, G., MARTÍNEZ-LEÓN, J. B., VILA, J. M., ALDASORO, M., OTERO, E. & LLUCH, S. 2000. Relaxation induced by cGMP phosphodiesterase inhibitors sildenafil and zaprinast in human vessels. *Annals of Thoracic Surgery,* 70**,** 1327-31.

MEHTA, P. K. & GRIENDLING, K. K. 2007. Angiotensin II cell signaling: physiological and pathological effects in the cardiovascular system. *American Journal of Physiology Cell Physiology,* 292**,** C82-97.

MENG, W., DONG, Y., LIU, J., WANG, Z., ZHONG, X., CHEN, R., ZHOU, H., LIN, M., JIANG, L., GAO, F., XU, T., CHEN, Q. & ZENG, X. 2009. A clinical evaluation of amlexanox oral adhesive pellicles in the treatment of recurrent aphthous stomatitis and comparison with amlexanox oral tablets: a randomized, placebo controlled, blinded, multicenter clinical trial. *Trials,* 10**,** 30.

MEYER, R. C., GIDDENS, M. M., SCHAEFER, S. A. & HALL, R. A. 2013. GPR37 and GPR37L1 are receptors for the neuroprotective and glioprotective factors prosaptide and prosaposin. *Proceedings of the National Academy of Sciences of the United States of America,* 110**,** 9529-34.

MIKOLAJCZYK, T. P., NOSALSKI, R., SZCZEPANIAK, P., BUDZYN, K., OSMENDA, G., SKIBA, D., SAGAN, A., WU, J., VINH, A., MARVAR, P. J., GUZIK, B., PODOLEC, J., DRUMMOND, G., LOB, H. E., HARRISON, D. G. & GUZIK, T. J. 2016. Role of chemokine RANTES in the regulation of perivascular inflammation, T-cell accumulation, and vascular dysfunction in hypertension. *FASEB Journal,* 30**,** 1987-99.

MILASTA, S., EVANS, N. A., ORMISTON, L., WILSON, S., LEFKOWITZ, R. J. & MILLIGAN, G. 2005. The sustainability of interactions between the orexin-1 receptor and beta-arrestin-2 is defined by a single C-terminal cluster of hydroxy amino acids and modulates the kinetics of ERK MAPK regulation. *Biochemical Journal,* 387**,** 573-584.

MILLIGAN, G. 2011. Orthologue selectivity and ligand bias: translating the pharmacology of GPR35. *Trends in Pharmacological Sciences,* 32**,** 317-325.

MILLS, P. A., HUETTEMAN, D. A., BROCKWAY, B. P., ZWIERS, L. M., GELSEMA, A. J., SCHWARTZ, R. S. & KRAMER, K. 2000. A new method for measurement of blood pressure, heart rate, and activity in the mouse by radiotelemetry. *Journal of Applied Physiology (1985),* 88**,** 1537-44.

MIN, K. D., ASAKURA, M., LIAO, Y., NAKAMARU, K., OKAZAKI, H., TAKAHASHI, T., FUJIMOTO, K., ITO, S., TAKAHASHI, A., ASANUMA, H., YAMAZAKI, S., MINAMINO, T., SANADA, S., SEGUCHI, O., NAKANO, A., ANDO, Y., OTSUKA, T., FURUKAWA, H., ISOMURA, T., TAKASHIMA, S., MOCHIZUKI, N. & KITAKAZE, M. 2010. Identification of genes related to heart failure using global gene expression

profiling of human failing myocardium. *Biochemical and Biophysical Research Communications,* 393, 55-60.

MOHAN, P., BRUTSAERT, D. L., PAULUS, W. J. & SYS, S. U. 1996. Myocardial contractile response to nitric oxide and cGMP. *Circulation,* 93, 1223-9.

MOORE, J. P., VINH, A., TUCK, K. L., SAKKAL, S., KRISHNAN, S. M., CHAN, C. T., LIEU, M., SAMUEL, C. S., DIEP, H., KEMP-HARPER, B. K., TARE, M., RICARDO, S. D., GUZIK, T. J., SOBEY, C. G. & DRUMMOND, G. R. 2015. M2 macrophage accumulation in the aortic wall during angiotensin II infusion in mice is associated with fibrosis, elastin loss, and elevated blood pressure. *American Journal of Physiology Heart and Circulatory Physiology,* 309, H906-17.

MORONI, F., COZZI, A., SILI, M. & MANNAIONI, G. 2012. Kynurenic acid: a metabolite with multiple actions and multiple targets in brain and periphery. *Journal of Neural Transmission (Vienna),* 119, 133-9.

MUJIĆ-DELIĆ, A., DE WIT, R. H., VERKAAR, F. & SMIT, M. J. 2014. GPCR-targeting nanobodies: attractive research tools, diagnostics, and therapeutics. *Trends in Pharmacological Sciences,* 35, 247-55.

MULVANY, M. J. & AALKJAER, C. 1990. Structure and function of small arteries. *Physiological Reviews,* 70, 921-61.

MULVANY, M. J. & HALPERN, W. 1977. Contractile properties of small arterial resistance vessels in spontaneously hypertensive and normotensive rats. *Circulation Research,* 41, 19-26.

MUNK, C., ISBERG, V., MORDALSKI, S., HARPSØE, K., RATAJ, K., HAUSER, A. S., KOLB, P., BOJARSKI, A. J., VRIEND, G. & GLORIAM, D. E. 2016. GPCRdb: the G protein-coupled receptor database - an introduction. *British Journal of Pharmacology,* 173, 2195-207.

NAKAMURA, Y., ISHII, J. & KONDO, A. 2016. Current Techniques for Studying Oligomer Formations of G-Protein-Coupled Receptors Using Mammalian and Yeast Cells. *Current Medicinal Chemistry,* 23, 1638-56.

NEDVETZKI, S., GONEN, E., ASSAYAG, N., REICH, R., WILLIAMS, R. O., THURMOND, R. L., HUANG, J. F., NEUDECKER, B. A., WANG, F. S., TURLEY, E. A. & NAOR, D. 2004. RHAMM, a receptor for hyaluronan-mediated motility, compensates for CD44 in inflamed CD44-knockout mice: a different interpretation of redundancy. *Proceedings of the National Academy of Sciences of the United States of America,* 101, 18081-6.

NEETOO-ISSELJEE, Z., MACKENZIE, A. E., SOUTHERN, C., JERMAN, J., MCIVER, E. G., HARRIES, N., TAYLOR, D. L. & MILLIGAN, G. 2013. High-throughput identification and characterization of novel, species-selective GPR35 agonists. *Journal of Pharmacology and Experimental Therapeutics,* 344, 568-78.

NGO, T., ILATOVSKIY, A. V., STEWART, A. G., COLEMAN, J. L., MCROBB, F. M., RIEK, R. P., GRAHAM, R. M., ABAGYAN, R., KUFAREVA, I. & SMITH, N. J. 2016a. Orphan receptor ligand discovery by pickpocketing pharmacological neighbors. *Nature Chemical Biology*, 13, 235-42.

NGO, T., KUFAREVA, I., COLEMAN, J. L., GRAHAM, R. M., ABAGYAN, R. & SMITH, N. J. 2016b. Identifying ligands at orphan GPCRs: current status using structure-based approaches. *British Journal of Pharmacology*, 173, 2934-51.

NISHIMURA, A., SUNGGIP, C., TOZAKI-SAITOH, H., SHIMAUCHI, T., NUMAGA-TOMITA, T., HIRANO, K., IDE, T., BOEYNAEMS, J. M., KUROSE, H., TSUDA, M., ROBAYE, B., INOUE, K. & NISHIDA, M. 2016. Purinergic P2Y6 receptors heterodimerize with angiotensin AT1 receptors to promote angiotensin II-induced hypertension. *Science Signaling,* 9, ra7.

NOBLES, K. N., XIAO, K., AHN, S., SHUKLA, A. K., LAM, C. M., RAJAGOPAL, S., STRACHAN, R. T., HUANG, T.-Y., BRESSLER, E. A., HARA, M. R., SHENOY, S. K., GYGI, S. P. & LEFKOWITZ, R. J. 2011. Distinct Phosphorylation Sites on the beta(2)-Adrenergic Receptor Establish a Barcode That Encodes Differential Functions of ß-Arrestin. *Science Signaling,* 4, ra51.

NOMA, T., LEMAIRE, A., NAGA PRASAD, S. V., BARKI-HARRINGTON, L., TILLEY, D. G., CHEN, J., LE CORVOISIER, P., VIOLIN, J. D., WEI, H., LEFKOWITZ, R. J. & ROCKMAN, H. A. 2007. ß -arrestin-mediated beta1-adrenergic receptor transactivation of the EGFR confers cardioprotection. *Journal of Clinical Investigation,* 117, 2445-58.

NORDSTRÖM, K. J., SÄLLMAN ALMÉN, M., EDSTAM, M. M., FREDRIKSSON, R. & SCHIÖTH, H. B. 2011. Independent HHsearch, Needleman-Wunsch-based, and motif analyses reveal the overall hierarchy for most of the G protein-coupled receptor families. *Molecular Biology and Evolution,* 28, 2471-80.

O'DOWD, B. F., NGUYEN, T., MARCHESE, A., CHENG, R., LYNCH, K. R., HENG, H. H., KOLAKOWSKI, L. F. & GEORGE, S. R. 1998. Discovery of three novel G-protein-coupled receptor genes. *Genomics,* 47, 310-3.

OAKLEY, R. H., HUDSON, C. C., SJAASTAD, M. D. & LOOMIS, C. R. 2006. The ligand-independent translocation assay: an enabling technology for screening orphan G protein-coupled receptors by arrestin recruitment. *Methods in Enzymology,* 414, 50-63.

OFFERMANNS, S., MANCINO, V., REVEL, J. P. & SIMON, M. I. 1997. Vascular system defects and impaired cell chemokinesis as a result of Gα13 deficiency. *Science,* 275, 533-6.

OHSHIRO, H., TONAI-KACHI, H. & ICHIKAWA, K. 2008. GPR35 is a functional receptor in rat dorsal root ganglion neurons. *Biochemical and Biophysical Research Communications,* 365, 344-8.

OKA, S., OTA, R., SHIMA, M., YAMASHITA, A. & SUGIURA, T. 2010. GPR35 is a novel lysophosphatidic acid receptor. *Biochemical and Biophysical Research Communications,* 395**,** 232-7.

OKUMURA, S., BABA, H., KUMADA, T., NANMOKU, K., NAKAJIMA, H., NAKANE, Y., HIOKI, K. & IKENAKA, K. 2004. Cloning of a G-protein-coupled receptor that shows an activity to transform NIH3T3 cells and is expressed in gastric cancer cells. *Cancer Science,* 95**,** 131-5.

ORSINI, M. J., PARENT, J. L., MUNDELL, S. J., MARCHESE, A. & BENOVIC, J. L. 1999. Trafficking of the HIV coreceptor CXCR4. Role of arrestins and identification of residues in the c-terminal tail that mediate receptor internalization. *Journal of Biological Chemistry,* 274**,** 31076-86.

OVERINGTON, J. P., AL-LAZIKANI, B. & HOPKINS, A. L. 2006. How many drug targets are there? *Nature Reviews Drug Discovery,* 5**,** 993-6.

PALUDAN, S. R. 1998. Interleukin-4 and interferon-gamma: the quintessence of a mutual antagonistic relationship. *Scandinavian Journal of Immunology,* 48**,** 459-68.

PEETERS, R. P., VAN DER GEYTEN, S., WOUTERS, P. J., DARRAS, V. M., VAN TOOR, H., KAPTEIN, E., VISSER, T. J. & VAN DEN BERGHE, G. 2005. Tissue thyroid hormone levels in critical illness. *Journal of Clinical Endocrinology and Metabolism,* 90**,** 6498-507.

PHILIPP, M. & HEIN, L. 2004. Adrenergic receptor knockout mice: distinct functions of 9 receptor subtypes. *Pharmacology and Therapeutics,* 101**,** 65-74.

PHROMMINTIKUL, A., TRAN, L., KOMPA, A., WANG, B., ADRAHTAS, A., CANTWELL, D., KELLY, D. J. & KRUM, H. 2008. Effects of a Rho kinase inhibitor on pressure overload induced cardiac hypertrophy and associated diastolic dysfunction. *American Journal of Physiology Heart and Circulatory Physiology,* 294**,** H1804-14.

POOLE-WILSON, P. A., SWEDBERG, K., CLELAND, J. G., DI LENARDA, A., HANRATH, P., KOMAJDA, M., LUBSEN, J., LUTIGER, B., METRA, M., REMME, W. J., TORP-PEDERSEN, C., SCHERHAG, A., SKENE, A. & INVESTIGATORS, C. O. M. E. T. 2003. Comparison of carvedilol and metoprolol on clinical outcomes in patients with chronic heart failure in the Carvedilol Or Metoprolol European Trial (COMET): randomised controlled trial. *The Lancet,* 362**,** 7-13.

POULIN, B., BUTCHER, A., MCWILLIAMS, P., BOURGOGNON, J. M., PAWLAK, R., KONG, K. C., BOTTRILL, A., MISTRY, S., WESS, J., ROSETHORNE, E. M., CHARLTON, S. J. & TOBIN, A. B. 2010. The M3-muscarinic receptor regulates learning and memory in a receptor phosphorylation/arrestin-dependent manner. *Proceedings of the National Academy of Sciences of the United States of America,* 107**,** 9440-5.

PRIHANDOKO, R., ALVAREZ-CURTO, E., HUDSON, B. D., BUTCHER, A. J., ULVEN, T., MILLER, A. M., TOBIN, A. B. & MILLIGAN, G. 2016. Distinct Phosphorylation

Clusters Determine the Signaling Outcome of Free Fatty Acid Receptor 4/G Protein-Coupled Receptor 120. *Molecular Pharmacology,* 89**,** 505-20.

PÉREZ-GÓMEZ, E., ANDRADAS, C., FLORES, J. M., QUINTANILLA, M., PARAMIO, J. M., GUZMÁN, M. & SÁNCHEZ, C. 2013. The orphan receptor GPR55 drives skin carcinogenesis and is upregulated in human squamous cell carcinomas. *Oncogene,* 32**,** 2534-42.

QI, G., JIA, L., LI, Y., BIAN, Y., CHENG, J., LI, H., XIAO, C. & DU, J. 2011. Angiotensin II infusion-induced inflammation, monocytic fibroblast precursor infiltration, and cardiac fibrosis are pressure dependent. *Cardiovascular Toxicology,* 11**,** 157-67.

RAM, R., MICKELSEN, D. M., THEODOROPOULOS, C. & BLAXALL, B. C. 2011. New approaches in small animal echocardiography: imaging the sounds of silence. *American Journal of Physiology Heart and Circulatory Physiology,* 301**,** H1765-80.

RASK-ANDERSEN, M., ALMÉN, M. S. & SCHIÖTH, H. B. 2011. Trends in the exploitation of novel drug targets. *Nature Reviews Drug Discovery,* 10**,** 579-90.

RASMUSSEN, S. G., CHOI, H. J., FUNG, J. J., PARDON, E., CASAROSA, P., CHAE, P. S., DEVREE, B. T., ROSENBAUM, D. M., THIAN, F. S., KOBILKA, T. S., SCHNAPP, A., KONETZKI, I., SUNAHARA, R. K., GELLMAN, S. H., PAUTSCH, A., STEYAERT, J., WEIS, W. I. & KOBILKA, B. K. 2011. Structure of a nanobody-stabilized active state of the ß(2) adrenoceptor. *Nature,* 469**,** 175-80.

REGAN, J. A., MAURO, A. G., CARBONE, S., MARCHETTI, C., GILL, R., MEZZAROMA, E., VALLE RALEIGH, J., SALLOUM, F. N., VAN TASSELL, B. W., ABBATE, A. & TOLDO, S. 2015. A mouse model of heart failure with preserved ejection fraction due to chronic infusion of a low subpressor dose of angiotensin II. *American Journal of Physiology Heart and Circulatory Physiology,* 309**,** H771-8.

REILLY, S. M., CHIANG, S. H., DECKER, S. J., CHANG, L., UHM, M., LARSEN, M. J., RUBIN, J. R., MOWERS, J., WHITE, N. M., HOCHBERG, I., DOWNES, M., YU, R. T., LIDDLE, C., EVANS, R. M., OH, D., LI, P., OLEFSKY, J. M. & SALTIEL, A. R. 2013. An inhibitor of the protein kinases TBK1 and IKK-ε improves obesity-related metabolic dysfunctions in mice. *Nature Medicine,* 19**,** 313-21.

REN, X. D., KIOSSES, W. B. & SCHWARTZ, M. A. 1999. Regulation of the small GTP-binding protein Rho by cell adhesion and the cytoskeleton. *EMBO Journal,* 18**,** 578-85.

REN, X. R., REITER, E., AHN, S., KIM, J., CHEN, W. & LEFKOWITZ, R. J. 2005. Different G protein-coupled receptor kinases govern G protein and ß -arrestin-mediated signaling of V2 vasopressin receptor. *Proceedings of the National Academy of Sciences of the United States of America,* 102**,** 1448-53.

RESTA, F., MASI, A., SILI, M., LAURINO, A., MORONI, F. & MANNAIONI, G. 2016. Kynurenic acid and zaprinast induce analgesia by modulating HCN channels through GPR35 activation. *Neuropharmacology,* 108**,** 136-43.

ROBINSON, J. E., VARDY, E., DIBERTO, J. F., CHEFER, V. I., WHITE, K. L., FISH, E. W., CHEN, M., GIGANTE, E., KROUSE, M. C., SUN, H., THORSELL, A., ROTH, B. L., HEILIG, M. & MALANGA, C. J. 2015. Receptor Reserve Moderates Mesolimbic Responses to Opioids in a Humanized Mouse Model of the OPRM1 A118G Polymorphism. *Neuropsychopharmacology,* 40**,** 2614-22.

ROCHA, R., CHANDER, P. N., KHANNA, K., ZUCKERMAN, A. & STIER, C. T. 1998. Mineralocorticoid blockade reduces vascular injury in stroke-prone hypertensive rats. *Hypertension,* 31**,** 451-8.

ROHRER, D. K. & KOBILKA, B. K. 1998. Insights from in vivo modification of adrenergic receptor gene expression. *Annual Review of Pharmacology and Toxicology,* 38**,** 351-73.

RONKAINEN, V. P., TUOMAINEN, T., HUUSKO, J., LAIDINEN, S., MALINEN, M., PALVIMO, J. J., YLÄ-HERTTUALA, S., VUOLTEENAHO, O. & TAVI, P. 2014. Hypoxia-inducible factor 1-induced G protein-coupled receptor 35 expression is an early marker of progressive cardiac remodelling. *Cardiovascular Research,* 101**,** 69-77.

ROZENFELD, R., GUPTA, A., GAGNIDZE, K., LIM, M. P., GOMES, I., LEE-RAMOS, D., NIETO, N. & DEVI, L. A. 2011. AT1R-CB_1R heteromerization reveals a new mechanism for the pathogenic properties of angiotensin II. *EMBO Journal,* 30**,** 2350-63.

RUDNICKI, M. A., BRAUN, T., HINUMA, S. & JAENISCH, R. 1992. Inactivation of MyoD in mice leads to up-regulation of the myogenic HLH gene Myf-5 and results in apparently normal muscle development. *Cell,* 71**,** 383-90.

RUIZ-ORTEGA, M., LORENZO, O., RUPÉREZ, M., ESTEBAN, V., SUZUKI, Y., MEZZANO, S., PLAZA, J. J. & EGIDO, J. 2001. Role of the renin-angiotensin system in vascular diseases: expanding the field. *Hypertension,* 38**,** 1382-7.

RYBERG, E., LARSSON, N., SJÖGREN, S., HJORTH, S., HERMANSSON, N. O., LEONOVA, J., ELEBRING, T., NILSSON, K., DRMOTA, T. & GREASLEY, P. J. 2007. The orphan receptor GPR55 is a novel cannabinoid receptor. *British Journal of Pharmacology,* 152**,** 1092-101.

SAKURAI, T., AMEMIYA, A., ISHII, M., MATSUZAKI, I., CHEMELLI, R. M., TANAKA, H., WILLIAMS, S. C., RICHARSON, J. A., KOZLOWSKI, G. P., WILSON, S., ARCH, J. R., BUCKINGHAM, R. E., HAYNES, A. C., CARR, S. A., ANNAN, R. S., MCNULTY, D. E., LIU, W. S., TERRETT, J. A., ELSHOURBAGY, N. A., BERGSMA, D. J. & YANAGISAWA, M. 1998. Orexins and orexin receptors: a family of hypothalamic neuropeptides and G protein-coupled receptors that regulate feeding behavior. *Cell,* 92**,** 1 page following 696.

SCHAPPI, J. M., KRBANJEVIC, A. & RASENICK, M. M. 2014. Tubulin, actin and heterotrimeric G proteins: coordination of signaling and structure. *Biochimica et Biophysica Acta,* 1838**,** 674-81.

SCHRAGE, R., SCHMITZ, A. L., GAFFAL, E., ANNALA, S., KEHRAUS, S., WENZEL, D., BÜLLESBACH, K. M., BALD, T., INOUE, A., SHINJO, Y., GALANDRIN, S., SHRIDHAR, N., HESSE, M., GRUNDMANN, M., MERTEN, N., CHARPENTIER, T. H., MARTZ, M., BUTCHER, A. J., SLODCZYK, T., ARMANDO, S., EFFERN, M., NAMKUNG, Y., JENKINS, L., HORN, V., STÖßEL, A., DARGATZ, H., TIETZE, D., IMHOF, D., GALÉS, C., DREWKE, C., MÜLLER, C. E., HÖLZEL, M., MILLIGAN, G., TOBIN, A. B., GOMEZA, J., DOHLMAN, H. G., SONDEK, J., HARDEN, T. K., BOUVIER, M., LAPORTE, S. A., AOKI, J., FLEISCHMANN, B. K., MOHR, K., KÖNIG, G. M., TÜTING, T. & KOSTENIS, E. 2015. The experimental power of FR900359 to study Gq-regulated biological processes. *Nature Communications,* 6**,** 10156.

SCHRÖDER, R., JANSSEN, N., SCHMIDT, J., KEBIG, A., MERTEN, N., HENNEN, S., MÜLLER, A., BLÄTTERMANN, S., MOHR-ANDRÄ, M., ZAHN, S., WENZEL, J., SMITH, N. J., GOMEZA, J., DREWKE, C., MILLIGAN, G., MOHR, K. & KOSTENIS, E. 2010. Deconvolution of complex G protein-coupled receptor signaling in live cells using dynamic mass redistribution measurements. *Nature Biotechnology,* 28**,** 943-9.

SCHRÖDER, R., SCHMIDT, J., BLÄTTERMANN, S., PETERS, L., JANSSEN, N., GRUNDMANN, M., SEEMANN, W., KAUFEL, D., MERTEN, N., DREWKE, C., GOMEZA, J., MILLIGAN, G., MOHR, K. & KOSTENIS, E. 2011. Applying label-free dynamic mass redistribution technology to frame signaling of G protein-coupled receptors noninvasively in living cells. *Nature Protocols,* 6**,** 1748-60.

SCHWARCZ, R., BRUNO, J. P., MUCHOWSKI, P. J. & WU, H. Q. 2012. Kynurenines in the mammalian brain: when physiology meets pathology. *Nature Reviews Neuroscience,* 13**,** 465-77.

SEIBOLD, A., WILLIAMS, B., HUANG, Z. F., FRIEDMAN, J., MOORE, R. H., KNOLL, B. J. & CLARK, R. B. 2000. Localization of the sites mediating desensitization of the beta(2)-adrenergic receptor by the GRK pathway. *Molecular Pharmacology,* 58**,** 1162-73.

SHENOY, S. K., DRAKE, M. T., NELSON, C. D., HOUTZ, D. A., XIAO, K., MADABUSHI, S., REITER, E., PREMONT, R. T., LICHTARGE, O. & LEFKOWITZ, R. J. 2006. β-arrestin-dependent, G protein-independent ERK1/2 activation by the beta2 adrenergic receptor. *Journal of Biological Chemistry,* 281**,** 1261-73.

SIEHLER, S. 2009. Regulation of RhoGEF proteins by G12/13-coupled receptors. *British Journal of Pharmacology,* 158**,** 41-9.

SINGH, N. S., BERNIER, M. & WAINER, I. W. 2016. Selective GPR55 antagonism reduces chemoresistance in cancer cells. *Pharmacological Research,* 111, 757-66.

SLUSARSKI, D. C., CORCES, V. G. & MOON, R. T. 1997. Interaction of Wnt and a Frizzled homologue triggers G-protein-linked phosphatidylinositol signalling. *Nature,* 390**,** 410-3.

SOERGEL, D. G., SUBACH, R. A., COWAN, C. L., VIOLIN, J. D. & LARK, M. W. 2013. First clinical experience with TRV027: pharmacokinetics and pharmacodynamics in healthy volunteers. *Journal of Clinical Pharmacology,* 53**,** 892-9.

SOUTHERN, C., COOK, J. M., NEETOO-ISSELJEE, Z., TAYLOR, D. L., KETTLEBOROUGH, C. A., MERRITT, A., BASSONI, D. L., RAAB, W. J., QUINN, E., WEHRMAN, T. S., DAVENPORT, A. P., BROWN, A. J., GREEN, A., WIGGLESWORTH, M. J. & REES, S. 2013. Screening β-arrestin recruitment for the identification of natural ligands for orphan G-protein-coupled receptors. *Journal of Biomolecular Screening,* 18**,** 599-609.

SPRANG, S. R., CHEN, Z. & DU, X. 2007. Structural basis of effector regulation and signal termination in heterotrimeric Gα proteins. *Advances in Protein Chemistry,* 74**,** 1-65.

STANDFUSS, J., EDWARDS, P. C., D'ANTONA, A., FRANSEN, M., XIE, G., OPRIAN, D. D. & SCHERTLER, G. F. 2011. The structural basis of agonist-induced activation in constitutively active rhodopsin. *Nature,* 471**,** 656-60.

STONE, T. W. & DARLINGTON, L. G. 2002. Endogenous kynurenines as targets for drug discovery and development. *Nature Reviews Drug Discovery,* 1**,** 609-20.

SUN, Y. V., BIELAK, L. F., PEYSER, P. A., TURNER, S. T., SHEEDY, P. F., BOERWINKLE, E. & KARDIA, S. L. 2008. Application of machine learning algorithms to predict coronary artery calcification with a sibship-based design. *Genetic Epidemiology,* 32**,** 350-60.

SURMA, M., WEI, L. & SHI, J. 2011. Rho kinase as a therapeutic target in cardiovascular disease. *Future Cardiology,* 7**,** 657-71.

SUTHERLAND, E. W. 1972. Studies on the mechanism of hormone action. *Science,* 177**,** 401-8.

SZCZEPEK, M., BEYRIÈRE, F., HOFMANN, K. P., ELGETI, M., KAZMIN, R., ROSE, A., BARTL, F. J., VON STETTEN, D., HECK, M., SOMMER, M. E., HILDEBRAND, P. W. & SCHEERER, P. 2014. Crystal structure of a common GPCR-binding interface for G protein and arrestin. *Nature Communications,* 5**,** 4801.

TAKAYANAGI, T., FORRESTER, S. J., KAWAI, T., OBAMA, T., TSUJI, T., ELLIOTT, K. J., NUTI, E., ROSSELLO, A., KWOK, H. F., SCALIA, R., RIZZO, V. & EGUCHI, S. 2016. Vascular ADAM17 as a Novel Therapeutic Target in Mediating Cardiovascular Hypertrophy and Perivascular Fibrosis Induced by Angiotensin II. *Hypertension,* 68**,** 949-55.

TAKAYANAGI, T., KAWAI, T., FORRESTER, S. J., OBAMA, T., TSUJI, T., FUKUDA, Y., ELLIOTT, K. J., TILLEY, D. G., DAVISSON, R. L., PARK, J. Y. & EGUCHI, S. 2015. Role of epidermal growth factor receptor and endoplasmic reticulum stress in vascular remodeling induced by angiotensin II. *Hypertension,* 65**,** 1349-55.

TAKEDA, N. & MAEMURA, K. 2011. Circadian clock and cardiovascular disease. *Journal of Cardiology,* 57**,** 249-56.

TAKEDA, S., YAMAMOTO, A., OKADA, T., MATSUMURA, E., NOSE, E., KOGURE, K., KOJIMA, S. & HAGA, T. 2003. Identification of surrogate ligands for orphan G protein-coupled receptors. *Life Sciences,* 74**,** 367-77.

TAKEFUJI, M., WIRTH, A., LUKASOVA, M., TAKEFUJI, S., BOETTGER, T., BRAUN, T., ALTHOFF, T., OFFERMANNS, S. & WETTSCHURECK, N. 2012. G(13)-mediated signaling pathway is required for pressure overload-induced cardiac remodeling and heart failure. *Circulation,* 126**,** 1972-82.

TANG, T., LI, L., TANG, J., LI, Y., LIN, W. Y., MARTIN, F., GRANT, D., SOLLOWAY, M., PARKER, L., YE, W., FORREST, W., GHILARDI, N., ORAVECZ, T., PLATT, K. A., RICE, D. S., HANSEN, G. M., ABUIN, A., EBERHART, D. E., GODOWSKI, P., HOLT, K. H., PETERSON, A., ZAMBROWICZ, B. P. & DE SAUVAGE, F. J. 2010. A mouse knockout library for secreted and transmembrane proteins. *Nature Biotechnology,* 28**,** 749-55.

TANIGUCHI, Y., TONAI-KACHI, H. & SHINJO, K. 2006. Zaprinast, a well-known cyclic guanosine monophosphate-specific phosphodiesterase inhibitor, is an agonist for GPR35. *FEBS Letters,* 580**,** 5003-8.

TE RIET, L., VAN ESCH, J. H., ROKS, A. J., VAN DEN MEIRACKER, A. H. & DANSER, A. H. 2015. Hypertension: renin-angiotensin-aldosterone system alterations. *Circulation Research,* 116**,** 960-75.

TEICHHOLZ, L. E., KREULEN, T., HERMAN, M. V. & GORLIN, R. 1976. Problems in echocardiographic volume determinations: echocardiographic-angiographic correlations in the presence of absence of asynergy. *American Journal of Cardiology,* 37**,** 7-11.

TELLO, J. A., KOHOUT, T., PINEDA, R., MAKI, R. A., SCOTT STRUTHERS, R. & MILLAR, R. P. 2013. Reproductive physiology of a humanized GnRH receptor mouse model: application in evaluation of human-specific analogs. *American Journal of Physiology Endocrinology and Metabolism,* 305**,** E67-77.

THOMPSON, S., CLARKE, A. R., POW, A. M., HOOPER, M. L. & MELTON, D. W. 1989. Germ line transmission and expression of a corrected HPRT gene produced by gene targeting in embryonic stem cells. *Cell,* 56**,** 313-21.

THOMSEN, A. R., PLOUFFE, B., CAHILL, T. J., SHUKLA, A. K., TARRASCH, J. T., DOSEY, A. M., KAHSAI, A. W., STRACHAN, R. T., PANI, B., MAHONEY, J. P., HUANG, L., BRETON, B., HEYDENREICH, F. M., SUNAHARA, R. K., SKINIOTIS, G., BOUVIER, M. & LEFKOWITZ, R. J. 2016. GPCR-G Protein-β-Arrestin Super-Complex Mediates Sustained G Protein Signaling. *Cell*, 166, 907-19.

THORBURN, A. N., MACIA, L. & MACKAY, C. R. 2014. Diet, metabolites, and "western-lifestyle" inflammatory diseases. *Immunity,* 40**,** 833-42.

TOBIN, A. B. 2008. G-protein-coupled receptor phosphorylation: where, when and by whom. *British Journal of Pharmacology,* 153 Suppl 1**,** S167-76.

TOBIN, A. B., BUTCHER, A. J. & KONG, K. C. 2008. Location, location, location...site-specific GPCR phosphorylation offers a mechanism for cell-type-specific signalling. *Trends in Pharmacological Sciences,* 29**,** 413-20.

TRAYNHAM, C. J., CANNAVO, A., ZHOU, Y., VOUGA, A. G., WOODALL, B. P., HULLMANN, J., IBETTI, J., GOLD, J. I., CHUPRUN, J. K., GAO, E. & KOCH, W. J. 2015. Differential Role of G Protein-Coupled Receptor Kinase 5 in Physiological Versus Pathological Cardiac Hypertrophy. *Circulation Research,* 117**,** 1001-12.

TSVETANOVA, N. G. & VON ZASTROW, M. 2014. Spatial encoding of cyclic AMP signaling specificity by GPCR endocytosis. *Nature Chemical Biology,* 10**,** 1061-5.

UNGERER, M., BÖHM, M., ELCE, J. S., ERDMANN, E. & LOHSE, M. J. 1993. Altered expression of beta-adrenergic receptor kinase and beta 1-adrenergic receptors in the failing human heart. *Circulation,* 87**,** 454-63.

VAN BERLO, J. H., MAILLET, M. & MOLKENTIN, J. D. 2013. Signaling effectors underlying pathologic growth and remodeling of the heart. *Journal of Clinical Investigation,* 123**,** 37-45.

VAN VLIET, B. N., CHAFE, L. L. & MONTANI, J. P. 2003. Characteristics of 24 h telemetered blood pressure in eNOS-knockout and C57Bl/6J control mice. *Journal of Physiology,* 549**,** 313-25.

VAN VLIET, B. N., MCGUIRE, J., CHAFE, L., LEONARD, A., JOSHI, A. & MONTANI, J. P. 2006. Phenotyping the level of blood pressure by telemetry in mice. *Clinical and Experimental Pharmacology and Physiology,* 33**,** 1007-15.

VENKATAKRISHNAN, A. J., DEUPI, X., LEBON, G., TATE, C. G., SCHERTLER, G. F. & BABU, M. M. 2013. Molecular signatures of G-protein-coupled receptors. *Nature,* 494**,** 185-94.

VIOLIN, J. D., DEWIRE, S. M., YAMASHITA, D., ROMINGER, D. H., NGUYEN, L., SCHILLER, K., WHALEN, E. J., GOWEN, M. & LARK, M. W. 2010. Selectively engaging β-arrestins at the angiotensin II type 1 receptor reduces blood pressure and increases cardiac performance. *Journal of Pharmacology and Experimental Therapeutics,* 335**,** 572-9.

VOGT, S., GROSSE, R., SCHULTZ, G. & OFFERMANNS, S. 2003. Receptor-dependent RhoA activation in G12/G13-deficient cells: genetic evidence for an involvement of Gq/G11. *Journal of Biological Chemistry,* 278**,** 28743-9.

VÖGLER, O., BARCELÓ, J. M., RIBAS, C. & ESCRIBÁ, P. V. 2008. Membrane interactions of G proteins and other related proteins. *Biochimica et Biophysica Acta,* 1778**,** 1640-52.

WACHTER, S. B. & GILBERT, E. M. 2012. Beta-adrenergic receptors, from their discovery and characterization through their manipulation to beneficial clinical application. *Cardiology,* 122**,** 104-12.

WALKER, J. K., GAINETDINOV, R. R., FELDMAN, D. S., MCFAWN, P. K., CARON, M. G., LEFKOWITZ, R. J., PREMONT, R. T. & FISHER, J. T. 2004. G protein-coupled receptor kinase 5 regulates airway responses induced by muscarinic receptor activation. *American Journal of Physiology Lung Cell and Molecular Physiology,* 286, L312-9.

WANG, J., SIMONAVICIUS, N., WU, X., SWAMINATH, G., REAGAN, J., TIAN, H. & LING, L. 2006. Kynurenic acid as a ligand for orphan G protein-coupled receptor GPR35. *Journal of Biological Chemistry,* 281, 22021-8.

WEI, H., AHN, S., SHENOY, S. K., KARNIK, S. S., HUNYADY, L., LUTTRELL, L. M. & LEFKOWITZ, R. J. 2003. Independent beta-arrestin 2 and G protein-mediated pathways for angiotensin II activation of extracellular signal-regulated kinases 1 and 2. *Proc Natl Acad Sci U S A,* 100, 10782-7.

WEISS, D., KOOLS, J. J. & TAYLOR, W. R. 2001. Angiotensin II-induced hypertension accelerates the development of atherosclerosis in apoE-deficient mice. *Circulation,* 103, 448-54.

WENZEL, P., KNORR, M., KOSSMANN, S., STRATMANN, J., HAUSDING, M., SCHUHMACHER, S., KARBACH, S. H., SCHWENK, M., YOGEV, N., SCHULZ, E., OELZE, M., GRABBE, S., JONULEIT, H., BECKER, C., DAIBER, A., WAISMAN, A. & MÜNZEL, T. 2011. Lysozyme M-positive monocytes mediate angiotensin II-induced arterial hypertension and vascular dysfunction. *Circulation,* 124, 1370-81.

WENZEL, U., TURNER, J. E., KREBS, C., KURTS, C., HARRISON, D. G. & EHMKE, H. 2016. Immune Mechanisms in Arterial Hypertension. *Journal of the American Society of Nephrology,* 27, 677-86.

WETTSCHURECK, N. & OFFERMANNS, S. 2005. Mammalian G proteins and their cell type specific functions. *Physiological Reviews,* 85, 1159-204.

WHALEN, E. J., RAJAGOPAL, S. & LEFKOWITZ, R. J. 2011. Therapeutic potential of ß-arrestin- and G protein-biased agonists. *Trends in Molecular Medicine,* 17, 126-39.

WHITE, J. K., GERDIN, A. K., KARP, N. A., RYDER, E., BULJAN, M., BUSSELL, J. N., SALISBURY, J., CLARE, S., INGHAM, N. J., PODRINI, C., HOUGHTON, R., ESTABEL, J., BOTTOMLEY, J. R., MELVIN, D. G., SUNTER, D., ADAMS, N. C., TANNAHILL, D., LOGAN, D. W., MACARTHUR, D. G., FLINT, J., MAHAJAN, V. B., TSANG, S. H., SMYTH, I., WATT, F. M., SKARNES, W. C., DOUGAN, G., ADAMS, D. J., RAMIREZ-SOLIS, R., BRADLEY, A., STEEL, K. P. & PROJECT, S. I. M. G. 2013. Genome-wide generation and systematic phenotyping of knockout mice reveals new roles for many genes. *Cell,* 154, 452-64.

WILLIAMS, B., POULTER, N. R., BROWN, M. J., DAVIS, M., MCINNES, G. T., POTTER, J. F., SEVER, P. S., THOM, S. M. & BHS GUIDELINES WORKING PARTY, F. T. B. H. S. 2004. British Hypertension Society guidelines for hypertension management 2004 (BHS-IV): summary. *BMJ,* 328, 634-40.

WIRTH, A., BENYÓ, Z., LUKASOVA, M., LEUTGEB, B., WETTSCHURECK, N., GORBEY, S., ORSY, P., HORVÁTH, B., MASER-GLUTH, C., GREINER, E., LEMMER, B., SCHÜTZ, G., GUTKIND, J. S. & OFFERMANNS, S. 2008. G12-G13-LARG-mediated signaling in vascular smooth muscle is required for salt-induced hypertension. *Nature Medicine,* 14**,** 64-8.

WIRTZ, S., NEUFERT, C., WEIGMANN, B. & NEURATH, M. F. 2007. Chemically induced mouse models of intestinal inflammation. *Nature Protocols,* 2**,** 541-6.

WISLER, J. W., DEWIRE, S. M., WHALEN, E. J., VIOLIN, J. D., DRAKE, M. T., AHN, S., SHENOY, S. K. & LEFKOWITZ, R. J. 2007. A unique mechanism of beta-blocker action: carvedilol stimulates ß -arrestin signaling. *Proceedings of the National Academy of Sciences of the United States of America,* 104**,** 16657-62.

WOODARD, G. E., JARDÍN, I., BERNA-ERRO, A., SALIDO, G. M. & ROSADO, J. A. 2015. Regulators of G-protein-signaling proteins: negative modulators of G-protein-coupled receptor signaling. *International Review of Cell and Molecular Biology,* 317**,** 97-183.

WORZFELD, T., WETTSCHURECK, N. & OFFERMANNS, S. 2008. G(12)/G(13)-mediated signalling in mammalian physiology and disease. *Trends in Pharmacological Sciences,* 29**,** 582-9.

WYNNE, B. M., CHIAO, C. W. & WEBB, R. C. 2009. Vascular Smooth Muscle Cell Signaling Mechanisms for Contraction to Angiotensin II and Endothelin-1. *Journal of the American Society of Hypertension,* 3**,** 84-95.

XIE, M., BURCHFIELD, J. S. & HILL, J. A. 2013. Pathological ventricular remodeling: therapies: part 2 of 2. *Circulation,* 128**,** 1021-30.

XU, F., WU, H., KATRITCH, V., HAN, G. W., JACOBSON, K. A., GAO, Z. G., CHEREZOV, V. & STEVENS, R. C. 2011. Structure of an agonist-bound human A2A adenosine receptor. *Science,* 332**,** 322-7.

YAMAMOTO, H., OKUZAKI, D., YAMANISHI, K., XU, Y., WATANABE, Y., YOSHIDA, M., YAMASHITA, A., GOTO, N., NISHIGUCHI, S., SHIMADA, K., NOJIMA, H., YASUNAGA, T., OKAMURA, H., MATSUNAGA, H. & YAMANISHI, H. 2013. Genetic analysis of genes causing hypertension and stroke in spontaneously hypertensive rats. *International Journal of Molecular Medicine,* 31**,** 1057-65.

YAMORI, Y. & HORIE, R. 1977. Developmental course of hypertension and regional cerebral blood flow in stroke-prone spontaneously hypertensive rats. *Stroke,* 8**,** 456-61.

YANG, Y., LU, J. Y., WU, X., SUMMER, S., WHORISKEY, J., SARIS, C. & REAGAN, J. D. 2010. G-protein-coupled receptor 35 is a target of the asthma drugs cromolyn disodium and nedocromil sodium. *Pharmacology,* 86**,** 1-5.

ZAMBROWICZ, B. P. & SANDS, A. T. 2003. Knockouts model the 100 best-selling drugs--will they model the next 100? *Nature Reviews Drug Discovery,* 2**,** 38-51.

ZENG, C., LUO, Y., ASICO, L. D., HOPFER, U., EISNER, G. M., FELDER, R. A. & JOSE, P. A. 2003. Perturbation of D1 dopamine and AT1 receptor interaction in spontaneously hypertensive rats. *Hypertension,* 42**,** 787-92.

ZHANG, J., BARAK, L. S., ANBORGH, P. H., LAPORTE, S. A., CARON, M. G. & FERGUSON, S. S. 1999. Cellular trafficking of G protein-coupled receptor/beta-arrestin endocytic complexes. *J Biol Chem,* 274**,** 10999-1006.

ZHAO, P. & ABOOD, M. E. 2013. GPR55 and GPR35 and their relationship to cannabinoid and lysophospholipid receptors. *Life Sciences,* 92**,** 453-7.

ZHAO, P., SHARIR, H., KAPUR, A., COWAN, A., GELLER, E. B., ADLER, M. W., SELTZMAN, H. H., REGGIO, P. H., HEYNEN-GENEL, S., SAUER, M., CHUNG, T. D., BAI, Y., CHEN, W., CARON, M. G., BARAK, L. S. & ABOOD, M. E. 2010. Targeting of the orphan receptor GPR35 by pamoic acid: a potent activator of extracellular signal-regulated kinase and ß-arrestin2 with antinociceptive activity. *Molecular Pharmacology,* 78**,** 560-8.

ZHU, W., PETRASHEVSKAYA, N., REN, S., ZHAO, A., CHAKIR, K., GAO, E., CHUPRUN, J. K., WANG, Y., TALAN, M., DORN, G. W., LAKATTA, E. G., KOCH, W. J., FELDMAN, A. M. & XIAO, R. P. 2012. Gi-biased ß2AR signaling links GRK2 upregulation to heart failure. *Circulation Research,* 110**,** 265-74.

ZIOLO, M. T., LEWANDOWSKI, S. J., SMITH, J. M., ROMANO, F. D. & WAHLER, G. M. 2003. Inhibition of cyclic GMP hydrolysis with zaprinast reduces basal and cyclic AMP-elevated L-type calcium current in guinea-pig ventricular myocytes. *British Journal of Pharmacology,* 138**,** 986-94.